

# Comparative analysis of the conformational dynamics of human and yeast Hsp90

**Stefan Riedl**

Vollständiger Abdruck der von der TUM School of Natural Sciences der Technischen Universität München zur Erlangung des akademischen Grades eines Doktors der Naturwissenschaften (Dr. rer. nat.) genehmigten Dissertation.

Vorsitz: Prof. Dr. Cathleen Zeymer

Prüfer\*innen der Dissertation:

1. Prof. Dr. Johannes Buchner
2. Prof. Dr. Michael Sattler

Die Dissertation wurde am 14.06.2023 bei der Technischen Universität München eingereicht und durch die TUM School of Natural Sciences am 13.07.2023 angenommen.



“There’s no scientific consensus that life is important.”  
- Professor Farnsworth, Futurama



# Content

Summary.....	1
Zusammenfassung.....	2
1 Introduction.....	4
1.1 Protein Folding in the Cell.....	4
1.2 Molecular Chaperones.....	7
1.3 The Molecular Chaperone Hsp90.....	10
1.3.1 Hsp90 Isoforms.....	11
1.3.2 Structure of Hsp90.....	12
1.3.3 The Conformational Cycle of Hsp90.....	15
1.3.4 Co-Chaperones of Hsp90.....	18
2 Objective.....	23
3 Material and Methods.....	25
3.1 Material.....	25
3.1.1 Chemicals.....	25
3.1.2 Instruments and Consumables.....	27
3.1.3 Software and Web-Based Tools.....	29
3.1.4 Kits and Markers.....	30
3.1.5 Nucleotides.....	30
3.1.6 Fluorophores.....	30
3.1.7 Enzymes.....	31
3.1.8 Media and Antibiotics.....	31
3.1.9 <i>E. coli</i> and <i>S. cerevisiae</i> Strains.....	32
3.1.10 Plasmids.....	32
3.1.11 DNA Oligonucleotides.....	34
3.2 Methods.....	37
3.2.1 Biomolecular Techniques.....	37
3.2.1.1 Cultivation of <i>E. coli</i> .....	37
3.2.1.2 Cultivation of <i>S. cerevisiae</i> .....	37
3.2.1.3 Transformation of <i>E. coli</i> .....	37
3.2.1.4 Transformation of <i>S. cerevisiae</i> .....	38
3.2.1.5 Polymerase Chain Reaction.....	39

3.2.1.6 Site-Directed Mutagenesis.....	40
3.2.1.7 Agarose Gel Electrophoresis.....	40
3.2.1.8 DNA Isolation and Purification.....	40
3.2.1.9 Restriction Digest and Ligation.....	41
3.2.1.10 Sequence- and Ligation-Independent Closing.....	41
3.2.2 Protein Expression and Purification.....	42
3.2.2.1 Protein Expression in <i>E. coli</i> .....	42
3.2.2.2 Cell Disruption.....	43
3.2.2.3 Affinity Chromatography.....	43
3.2.2.4 Proteolytic His-Tag Cleavage.....	44
3.2.2.5 Reverse Affinity Chromatography.....	45
3.2.2.6 Ion-Exchange Chromatography.....	45
3.2.2.7 Hydroxyapatite Chromatography.....	46
3.2.2.8 Size-Exclusion Chromatography.....	46
3.2.3 Biochemical Methods.....	47
3.2.3.1 SDS-Polyacrylamide Gel Electrophoresis.....	47
3.2.3.2 Coomassie Staining.....	48
3.2.3.3 Western Blot.....	49
3.2.3.4 Native Polyacrylamide Gel Electrophoresis.....	50
3.2.3.5 Limited Proteolysis.....	50
3.2.3.6 Crosslinking of Co-Chaperones.....	51
3.2.3.7 Crosslinking Closing Kinetics.....	51
3.2.3.8 Crosslink MS/MS Measurements.....	51
3.2.3.9 Protein Labeling.....	52
3.2.3.10 Expressed Protein Ligation.....	53
3.2.3.11 Sortase A Mediated Protein Ligation.....	53
3.2.4 Biophysical Methods.....	55
3.2.4.1 Circular Dichroism Spectroscopy.....	55
3.2.4.2 Thermo Shift Assay.....	55
3.2.4.3 Absorbance Spectroscopy.....	56
3.2.4.4 Analytical Ultracentrifugation.....	56
3.2.4.5 Transmission Electron Microscopy.....	57

3.2.4.6 Hydrogen Deuterium Exchange Mass Spectrometry.....	57
3.2.4.7 Evolutionary Residue Conservation.....	58
3.2.4.8 Molecular Dynamic Simulations.....	58
3.2.4.9 Size Exclusion Chromatography with Multi Angle Light Scattering.....	59
3.2.4.10 Ensemble Förster Resonance Energy Transfer Spectroscopy.....	60
3.2.4.11 Single Molecule Förster Resonance Energy Transfer Spectroscopy.....	60
3.2.5 <i>In Vitro</i> and <i>In Vivo</i> Activity Assays.....	61
3.2.5.1 Regenerative ATPase Assay.....	61
3.2.5.2 5'-FOA Plasmid Shuffling Assay.....	62
3.2.5.3 Temperature Sensitivity.....	62
3.2.5.4 Radicol Sensitivity.....	62
4 Results.....	64
4.1 Establishing a Human Hsp90 FRET-System.....	64
4.1.1 Design of Hsp90 Fragments for Expressed Protein Ligation.....	66
4.1.2 Expressed Protein Ligation of Hsp90.....	68
4.1.3 Optimization of the Hsp90 Expressed Protein Ligation.....	70
4.1.4 Design of Hsp90 Fragments for SrtA Mediated Ligation.....	72
4.1.5 SrtA Mediated Ligation of Hsp90.....	74
4.1.6 Optimization of the SrtA Mediated Protein Ligation.....	76
4.1.7 <i>In Vitro</i> Characterization of SrtA Ligated Hsp90.....	78
4.1.8 <i>In Vitro</i> Characterization of Labeled Hsp90.....	80
4.1.9 Single Molecule Characterization of SrtA Ligated Hsp90.....	83
4.2 Defining the Closed State Formation of Hsp90.....	86
4.2.1 Oligomer Formation during Hsp90 Closing.....	86
4.2.2 Ionic Components Modulate Hsp90 Stability and Closing.....	89
4.2.3 Time-Resolved Closing of Hsp90.....	91
4.2.4 Temperature Influence on the Hsp90 Closing Kinetics.....	94
4.3 Evolutionary Differences of Hsp82 and Hsp90 $\beta$ .....	96
4.3.1 Nucleotide-induced Closed State Formation.....	97
4.3.2 Correlation of Hsp90 Closing Kinetics and ATPase Activity.....	100
4.3.3 Modulation of the Hsp90 Activity by Hydrophobic Interactions.....	102
4.3.4 Influence of Mutations on Hsp90.....	105

4.3.5 Dimer Re-Opening via Nucleotide Exchange.....	107
4.3.6 Domain Rearrangements during the Closed State Formation.....	111
4.3.7 Evolutionary Divergence of Yeast and Human Hsp90.....	113
4.3.8 <i>In Vitro</i> Characterization of Chimeric Human/Yeast-Mutants.....	116
4.3.9 <i>In Vivo</i> Characterization of Chimeric Human/Yeast-Mutants.....	117
5 Discussion.....	118
References.....	128
Abbreviations.....	148
Acknowledgments.....	150
Declaration.....	151



## Summary

Molecular chaperones are essential for the proper folding and stabilization of proteins. Among them, Hsp90 is a highly conserved ATP-dependent folding factor that plays a critical role in regulating the folding, activation, and degradation of a diverse set of client proteins. The Hsp90 monomer consists of three domains: an N-terminal domain that contains the ATP-binding site, a middle domain that binds to client proteins and interacts with co-chaperones, and a C-terminal domain that is required for dimerization. The chaperoning function of Hsp90 is facilitated by its dynamic nature, allowing for conformational changes from an open to a closed state that aid in protein folding and client-protein interaction. In recent years, the ATPase cycle of the yeast analogue Hsp82 has been well characterized. However, human Hsp90 is far less well studied and leaves open many questions.

The first part of the thesis focuses on the development of an N-terminal FRET system to investigate the conformational dynamics of human Hsp90. Due to the presence of six native cysteines in human Hsp90, the labeling of the protein with fluorescent dyes is challenging compared to yeast Hsp82. To overcome this issue, the protein was expressed in two fragments: the N-terminal fragment to which the fluorescent label should be connected and the C-terminal fragment containing the native cysteines. The ligation of the two fragments was attempted via expressed protein ligation and Sortase A mediated ligation. However, the Sortase A-mediated ligation was the only approach that provided sufficient yields. The resulting site-specific labeled Hsp90 revealed nucleotide-dependent changes in populations of open and closed conformations in single molecule FRET experiments.

The second part of the thesis describes the formation of the closed state of unlabeled Hsp90 by SEC and the comparison to the yeast analogue Hsp82. First, the buffer conditions were optimized to promote closed state formation and the kinetics of the closed state formation in the presence of ATP $\gamma$ S were determined. Differences between yeast and human Hsp90 were observed in ATPase activity and structural transitions. Notably, the use of kosmotropic buffers significantly enhanced the activity and closing kinetics of human Hsp90, but not of yeast Hsp90. However, mutations modulating Hsp90 activity suggest a common mechanism between the two proteins, as well as a correlation between closing kinetics and ATPase activity.

Two highly conserved residues in the lid and  $\alpha$ 1-helix of the human N-terminal domain were identified, which differ between Hsp82 and Hsp90 and affect crucial elements of the ATPase cycle. Molecular dynamics simulations, as well as the *in vivo* and *in vitro* characterization of mutants, revealed their impact on conformational dynamics and enzymatic activity.

## Zusammenfassung

Molekulare Chaperone sind essentiell für die korrekte Faltung und Stabilisierung von Proteinen. Hsp90 ist ein hochkonservierter, ATP-abhängiger Faltungsfaktor, der eine entscheidende Rolle bei der Regulation der Faltung, Aktivierung und Degradation einer breiten Gruppe von *Client*-Proteinen spielt. Das Hsp90-Monomer besteht aus drei Domänen: einer N-terminalen Domäne, die die ATP-Binde-Stelle enthält, einer mittleren Domäne, die an *Client*-Proteine bindet und mit Co-Chaperonen interagiert und einer C-terminalen Domäne, die essentiell für die Dimerisierung ist. Die Chaperon-Funktion von Hsp90 wird durch den ATPase Zyklus ermöglicht, der strukturelle Konformationsänderungen hervorruft, welche bei der Proteinfaltung und Interaktion mit *Client*-Proteinen involviert sind. In den letzten Jahren wurde der ATPase-Zyklus des Hefe-Analogons Hsp82 umfassend erforscht. Das menschliche Hsp90 ist jedoch weit weniger gut charakterisiert und wirft viele Fragen auf.

Der erste Teil der Arbeit konzentriert sich auf die Entwicklung eines N-terminalen FRET-Systems, um die konformationellen Dynamiken von humanem Hsp90 zu erforschen. Aufgrund der Anwesenheit von sechs nativen Cysteinen in Hsp90 beim Menschen ist die Markierung des Proteins mit fluoreszierenden Farbstoffen im Vergleich zu Hsp82 erschwert. Um eine selektive Fluoreszenzmarkierung zu erhalten, wurde das Protein deshalb in zwei Fragmenten exprimiert: das N-terminale Fragment, welches mit einem fluoreszierenden Farbstoff verknüpft wird, und das C-terminale Fragment, das die nativen Cysteine enthält. Die Ligation der beiden Fragmente wurde via *Expressed Protein Ligation* und SortaseA-Ligation versucht. Jedoch resultierte nur der Ansatz mit SortaseA in ausreichenden Mengen an Protein für weitere Experimente. Das gelabelte Hsp90 wies in Einzelmolekülmessungen unterschiedliche Populationen des offenen und geschlossenen Zustands auf, abhängig vom verwendeten Nukleotid.

Der zweite Teil der Arbeit befasst sich mit der Ausbildung des geschlossenen Zustands von ungelabelten Hsp90 via SEC. Zusätzlich wurde das humane Hsp90 mit dem Hefe-Analog Hsp82 verglichen. Zunächst wurden die Pufferbedingungen optimiert, um die Formierung des geschlossenen Zustands zu begünstigen und die Kinetik der Formierung des geschlossenen Zustands in Gegenwart von ATP $\gamma$ S bestimmt. Unterschiede zwischen Hefe und humanem Hsp90 wurden hinsichtlich ATPase-Aktivität und strukturellen Übergängen beobachtet. Insbesondere führte die Verwendung von kosmotropen Puffern zur Verbesserung der Aktivität und Schließkinetik bei humanem Hsp90, jedoch nicht bei Hsp82. Mutationen, die die Aktivität von Hsp90 modulieren, legen jedoch einen gemeinsamen Mechanismus zwischen den beiden Proteinen sowie eine Korrelation zwischen Schließkinetik und ATPase-Aktivität nahe.

Zwei konservierte Aminosäuren im *ATP-Lid* und in der  $\alpha$ 1-Helix der humanen N-terminalen Domäne konnten identifiziert werden, die sich zwischen Hsp82 und Hsp90 unterscheiden und wichtige Elemente

des ATPase-Zyklus beeinflussen. Molekulardynamik-Simulationen sowie die *in vivo*- und *in vitro*-Charakterisierungen von Mutanten zeigten deutliche Auswirkungen auf die Schließkinetik und die Aktivität.

# 1 Introduction

## 1.1 Protein Folding in the Cell

Proteins are complex biomolecules and macromolecules consisting of one or more chain of amino acid residues. They fulfill a wide range of vital roles within every organisms, such as aiding in DNA replication, intracellular transport via motor proteins, providing stability through cytoskeletal proteins or catalyzing metabolic processes *via* various enzymes (Whitford, 2013). For this purpose, mammalian cells possess a diverse repertoire of different proteins, ranging between 10,000 and 20,000 (Balchin et al., 2016). Proteins acquire their distinct characteristics primarily from the precise arrangement of amino acid sequences, dictated by the nucleotide sequence of their genes (Dill et al., 1995). This sequence governs the folding of proteins into unique three-dimensional structures that directly influence their functionality. Although a notable fraction (20% to 30%) of proteins exist in an unfolded state, referred to as intrinsically disordered proteins, the majority of proteins must adopt this precise structures to fulfill their cellular function optimally (Dunker et al., 2002). The Levinthal paradox presents a perplexing contradiction: proteins fold into their native three-dimensional structures with remarkable speed, despite the astronomical number of possible conformations (Levinthal, 1968). This paradox arises because it would be practically impossible for proteins to systematically explore all possible configurations before settling into the correct structure, yet they do so rapidly and efficiently. To explain this paradox, the “folding funnel” model is used to describe the process by which proteins attain their biologically active structure (Fig. 1) (Bryngelson et al., 1995; Onuchic et al., 1997). The model suggests that as proteins fold, they navigate on a three-dimensional energy landscape, which resembles a funnel. Proteins initially exhibit a broad range of conformations with higher energy levels, but during folding, they converge towards a narrow funnel-shaped region representing stable, low-energy conformations. This funnel guides the folding process, facilitating rapid exploration and convergence towards the native state while preventing non-functional or misfolded structures (Zwanzig et al., 1992). However, intermediate folding states may act as local kinetic traps along the funnel's surface (Dill & Chan, 1997). The folding dynamics of proteins differ based on their size. Smaller proteins fold efficiently along smooth free-energy landscapes, undergoing direct transitions without significant intermediates (Jackson, 1998). On the other hand, larger proteins face obstacles in the form of rate-limiting steps, such as prolyl *cis/trans* isomerization or disulfide bond formation, which introduce substantial kinetic barriers during the folding process (Bai et al., 1995). Consequently, larger proteins commonly populate intermediates and require multiple sequential steps to achieve their final native fold. Initially, it was believed that newly synthesized proteins could spontaneously reach their folded state *in vivo* through the burial of hydrophobic surfaces within the protein's core, without the need for catalysis or metabolic assistance (Anfinsen, 1973). However, the cytosol of eukaryotic cells presents a significant challenge for proper protein folding due to its high intracellular protein concentration. The crowded physiological environment, with approximately 200 – 300 mg/mL of proteins (Zimmerman & Trach, 1991), reduces

the entropic freedom and creates excluded volume, leading to increased misfolding and aggregation (Ellis & Minton, 2006). This is because compact aggregates are favored over the generally less compact native folds in such conditions (Hong & Gierasch, 2010). Moreover, the exposure of hydrophobic regions in folding intermediates increases the likelihood of non-native intra- and intermolecular interactions, further promoting protein aggregation. Such aggregated proteins have the potential to form stable complexes, including well-known examples like the tau protein or  $\alpha$ -synuclein. In particular, these proteins can undergo a process of  $\beta$ -strand stacking, leading to the formation of stable amyloid fibers (Fink, 1998). These amyloid fibers are strongly implicated in neurodegenerative disorders such as Alzheimer's and Parkinson's disease (Irvine et al., 2008).

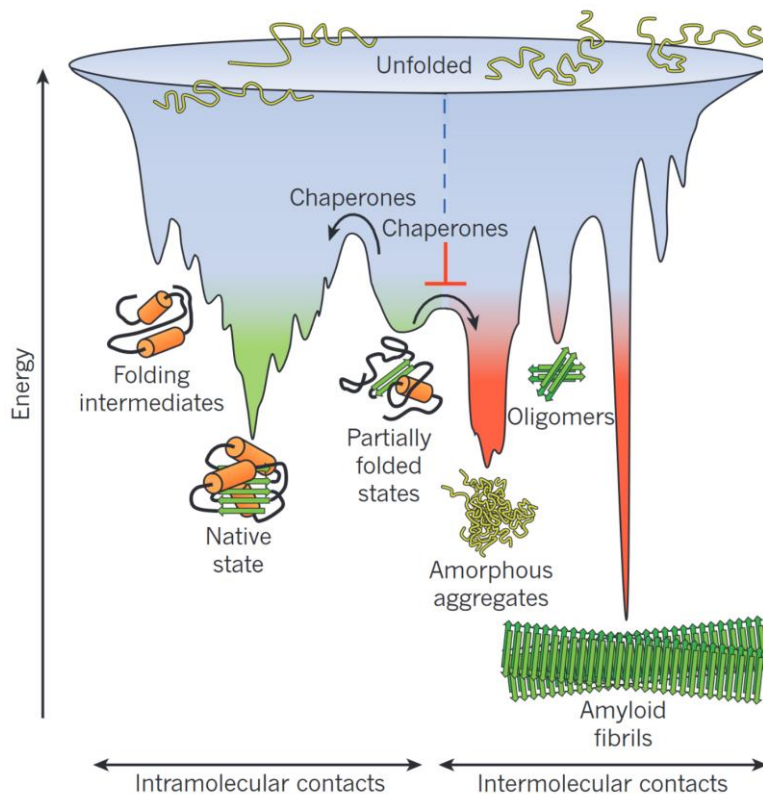


**Figure 1: The interplay between protein folding and aggregation.** Schematic illustration of the *in vivo* folding process of proteins. To reach their native folding state, proteins navigate a funnel-shaped energy landscape, forming intramolecular contacts. This landscape's ruggedness leads to trapped conformations that must overcome energy barriers. Chaperones can accelerate these steps. However, simultaneous folding of molecules can overlap with intermolecular aggregation, resulting in the formation of disordered aggregates, harmful oligomers, or organized amyloid fibrils. Fibrillar aggregation occurs through nucleation-dependent polymerization, starting from folding intermediates or destabilized native states. Molecular chaperones typically prevent this aggregation. Illustration adapted from (Hartl et al., 2011).

In addition to its role in folding-related diseases, protein aggregation profoundly affects various cellular processes. These include organelle localization, intracellular transport, metabolic changes, cytoskeletal integrity, and can ultimately result in cell cycle arrest and lethality (Richter et al., 2010; Verghese et al., 2012; Woerner et al., 2016). Besides the loss of protein activity, protein aggregates also exhibit toxicity

by disrupting membrane integrity and interfering with calcium homeostasis (Butterfield & Lashuel, 2010; Kawahara & Kuroda, 2000). It is important to note that the toxicity is predominantly attributed to smaller oligomers and intermediate aggregate species rather than the fully formed high molecular weight complexes. These smaller species are believed to have a more detrimental impact on cellular function and contribute significantly to the observed toxicity associated with protein aggregation (Verma et al., 2015). To prevent the aggregation of unfolded proteins *in vivo*, a diverse set of proteins called molecular chaperones has evolved (Buchner, 1996; Hartl, 1996). The expression of certain molecular chaperones is upregulated as part of the cellular heat shock response (HSR), which serves to counteract the effects of cellular stress and protein unfolding (Lindquist, 1986). These chaperones bind to non-native and unfolded proteins, stabilizing their structure and assisting them in reaching their native functional state (Fig. 2). While they are not directly involved in the folding process, they prevent incorrect non-native interactions within the protein (Hartl, 1996). Additionally, molecular chaperones play various roles in folding and protein homeostasis processes, including *de novo* protein folding, refolding of denatured proteins, proteolytic degradation, and complex assembly (Ellis & Minton, 2006; Walter & Buchner, 2002). These functions collectively contribute to maintaining cellular protein integrity and function.

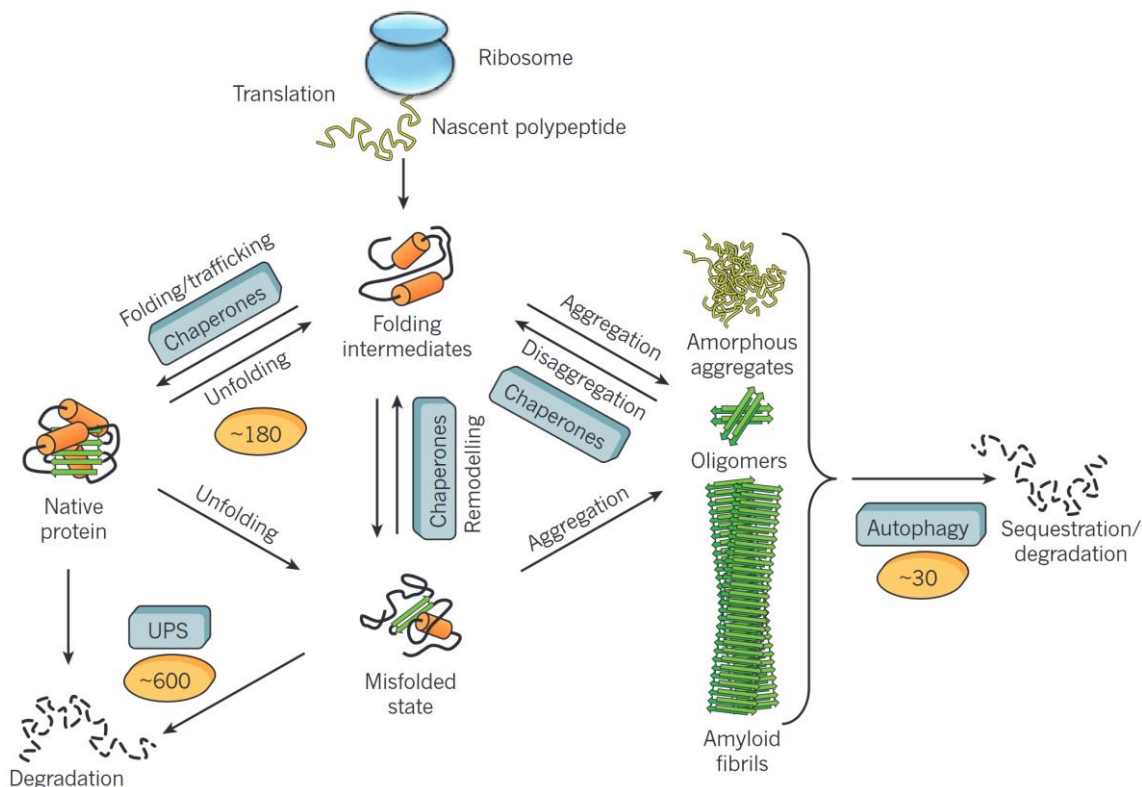


**Figure 2: Protein fates in the proteostasis network.** The proteostasis network combines chaperone pathways to facilitate the folding of newly synthesized proteins, remodel misfolded states, and aid in disaggregation. This network works in conjunction with protein degradation mechanisms such as the UPS (ubiquitin-proteasome system) and the autophagy system. Illustration adapted from (Hartl et al., 2011).

## 1.2 Heat-Shock Proteins

Molecular chaperones play a crucial role throughout the entire lifespan of a protein. They are involved in interactions starting from the nascent protein chain's initial amino acids at the exit tunnel of the ribosome, all the way to their interaction with E3 ligases, which leads to ubiquitination and subsequent degradation (Esser et al., 2005; Wegrzyn & Deuring, 2005). Heat stress induces the upregulation of most molecular chaperones, resulting in their classification as heat shock proteins (Hsps) (Finkelstein et al., 1982). These Hsps can be further divided into different families based on their molecular weight, including small Hsps, Hsp40, Hsp60, Hsp70, Hsp90 and Hsp100.

Unlike other heat shock proteins that rely on ATP for their chaperone activity, sHsps (small heat shock proteins) exhibit ATP independence (Jakob et al., 1993). To fulfill their role as chaperones, sHsps form polydisperse multimeric assemblies. By binding to folding intermediates, the oligomeric sHsp complexes prevent the aggregation of proteins (Fig. 3). This unique ability has led to their definition as "holdases" since they hold unfolded or misfolded proteins in a soluble state (Haslbeck & Buchner, 2015). Additionally, sHsps can co-aggregate with other proteins, which facilitates subsequent deaggregation in cooperation with other chaperones (Nakamoto & Vigh, 2007). This cooperative behavior is crucial for maintaining protein homeostasis within the cell. Among the sHsps,  $\alpha$ -crystallin is the most prominent member and has been extensively studied. It is predominantly found in the vertebrate eye, where it plays a crucial role in maintaining lens transparency. The presence of an evolutionarily conserved domain, known as the  $\alpha$ -crystallin domain, is a defining feature of all sHsps (Bagneris et al., 2009). Functional and structural variations among sHsps arise from the flanking N- and C-terminal regions, which can modulate the chaperone activity and substrate specificity of sHsps (Basha et al., 2012; Kriehuber et al., 2010). This allows them to adapt to specific cellular demands and stress conditions. While sHsps play a vital role in preventing protein aggregation, they require the assistance of ATP-dependent chaperones, such as Hsp70 or Hsp100, to fully resolve misfolded or aggregated proteins (Mogk et al., 2003). Furthermore, recent studies have revealed an association between sHsps and cellular membranes, suggesting their potential involvement in membrane quality control, particularly under stress conditions (Nakamoto & Vigh, 2007).

Contrary to sHsps, the remaining Hsps, termed "foldases", share a common reliance on ATP for their folding activity. Nevertheless, their structures and mechanisms exhibit significant variations. Foldases engage in repetitive cycles of substrate binding and release, utilizing the energy derived from ATP hydrolysis to facilitate substrate folding (Saibil, 2013). Hsp60s, or chaperonins, are a specific type of molecular chaperone that actively contribute to the correct folding of proteins (Fig. 3) (Fenton & Horwich, 2003). Chaperonins are distinguished by their formation of large oligomeric ring structures and can be divided into two classes: group I and group II chaperonins. Group I chaperonins, such as GroEL, are present in bacteria and endosymbiotic organelles like chloroplasts or mitochondria. GroEL,

extensively studied as a representative of group I chaperonins, consists of two identical heptameric rings stacked upon one another (Sigler et al., 1998). Unfolded proteins bind to the cavity created by these rings, and their folding occurs in an ATP-dependent and cooperative manner (Spiess et al., 2004). The activity of GroEL is regulated by a cofactor called GroES (Hsp10). Once the substrate binds to the GroEL complex, GroES attaches to the top, enveloping the substrate within the complex. This encapsulation facilitates proper folding within the central cavity. Hsp60s are associated with several critical proteins and play a vital role in modulating their functionality. Notably, they interact with essential components of the transcription/translation machinery and metabolic enzymes (Houry et al., 1999). In contrast, group II chaperonins, for example the T-complex protein Ring Complex (TRiC), are found in archaea and the cytosol of eukaryotic cells. Unlike group I chaperonins, group II chaperonins form heterooligomeric ring complexes with a wide range of subunits (Valpuesta et al., 2002). They possess an integrated lid and exhibit functional asymmetry across the complex due to the differential net charge and ATP binding affinity of their constituent paralogous subunits. Folding in group II chaperonins occurs through a nucleotide-driven conformational cycle, involving highly coordinated allosteric communication among the subunits, leading to a global expansion and contraction of the complex (Leitner et al., 2012; Reissmann et al., 2012).

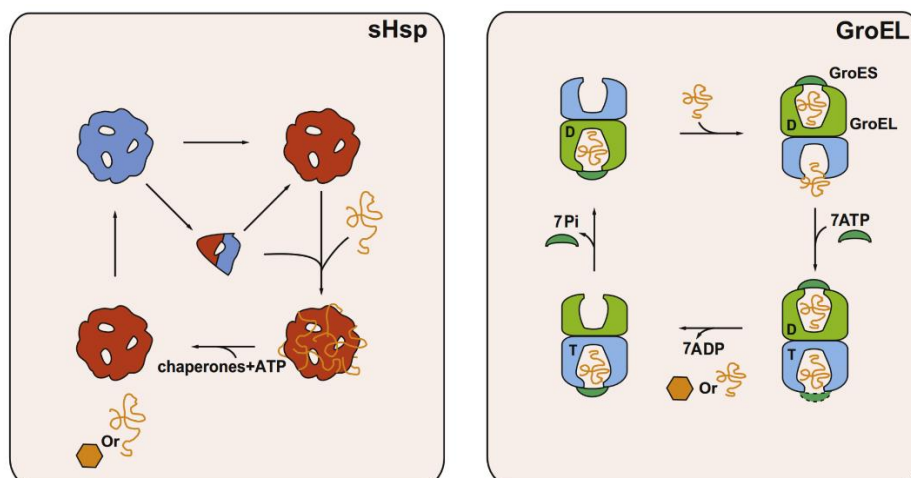


**Figure 3: Molecular Chaperone Mechanism of sHsps and Chaperonins.** Small heat shock proteins (sHsps) can form oligomeric complexes and bind unfolded or aggregated proteins, allowing them to be refolded with the assistance of ATP-dependent chaperones. Chaperonins, including GroEL, possess a central cavity where substrate proteins can undergo ATP-dependent folding. GroEL actively associates with GroES to form a functional complex. Illustration adapted from (Richter et al., 2010).

The Hsp100 protein family, also known as AAA+ proteins (ATPases Associated with diverse cellular Activities), plays a crucial role in the disaggregation and refolding of protein aggregates (Fig. 4) (Schirmer et al., 1996). Proteins from this family assemble into hexameric complexes, forming a ring structure comprising six identical protomers (Doyle & Wickner, 2009). Hsp100s, such as Hsp104 in yeast or ClpB in bacteria, work in conjunction with the Hsp70/DnaK system to solubilize and extract

aggregated proteins (Mogk et al., 2015). While Hsp70 recognizes and binds to misfolded or aggregated proteins, Hsp100 utilizes the energy derived from ATP hydrolysis to unfold the protein aggregates. ATP binding and hydrolysis induce conformational changes in the Hsp100 hexameric ring, leading to the threading of the protein substrate through a central pore within the complex (Weber-Ban et al., 1999). This threading mechanism allows for the substrate's release from the protein aggregate, facilitating its subsequent refolding. In addition to their disaggregation function, some Hsp100 members, such as ClpA in bacteria, form an active complex with a separate peptidase subunit (ClpP). The ClpAP complexes possess the ability to not only unfold but also directly degrade protein aggregates (Kim et al., 2001; Reid et al., 2001). The unfolded proteins are delivered to the ClpP peptidase, which acts as a proteolytic chamber, breaking down the proteins into smaller peptides (Wang et al., 1997).

Hsp70 is highly conserved and ubiquitously expressed in almost all living organisms (Boorstein et al., 1994). It plays a crucial role as part of the cellular folding machinery, ensuring the proper folding and activation of client proteins (Fig. 4). Hsp70 functions closely with Hsp40 proteins, to facilitate the folding process (Rosenzweig et al., 2019). The structure of Hsp70 consists of two distinct domains: the N-terminal nucleotide binding domain (NBD) and the C-terminal substrate binding domain (SBD) (Fernandez-Fernandez & Valpuesta, 2018). The SBD contains an alpha-helical lid that can close upon substrate binding (Mayer et al., 2000). Additionally, the lid contains the EEVD motif, which is essential for interacting with TPR (tetratricopeptide repeat)-containing co-chaperones (Zuiderweg et al., 2017). The two domains are connected by a short linker, allowing for allosteric changes in the protein's conformation. Studies have shown that the linker plays a crucial role in the chaperone function of Hsp70. Nucleotide binding in the NBD of Hsp70 plays a key role in the lid closing mechanism (Qi et al., 2013). When ATP is bound to the NBD, the lid remains open, enabling substrate binding and release. However, upon ATP hydrolysis, the lid closes, capturing the substrate in a high-affinity state (Kityk et al., 2018). This conformational change is essential for the proper folding of client proteins. Hsp70 operates through repetitive cycles of substrate binding and ATP hydrolysis (Kohler & Andreasson, 2020; Moran Luengo et al., 2019). By selectively binding to hydrophobic protein segments, typically consisting of five amino acids, Hsp70 interacts with unfolded or misfolded regions, aiding in their correct folding and preventing aggregation (Rudiger et al., 1997).

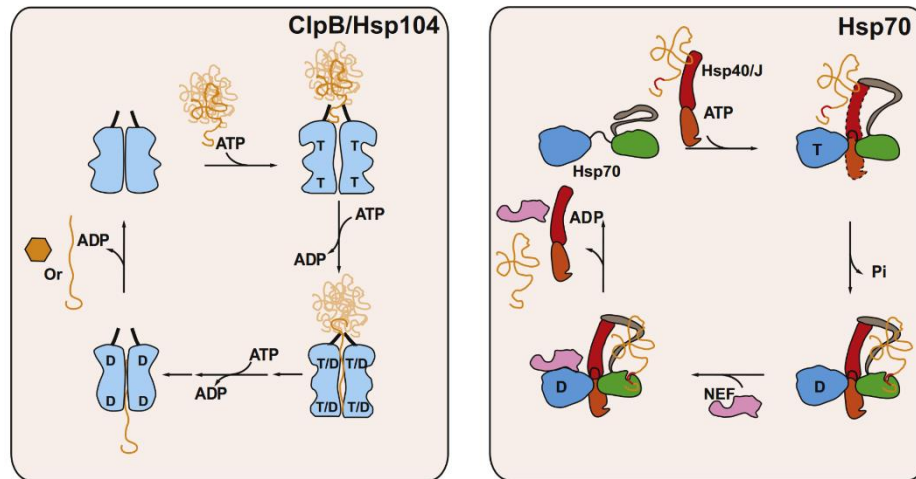


**Figure 4: Molecular Chaperone Mechanism of Hsp100 and Hsp70.** Hsp100 chaperones, such as CplB, CplA, and CplP, feature a central pore through which substrate proteins are threaded in an ATP-dependent manner, leading to refolding or proteolysis. Hsp70 chaperones coordinate N-terminal nucleotide hydrolysis with conformational changes in the substrate binding domain. The repetitive cycle of hydrolysis and nucleotide exchange, facilitated by NEFs (Nucleotide Exchange Factors), actively drives protein refolding. Illustration adapted from (Richter et al., 2010).

### 1.3 The Molecular Chaperone Hsp90

The 90 kDa large heat shock protein (Hsp90) was historically identified and named based on its upregulated cellular transcription upon thermal stress and its molecular weight, along with other heat shock proteins (Kampinga et al., 2009). However, despite their nomenclature, the transcription of Hsps is increased likewise by various other stressors, including cold, wound healing or UV light (Cao et al., 1999; Laplante et al., 1998; Matz et al., 1996). Hsp90 is an essential ATP-dependent molecular chaperone that is ubiquitously expressed and highly conserved in eukaryotes (Borkovich et al., 1989). As a chaperone, Hsp90 stabilizes other proteins, termed clients, and prevents their aggregation by ensuring a correctly folded tertiary structure (Richter et al., 2010). Hsp90 exhibits a preference for binding to clients in later folding states, misfolded proteins, or intrinsically unstable proteins (Rutledge et al., 2022; Tomoyasu et al., 1995). Even under physiological conditions, Hsp90 is engaged in a broad spectrum of essential cellular processes, which involve client activation (Kovacs et al., 2005), DNA repair (Pennisi et al., 2015), proteostasis (van Oosten-Hawle et al., 2013) and the immune response (Mayor et al., 2007). Furthermore, Hsp90 can be associated with certain types of cancer and neurodegenerative diseases. Alzheimer's disease, as well as Parkinson's, correlate with the aggregation of  $\beta$ -amyloids, hyperphosphorylated tau proteins or  $\alpha$ -synuclein, which are clients of Hsp90 (Daturpalli et al., 2013; Dickey et al., 2007; Evans et al., 2006). In 'stressed' cancer cells, upregulated Hsp90 maintains the integrity and conformation of overexpressed oncoproteins and activates important clients related to tumor growth, tissue development and survival. Consequently, in the last decade many clinical trials aimed at the modulation of Hsp90 activity as potential cancer therapy or for targeted treatment of

folding-related diseases (Sanchez et al., 2020; Trepel et al., 2010). Hsp90 functions as a chaperone in collaboration with the Hsp70 system, playing a role in late-stage protein folding unlike other chaperones. The transfer of clients from Hsp70 to Hsp90 occurs through the adapter protein Hop (known as Sti1 in yeast) (Alvira et al., 2014). To accommodate a wide range of client proteins, Hsp90 possesses several crucial features. One fundamental aspect of client interaction is that Hsp90 recognizes exposed hydrophobic residues regardless of the protein's folding state. The binding strength appears to be significantly influenced by the structural flexibility of the substrate protein (Wandinger et al., 2008). Additionally, unlike other chaperones, Hsp90 differs in terms of its binding sites, as it lacks a specific site and instead possesses a broad interaction surface spanning the entire protomer (Mayer & Le Breton, 2015). Hsp90 undergoes significant conformational changes throughout its ATP-dependent chaperone cycle, with each change being essential for cycle progression (Hellenkamp et al., 2017; Hessling et al., 2009). Given Hsp90's critical role in various cellular processes, precise regulation of client interaction and cycle progression is necessary, which is achieved through the involvement of co-chaperones and posttranslational modifications (Schopf et al., 2017).

### 1.3.1 Hsp90 Isoforms

The family of Hsp90 proteins are present in all kingdoms of life, with the exception of archaea. The high temperature protein G (HtpG) is a specific isoform of Hsp90 found only in bacteria, such as *E. coli*, which typically have only one isoform of Hsp90 (Harris et al., 2004). In contrast, higher evolved species encode several isoforms due to a gene duplication occurring 500 million years ago (Gupta, 1995). However, popular model organisms, like *Drosophila melanogaster* (Hsp83) or *Caenorhabditis elegans* (Daf-21), exhibit a single copy of the Hsp90 gene in their genomes, suggesting the loss of one of the gene duplications (Arrigo & Tanguay, 1991; Gaiser et al., 2011). Surprisingly, the yeast organism *Saccharomyces cerevisiae* is a unique fungal species encoding already two cytoplasmic homologs: the constitutive expressed Hsp82 and the heat-induced Hsc82, which possess a 97 % sequence identity. However, the two isoforms slightly differ in their ATPase rate, conformational cycle, thermal stability and Radicol sensitivity (Girstmair et al., 2019). Similar to yeast, vertebrates express two major cytoplasmic isoforms: Hsp90 $\alpha$  (HSP90AA1), the stress-induced isoform, and Hsp90 $\beta$  (HSP90AB1), which is constitutively expressed but also upregulated upon stress (Sreedhar et al., 2004). Although Hsp90 $\alpha$  and Hsp90 $\beta$  share over 80% sequence identity and have nearly identical biochemical properties, their expression and secretion patterns differ, indicating that they may have distinct roles in biological processes (Taherian et al., 2008). In addition to the two cytoplasmic Hsp90s, Grp94 (HSP90B1) is specifically expressed in the endoplasmic reticulum (Sreedhar et al., 2004), whereas the TNF receptor associated protein 1 (Trap1/TRAP1) is located in the mitochondrial matrix (Felts et al., 2000). While Grp94 has a comparable domain structure and ATPase activity to other Hsp90 proteins (Marzec et al., 2012), Trap1 lacks the charged linker region, similar to the bacterial HtpG, and exhibits an asymmetric

closing behavior (Lavery et al., 2014). Unlike the cytosolic isoforms, no co-chaperones have been identified for Grp94 and Trap1. Recent studies suggest the presence of an additional isoform termed Hsp90N (Grammatikakis et al., 2002). Although the protein exhibits high sequence homology to other Hsp90s, it lacks the conserved N-terminal ATPase domain.

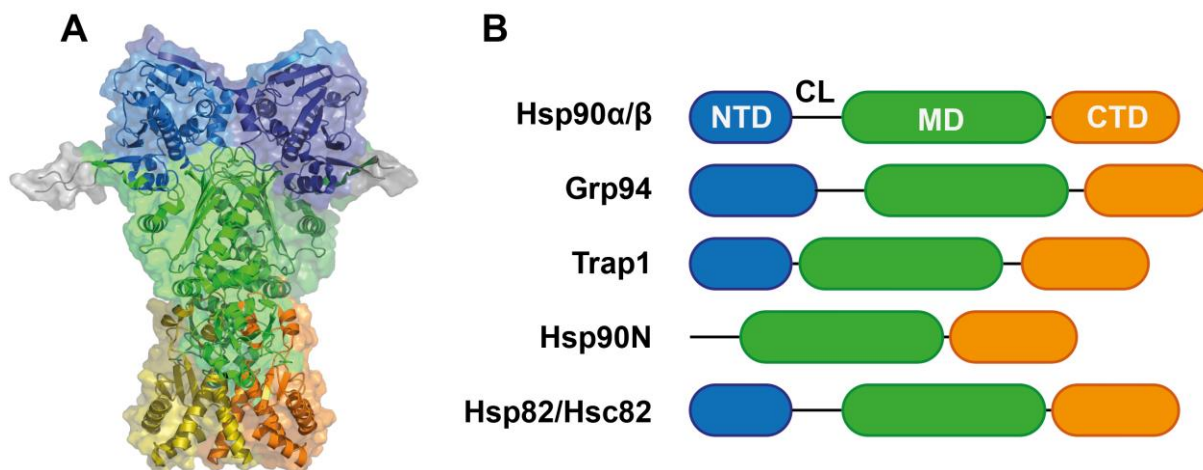


**Figure 5: Conserved domain structure of the Hsp90 family.** **A)** Surface model of closed human Hsp90 $\beta$  superimposed with secondary structure elements (PDB ID: 5FWK). Specific domains are highlighted: NTD blue, charged linker (CL) grey, MD, green, CTD yellow. **B)** Schematic illustration comparing the domain arrangements of the human Hsp90 isoforms with yeast Hsp82 and Hsc82. Domains are color-coded according to (A).

### 1.3.2 Structure of Hsp90

In vivo Hsp90 activity depends on the dimerization of two subunits into a V-shaped homodimer (Wayne & Bolon, 2007). Each protomer consists of three distinct structural domains with specific functionality. The N-terminal domain (NTD) houses the ATPase active site and connects to the middle domain (MD) through a flexible charged linker. The MD plays a crucial role in interacting with clients, co-chaperones, and participates in ATP hydrolysis. On the other hand, the C-terminal domain (CTD) facilitates the dimerization of the dimer.

The NTD contains the nucleotide-binding site, which belongs to the GHKL ATPase superfamily (Gyrase, Hsp90, histidine kinase, MutL) (Dutta & Inouye, 2000; Richter et al., 2001). The Hsp90 GHKL domain comprises multiple aligned  $\beta$ -sheets, framed by  $\alpha$ -helices, and a flexible,  $\alpha$ -helical ‘lid’ on top (Verma et al., 2016). The ATP pocket, situated at the core of the  $\alpha$ -helical side, serves as a central feature of the NTD. Several Hsp90 inhibitors, including Radicol and Geldanamycin, exhibit nanomolar affinities specifically towards this Bergerat ATP-binding fold (Schulte et al., 1998; Whitesell et al., 1994). The initial structure of the yeast Hsp90 NTD identified several essential residues, participating in ATP binding and hydrolysis (Prodromou et al., 1997). The ribose part of ATP engages in hydrogen bonds and electrostatic interactions with specific residues, including Leu-34, Asn-37, Asp-40, Asp-79, Gly-83, Asn-92, and Thr-171. Notably, Asp-79 directly interacts with the exocyclic N6 amino group. In

yeast, substituting this residue with asparagine (D79N) leads to lethality as it impairs ATP binding (Obermann et al., 1998). The co-factor  $Mg^{2+}$  adopts an approximately octahedral conformation and interacts with the  $\alpha$  and  $\beta$ -phosphate groups of ATP, as well as Asn-37 and three solvent molecules. Glu-33, Lys-98, Gly-118, Gly-121, Phe-124, and Gly-123 participate in the hydrolysis of ATP, facilitating its conversion into ADP and Pi while interacting with the phosphate groups. Replacing Glu-33 with alanine (E33A) allows ATP binding but eliminates hydrolysis. This mutation was initially reported to be lethal in yeast (Panaretou et al., 1998; Young & Hartl, 2000), but recent studies have demonstrated its viability (Reidy & Masison, 2020; Zierer et al., 2016). In addition to the ATP binding pocket, the N-terminal domain (NTD) of Hsp90 contains other crucial structural elements that play important mechanistic roles. Upon nucleotide binding, the ATP lid, which consist of a flexible helix-loop-helix motif (residue 94-125), closes over the ATP binding pocket (Prodromou et al., 2000). This closure also exposes hydrophobic residues on the  $\alpha$ 1-helix and establishes interactions of the lid with the  $\beta$  and  $\gamma$ -phosphate of ATP, promoting dimerization and hydrolysis together with the catalytic loop from the middle domain (Ali et al., 2006; Cunningham et al., 2012). Additionally, the  $\beta$ 1-strand interchanges with the strand from the opposing dimer.

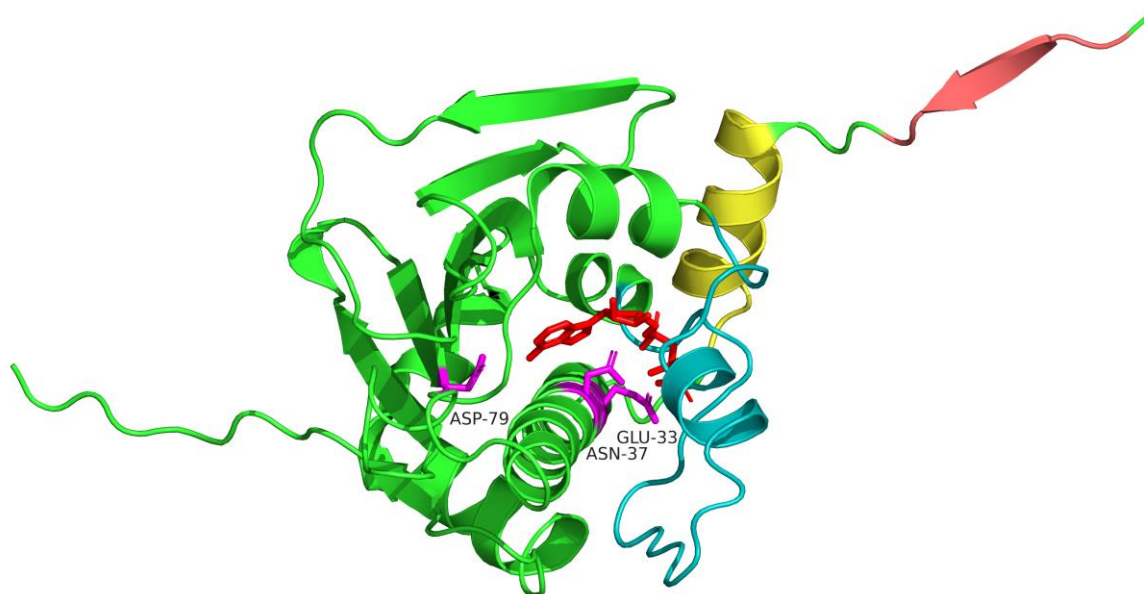


**Figure 6: The N-terminal domain of yeast Hsp90.** Crystal structure of the NTD of yeast Hsp902 (PDB ID: 2CG9) in the closed state. Bound ATP (red) is enclosed by the ATP binding pocket and the ATP lid (teal). The  $\alpha$ 1-helix (yellow), the  $\beta$ 1-strand (salmon) and important functional residues (magenta) are highlighted.

The NTD connects to the middle domain (MD) by a highly flexible, charged linker that modulates the dynamics of the NTD and influences the chaperone's function (Hainzl et al., 2009; Jahn et al., 2014). Moreover, recent studies have highlighted the regulatory function of the linker in client binding, which is attributed to its transient interactions with the  $\beta$ 8-strand located in the NTD (Lopez, Elimelech, et al., 2021). However, genetic studies have demonstrated that the region is non-essential for vital functions

of Hsp90 (Louvion et al., 1996). Therefore, it likely serves as a regulatory component (Csermely et al., 1998).

The MD is responsible for substrate recognition, co-chaperone interaction and interacts with the ATP  $\gamma$ -phosphate through a catalytic loop during hydrolysis (Cunningham et al., 2012; Meyer et al., 2003). The affiliation of Hsp90 to the GHKL ATP superfamily is demonstrated by the structure of the middle domain. The MD comprises two  $\alpha\beta$  sub-domains linked via a helical coil, which resembles the folds of GyrB and MutL (Ali et al., 2006). Furthermore, the structure revealed the presence of a flexible catalytic loop, which is involved in hydrolysis. A highly conserved Arg-380 is orientated towards the nucleotide-binding pocket and directly contacts the  $\gamma$ -phosphate of ATP (Fig. 7). However, recent studies suggest a stabilizing role of the closed state instead of a direct participation of Arg-380 (Cunningham et al., 2012). This is demonstrated by mutagenesis, as a replacement of Arg-380 by alanine reduces ATPase activity and is lethal in yeast cells (Meyer et al., 2003). Furthermore, investigation of different mutants demonstrated the significance of Try-300 in facilitating conformational changes necessary for the development of a semi-closed structure capable of efficiently processing the ligand-binding domain (LBD) of the glucocorticoid receptor. Therefore, this residue plays a crucial role in inter-domain communication within Hsp90, linking client binding to alterations in the Hsp90 cycle (Rutz et al., 2018).

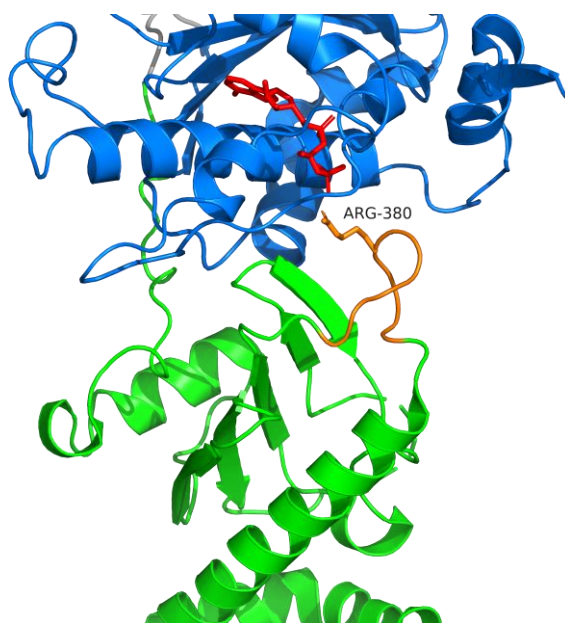


**Figure 7: The catalytic loop of the middle domain contacts the ATP  $\gamma$ -phosphate.** Structure of the yeast Hsp90 NTD (blue) and MD (green) in the closed state (PDB ID: 2CG). The essential Arg-380 of the catalytic loop (orange) interacts with the ATP  $\gamma$ -phosphate located in the ATP binding pocket during hydrolysis.

The carboxy-terminal domain (CTD) is the primary dimerization site. At its C-terminal end it has a peptide extension containing a highly conserved Met-Glu-Glu-Val-Asp (MEEVD) motif, which enables

the recruitment of co-chaperones with the tetratricopeptide repeat domain (Brinker et al., 2002; Harris et al., 2004; Scheufler et al., 2000). Dimerization plays an essential role for the *in vivo* function of Hsp90 (Minami et al., 1994). However, evidence from both *in vivo* and *in vitro* experiments suggests that subunit exchange occurs within the Hsp90 dimer, a process that can be influenced by co-chaperones (Retzlaff et al., 2010). Moreover, the cytoplasmic isoforms of Hsp90 are capable of undergoing subunit exchange, leading to the formation of  $\alpha\beta$  heterodimers (Csermely et al., 1998). The C-domain of Hsp90 comprises an extended loop that connects the middle segment to the beginning of a curved  $\alpha$ -helix (Fig. 8). Furthermore, the C-domain includes a three-stranded  $\beta$ -sheet positioned next to the curved helix, which contacts one face of a three-helix coil. The other face of this three-helix coil, which includes a helix-loop-helix motif, serves as the constitutive dimerization interface with the second protomer (Ali et al., 2006).



**Figure 8: The C-terminal domain of Hsp90 facilitates dimerization.** Structure of the yeast Hsp90 CTD in the closed state (PDB ID: 2CG9). Respective protomers of the dimer are indicated in orange/yellow.

### 1.3.3 The Conformational Cycle of Hsp90

During its ATP-dependent chaperone cycle, Hsp90 undergoes crucial conformational changes for cycle progression (Hellenkamp et al., 2017; Hessling et al., 2009). The crystal structures of the *E. coli* homolog HtpG and yeast Hsp82 (Fig. 9) provided initial insights into these structural rearrangements. However, these structures merely represent snapshots of the extensive conformational changes that Hsp90 undergoes. Electron microscopy analyses of HtpG revealed that it exists in various conformational states (Shiau et al., 2006). Apo-HtpG predominantly populates an open V-shaped conformation with distant NTDs, but dimerized CTDs. In the presence of the non-hydrolyzable ATP analog AMP-PNP, it adopts a closed elongated conformation. Similar to HtpG, Hsp82 was crystallized in complex with AMP-PNP and the co-chaperone Sba1/p23, both components stabilizing the closed compact conformation of

Hsp90. The resulting structure included both dimerization of the C-domains and association of the N-domains (Ali et al., 2006). Differences between the open and closed conformations have led to the identification of functionally important elements, including the ATP lid, the catalytic loop, and  $\beta$ 1-strand. To gain a more comprehensive understanding of the conformational rearrangements, a Förster resonance energy transfer (FRET) system was developed for yeast Hsp90, leading to the discovery of two additional intermediate states (Hessling et al., 2009). Moreover, single-molecule FRET spectroscopy demonstrated that even in the absence of nucleotides, the protein exhibits spontaneous fluctuations between the open and closed conformations, highlighting its inherent flexibility (Ratzke et al., 2014). However, upon the addition of nucleotides, Hsp90 follows a directed conformational cycle (Hessling et al., 2009). After a relatively fast binding of ATP, the N-terminal ATP lid closes over the bound nucleotide, exposing the  $\alpha$ 1-helix to the solvent (Ali et al., 2006; Cunningham et al., 2008; Weikl et al., 2000). The hydrophobic interactions between the  $\alpha$ 1-helices of the opposing dimer as well as the  $\beta$ 1-strand swap drive the formation of an intermediate closed state with dimerized NTDs (closed-1) (Schulze et al., 2016). Subsequently, the MD domain rearranges in a manner that allows contact with the NTD and the catalytic loop to interact with the ATP  $\gamma$ -phosphate (closed-2) (Meyer et al., 2003). In the ATPase active closed conformation the two protomers wrap around each other, and the NTDs undergo rotation (Lopez, Dahiya, et al., 2021; Pearl, 2016). From this twisted state, the irreversible hydrolysis of ATP into ADP and inorganic phosphate ( $P_i$ ) leads to substrate release and dissociation of the N-terminal domains leaving Hsp90 in its apo-state. The major limiting steps in this cycle are the extensive conformational rearrangements that Hsp90 undergoes in order to facilitate ATP hydrolysis (Hessling et al., 2009; Weikl et al., 2000).

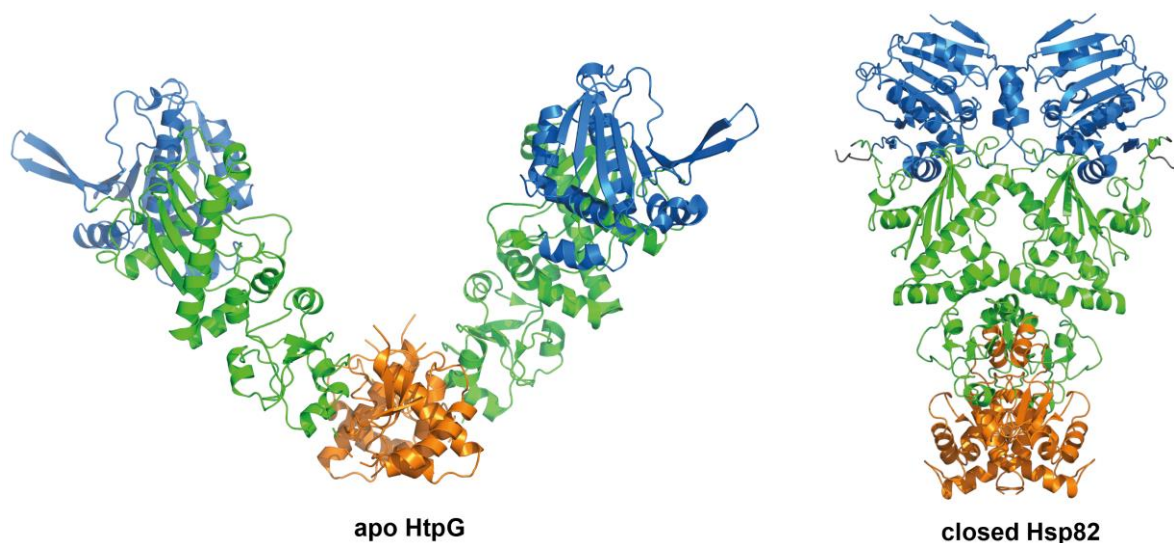


**Figure 9: Open and closed conformation of Hsp90.** Crystal structure of the *E. coli* HtpG (PDB ID: 2IOQ) in the open V-shaped conformation and the closed state of yeast Hsp82 (PDB ID: 2CG9). Respective domains are color-coded according to figure 5.

Hsp90's conformational cycle and ATPase activity can be regulated through multiple mechanisms, which are believed to enable the adaptation of Hsp90's function to the specific requirements of its clients. In addition to various co-chaperones, crucial regulatory mechanisms involve post-translational modifications, including acetylation (Scroggins et al., 2007), nitrosylation (Martinez-Ruiz et al., 2005), phosphorylation (Soroka et al., 2012) and ubiquitination (Kundrat & Regan, 2010). The ability of Hsp90 to hydrolyze ATP is crucial for the survival of cells (Obermann et al., 1998; Panaretou et al., 1998). However, the precise connection between the conformational changes of Hsp90 and the processing of its client proteins remains an important unanswered question. Additionally, there is limited information available regarding the conformational cycle of human Hsp90. While there is an overall conserved mechanism among Hsp90 species, involving N-terminal rearrangements upon ATP binding followed by transitions to the closed state (Richter et al., 2008; Vaughan et al., 2009), notable differences exist between bacteria, yeast, and human Hsp90. ATPase, H/DX, and EM data reveal variations in enzymatic activity and closed state population among these homologs (Graf et al., 2014; Richter et al., 2008; Southworth & Agard, 2008). Therefore, it remains unclear whether the observed conformational rearrangements can be extended in all aspects to the entire Hsp90 family, including human Hsp90.

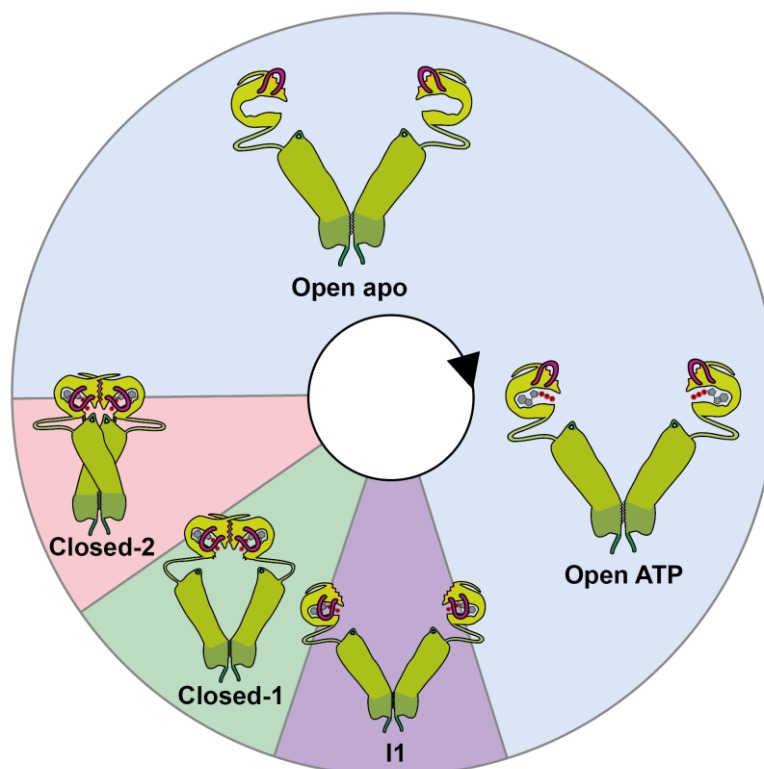


**Figure 10: The conformational cycle of Hsp90.** Schematic illustration representing the different dwell times of the conformational states (blue: open; violet: I1, green: closed-1, red: closed-2) during the Hsp90 hydrolysis cycle. The size of the sectors indicate the relative time spent at each state required for the hydrolysis of one ATP molecule per protomer. Illustration designed based on the publication of Zierer et al. (2016). After ATP binding, the ATP-lid rearranges over the nucleotide binding pocket forming the intermediate state 1 (I1). Hydrophobic interactions of the exposed  $\alpha$ 1-helix and the  $\beta$ 1-strand swap promote N-terminal dimerization (closed-1). The subsequent interaction of the catalytic loop from the middle domain (closed-2) initiate the hydrolysis of ATP.

### 1.3.4 Co-Chaperones of Hsp90

Due to Hsp90's involvement in crucial cellular processes, a strict regulation of client interaction and cycle progression by co-chaperones is required. Co-chaperones are defined as proteins that assist or modulate the functionality of Hsp90, but they are not considered clients. Therefore, they can act as scaffold proteins for client recruitment, impact the ATPase cycle or even carry out both tasks simultaneously. Co-chaperone interaction sites are present at every Hsp90 domain, which allows antagonistic, simultaneous or synergistic binding (Schopf et al., 2017). Together with posttranslational modifications (PTMs), complex and situational fine-tuning of Hsp90 function and client interaction is possible (Rohl et al., 2013).

#### *Hop/Sti1*

One of the earliest discovered and best-characterized interactors of Hsp90 is the Hsp70/Hsp90 organizing protein (Hop), known as the stress-inducible protein 1 (Sti) in yeast (Honore et al., 1992; Nicolet & Craig, 1989). Hop belongs to the group of tetratricopeptide repeat (TPR) containing co-chaperones, which interact with the MEEVD motif located at the C-terminus of Hsp90 (Perez-Riba & Itzhaki, 2019). The protein contains three separate TPR domains, which are constructed from three helix-turn-helix motifs (Blatch & Lassle, 1999). Furthermore, the TPR domains are separated by two aspartate-proline (DP) rich regions, resulting in the TPR1-DP1-TRPR2A-TPR2B-DP2 structure of Hop (Schmid et al., 2012). Previous studies revealed that TRP1 predominantly interacts with Hsp70, whereas the interaction with Hsp90 is modulated by its TPR2A domain (Rohl et al., 2015; Scheufler et al., 2000). Therefore, the protein can simultaneously bind to Hsp70 and Hsp90 in a ternary multi-chaperone complex, serving as a scaffold and facilitating client transfer (Alvira et al., 2014; Johnson et al., 1998). As a result, Hop plays a crucial role in the proper folding and maturation of client proteins targeted by Hsp90 (Kimmins & MacRae, 2000). Although Hop is conserved among various species, there are indications that it may exhibit structural and functional variations across different organisms. For instance, while Hop is an essential gene in mice (Beraldo et al., 2013), it is not deemed essential in yeast (Chang et al., 1997). In addition to its role in the Hsp70/Hsp90 machinery, Hop can interact with Hsp90 in the open conformation (Fig. 12C), inhibiting its ATPase activity, while having no influence on the ATP affinity (Richter et al., 2003).

#### *p23*

Contrary to Hop, the co-chaperone p23 (Sba1 in yeast) acts during the later stages of the chaperone cycle (Johnson & Toft, 1995). Once Hsp90 reaches the closed state during its conformational rearrangements, p23 can bind into the formed groove in between dimerized NTDs (Fig. 12A), stabilizing the closed state (Ali et al., 2006; Martinez-Yamout et al., 2006). The resulting inhibition of ATPase activity has been proven beneficial for steroid hormone receptor (SHR) maturation (Johnson & Toft, 1994; Rehn & Buchner, 2015). However, the exact mechanism by which p23 inhibits Hsp90 is still uncertain. It is

unclear whether p23 blocks the interdomain contacts required for ATP hydrolysis (Ali et al., 2006) or prevents the product release following hydrolysis (Karagoz, Duarte, et al., 2011). Besides interacting with Hsp90, p23 also exhibits a passive chaperone-like activity by suppressing the aggregation of denatured proteins (Bose et al., 1996). Furthermore, it is probable that p23 continues to interact with client proteins after they are released from Hsp90 (Freeman et al., 2000). Alternatively, p23 may promote structural movements in Hsp90. Studies suggested that p23 couples Hsp90's ATPase activity to the release of client proteins by facilitating the dissociation of receptor-Hsp90 complexes in the presence of ATP (Young & Hartl, 2000). Similar to the  $\alpha$ -crystallin subunit of sHsps, p23 consists of a single domain, which is made out of two opposing  $\beta$ -sheet layers (Weaver et al., 2000). Additionally, the protein possesses an unstructured C-terminal tail, which is postulated to stabilize the core domain of p23 in the absence of substrate (Seraphim et al., 2015). The core domain of p23 houses the active site, which interacts with the MD and catalytic loop of Hsp90, thus inhibiting ATPase activity (Biebl et al., 2021). The C-terminal tail residues are essential for the ability of p23 to bind clients and its chaperone function (Noddings et al., 2022; Weikl et al., 1999). p23, along with the co-chaperone Hop, plays a significant role in the glucocorticoid receptor (GR) maturation process. The activation of the receptor involves the transition from the "loading" complex (GR-Hsp90-Hsp70-Hop) to the "maturation" complex (GR-Hsp90-p23) (Noddings et al., 2022; Wang et al., 2022). In the "loading" complex structure, two Hsp70 proteins are present, with one delivering the GR and the other serving as a scaffold for the Hop co-chaperone (Fig. 11A). Hop interacts with all components of the complex, including GR, and primes Hsp90 for subsequent ATP hydrolysis. In the "maturation" complex, p23 stabilizes the native form of GR, which is threaded through the lumen of Hsp90 (Fig. 11B).

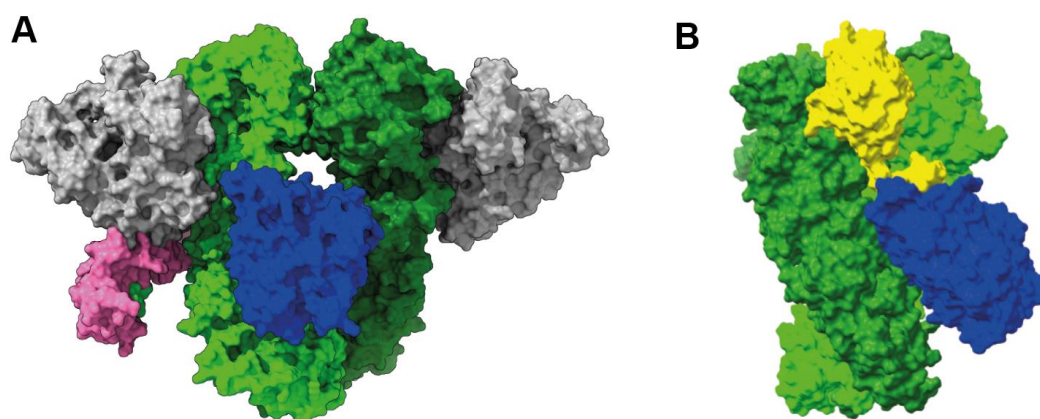


**Figure 11: Maturation of the glucocorticoid receptor.** **A)** Surface structure of the GR-Hsp90-Hsp70-Hop "loading" complex. The Hsp70 (grey) proteins interact with Hop (pink) and deliver the inactive GR (blue) to the semi-closed Hsp90 (green) (PDB ID: 7KW7 (Wang et al., 2022)). **B)** Surface structure of the GR-Hsp90-p23 "maturation" complex. Closed Hsp90 (green) threads GR (blue) through its lumen, leading to its refolding and subsequent activation. p23 (yellow) stabilizes the closed Hsp90 conformation and interacts with the GR *via* a C-terminal helix (PDB ID: 7KRJ (Noddings et al., 2022)).

*Aha1*

The co-chaperone Aha1 (activator of Hsp90 ATPase) enhances the ATPase activity of Hsp90 and is able to displace Hop/Sti1 from the Hsp90/Hop-complex (Krukenberg et al., 2011). Aha1 initiates the formation of a preliminary closed state of Hsp90 (Li et al., 2013), accelerating the conformational rearrangements required for folding and maturation of client proteins (Koulov et al., 2010). Research suggests that Aha1 enhances the interaction of the catalytic loop with the bound nucleotide and thereby elevating the ATPase activity (Horvat et al., 2014; Panaretou et al., 2002). The conserved RKxK-motif within the Aha1 family is responsible for facilitating this interaction (Meyer et al., 2004). Hsp90 is stimulated by the co-chaperone in an asymmetric way, where one Aha1 protein is sufficient to accelerate the ATPase activity of the Hsp90 dimer (Retzlaff et al., 2010). Furthermore, Aha1 can interact with Hsp90 regardless of its nucleotide state, but it exhibits higher binding affinities for the nucleotide-bound state (Li et al., 2013). Aha1 consists of two structured domains, which are connected by a linker region (Meyer et al., 2004). The N-terminal domain of the protein interacts with the middle domain of Hsp90 and induces structural rearrangements, which results in N-terminal dimerization. Subsequently, the C-terminal Aha1 domain binds in the exposed hydrophobic groove (Fig. 12B), stabilizing the conformation initiated by the N-terminal domain (Oroz et al., 2019; Retzlaff et al., 2010). Although the N- and C-terminal domains of Aha1 have been extensively characterized (Meyer et al., 2004; Retzlaff et al., 2010), the flexible nature of both Aha1 and Hsp90 has prevented the determination of a crystal structure of the full-length co-chaperone complex to date.

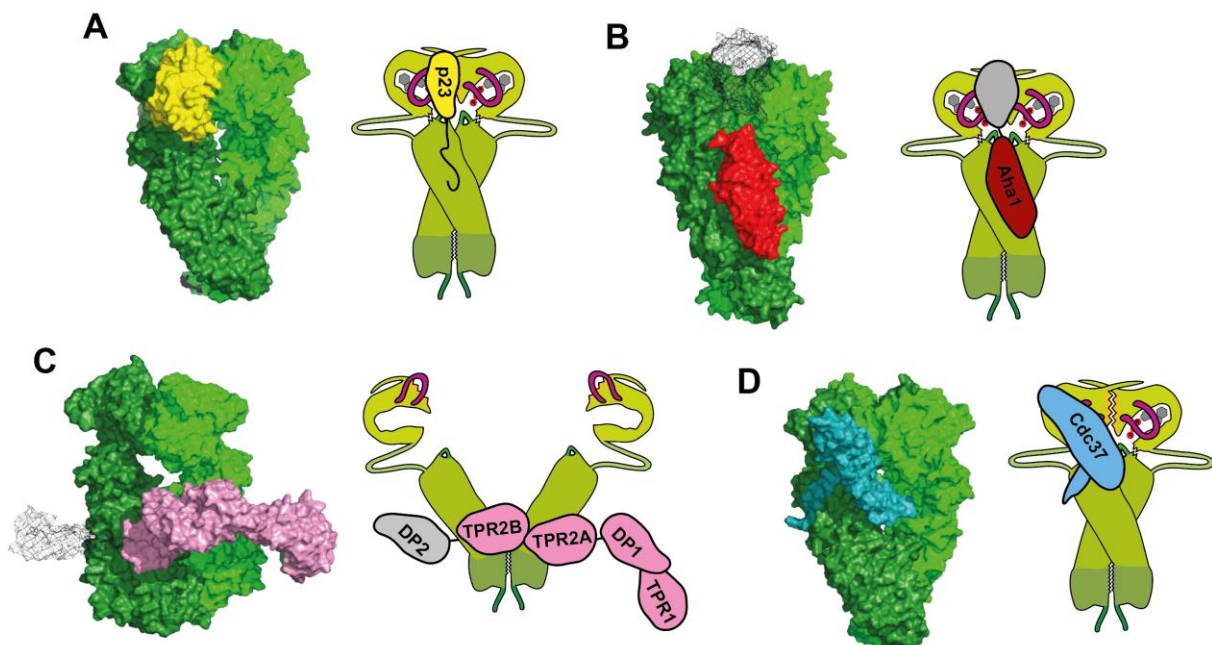


**Figure 12: The binding of co-chaperones to the Hsp90 dimer.** **A)** Surface structure and schematic illustration of p23 (Sba1 from yeast; yellow) bound to the closed yeast Hsp90 dimer (PDB ID: 2CG9 (Ali et al., 2006)). The flexible tail of p23 is missing in the structure, but illustrated in the schematic representation. Functional elements of Hsp90 are colored according to figure 5. **B)** Aha1 bound to yeast Hsp90 in the closed state (PDB ID: 1USV (Meyer et al., 2004)). Full length Hsp90 was

reconstructed from the closed yeast Hsp90 structure (2CG9). The Aha1 NTD (grey; PDB ID: 7DME (Hu et al., 2021)) was representatively modeled onto the structure. **C)** Hop bound to the partially closed human Hsp90 (PDB ID: 7KW7 (Noddings et al., 2022)). The missing DP2 domain (grey) was reconstructed from the available solution NMR structure (PDB ID: 2LLW (Schmid et al., 2012)). **D)** Cdc37 bound to human Hsp90 in the closed state (PDB ID: 5FWK). Inspired by Schopf et al. (2017).

In addition to Hop, p23, and Aha1, several other co-chaperones have been identified to modulate Hsp90 and/or serve as scaffold proteins for client recruitment (Table 1). TPR-containing co-chaperones, which interact with the MEEVD motif, often contain an additional peptidyl-prolyl cis-trans isomerase (PPIase) domain, including Fkbp51, Fkbp52, and Cyp40 (Cpr6 and Cpr7 in yeast) (Mayr et al., 2000; Noddings et al., 2023; Pirkel & Buchner, 2001). These proteins regulate the conformational cycle progression and are involved in receptor maturation and nuclear translocation (Storer et al., 2011; Sun et al., 2022). The co-chaperone Cdc37 inhibits the dimerization of Hsp90 NTDs as well as lid closing and participates specifically in the maturation of kinases (Fig. 12D) (Pearl, 2005). In yeast, besides Cdc37, only the two co-chaperones Sgt1 (Sugt in human) and Cns1 are essential for viability (Johnson & Brown, 2009), with Sgt1 being involved in kinetochore assembly (Kitagawa et al., 1999), whereas Cns1 is involved in translation elongation (Schopf et al., 2019). The co-chaperone CHIP (C-terminus of Hsc70-interacting protein) links chaperones with the protein degradation machinery by containing a U-box domain, which displays E3 ubiquitin ligase activity and promote the ubiquitination of misfolded chaperone-bound proteins (Murata et al., 2003).

**Table 1:** List of common yeast and human co-chaperones

<b>Human co-chaperone</b>	<b>Yeast co-chaperone</b>	<b>Binding site in Hsp90</b>	<b>Function</b>
Hop	Sti1	MEEVD, MD, CTD	Stabilizes the open Hsp90 conformation; client transfer from Hsp70/Hsp40 to Hsp90
Cdc37	Cdc37	NTD, MD	Prevents ATP lid closure; specific for maturation of kinases
Sugt	Sgt1	NTD	Involved in the kinetochore assembly in yeast
p23	Sba1	NTD, MD	Stabilizes the closed Hsp90 conformation; Inhibition of ATPase activity
Aha1	Aha1	NTD, MD	Stimulates ATPase activity
PP5	Ppt1	MEEVD	Dephosphorylates Hsp90; Maturation of kinases
Cyp40	Cpr6, Cpr7	MEEVD	PPIase
TTC4	Cns1	MEEVD	Affects translation
Hsp110	Sse1	-	Nucleotide exchange factor for Hsp70
Hdj2	Ydj1	-	Stimulates ATPase activity of Hsp70
-	Tah1	MEEVD	Component of the R2TP complex
Chip	-	MEEVD	E3 ubiquitin ligase
Fkbp51	-	MEEVD	PPIase
Fkbp52	-	MEEVD	PPIase
XAP2	-	MEEVD	Alters importin beta recognition
AIPL1	-	MEEVD	Associated with retinal diseases
Unc45	-	MEEVD	Involved in myosin-related processes
NudC	-	MD	Client transfer from Hsp40 to Hsp90

(Schopf et al., 2017; Zuehlke & Johnson, 2010)

## 2 Objective

Hsp90 is a highly conserved molecular chaperone that is essential for the proper folding, stability, and activation of a diverse range of client proteins. The homodimer undergoes large conformational changes between an open and closed state as part of its functional cycle, which is driven by ATP binding and hydrolysis. However, the dynamics of human Hsp90 during its structural rearrangements are not well understood, as cryo EM structures of only the closed state and the loading/maturation complex of Hsp90 are available (Verba et al., 2016; Wang et al., 2022). Hsp82, the yeast ortholog, and human Hsp90 share a high degree of sequence and structural similarity, including a conserved ATPase hydrolysis mechanism and a similar affinity for ATP (Richter et al., 2008). Additionally, both chaperones require co-chaperones for their function and are regulated by post-translational modifications (Backe et al., 2020; Prodromou et al., 1999). Despite several common mechanistic features, Hsp82 and Hsp90 drastically differ in their enzymatic activity (Vaughan et al., 2009). Consequently, human Hsp90 remains enigmatic in several aspects, including its structural plasticity, its interactions with client proteins, and the precise role of its extended co-chaperones in regulating its activity. Therefore, an important question that remains unresolved is whether the Hsp90 conformational cycle can be applied universally to the entire Hsp90 family.

One way to investigate the conformational changes during the ATPase cycle is through Förster resonance energy transfer (FRET) experiments, which monitor changes in distance and orientation between fluorophores attached to specific domains of the protein. Hsp82 has been successfully characterized using a FRET system, demonstrating the utility of this technique for studying Hsp90 conformational dynamics (Hessling et al., 2009). In this context, the development of a human Hsp90 FRET system could provide new insights into the molecular mechanisms that govern its function. By monitoring changes in distance and orientation between fluorescent probes attached to specific domains of the protein, it may be possible to unravel the conformational changes that occur during the functional cycle of Hsp90 and shed light on its interactions with co-chaperones and client proteins. Such a system could also have important implications for the design of novel therapeutic agents that modulate Hsp90, a promising target for cancer therapy.

Furthermore, the objective of this study is to investigate the common conformational mechanism of two proteins, which has already been investigated by previous studies (Vaughan et al., 2009). However, despite similar structural rearrangements, there are still significant gaps in our understanding of the mechanistic differences between these proteins. Although differences in ATPase rate and populations of conformational states have been observed (Graf et al., 2014; Southworth & Agard, 2008), there are other elusive mechanistic differences that remain unexplored. To bridge this knowledge gap an in-depth characterization of yeast and human Hsp90 using a variety of bioanalytical approaches, including size exclusion chromatography, hydrogen/deuterium exchange, and molecular dynamic simulations would

## *Objective*

---

yield valuable insights. Through these techniques, we aim to identify and elucidate the inherent differences in conformational dynamics between the two proteins. By examining these differences, we can gain insights into the evolutionary discrepancies of the two proteins and shed light on the elusive ATPase cycle of human Hsp90.

## 3 Material and Methods

### 3.1 Material

#### 3.1.1 Chemicals

Chemical	Manufacturer
1,4-Dithiothreitol (DTT)	Roth (Karlsruhe, Germany)
2-Mercaptoethanol	Roth (Karlsruhe, Germany)
3-[(3-cholamidopropyl)dimethylammonio]-1-propanesulfonate (CHAPS)	Roth (Karlsruhe, Germany)
4-(2-hydroxyethyl)-1-piperazineethanesulfonic acid (HEPES)	Serva (Heidelberg, Germany)
5-Fluorootic acid (5-FOA)	Thermo Fisher Scientific (Waltham, USA)
Acetic acid	Merck (Darmstadt, Germany)
Acetonitrile	Merck (Darmstadt, Germany)
Acrylamide (38 %, 2 % bisacrylamide)	Serva (Heidelberg, Germany)
Agar agar, powder	Serva (Heidelberg, Germany)
Agarose, ultra pure	Serva (Heidelberg, Germany)
Aluminium chloride (AlCl <sub>3</sub> ) hexahydrate	Sigma Aldrich (St. Louis, USA)
Amino acids	Sigma Aldrich (St. Louis, USA)
Ammonium sulfate (NH <sub>4</sub> ) <sub>2</sub> SO <sub>4</sub>	Merck (Darmstadt, Germany)
Ammoniumperoxodisulfat	Roth (Karlsruhe, Germany)
Bacto Peptone	Thermo Fisher Scientific (Waltham, USA)
Bacto Tryptone	Thermo Fisher Scientific (Waltham, USA)
Bacto Yeast Extract	Thermo Fisher Scientific (Waltham, USA)
Bromphenolblue S	Serva (Heidelberg, Germany)
Calcium chloride (CaCl <sub>2</sub> ) dihydrate	Merck (Darmstadt, Germany)
Coomassie Brilliant Blue R-250	Serva (Heidelberg, Germany)
Deoxyribonucleic acid, single stranded from salmon testes	Sigma Aldrich (St. Louis, USA)
Deuteriumoxide (D <sub>2</sub> O)	Roth (Karlsruhe, Germany)
Dimethylsulfoxide (DMSO)	Sigma Aldrich (St. Louis, USA)
Dipotassium hydrogen phosphate (K <sub>2</sub> HPO <sub>4</sub> ) trihydrate	Merck (Darmstadt, Germany)
Disodium hydrogen phosphate (Na <sub>2</sub> HPO <sub>4</sub> ) dihydrate	Merck (Darmstadt, Germany)
Disuccinimidyl glutarate (DSG)	Thermo Fisher Scientific (Waltham, USA)
DNA stain G	Serva (Heidelberg, Germany)
D(+)-Glucose monohydrate	Merck (Darmstadt, Germany)
Glycerol, 99 %	Sigma Aldrich (St. Louis, USA)
Hydrochloric acid (32 %)	Sigma Aldrich (St. Louis, USA)

*Material and Methods*

---

Imidazole	Sigma Aldrich (St. Louis, USA)
2-Iodacetamide	Merck (Darmstadt, Germany)
Isopropanol	Roth (Karlsruhe, Germany)
Isopropyl- $\beta$ -D-thiogalactopyranoside (IPTG)	Roth (Karlsruhe, Germany)
LB-medium, powder	Serva (Heidelberg, Germany)
Lithium acetate	Roth (Karlsruhe, Germany)
Magnesium chloride (MgCl <sub>2</sub> ) hexahydrate	Merck (Darmstadt, Germany)
Methanol	Roth (Karlsruhe, Germany)
Milk powder (blotting grade)	Roth (Karlsruhe, Germany)
Nickel sulfate (NiSO <sub>4</sub> ) hexahydrate	Merck (Darmstadt, Germany)
Nicotinamideadenine dinucleotide (NADH)	Roche Diagnostics (Mannheim, Germany)
Phenylmethylsulfonyl fluoride (PMSF)	Sigma Aldrich (St. Louis, USA)
Phosphoenolpyruvate (PEP)	Roche Diagnostics (Mannheim, Germany)
Polyethylene glycol (PEG-6000/4000)	Merck (Darmstadt, Germany)
Polyoxyethylen sorbitan monolaurate (Tween 20)	Merck (Darmstadt, Germany)
Potassium chloride (KCl)	Roth (Karlsruhe, Germany)
Potassium dihydrogen phosphate (KH <sub>2</sub> PO <sub>4</sub> )	Merck (Darmstadt, Germany)
Protease inhibitor mix HP	Merck (Darmstadt, Germany)
Radicicol	Roth (Karlsruhe, Germany)
Sodium dihydrogen phosphate (NaH <sub>2</sub> PO <sub>4</sub> ) monohydrate	Merck (Darmstadt, Germany)
Sodium 2-mercaptoethanesulfonate (MESNA)	Sigma Aldrich (St. Louis, USA)
Sodium chloride (NaCl)	Sigma Aldrich (St. Louis, USA)
Sodium dodecyl sulfate (SDS)	Merck (Darmstadt, Germany)
Sodium fluoride (NaF)	Sigma Aldrich (St. Louis, USA)
Sodium hydroxide (NaOH)	Merck (Darmstadt, Germany)
SYPRO orange protein gel stain	Thermo Fisher Scientific (Waltham, USA)
N,N,N',N'-Tetramethylethylenediamin (TEMED)	Roth (Karlsruhe, Germany)
Titriplex III (EDTA)	Merck (Darmstadt, Germany)
Tris(2-carboxyethyl)phosphine (TCEP)	Sigma Aldrich (St. Louis, USA)
Tris-(hydroxymethyl)-aminomethan (Tris)	Roth (Karlsruhe, Germany)
Uranyl acetate	Science Services (Munich, Germany)
Yeast nitrogen base	Thermo Fisher Scientific (Waltham, USA)
YPD-medium, powder	Thermo Fisher Scientific (Waltham, USA)

### 3.1.2 Instruments and Consumables

Device	Origin
<b>Absorption Spectrophotometer</b>	
Nanodrop ND-1000 UV/VIS Spectrophotometer	Thermo Fisher Scientific (Waltham, USA)
Quartz Cuvettes High Precision Cell 10 mm	Hellma Analytics (Müllheim, Germany)
Sunrise Absorbance Microplate Reader	Tecan Group (Männedorf, Switzerland)
Ultrospec 1100 Pro UV/Vis Spectrometer	GE Healthcare (Freiburg, Germany)
Cary 50 Bio UV-Vis Spectrophotometer	Varian (Palo Alto, USA)
<b>Centrifuges</b>	
Analytical Ultracentrifuge XL-A	Beckman Coulter (Krefeld, Germany)
Avanti J25	Beckman Coulter (Krefeld, Germany)
Avanti J-26 XP	Beckman Coulter (Krefeld, Germany)
Eppendorf Centrifuge 5418	Eppendorf (Hamburg, Germany)
Eppendorf Centrifuge 5810	Eppendorf (Hamburg, Germany)
Heraeus Biofuge Stratos	Thermo Fisher Scientific (Waltham, USA)
Hettich-Centrifuge Mikro 185	Hettich (Tuttlingen, Germany)
JA 10 rotor	Beckman Coulter (Krefeld, Germany)
JA 25.50 rotor	Beckman Coulter (Krefeld, Germany)
<b>Chromatography Equipment</b>	
Äkta Explorer	GE Healthcare (Freiburg, Germany)
Äkta FPLC-System	GE Healthcare (Freiburg, Germany)
CFT Hydroxyapatite, 50 mL	BioRad (Munich, Germany)
His-Trap FF, 5 mL	GE Healthcare (Freiburg, Germany)
His-Trap HP, 5 mL	GE Healthcare (Freiburg, Germany)
Loop 2 mL/5 mL/10 mL	GE Healthcare (Freiburg, Germany)
PD-10 desalting columns	GE Healthcare (Freiburg, Germany)
ResourceQ , 6 mL	GE Healthcare (Freiburg, Germany)
Superdex Prep Grade 200 (16/60, 10/300)	GE Healthcare (Freiburg, Germany)
Superdex Prep Grade 75 (16/60, 26/60)	GE Healthcare (Freiburg, Germany)
Superloop 150 mL	GE Healthcare (Freiburg, Germany)
<b>Circular dichroism Spectropolarimeter</b>	
CD cuvettes	Hellma Analytics (Müllheim, Germany)
Chirascan CD Spectropolarimeter	Applied Photophysics (Leatherhead, UK)
Jasco J715	Jasco (Groß-Umstadt, Germany)
PTC 343 Peltier temperature device	Jasco (Groß-Umstadt, Germany)
<b>Fluorescence Spectrophotometer</b>	
Fluoromax 3 Fluorescence Spectrometer	Horiba Scientific (Munich, Germany)

FP 8250/8550 Spectrofluorometer	Jasco (Groß-Umstadt, Germany)
Quartz Cuvettes (10mm, 3 Windows)	Hellma Analytics (Müllheim, Germany)
<b>Gel Electrophoresis and Western Blotting</b>	
ECL Prime Western Blotting Detection Reagent	GE Healthcare (Freiburg, Germany)
Electrophoresis Power Supply EPS 1001	GE Healthcare (Freiburg, Germany)
Electrophoresis Power Supply EPS 3501 XL	GE Healthcare (Freiburg, Germany)
Electrophoresis Power Supply EPS 601	GE Healthcare (Freiburg, Germany)
Epson ImageScanner III	GE Healthcare (Freiburg, Germany)
Fastblott B44	Biometra (Göttingen, Germany)
Gel Loading Dye, Purple (6x)	New England Biolabs (Ipswich, USA)
Hofer Dual Gel Caster	Hofer (Holliston, USA)
Hofer Mighty Small II SE 250 / 260 Mini-Vertical Units	Hofer (Holliston, USA)
ImageQuant LAS 4000	GE Healthcare (Freiburg, Germany)
ImageQuant LAS 500	GE Healthcare (Freiburg, Germany)
Native Anode Buffer for BN/CN (10x)	Serva (Heidelberg, Germany)
Native Cathode Buffer for BN/CN (10x)	Serva (Heidelberg, Germany)
PVDF Membranes	Roth (Karlsruhe, Germany)
Sample Buffer for Clear Native (2x)	Serva (Heidelberg, Germany)
SDS-Gel TG PRiME 8 % / 4 - 20 %	Serva (Heidelberg, Germany)
Typhoon 9200 Variable Mode Imager	Amersham (Uppsala, Sweden)
Vertical Native Gel 4 - 16 %	Serva (Heidelberg, Germany)
WesternBright ECL Spray	Advansta (Menlo Park, USA)
Whatman chromatography paper (3mm)	Whatman (Maidstone, England)
Wide Mini-Sub Cell GT	BioRad (Munich, Germany)
<b>PCR Equipment</b>	
BioRad T-100 Thermal Cycler	BioRad (Munich, Germany)
PCR tubes	Nerbe Plus (Winsen, Germany)
Thermocycler MJ Mini	BioRad (Munich, Germany)
Thermocycler MWG Biotech Primus 25	MWG-Biotech (Ebersberg, Germany)
<b>Scales</b>	
Sartorius BL 310	Sartorius (Göttingen, Germany)
Sartorius BP 121S	Sartorius (Göttingen, Germany)
Sartorius Universal	Sartorius (Göttingen, Germany)
<b>Additional Equipment</b>	
Amicon Ultra-15 Centrifugal Filter Units	Merck (Darmstadt, Germany)
Bandelin Sonoplus HD2200	Branson (Danbury, USA)
Cell disruption apparatus Basic Z Constant system	Constant Systems (Warwick, UK)
Chitin Resin	New England Biolabs (Ipswich, USA)
Cuvettes (plastic)	Brand GmbH (Wertheim, Germany)

Dialysis membrane Spectra/Por	Spectrum Laboratories (Breda, Netherlands)
Dialysis tubes Spectra/Por	Spectrum (Houston, USA)
Eppendorf Thermomixer Compact	Eppendorf (Hamburg, Germany)
Eppendorf-Tubes (0.5/1/2 mL)	Eppendorf (Hamburg, Germany)
Homogenisator DIAX 900	Heidolph (Kehlheim, Germany)
Incubator Binder KB 115	Binder GmbH (Tuttlingen, Germany)
Incubator Certomat BS-1	Sartorius (Göttingen, Germany)
Incubator Mytron WB	Mytron (Heiligenstadt, Germany)
Magnetic stirrer MR 2000	Heidolph (Kehlheim, Germany)
Magnetic stirrer MR 3100	Heidolph (Kehlheim, Germany)
Petri dishes PS, 94 mm	Greiner Bio One (Kremsmünster, Austria)
pH-Meter 538 MultiCal	WTW (Weilheim, Germany)
pH-meter pH526	WTW (Weilheim, Germany)
Shimadzu HPLC System	GE Healthcare (Freiburg, Germany)
Varioklav	HP (Oberschleißheim, Germany)
Vortexer REAX top	Heidolph (Kehlheim, Germany)

### 3.1.3 Software and Web-Based Tools

<b>Program</b>	<b>Developer</b>
Adobe Illustrator 2021	Adobe Inc. (San José, USA)
Adobe Photoshop 2020	Adobe Inc. (San José, USA)
ChimeraX 1.4	UCSF-RBVI (San Francisco, USA)
Clustal Omega	EMBL-EBI (Cambridge, UK)
ConSurf	ConSurf ( <a href="http://consurf.tau.ac.il/consurf_index.php">consurf.tau.ac.il/consurf_index.php</a> )
EndNote 20	Adept Scientific (Herts, GB)
ImageJ	Wayne Rasband ( <a href="http://imagej.net/ij/docs/index.html">imagej.net/ij/docs/index.html</a> )
Microsoft Office 2016	Microsoft Corporation (Redmond, USA)
NEB Tm Calculator	NEB ( <a href="http://tmcalculator.neb.com">tmcalculator.neb.com</a> )
NEBaseChanger	NEB ( <a href="http://nebasechanger.neb.com">nebasechanger.neb.com</a> )
NEBuilder	NEB ( <a href="http://nebuilder.neb.com">nebuilder.neb.com</a> )
OriginPro 2021b	Originlab (Northampton, USA)
ProtParam tool	Expasy ( <a href="http://web.expasy.org/protparam">web.expasy.org/protparam</a> )
Prox1	Prox1 Server ( <a href="http://prox1-ms.org/">prox1-ms.org/</a> )
Pymol 2	Schrödinger (Mannheim, Germany)
Sedfit	Peter Schuck ( <a href="http://sedfitsedphat.github.io">sedfitsedphat.github.io</a> )
Sednterp 3	John Philo ( <a href="http://jphilo.mailway.com/index.htm">jphilo.mailway.com/index.htm</a> )
Sedview	Hayes D.B. & Stafford W.F. (Hayes and Stafford, 2010)
SerialCloner 2.6.1	SerialBasics ( <a href="http://serialbasics.free.fr/Serial_Cloner.html">serialbasics.free.fr/Serial_Cloner.html</a> )

### 3.1.4 Kits and Markers

<b>Name</b>	<b>Origin</b>
Color Prestained Protein Standard, Broad Range	New England Biolabs (Ipswich, USA)
Dual Color Protein Standard III	Serva (Heidelberg, Germany)
FastLoad 1 kb DNA Ladder	Serva (Heidelberg, Germany)
NativeMark™ Unstained Protein Standard	Thermo Fisher Scientific (Waltham, USA)
Protein Test Mixture 6	Serva (Heidelberg, Germany)
Q5® Site-Directed Mutagenesis Kit	New England Biolabs (Ipswich, USA)
Wizard® Plus SV Minipres DNA Purification System	Promega (Madison, USA)
Wizard® SV Gel and PCR Clean-Up System	Promega (Madison, USA)

### 3.1.5 Nucleotides

<b>Name</b>	<b>Manufacturer</b>
Adenosin-5'-diphosphate (ADP) disodium salt	Roche Diagnostic International AG (Rotkreuz, Switzerland)
Adenosin-5'-triphosphate (ATP) disodium salt	Roche Diagnostic International AG (Rotkreuz, Switzerland)
Adenosin-5'-(β,γ-imido)triphosphate (AMP-PNP) tetralithium salt	Roche Diagnostic International AG (Rotkreuz, Switzerland)
Adenosin-5'-o-(3-thio-triphosphat) (ATPγS) tetralithium salt	Roche Diagnostic International AG (Rotkreuz, Switzerland)
Adenosin-5'-o-(3-thio-triphosphat) (ATPγS) lithium salt, solution	Roche Diagnostic International AG (Rotkreuz, Switzerland)
Desoxynucleotidetriphosphates (dNTPs)	New England Biolabs (Ipswich, USA)

### 3.1.6 Fluorophores

<b>Name</b>	$\lambda_{\text{abs}}$ (nm)	$\lambda_{\text{fl}}$ (nm)	$\epsilon$ (M <sup>-1</sup> cm <sup>-1</sup> )	<b>Origin</b>
ATTO 488-maleimid	500	520	9.000	Atto-Tec(Siegen, Germany)
ATTO 523-maleimid	532	552	115.000	Atto-Tec(Siegen, Germany)
ATTO 550-maleimid	554	576	120.000	Atto-Tec(Siegen, Germany)
ATTO 643-maleimid	643	665	150.000	Atto-Tec(Siegen, Germany)

### 3.1.7 Enzymes

<b>Name</b>	<b>Origin</b>
Apyrase (grade 3)	Sigma Aldrich (St. Louis, USA)
BamHI-HF	New England Biolabs (Ipswich, USA)
Bovine serum albumin (BSA)	Sigma Aldrich (St. Louis, USA)
$\alpha$ -Chymotrypsin (from bovine pancreas)	Sigma Aldrich (St. Louis, USA)
DNase I	Invitrogen Life Sciences (Paisley, UK)
DpnI	New England Biolabs (Ipswich, USA)
KLD enzyme mix	New England Biolabs (Ipswich, USA)
L-Lactate dehydrogenase (LDH)	Roche (Mannheim, Germany)
NdeI	New England Biolabs (Ipswich, USA)
Phusion polymerase	New England Biolabs (Ipswich, USA)
Pyruvate kinase (PK)	Roche (Mannheim, Germany)
Q5 polymerase	New England Biolabs (Ipswich, USA)
T4 DNA ligase	New England Biolabs (Ipswich, USA)
T4 polymerase	New England Biolabs (Ipswich, USA)
Trypsin (Sequencing grade)	Promega (Madison, USA)
XhoI	New England Biolabs (Ipswich, USA)

### 3.1.8 Media and Antibiotics

<b>Name</b>	<b>Compounds</b>
LB <sub>0</sub>	5 g/L NaCl 10 g/L Bacto Yeast extract 16 g/L Bacto Tryptone For plates: 15 g/L Agar agar
2x YT	5 g/L NaCl 10 g/L Bacto Yeast extract 17 g/L Bacto Tryptone
YPD	20 g/L Bacto Peptone 10 g/L Bacto Yeast extract 20 g/L D(+)-Glucose For plates: 24 g/L Agar agar
Yeast selection media	6.7 g/L Yeast nitrogen base 0.1 % (v/v) 1 M NaOH 2 g/L selective aa-mix 20 g/L D(+)-Glucose For plates 20 g/L Agar agar

Selective aa-mix	0.5 g adenine, 2 g arginine, 2 g aspartic acid, 2 g histidine, 10 g leucine, 2 g lysine, 2 methionine, 2 g phenylalanine, 2 g threonine, 2 g tyrosine, 2 g tryptophane, 2 g uracil
------------------	--

Depending on the used strain and plasmid, 35 µg/mL Kanamycin, 25 µg/mL Chloramphenicol or 100 µg/mL Ampicillin were added to the medium. Auxotrophic selection was achieved by omitting specific amino acids from the selective amino acid mix.

### 3.1.9 *E. coli* and *S. cerevisiae* Strains

*E. coli* XL-1 blue and *E. coli* Mach1 strains were used for plasmid amplification and molecular cloning. Competent *E. coli* BL21 and Rosetta cells were used for protein expression. The *S. cerevisiae* hsp82Δ hsc82Δ strain, used for plasmid shuffling experiments, was based on the ΔPCLDα strain, which was obtained as a gift from Susan Lindquist (Nathan & Lindquist, 1995).

Organism	Strain	Genotype	Origin
<i>E. coli</i>	BL21 (DE3)	F <sup>-</sup> <i>dcm ompT hsdS</i> (r <sub>B</sub> <sup>-</sup> m <sub>B</sub> <sup>-</sup> ) <i>gal λ</i> (DE3)	Stratagene (La Jolla, USA)
<i>E. coli</i>	Mach1	F <sup>-</sup> φ80 <i>lacZ</i> ΔM15 Δ <i>lacX</i> 74 <i>hsdS</i> (r <sub>K</sub> <sup>-</sup> m <sub>K</sub> <sup>-</sup> ) <i>tonA</i> Δ <i>recA</i> 1398 <i>endA</i> 1	Invitrogen (Karlsruhe, Germany)
<i>E. coli</i>	Rosetta (DE3)	F <sup>-</sup> <i>dcm ompT hsdS</i> (r <sub>B</sub> <sup>-</sup> m <sub>B</sub> <sup>-</sup> ) <i>gal λ</i> (DE3) pRARE (Cam <sup>R</sup> )	Dr. Florent Delhommel (TUM)
<i>E. coli</i>	XL-1 blue	<i>recA1 endA1 gyrA96 thi-1 hsdR17 supE44</i> <i>relA1 lac</i> [F <sup>'</sup> <i>proAB lacI</i> <sup>q</sup> ΔM15 Tn10 (Tet <sup>R</sup> )]	Stratagene (La Jolla, USA)
<i>S. cerevisiae</i>	BY4741	MATα <i>his3</i> Δ1 <i>leu2</i> Δ0 <i>met15</i> Δ0 <i>ura3</i> Δ0	Euroscarf (Frankfurt, Germany)
<i>S. cerevisiae</i>	hsp82Δ hsc82Δ [HSP82]	MATα <i>his3</i> Δ1 <i>leu2</i> Δ0 <i>ura3</i> Δ0 <i>lys2</i> Δ0 <i>arg4</i> Δ::kanMX <i>hsc82</i> Δ::kanMX <i>hsp82</i> Δ::natMX [pKAT-HSC82-URA3]	Dr. Florian Schopf (TUM)

### 3.1.10 Plasmids

Insert	Vector	Source
-	pET28b	Novagen
-	pET28b-SUMO	Dr. Oliver Lorenz (TUM)
Hsp82 WT	pET28b	Dr. Alina Röhl (TUM)
Hsp82 T101I	pET28b	Dr. Bettina Zierer (TUM)

*Material and Methods*

Hsp82 A107N	pET28b	Dr. Bettina Zierer (TUM)
Hsp82 L15R	pET28b	Dr. Bettina Zierer (TUM)
Hsp82 T22I	pET28b	Dr. Bettina Zierer (TUM)
Hsp82 T13A	pET28b	This work
Hsp82 S109Q	pET28b	This work
Hsp82 T13A S109Q	pET28b	This work
-	P432 GPD	ATCC (Manassas, USA)
Hsp82 WT	P432 GPD	Dr. Bettina Zierer (TUM)
Hsp82 T101I	P432 GPD	Dr. Bettina Zierer (TUM)
Hsp82 A107N	P432 GPD	Dr. Bettina Zierer (TUM)
Hsp82 T22I	P432 GPD	Dr. Bettina Zierer (TUM)
Hsp82 T13A	P432 GPD	This work
Hsp82 S109Q	P432 GPD	This work
Hsp82 T13A S109Q	P432 GPD	This work
Aha1 (yeast)	pET28b	Dr. Klaus Richter (TUM)
Sti1	pET28b-SUMO	Dr. Andreas Schmid (TUM)
Sba1	pET28b	Dr. Martin Hessling (TUM)
Hsp90 $\beta$ WT	pET28b-SUMO	Dr. Klaus Richter (TUM)
Hsp90 $\beta$ L24R	pET28b-SUMO	This work
Hsp90 $\beta$ T31I	pET28b-SUMO	This work
Hsp90 $\beta$ T110I	pET28b-SUMO	This work
Hsp90 $\beta$ A116N	pET28b-SUMO	This work
Hsp90 $\beta$ A22T	pET28b-SUMO	This work
Hsp90 $\beta$ Q118S	pET28b-SUMO	This work
Hsp90 $\beta$ A22T Q118S	pET28b-SUMO	This work
Hsp90 $\beta$ 1-265LPXTG	pET28b-MBP-TEV	Dr. Franziska Toppel
Hsp90 $\beta$ 1-265LPXTG	pET28b-MBP-TEV-1MA	This work
Hsp90 $\beta$ G265-724	pET28b-MBP-TEV	Dr. Franziska Toppel
Hsp90 $\beta$ 265LPXTG	pET28b-MBP-TEV	Dr. Franziska Toppel
Hsp90 $\beta$ 1-90LPDTG	pET28b-MBP-TEV-1MA	This work
Hsp90 $\beta$ 1-90LPDTG	pET28b-SUMO	This work
Hsp90 $\beta$ 1-90LADTG	pET28b-SUMO	This work
Hsp90 $\beta$ G90-724	pETM11	This work
Hsp90 $\beta$ G90-724	pET28b-SUMO	This work
Hsp90 $\beta$ 90LPDTG	pET28b-SUMO	This work
Hsp90 $\beta$ 1-215LPITG	pET28b-SUMO	This work
Hsp90 $\beta$ G215-724	pET28b-SUMO	This work
Hsp90 $\beta$ G215-724	pETM11	This work
Hsp90 $\beta$ 215LPITG	cc	This work

-	pTXB1	Addgene
Hsp90 $\beta$ 1-68-Intein-CBD	pTXB1	This work
Hsp90 $\beta$ 1-68-Intein-CBD	pET28b-SUMO	This work
Hsp90 $\beta$ 1-68-Intein-CBD 67N	pET28b-SUMO	This work
Hsp90 $\beta$ G68C-724	pETM11	This work
Hsp90 $\beta$ S67N G68C	pET28b-SUMO	This work
Hsp90 $\beta$ 1-365-Intein-CBD	pET28b-SUMO	This work
Hsp90 $\beta$ 1-365-Intein-CBD 364N	pET28b-SUMO	This work
Hsp90 $\beta$ 365-724	pET28b-SUMO	This work
Hsp90 $\beta$ 365-724	pETM11	This work
Hsp90 $\beta$ G68C S364N	pET28b-SUMO	This work
Hsp90 $\beta$ 1-235-Intein-CBD	pET28b-SUMO	This work
Hsp90 $\beta$ G235C-724	pETM11	This work
Hop	pET28b	Dr. Andreas Schmid (TUM)
Aha1	pET28b	Dr. Marco Retzlaff (TUM)
p23	pET28b	Dr. Martin Hessling (TUM)
Sortase 5M	pET28b	Dr. Maximilian Fottner (TUM)
Sortase 2A.9	pET28b	Dr. Maximilian Fottner (TUM)
TEV protease	pET28b	David S. Waugh (NCI)
SUMO protease	pET28b	Dr. Alexander Bepperling (TUM)

### 3.1.11 DNA Oligonucleotides

All DNA Oligonucleotides were designed with NEB Builder or NEB Base Changer. Synthesis was carried out by Eurofins Genomics (Ebersberg, Germany). DNA Oligonucleotides were dissolved in ddH<sub>2</sub>O to a final concentration of 100 pmol/ $\mu$ L prior to usage.

<b>Primer to introduce cysteins for labeling</b>		
h90b_S63C_fwd	GACAGACCCTtgCAGTTGGACAG	pET28b/pETM11
h90b_S63C_rev	AGGCTCTCATAGCGAATC	pET28b/pETM11
h90b_S67C_fwd	GAAGTTGGACTgcGGTAAAGAGCTGAAAATTG	pET28b/pETM11
h90b_S67C_rev	GAAGGGTCTGTCAGGCTC	pET28b/pETM11
h90b_G68C_fwd	GTTGGACAGTtGTAAGAGCTG	pET28b/pETM11
h90b_G68C_rev	TTCGAAGGGTCTGTCAGG	pET28b/pETM11
h90b_S63C_rev	GACCGATCCGtGCAAAGCTGGA	pTXB1
h90b_S67C_fwd	AGGCTTTCATAACGGATTTTATC	pTXB1
<b>Primer for ATPase mutants</b>		
h90b_T31I_fwd	ATCATCAATAtCTTCTATTCCAACAAGG	pET28b/pETM11
h90b_T31I_rev	GAGGGACATGAGTTGGGC	pET28b/pETM11
h90b_L24R_fwd	ATTGCCCAACgCATGTCCCTC	pET28b/pETM11

*Material and Methods*

h90b_L24R_rev	TTCTGCCTGAAAGGCAAAAG	pET28b/pETM11
h90b_T110I_fwd	AAGTCTGGTAtTAAAGCATTTCATG	pET28b/pETM11
h90b_T110I_rev	GGCAATGGTTCCCAAATTATTTATG	pET28b/pETM11
h90b_A116N_fwd	ATTCATGGAGaaTCTTCAGGCTG	pET28b/pETM11
h90b_A116N_rev	GCTTTAGTACCAGACTTG	pET28b/pETM11
h90b_A22T_fwd	GGCAGAAATtCCCAACTCATG	pET28b/pETM11
h90b_A22T_rev	TGAAAGGCAAAAAGTCTCC	pET28b/pETM11
h90b_Q118S_fwd	GGAGGCTCTtagcGCTGGTGCAG	pET28b/pETM11
h90b_Q118S_rev	ATGAATGCTTTAGTACCAG	pET28b/pETM11
h90b_T22A_fwd	GGCAGAAATtGCCAACTCATG	pET28b/pETM11
h90b_T22A_rev	TGAAAGGCAAAAAGTCTCC	pET28b/pETM11
hsp82_T13A_fwd	AGCTGAAATtGCTCAGTTGATG	pET28b
hsp82_T13A_rev	TGAAATTCAAAAGTTTCACTAG	pET28b
hsp82_S109Q_fwd	GGAAGCTCTAcagGCTGGTGCCGATG	pET28b
hsp82_S109Q_rev	ATGAAGGCTTTGGTACCAG	pET28b
hsp82_A13T_fwd	AGCTGAAATtCTCAGTTGATG	pET28b
hsp82_A13T_rev	TGAAATTCAAAAGTTTCACTAG	pET28b
<b>Primer for Sortase 2A and 5M ligation of Hsp90<math>\beta</math> at residue 90</b>		
MG1MA_fwd	CTCCTTCTTAAAGTTAAACAAAATTATTC	pET28b-MBP
MG1MA_rev	ATATACCATGGCCAGCCATCACC	pET28b-MBP
1-90_LPXTG_fwd	accggcTAGGCGGCCGCACTCGAG	pET28b-Sumo
1-90_LPXTG_rev	aatcggCAAAGTCAGGGTACGTTCTGAGG	pET28b-Sumo
1-90_LPXTG_fwd	CTGCCAAGACCGGCGCG	pET28b-MBP
1-90_LPXTG_rev	AGTCAGGGTACGTTCTGAGGG	pET28b-MBP
1-90_LPXTG_fwd	aggctaaTTGGCATGACCAAAGCTG	pET28b-Sumo
1-90_LPXTG_rev	gtgtccgcCAAAGTCAGGGTACGTTT	pET28b-Sumo
G90-724_fwd	GGCATTGGCATGACCAAA	pET28b-Sumo
G90-724_rev	TCCACCAATCTGTTCTCTG	pET28b-Sumo
G90-724_fwd	GGCATTGGCATGACCAAA	pETM11
G90-724_rev	CTGAAAATAAAGATTCTCAGTAGTG	pETM11
90b_LPXTG90_fwd	CCTGACTTTGccgGACACAGGCATTG	pET28b-Sumo
90b_LPXTG90_rev	GTACGTTCTGAGGGTTG	pET28b-Sumo
<b>Primer for Sortase 5M ligation of Hsp90<math>\beta</math> at residue 215</b>		
1-215_LPITG_fwd	accggttagTTGGAGAAGGAACGAGAG	pET28b-Sumo
1-215_LPITG_rev	gatgggaagGCCTATGAACTGAGAATG	pET28b-Sumo
90b_LPITG*215_fwd	taccggcTAGGCGGCCGCACTCGAG	pET28b-Sumo
90b_LPITG*215_rev	atcggcagGCCTATGAACTGAGAATGCTTCTTCACTAC	pET28b-Sumo
G215-724_fwd	GGCTATTTGGAGAAGGAACGAG	pET28b-Sumo
G215-724_rev	TCCACCAATCTGTTCTCTG	pET28b-Sumo
G215-724_fwd	TATTTGGAGAAGGAACGAG	pETM11
G215-724_rev	GCCCTGAAAATAAAGATTC	pETM11
90b_LPITG215_fwd	taccggcTATTTGGAGAAGGAACGAG	pET28b-Sumo
90b_LPITG215_rev	atcggcagGCCTATGAACTGAGAATG	pET28b-Sumo

<b>Primer for EPL of Hsp90<math>\beta</math> at residue 68</b>		
1-68-Intein_fwd	tcacagagaacagattggtggatccatgcctgaggaagtgcac	pET28b-Sumo /slic
1-68-Intein_rev	ccgtgatgcaactgtccaacttcgaagg	pET28b-Sumo /slic
1-68-Intein_fwd	gttggacagttgcatcacgggagatgcac	pTXB1 /slic
1-68-Intein_rev	agtgggtggtggtggtgctcgagtcattgaagctgccacaagg	pTXB1 /slic
Sumo-1-68-Intein_fwd	TGTATTACCGGTGATGCC	pET28b-Sumo-Int
Sumo-1-68-Intein_rev	GCTATCCAGTTTGCTCGG	pET28b-Sumo-Int
S67N_fwd	AAACTGGATAaCTGTATTACCGGTGATG	pET28b-Sumo-Int
S67N_rev	GCTCGGATCGGTCAGGCT	pET28b-Sumo-Int
G68C-724_fwd	TGTAAGAGCTGAAAATTGA	pETM11
G68C-724_rev	CTGAAAATAAAGATTCTCAGTAG	pETM11
90b_S67N-G68C_fwd	AAGTTGGACAactGTAAAGAGCTGAAAATTGACATCATC	pET28b-Sumo
90b_S67N-G68C_rev	CGAAGGGTCTGTCAGGCT	pET28b-Sumo
<b>Primer for EPL of Hsp90<math>\beta</math> at residue 365</b>		
1-365-Intein_fwd	cttaagaaggagatatacatatgATGCCTGAGGAAGTGCAC	pET28b-Sumo /slic
1-365-Intein_rev	actagtgcactcccgtgatgcaGCTGTCCATGATGAACAC	pET28b-Sumo /slic
C365-724_fwd	TGTGATGAGTTGATACCAG	pET28b-Sumo
C365-724_rev	TCCACCAATCTGTTCTCTG	pET28b-Sumo
C365-724_fwd	TGTGATGAGTTGATACCAG	pETM11
C365-724_rev	CTGAAAATAAAGATTCTCAGTAG	pETM11
S364N_fwd	ATTATGGATAaCTGTATTACCGGTGATG	pET28b-Sumo-Int
S364N_rev	AAACACGCGACGCACGTA	pET28b-Sumo-Int
90b_S364N_fwd	ATCATGGACAaCTGTGATGAGTTG	pET28b-Sumo
90b_S364N_rev	GAACACACGGCGGACATA	pET28b-Sumo
<b>Primer for EPL of Hsp90<math>\beta</math> at residue 235</b>		
1-235-Intein_fwd	TGTATTACCGGTGATGCC	pET28b-Sumo-Int
1-235-Intein_rev	TTTTTCTTCTTCGGCTTCATC	pET28b-Sumo-Int
G235C-724_fwd	GAGAAAGAAGAGGAAGATAAAG	pETM11
G235C-724_rev	ACACTGAAAATAAAGATTCTCAG	pETM11
pTXB1- $\Delta$ CBD-His_fwd	CACCACCACTAACTCGAGCACCACCAC	pET28b-Sumo-Int
pTXB1- $\Delta$ CBD-His_rev	ATGATGATGCAGACCGCTATTTCAGACC	pET28b-Sumo-Int

## 3.2 Methods

### 3.2.1 Biomolecular Techniques

#### 3.2.1.1 Cultivation of *E. coli*

All used *E. coli* strains were cultivated in liquid LB<sub>0</sub> media or kept on LB<sub>0</sub> agar plates. For short-term storage, *E. coli* cultures were kept on LB<sub>0</sub> plates at 4 °C. For prolonged storage, *E. coli* cells were stored in liquid media containing 15 % (v/v) glycerol at -70 °C. For plasmid amplification, 2 mL of liquid culture were directly inoculated with single *E. coli* colonies, obtained after transformation, and incubated at 37 °C over night. For larger volumes, 100 mL liquid media were inoculated with bacteria and incubated over night at 37 °C under constant shaking. The next day, the cell suspension was transferred to a 5 L flask containing 2 L of media and further incubated at 37 °C. To monitor bacterial growth in solution, the optical density of the suspension was measured via UV/Vis spectrometry at 600 nm (OD<sub>600</sub>). To prevent contamination or for positive/negative selection, all media contained antibiotics according to the respective resistance on the plasmid.

#### 3.2.1.2 Cultivation of *S. cerevisiae*

All used *S. cerevisiae* strains were cultivated in liquid YPD media or kept on YPD agar plates. For short-term storage, *S. cerevisiae* cultures were kept on YPD plates at 4 °C. For prolonged storage, *S. cerevisiae* cells were stored in liquid media containing 15 % (v/v) glycerol at -70 °C. 2 mL of liquid culture were directly inoculated with single *S. cerevisiae* colonies, obtained after transformation, and incubated at 30 °C over night. For larger volumes, 100 mL liquid media were inoculated with a single colony and incubated over night at 30 °C under constant shaking. The next day, the cell suspension was transferred to a 5 L flask containing 2 L of media and further incubated at 30 °C. To monitor yeast growth in solution, the optical density of the suspension was measured via UV/Vis spectrometry at 595 nm (OD<sub>595</sub>). Positive/negative selection was performed using yeast strains auxotroph for histidine, leucine, uracil, lysine and arginine, and incubation in media with a corresponding amino acid mixture.

#### 3.2.1.3 Transformation of *E. coli*

Chemical transformation of CaCl<sub>2</sub> competent *E. coli* cells was used for introducing DNA into the cells via heat-shock. Freshly thawed aliquots of chemically competent cells were prepared according to the published protocol of Sambrook (Sambrook et al., 1989). 1 – 2 µL (100 ng) of plasmid DNA were mixed with 200 µL of competent *E. coli* and kept on ice for 5 min. For PCR products with non-overlapping primer or ligation constructs, 10 µL of KLD reaction mix (see 3.2.1.6) or ligation mix were used instead. The heat-shock was conducted for 1 min at 42 °C and 400 rpm in an Eppendorf Thermomix. Afterwards,

1.2 mL of cold LB<sub>0</sub> media were added and the cells were put on ice for 2 min. After 60 min of incubation at 37 °C and 400 rpm, the cells were centrifuged for 2 min at 10000 rpm. 1.2 mL of supernatant was removed and the cells resuspended in the remaining LB<sub>0</sub> media. The cell suspension was distributed via glass beads on LB<sub>0</sub> agar plates, containing the respective antibiotic for selection, and incubated overnight at 37 °C.

### 3.2.1.4 Transformation of *S. cerevisiae*

For the transformation of *S. cerevisiae* strains, 5 mL YPD liquid culture was inoculated with a single colony of the respective strain and incubated at 30 °C over night. The yeast suspension was transferred to 50 mL of YPD media to obtain an OD<sub>595</sub> of 0.15 after dilution. Further incubation for approximately 4.5 h at 30 °C yielded an OD<sub>595</sub> of 0.6 (two full cell cycles). Subsequently, cells were pelleted by centrifugation (5 min, 3000 x g) at room temperature and washed with 25 mL ddH<sub>2</sub>O after the supernatant was discarded. After the cells were spun down once more (5 min, 3000 x g), the pellet was resuspended in 1 mL of 0.1 M lithiumacetate (LiOAc) and transferred to a 1.5 mL reaction tube. Again, the cells were pelleted via centrifugation (7000 rpm, 1 min) and resuspended in 500 µL 0.1 M LiOAc. 50 µL of the suspension were used for the transformation, transferred to a fresh reaction tube and centrifuged for 1 min at 7000 rpm. The supernatant was discarded and the pellet resuspended in 360 µL PLATE mix.

**Table 2:** Components of the PLATE mix.

Compound	Volume
PEG 3000 50 % (w/v)	240 µL
LiOAc (1 M)	36 µL
Salmon ssDNA	10 µL
Plasmid DNA	100 – 400 ng
Sterile ddH <sub>2</sub> O	ad 360 µL

Resuspended cells were incubated at 30 °C for 30 min and heat-shocked at 42 °C for 30 min afterwards. The cells were pelleted (1 min, 7000 rpm) and resuspended in 1 mL sterile ddH<sub>2</sub>O after the supernatant was discarded. 50 – 200 µL of the yeast cell suspension were plated on auxotrophy-selection YPD plates and incubated at 30 °C for 3 days.

### 3.2.1.5 Polymerase Chain Reaction

Polymerase chain reaction can be used to edit, delete and introduce new nucleobases on a template plasmid or to amplify specific DNA sequences for further molecular cloning. Reactions were carried out according to the manufacturer's protocol for the Phusion High-Fidelity DNA Polymerase (New England Biolabs). All components were combined on ice with Phusion polymerase added last to avoid primer degradation by exonuclease activity. All experiments were performed in a BioRad Thermal Cycler with a heated lid in a 50  $\mu$ L scale.

**Table 3:** Components used for the polymerase chain reaction.

<b>Compound</b>	<b>Concentration</b>	<b>Volume (<math>\mu</math>L)</b>
5x Phusion HP-Buffer	-	10
Forward Primer	0.5 $\mu$ M	2.5
Reverse Primer	0.5 $\mu$ M	2.5
dNTP Mix	200 $\mu$ M	1
Template DNA	10 ng	varying
DMSO (optional)	-	(1.5 $\mu$ L)
Phusion Polymerase	0.02 units/ $\mu$ L	0.5
ddH <sub>2</sub> O	-	add 50 $\mu$ L

Depending on the primer length and the percentage of guanine and cytosine the annealing temperature was adjusted. The length of the amplified DNA sequence determined the elongation time.

**Table 4:** Temperature program used during PCR.

<b>Step</b>	<b>Temperature (<math>^{\circ}</math>C)</b>	<b>Time</b>	<b>Cycles</b>
Initial Denaturation	95	30 s	1x
Denaturation	95	10 s	
Annealing	varying	30 s	35x
Elongation	72	30 s/kb	
Storage	4	$\infty$	1x

### 3.2.1.6 Site-Directed Mutagenesis

To introduce site-specific mutations or for sequence deletions, primers designed with the NEB base changer tool (New England Biolabs) were used. The designed reverse-complementary and non-overlapping primers, together with the target plasmid were subjected to a PCR according to the manufacturer's protocol. For sequence deletions, either primers flanking the deleted region or primers introducing an additional stop codon were used. Proper amplification of the desired sequence was confirmed by agarose gel electrophoresis afterwards. Designed primers generate a linear DNA double strand with blunt ends. Phosphorylation and ligation of amplified DNA, as well as digestion of the template DNA was accomplished with the KLD enzyme mix of the Q5 site directed mutagenesis kit (New England Biolabs). Subsequently, the mixture was transformed into competent *E. coli* XL-1 or Mach1 cells.

### 3.2.1.7 Agarose Gel Electrophoresis

Linear DNA strands, obtained as PCR products or as fragments from vector digestion with restriction enzymes, as well as circular plasmids can be separated and analyzed via agarose gel electrophoresis. 1 % gels were prepared by boiling 1 g of agarose with 100 mL 1x TAE buffer (40 mM Tris, 20 mM acetic acid, 1 mM EDTA, pH = 8) and 0.003 % DNA stain G until complete homogeneity of the mixture was achieved. 10 – 50  $\mu$ L of the DNA sample, mixed with 6x Purple Gel Loading Dye New England Biolabs), were loaded onto the cooled down gel. Additionally, SERVA FastLoad 1 kB DNA Ladder was used as a reference marker. The electrophoresis was carried out in 1x TAE buffer at a constant voltage of 120 V for at least 30 min at room temperature. Separated DNA fragments were detected by DNA stain G excitation with UV-light in a BioDoc Analyzer (Biometra).

### 3.2.1.8 DNA Isolation and Purification

*E. coli* can be used to amplify and ligate vector DNA or for plasmid selection via antibiotics. In all cases, appropriate DNA needs to be transformed into chemically competent bacteria before. For the isolation of the DNA afterwards, 5 mL of LB<sub>0</sub> liquid culture containing the respective antibiotic (35  $\mu$ g/mL kanamycin, 100  $\mu$ g/mL ampicillin, 10  $\mu$ g/mL tetracyclin) were inoculated with a single colony from an agar plate. After overnight incubation at 37 °C on a tube rotator, plasmid DNA was extracted with a Wizard® Plus SV Minipres DNA Purification System (Promega) according to the manufacturer's protocol. Subsequently, the DNA concentration and purity of the sample were determined via UV/Vis spectroscopy. Measurements were carried out on a Nanodrop ND-100 UV/Vis spectrometer with 2.5  $\mu$ L of sample volume. The calculation of the concentration is based on the Lamber-Beer equation with

regard of the absorbance at 260 nm. Plasmid identity was verified via DNA sequencing conducted by Eurofins.

### 3.2.1.9 Restriction Digest and Ligation

Restriction enzymes can be utilized to linearize a target plasmid, excise DNA fragments or to generate sticky ends. Enzymes were chosen based on the desired restriction recognition site with regard to the manufacturer's protocol (New England Biolabs). Digestion was conducted with 1  $\mu$ L of the respective restriction enzyme, 1  $\mu$ g of amplified DNA and 10x NEB CutSmart buffer at a total volume of 50  $\mu$ L. After 1 h at 37 °C, the reaction mixture was purified and the final DNA concentration determined. Ligation of a purified and digested vector backbone with a DNA fragment with matching sticky end was accomplished with T4-DNA ligase (New England Biolabs). For the ligation, 100 ng of vector DNA were mixed with the insert at a 1:3 to 1:5 molar ratio (vector DNA : insert DNA).

**Table 5:** Compounds used for the ligation of DNA.

<b>Compound</b>	<b>Amount</b>
Vector DNA	100 ng
Insert DNA	varying
T4 DNA Ligase	1 $\mu$ L
5x T4 DNA Ligase Buffer	2 $\mu$ L
ddH <sub>2</sub> O	add 20 $\mu$ L

The reaction mixture was incubated in a water bath at 16 °C over night. Subsequently, the mixture was transformed into competent *E. coli* XL-1 or Mach1 cells.

### 3.2.1.10 Sequence- and Ligation-Independent Cloning

With sequence- and ligation-independent cloning one or more fragments can be introduced into a vector backbone simultaneously (Li & Elledge, 2012). All DNA fragments were amplified by PCR with primers, which generate 15 bp long overlaps, homologous with either neighboring fragments or the vector backbone. Primer design was carried out with the NEBuilder web tool (New England Biolabs) and the PCR conducted accordingly. Afterwards, the desired vector backbone was linearized by restriction digest with restriction enzymes to create matching pairs with the DNA fragments. The SLIC mixture contained 100 ng of the digested vector and the desired insert at a 1:2 molar ration (vector DNA : insert DNA).

**Table 6:** Compounds used for the SLIC reaction.

<b>Compound</b>	<b>Amount</b>
Linearized Vector DNA	100 ng
Insert DNA	varying
NEB 2.1 buffer	1.0 $\mu$ L
T4 DNA polymerase	0.4 $\mu$ L
ddH <sub>2</sub> O	Add 10 $\mu$ L

T4 DNA polymerase was added as last component to the mixture. In the absence of dNTPs the intrinsic exonuclease activity creates the 5' overhangs required for the ligation. The reaction was incubated at room temperature for exactly 2.5 min and placed on ice for at least 10 min immediately afterwards. Subsequently, the mixture was transformed into competent *E. coli* XL-1 or Mach1 cells.

### 3.2.2 Protein Expression and Purification

#### 3.2.2.1 Protein Expression in *E. coli*

To achieve recombinant protein expression, the plasmid, encoding the desired protein sequence, was transformed into either the *E. coli* BL21 (DE3) or Rosetta (DE3) strain. The bacteria were plated on agar plates or directly used for the inoculation of 150 mL LB<sub>0</sub> media and incubated at 37 °C over night. To prevent contamination and ensure selective growth of bacteria containing the plasmid, all media used were supplemented with respective antibiotics. 2 – 12 L of warm LB<sub>0</sub> or 2xYT media were inoculated with sufficient pre-culture to obtain an OD<sub>600</sub> of 0.1 - 0.2 and were further incubated at 37 °C and 150 rpm. After an OD<sub>600</sub> of 0.6 – 0.9 was reached, the addition of 1 mM isopropyl- $\beta$ -D-thiogalactopyranoside (IPTG) induced protein expression. Depending on the protein, the expression time and temperature was varied.

**Table 7:** Expression conditions of different proteins.

<b>Protein</b>	<b>Media</b>	<b>Temperature</b>	<b>Time</b>	<b>Antibiotic</b>
Hsp82 wt and ATPase mutants	2xYT	37 °C	4 h	50 $\mu$ g/mL kanamycin
Hsp90 $\beta$ wt and ATPase mutants	2xYT	37 °C	4 h	50 $\mu$ g/mL kanamycin
Hsp90 $\beta$ EPL N-terminal	LB <sub>0</sub>	16 °C	ON	50 $\mu$ g/mL kanamycin
Hsp90 $\beta$ EPL C-terminal	LB <sub>0</sub>	25 °C	ON	50 $\mu$ g/mL kanamycin
Hsp90 $\beta$ SrtA N-terminal	LB <sub>0</sub>	37 °C	4 h	50 $\mu$ g/mL kanamycin

Hsp90 $\beta$ SrtA C-terminal	LB <sub>0</sub>	37 °C	4 h	50 $\mu$ g/mL kanamycin
p23	LB <sub>0</sub>	25 °C	ON	100 $\mu$ g/mL ampicillin
Sba1	LB <sub>0</sub>	37 °C	4 h	50 $\mu$ g/mL kanamycin
Hop	LB <sub>0</sub>	25 °C	ON	50 $\mu$ g/mL kanamycin
Sti1	LB <sub>0</sub>	37 °C	4 h	50 $\mu$ g/mL kanamycin
hAha1 & yAha1	LB <sub>0</sub>	37 °C	4 h	50 $\mu$ g/mL kanamycin
Sumo-Protease	LB <sub>0</sub>	37 °C	4 h	50 $\mu$ g/mL kanamycin
TEV-Protease	LB <sub>0</sub>	37 °C	4 h	50 $\mu$ g/mL kanamycin
Sortase 2A/5M	LB <sub>0</sub>	37 °C	4 h	50 $\mu$ g/mL kanamycin

A Beckman Avanti J25 centrifuge equipped with a JA10 rotor was used to harvest the cells at 6000 g (7000 rpm) for 10 min at 8 °C. Cell pellets were resuspended in 75 mL buffer of the first purification step, snap-frozen with liquid nitrogen and stored at -80 °C until further usage.

### 3.2.2.2 Cell Disruption

Frozen bacterial cell suspensions were thawed on ice, treated with one aliquot of SERVA Protease Inhibitor Mix HP and DNaseI. Homogeneity of the sample was accomplished by a Heidolph homogenisator operating at 7000 rpm. Cells were either disrupted via sonification at 3 x 90 s, 5 x 10 % duty cycles at 50 % output (Bandelin Sonoplus HD2200) or at 1.8 bar with the Cell Disruption System Basic Z. To slow down unwanted proteolysis, cells and lysate were kept on ice at all times. To separate soluble proteins from cell fragments, obtained lysate was subjected to centrifugation at Beckman Avanti J25 centrifuge equipped with a JA25.50 rotor for 1 h at 6 °C and 27000 g (18000 rpm). Afterwards, the cleared supernatant was separated and used for purification.

### 3.2.2.3 Affinity Chromatography

Purification of proteins was carried out on Äka fast protein liquid chromatography (FPLC) systems equipped with a UV-900 detector (GE Healthcare). A majority of used constructs and proteins were tagged N-terminally with six histidines (6xHis) which enables the purification via immobilized nickel (II) nitriloacetate (Ni-NTA) residues. The Ni-NTA is chelated by the imidazole groups of the His-tag leading to selective binding of the target protein to the affinity column. Therefore, in a first step the cleared cell lysate was loaded onto a 5 mL HisTrap FF or HisTrap HP (GE Healthcare) column with Ni-NTA buffer A at 3 mL/min. To remove proteins with weak or unspecific interaction, the column was washed with 100 mL of 6 % buffer B. Imidazole, contained in buffer B, competes with the bound imidazole ring of histidine and other proteins, leading to their displacement from the complex and

elution. A step-gradient with 10 column volumes of 75 % buffer B leads to the final elution of the 6xHis-tagged protein, which was collected in 3 mL fractions. Since the protease inhibitor is removed during the purification, 1 mM EDTA was added to the collection tubes to inhibit metalloproteases. Fractions containing protein, detected via their absorption at 280 nm, were analyzed by SDS-PAGE and pooled afterwards if the target protein was contained.

**Table 8:** Affinity chromatography buffers of different proteins.

<b>Proteins</b>	<b>Ni-NTA Buffer A</b>	<b>Ni-NTA Buffer B</b>
Hsp82 wt & mutants Hsp90 $\beta$ wt/LPKTG & mutants Hsp90 $\beta$ SrtA N-terminal Hsp90 $\beta$ EPL/SrtA C-terminal Sba1	50 mM Na <sub>2</sub> HPO <sub>4</sub> pH 7.5 500 mM NaCl 10 mM Imidazole 1 mM DTT	50 mM Na <sub>2</sub> HPO <sub>4</sub> pH 7.5 500 mM NaCl 500 mM Imidazole 1 mM DTT
Hsp90 $\beta$ EPL N-terminal Sortase 2A/5M Sumo/TEV-Protease	50 mM Na <sub>2</sub> HPO <sub>4</sub> pH 7.8 500 mM NaCl 10 mM Imidazole	50 mM Na <sub>2</sub> HPO <sub>4</sub> pH 7.8 500 mM NaCl 500 mM Imidazole
hAha1 & yAha1	50 mM Na <sub>2</sub> HPO <sub>4</sub> pH 8.5 300 mM NaCl 10 mM Imidazole	50 mM Na <sub>2</sub> HPO <sub>4</sub> pH 8.5 300 mM NaCl 500 mM Imidazole
Sti1	50 mM Na <sub>2</sub> HPO <sub>4</sub> pH 7.8 300 mM NaCl 10 mM Imidazole	50 mM Na <sub>2</sub> HPO <sub>4</sub> pH 7.8 300 mM NaCl 500 mM Imidazole

### 3.2.2.4 Proteolytic His-Tag Cleavage

Proteins expressed via the pET28b-Sumo, pET28b-MBP or the pETM11 vector include a protease cleavage site, enabling the removal of the His-tag and the fusion protein. After the proteins from the affinity chromatography were pooled, the respective protease as added. For pET28b-Sumo expressed proteins, one aliquot of Sumo-Protease, which recognizes the Sumo domain and hydrolyzes the peptide bond after the glycine-glycine motif, was added. Proteins originating from the pET28b-MBP and pETM11 vector were treated with TEV-Protease, which cleaves specifically after the Glu-Asn-Leu-Tyr-Phe-Gln (ENLYFQ) sequence. Digestion was carried out overnight at 4 °C with simultaneous dialysis of the protein. To remove imidazole from the eluted protein sample, pooled fractions were filled into Spectra/Por dialysis tubes (Spectrum) and dialyzed against 3 L of the respective Ni-NTA buffer A overnight at 4 °C.

### 3.2.2.5 Reverse Affinity Chromatography

To remove cleaved solubility tags, the His-tag and proteins displaying affinity to the HisTrap columns, reverse affinity chromatography was carried out. Digested protein sample was loaded onto a 5 mL HisTrap FF or HisTrap HP (GE Healthcare) column with respective Ni-NTA buffer A at 3 mL/min and the flowthrough was fractionated. Therefore, proteins with unspecific interactions, proteases and His-tag containing fragments can be separated from the protein in the flowthrough, since they still interact with the Ni<sup>2+</sup> ions. Fractions containing the target protein, detectable via their absorption at 280 nm, were analyzed by SDS-PAGE and pooled afterwards if the target protein was contained.

### 3.2.2.6 Ion-Exchange Chromatography

During anion ion exchange chromatography (IEX), negative charged protein residues are reversible adsorbed to the stationary phase. Quaternary ammonium ions, the functional group of the ResourceQ or Q Sepharose column (GE Healthcare), interact via electrostatic interactions with the protein. Afterwards, elution can be achieved by either modifying the pH value or by modulating the concentration of exchangeable counter-ions. The 6 mL column was equilibrated with according to the manufacturer's protocol and the protein was diluted with buffer A to 150 mL. Subsequently, the protein was loaded onto the column and washed with 10 column volumes at a constant flow of 3 mL/min. For the ResourceQ column, a two-phase gradient was used for the elution of bound proteins. In a first step, the buffer B concentration was linearly increased to 20 % in 20 mL. The target protein was eluted after a further increase to 60 % buffer B in 150 mL. For Q Sepharose media, a gradient from 0 – 100 % B in 400 mL was applied. Fractions containing protein, detectable via their absorption at 280 nm, were analyzed by SDS-PAGE and pooled afterwards if the target protein was contained.

**Table 9:** Ion-exchange chromatography buffers of different proteins.

<b>Proteins</b>	<b>ResQ Buffer A</b>	<b>ResQ Buffer B</b>
Hsp82 wt & mutants	40 mM HEPES pH 7.5	40 mM HEPES pH 7.5
Hsp90β wt/LPKTG & mutants	20 mM KCl	1000 mM KCl
Hsp90β SrtA N-terminal	1 mM EDTA	1 mM EDTA
Sba1	1 mM DTT	1 mM DTT
Hsp90β EPL N-terminal	40 mM HEPES pH 7.5 20 mM KCl 1 mM EDTA	40 mM HEPES pH 7.5 1000 mM KCl 1 mM EDTA
	<b>Q-Seph Buffer A</b>	<b>Q-Seph Buffer B</b>
p23	20 mM MES pH 6.0 5 mM MgCl <sub>2</sub>	20 mM MES pH 6.0 600 mM MgCl <sub>2</sub>

	1 mM DTT	1 mM DTT
Hop	20 mM HEPES pH 7.6	20 mM HEPES pH 7.6
	5 mM MgCl <sub>2</sub>	600 mM MgCl <sub>2</sub>
	1 mM DTT	1 mM DTT

### 3.2.2.7 Hydroxyapatite Chromatography

Hydroxyapatite chromatography is defined as a mixed-mode chromatography approach (Zhao et al., 2009). The stationary phase consists a calcium-phosphate complex (Ca<sub>10</sub>(PO<sub>4</sub>)<sub>6</sub>(OH)<sub>2</sub>), which combines the different attributes of metal ions and the phosphate. Calcium displays anion-exchange properties as well as metal affinity, whereas phosphate serves as cation-exchanger. Before the protein was loaded onto the 30 mL column, it was dialyzed against 5 L of HAT buffer A overnight at 4 °C. The sample was loaded on the pre-equilibrated column and washed with 600 mL of buffer A at a flowrate of 1.2 mL/min. Elution was initiated with a linear gradient from 0 – 100 % buffer B in 200 mL. Fractions containing protein, detectable via their absorption at 280 nm, were analyzed by SDS-PAGE and fractions containing the target protein were pooled afterwards.

**Table 10:** Hydroxyapatite chromatography buffers of different proteins.

Proteins	HAT Buffer A	HAT Buffer B
p23	10 mM KH <sub>2</sub> PO <sub>4</sub> pH 7.0	400 mM KH <sub>2</sub> PO <sub>4</sub> pH 7.0
Hop	10 mM KH <sub>2</sub> PO <sub>4</sub> pH 7.5	400 mM KH <sub>2</sub> PO <sub>4</sub> pH 7.5

### 3.2.2.8 Size-Exclusion Chromatography

Size exclusion chromatography was used as the last purification step for all proteins. The porous column material allows the separation of proteins according to their size and shape. Small proteins are trapped in the pores of the stationary phase as they pass through the column, which retards their elution. The larger the protein, the less likely it will enter the pores of the adsorbent. Consequently, proteins with a large hydrodynamic volume flow through the column more quickly and can be separated from smaller proteins. For proteins larger than 60 kDa a HiLoad Superdex 16/600 with 200 µg was used (GE Healthcare). Otherwise a HiLoad Superdex 16/600 with 75 µg for smaller proteins or a HiLoad Superdex 10/300 (200 µg) for Intein removal was utilized. Before the protein was loaded onto the equilibrated column, the sample volume was reduced to 2 mL via Amicon Ultra Centrifugal Filters (Merck). After protein injection, chromatography was carried out at a flow of 1 mL/min with 3 mL fractions. Fractions containing protein, detectable via their absorption at 280 nm, were analyzed by SDS-PAGE and pooled afterwards if the target protein was contained. Afterwards, the sample volume was reduced by

centrifugation with Amicon Filters to obtain a final protein concentration between 100 – 200  $\mu$ M. Pure protein was aliquoted in PCR tubes (Nerbe), frozen and stored at -70 °C until further use.

**Table 11:** Size-exclusion chromatography buffers of different proteins.

<b>Proteins</b>	<b>SEC Buffer</b>
Hsp82 wt & mutants Hsp90 $\beta$ wt & mutants Hsp90 $\beta$ EPL/SrtA C-terminal Sba1 Sti1	40 mM HEPES pH 7.5 150 mM KCl 5 mM MgCl <sub>2</sub> 1 mM DTT
Hsp90 $\beta$ EPL/SrtA N-terminal Sortase 2A/5M Sumo/TEV-Protease	40 mM HEPES pH 7.5 150 mM KCl 5 mM MgCl <sub>2</sub>
p23 Hop	25 mM HEPES pH 7.6 150 mM KCl 5 mM MgCl <sub>2</sub> 2 mM DTT
yAha1 & hAha1	40 mM HEPES pH 8.5 300 mM KCl 1 mM DTT

### 3.2.3 Biochemical Methods

#### 3.2.3.1 SDS-Polyacrylamide Gel Electrophoresis

Discontinuous SDS-PAGE, developed by Ulrich K. Laemmli, allows the separation of proteins solely based on their molecular weight. Furthermore, the estimated size of a protein or the purity of a sample can be determined (Laemmli, 1970). Protein treatment with anionic SDS and  $\beta$ -mercaptoethanol prior to the electrophoresis eliminates any sterically influences and masks the proteins with a constant charge to mass ratio. Therefore, protein migration within the applied electric field depends only on the size of the protein and the used acrylamide concentration of the gel. Depending on the protein size, different fixed acrylamide concentration or a gradient of varying concentrations can enhance the separation of a sample mixture. A sample composition for a self-cast gel with 12.5 % acrylamide was comprised of the following chemicals.

**Table 12:** Compounds used for the preparation of SDS-gels.

	<b>Resolving gel (12.5%)</b>	<b>Stacking gel (5%)</b>
<b>Acrylamid / Bisacrylamid (40% w/v)</b>	3.125 mL	0.625 mL
<b>Resolving gel buffer (4x)</b>	2.5 mL	-
<b>Stacking gel buffer (2x)</b>	-	2.5 mL
<b>APS</b>	100 $\mu$ L	100 $\mu$ L
<b>TEMED</b>	10 $\mu$ L	10 $\mu$ L
<b>ddH<sub>2</sub>O</b>	4.375 mL	1.875 mL

Premade or freshly prepared gels were fixed in a Hoefer™ Mighty Small™ II Mini Vertical Electrophoresis System and 1x SDS running buffer was added. Protein samples were mixed with 5x Laemmli loading buffer and denatured at 95 °C for 1 min. 10 – 20  $\mu$ L protein sample and a prestained protein standard as reference were loaded into the gel pockets. Afterwards, electrophoresis was carried out at a constant current of 35 mA per gel for up to 1 h.

**Table 13:** Buffers used during SDS-PAGE.

<b>Buffer</b>	<b>Compounds</b>
<b>5x Laemmli loading buffer</b>	0.3 M Tris/HCl, pH = 6.8 50 % (v/v) glycerol 10 % (w/v) SDS 5 % (w/v) $\beta$ -mercaptoethanol 0.5 % (w/v) bromphenol blue
<b>10x SDS running buffer</b>	0.25 M Tris/HCl, pH = 8 2 M glycine 1 % (w/v) SDS
<b>4x resolving gel buffer</b>	1.5 M Tris/HCl, pH = 8.8 0.8 % (w/v) SDS
<b>2x stacking gel buffer</b>	0.25 M Tris/HCl, pH = 6.8 0.4 % (w/v) SDS

### 3.2.3.2 Coomassie Staining

To visualize proteins after protein separation by gel electrophoresis, Coomassie Brilliant blue R was used. The dye attaches to basic amino acid side chains enabling unspecific staining of all proteins on the gel. For this purpose, gels were heated up in Fairbanks A solution and rinsed with water afterwards

(Fairbanks et al., 1971). Destaining was achieved by incubating the gel in hot Fairbanks D solution until protein bands became visible. Pivoting of the gel on a shaker as well as the addition of a paper towel to the Fairbanks A solution accelerated the destaining process.

**Table 14:** Buffers used for coomassie staining of gels.

<b>Buffer</b>	<b>Compounds</b>
<b>Fairbanks A</b>	25 % (v/v) isopropanol
	10 % (v/v) acetic acid
	0.05 % (w/v) Coomassie Brilliant blue R
<b>Fairbanks D</b>	10 % (v/v) acetic acid

### 3.2.3.3 Western Blot

To detect, identify and quantify target proteins in a sample mixture, the combination of SDS-PAGE with a subsequent western blot can be used (Renart et al., 1979). Therefore, gels with separated proteins from a preceding electrophoresis were used for the assembly of the western blot sandwich. Prior to the semi-dry blot, six cut to size sheets of Whatman filter paper were soaked in Western-Blot-Transfer buffer. Additionally, a PVDF-membrane, activated in methanol for 15 s, together with three layers of the Whatman filter paper on top and bottom of the gel formed the transfer stack. The protein transfer from the gel onto the stable membrane was conducted in a Fastblot B44 (Biometra) for 90 min at 72 mA per gel. Blocking of the membrane was achieved by incubation with 5 % milk powder in PBS-T buffer (ON, 4 °C). Afterwards, the membrane was washed three times with PBS-T buffer for 10 min. The primary antibody was used at a 1:10,000 dilution and incubated with the membrane for 1 h at room temperature or overnight at 4 °C. To remove excess antibodies, the membrane was washed three times with PBS-T buffer for 10 min. Analogous to before, the secondary antibody was added and incubation took place for 1 h at room temperature. After a third washing step with PBS-T, the membrane was treated with Westernbright ECL Spray (Advansta) or ECL Prime Western Blotting Detection Reagent (GE Healthcare). Subsequently, the luminescence was detected in an ImageQuant LAS 500 or 4000 (GE Healthcare).

**Table 15:** Buffers used for western blotting.

<b>Buffer</b>	<b>Amount</b>
<b>Western-Blot-Transfer Buffer</b>	25 mM Tris/HCl, pH 7.4
	192 mM Glycine
	20 % (v/v) Methanol
	0.12 g/L SDS
<b>PBS 10x</b>	160 mM Na <sub>2</sub> HPO <sub>4</sub> , pH 8.3

	40 mM KH <sub>2</sub> PO <sub>4</sub> 1.12 M NaCl 27 mM KCl
<b>PBS-T</b>	PBS 1x 0.1 % (v/v) Tween-20

### 3.2.3.4 Native Polyacrylamide Gel Electrophoresis

To separate proteins in their native folding state, Native-PAGE was applied. Contrary to the SDS-PAGE, neither  $\beta$ -mercaptoethanol nor SDS are contained in any buffer. Therefore, proteins are only separated by their isoelectric point and their hydrodynamic volume. This allows the detection of protein-protein interactions or different conformational states. Protein samples were prepared at a concentration of 0.3 mg/ml and mixed with 2x Sample Buffer for Clear Native (Serva). For the separation of the proteins, Serva Vertical Native Gels (4 - 16 %) were used. 10x Native Anode/Cathode Buffer (Serva) was diluted with ddH<sub>2</sub>O and filled into the respective chamber of the electrophoresis unit (Hoefer). Electrophoresis was carried out at constant voltage of 50 V for 10 min. Subsequently, the voltage was increased to 200 V for additional 120 min. To visualize proteins after protein separation by the gel electrophoresis, Coomassie staining was applied.

### 3.2.3.5 Limited Proteolysis

Limited proteolysis can be used to determine the stability of a target protein against a specific protease. The digestive enzyme  $\alpha$ -chymotrypsin, a component of pancreatic juice and active in the duodenum, cleaves peptide bonds after large hydrophobic amino acids. However, inaccessible or buried hydrophobic side chains are exempt from cleavage. Therefore, conformational differences between a wildtype and a mutant protein or between open and closed Hsp90 can be distinguished. 0.3 mg/mL of Hsp90 $\beta$  or Hsp82 were incubated with 20:1 (w/w)  $\alpha$ -chymotrypsin (Sigma) in 20 mM Hepes/KOH pH 7.5, 5 mM MgCl<sub>2</sub>, 200 mM KCl, 6 mM  $\beta$ -mercaptoethanol at room temperature for up to 90 min. To induce closing, proteins were incubated with 2 mM ATP $\gamma$ S prior to proteolysis. The reaction was quenched with the addition of 2 mM phenylmethylsulfonyl fluoride (Sigma) after 0, 2, 5, 10, 30, 60 and 90 min. Afterwards, samples were directly mixed with 5x Laemmli buffer, analyzed by SDS-PAGE (4 – 12 %) and Coomassie staining.

### 3.2.3.6 Crosslinking of Co-Chaperones

Protein-protein interactions usually require close proximity of the interactors *in vivo* and *in vitro*. Therefore, chemical crosslinking agents can permanently link proteins in proximity and capture protein complexes or even transient interactions. For all crosslinking purposes, disuccinimidyl glutarate (DSG) was used. N-hydroxysuccinimide esters at both ends display selective reactivity towards primary amine groups, which leads to the formation of chemically stable crosslinks at a distance of 7.7 Å. To probe the interaction of co-chaperones with Hsp90 in different conformational states, Hsp90 was incubated with or without ATP $\gamma$ S with the respective interactor. Hsp90 was diluted with closing buffer (20 mM Hepes/KOH pH 7.5, 5 mM MgCl<sub>2</sub>, 200 mM KCl, 6 mM  $\beta$ -mercaptoethanol) to a concentration of 0.35 mg/mL. Afterwards, co-chaperones (1:2 molar ratio Hsp90:co-chaperone) and 2 mM ATP $\gamma$ S were added and the sample was incubated at 37 °C for 1 h (30 °C for Hsp82). 50 mM DSG, dissolved in DMSO, was diluted with closing buffer to 10 mM and mixed with the sample to a final concentration of 2 mM. After 45 min of incubation at room temperature and in the absence of light, 8 mM Tris/HCl pH 7.4 was added and the reaction was quenched for 15 min. Subsequently, the sample was mixed with 5x Laemmli loading buffer, denatured and analyzed via SDS-PAGE.

### 3.2.3.7 Crosslinking Closing Kinetics

During its ATPase cycle, Hsp90 undergoes several large conformational changes and domain rearrangements. This includes the dimerization of the NTDs and the overall formation of a more compact structure. Chemical crosslinking can distinguish between conformational states of Hsp90 by additional contact sites in the closed ATP bound state. Hsp90 was diluted in closing buffer (see 3.2.3.6) to a concentration of 0.35 mg/mL, 2 mM ATP $\gamma$ S was added and incubation started at 37 °C (30 °C for Hsp82). After 0, 1, 3, 5, 7, 10 and 30 min (0, 0.5, 1, 1.5, 3, 5 and 8 min for Hsp82) 20  $\mu$ L of sample were mixed with 2 mM DSG according to 3.2.3.6 and incubated for 45 min. Analogous, the reaction was quenched with Tris/HCl pH 7.4, mixed with 5x Laemmli and analyzed via SDS-PAGE. For the analysis of the gels, ImageJ was used. Hsp90 monomer and dimer fractions were calculated via integration of the respective gel band and subsequently plotted and fitted in OriginPro. Obtained kinetic curves were measured in triplicates and analyzed from three independent gels.

### 3.2.3.8 Crosslink MS/MS Measurements

#### *Sample preparation:*

To assess the exact location of crosslinks and determine different reaction sites in combination with the conformational states of Hsp90, chemical crosslinking was combined with MS/MS measurements. The existing and published protocol was adapted to determine crosslinks of Hsp90 in the open and closed

state (Muhlhofer et al., 2021). 35 µg of Hsp90 in 40 µL of the closing buffer (see 3.2.3.6) was incubated for 1 h at 37 °C (30 °C for Hsp82) with or without 2 mM ATP $\gamma$ S to initiate closing. Crosslinking was carried out as described in 2.2.3.6 with 2 mM DSG for 45 min and quenched with 6 µL of 1 M Tris/HCl pH 7.4 for 15 min. For the denaturation of the proteins, 29.5 µL of 6 M urea, 50 mM Tris/HCl pH 7.4 were added. After 30 min of incubation at 56 °C, the samples were cooled to room temperature and 6.3 µL 100 mM iodacetamide, 50 mM Tris/HCl pH 7.4 were added. The samples were incubated for 20 min at room temperature and in the absence of light. Digestion of the proteins was initiated by the addition of 1 µL trypsin (sequencing grade, Promega) and carried out over night at 37 °C. 1 µL of formic acid (FA) was directly added to stop the reaction. For desalting, the samples were applied onto double C18 layer stage tips (Thermo Fisher Scientific), pre-equilibrated with methanol containing 0.5 % formic acid. After three washing steps with the equilibration solution, the peptides were eluted with 60 µL of 80 % acetonitrile and 0.5 % formic acid. The solvent was removed by vacuum centrifugation and dissolved again in 25 µL 0.5 % FA. After 15 min of incubation in an ultrasonic bath, peptide samples were filtered via centrifugal filters (0.22 µm, Merck) and transferred into Chromacol vials (Thermo Fischer Scientific).

#### *MS/MS Measurements*

MS/MS measurements and analysis of the crosslinked protein samples was carried out by Katja Bäuml (TUM, Sieber) analogous to the published protocol (Muhlhofer et al., 2021). Protein separation was achieved by an Ultimate3000 Nano-HPLC, coupled to an Orbitrap Fusion via electrospray EASY™-source (Thermo Fischer Scientific). Peptide samples were loaded onto a 2 cm Nano Trap Column (75 µm i.d., Acclaim PepMap100, C18, 3 µm, 100 Å, Thermo Fischer Scientific) and separated via Acclaim PepMap RSLC Column (75 µm i.d., C18, 2 µm, 100 Å, Thermo Fischer Scientific) at 40 °C. Elution was carried out with a multi-step elution gradient from 5 to 90 % acetonitrile with 0.1 % FA (5 % ACN for 7 min, 5-28 % ACN in 30 min, 38-35 % ACN in 5 min, 90 % ACN for 10 min) at 0.4 µL/min. The m/z range for survey scans was set to 300 - 1,500 with a resolution of 120,000. For the automatic gain control, 2.0\*e5 was set as target value with a maximum allowed injection time of 80 ms. The most intense charge states were selected for HCD fragmentation and the collision energy set to 30 %. For the ion trap, the automatic gain control was set to 5.0\*e4 with a maximum allowed injection time of 100 ms. During the measurement generated fluoroanthene ions were used for the mass calibration of the peptides. Data acquisition was executed with the Xcalibur software (Thermo Fischer Scientific), processed with Kojak and visualized with the ProXL web tool (Riffle et al., 2016).

#### **3.2.3.9 Protein Labeling**

Fluorescent probes allow the specific detection and localization of a labeled protein at low concentrations and provide the means for a broad spectrum of fluorescent-based methods. Fluorescent

ATTO-maleimide dyes (Atto-Tec) covalently bind to the thiol group of exposed cysteine residues, enabling site-specific labeling. To remove excess DTT, buffer exchange to HKM buffer (40 mM Hepes/KOH pH 7.5, 5 mM MgCl<sub>2</sub>, 150 mM KCl) was performed via a PD-10 desalting column following the manufacturers protocol (GE Healthcare). The fluorescent dye was dissolved in DMSO and the concentration determined by UV/VIS absorbance at the respective wavelength. The dye was added to the protein at a twofold molar excess. If the final DMSO concentration exceeded 1 % (v/v), additional buffer was added. After 2 h of incubation in the dark at room temperature, 5 mM DTT was added to quench the labeling reaction. Excess dye was removed via PD-10 column, equilibrated in HKM buffer, and eluted protein was pooled and concentrated via Amicon centrifugation filters. Afterwards, the labeling efficiency was determined by UV/VIS spectrophotometry. To calculate the degree of labeling (DOL), the equation provided by the manufacturer was utilized (equation 1).

**equation 1:**

$$DOL = \frac{A_{max} / \epsilon_{max}}{A_{prot} / \epsilon_{prot}} = \frac{A_{max} * \epsilon_{prot}}{(A_{280} - A_{max} * CF_{280}) * \epsilon_{max}}$$

### 3.2.3.10 Expressed Protein Ligation

To circumvent the limitations of protein synthesis, numerous approaches can be employed. Most common is the synthesis of a target protein in multiple parts, followed by the subsequent ligation to the full-length protein in vitro (Muir et al., 1998). However, for many methods, the resulting protein backbone differs or additional amino acids are required at the site of ligation. The native chemical ligation (NCL), which includes the expressed protein ligation (EPL), generates a native amide bond in the fusion of multiple peptide fragments (Dawson et al., 1994). The reaction requires the transthioesterification of a C-terminal thioester with the thiol group of an N-terminal cysteine residue. The reversible first step is followed by an irreversible S-N-acyl-shift, restoring the native amide backbone of the ligated protein. The generation a C-terminal thioester can be achieved in multiple ways. Synthetically specific resins can be utilized, which form a terminal thioester on the peptide after cleavage, or recombinant via inteins. In nature, an intein can excise itself from an expressed protein, leading to a native peptide bond of the adjacent exons. Similar to the NCL, the underlying mechanism is based on the combination of an N-S-acyl-shift followed by transthioesterification. Modified inteins in combination with specific thiols are required for the formation of reactive thioesters in vitro. After the transthioesterification of the intein with the added thiol, the intein is removed and the second protein fragment, containing the N-terminal cysteine, introduced. The subsequent transthioesterification and irreversible N-S-acyl-shift lead to the formation of the ligated target protein. The N-terminal fragment was cloned and purified with a His-Sumo solubility tag and an intein originating from a pTXB1 plasmid (New England Biolabs). Additionally, to improve the formation of the thioester the amino acid N-terminal of the cysteine was replaced with an asparagine. After affinity (see 3.2.2.3), ion exchange (see 3.2.2.6) and size exclusion chromatography (see 3.2.2.8), the cleavage of the intein and thioester

formation was initiated. 5 mg of protein in Cleavage Buffer (20 mM Hepes pH 8.5, 500 mM NaCl, 50 mM 2-mercaptoethanesulfonic acid, 1 mM EDTA) was incubated for up to 40 h at either room temperature or 4 °C. The spliced intein was removed by gel filtration (Superdex Prep Grade 200, 10/300) or incubation with pre-equilibrated chitin beads (New England Biolabs). Obtained fractions, containing the thioester, were concentrated via Amicon centrifugation filters. The C-terminal cysteine fragment was cloned in the pETM11 vector, which enabled the cleavage via TEV protease after affinity chromatography (Dummler et al., 2005). The protein, containing the free cysteine, was further purified via reverse affinity (see 3.2.2.4) and size exclusion chromatography (see 3.2.2.8). For the ligation of the fragments, thioester and C-terminal protein were mixed in a 1:4 (N-term. : C.-term.) molar ratio in ligation buffer (20 mM HEPES pH 8.5, 10 mM MESNA, 500 mM NaCl) and incubated overnight at 4 °C according to the manufacturers protocol (New England Biolabs). Purification, thioester formation and ligation were analyzed via SDS-PAGE.

### 3.2.3.11 Sortase A Mediated Protein Ligation

The ligation of two protein fragments with a resulting amid bond can be mediated by the transpeptidase Sortase A (SrtA). *In vivo*, the membrane protein SrtA catalyzes the fusion of proteins containing the Leu-Pro-Xxx-Thr-Gly (LPXTG) motif with glycines of peptidoglycans located at the cell wall (Mazmanian et al., 1999). Sortase A cleaves the peptide bond between the threonine and glycine and covalently links the threonine carboxyl group to an active cysteine of the enzyme. The resulting reactive thioester-acyl is then transferred to the glycine of a second protein, resulting in a newly formed peptide bond (Mao et al., 2004). For the *in vitro* SrtA-mediated protein ligation, the first protein fragment was modified with the LPXTG motif at the carboxyl-terminus. To obtain a second protein fragment with a glycine at the amino-terminus, the His-MBP-tag was cleaved of via TEV protease. Because of the protease, the peptide bond of the ENLYFQG motif between the glutamine and the desired glycine is hydrolyzed, leading to the formation of an N-terminal glycine (Polayes et al., 1998). 5 mg of each purified fragment and 5 mg of the corresponding Sortase A (5M for LPXTG; 2A.9 for LAXTG) were mixed to obtain a final volume of 15 mL with ligation buffer (50 mM Tris/HCl pH 8.0, 150 mM NaCl, 20 mM CaCl<sub>2</sub>). After 60 min of incubation at room temperature, and in case of labeled proteins in the dark, the reaction was stopped, diluted with ResQ low salt buffer (40 mM HEPES pH 7.5, 20 mM KCl, 1 mM EDTA, 1 mM DTT) to a volume of 150 mL and purified via ion exchange chromatography (see 3.2.2.6). Fractions containing the ligated protein were pooled and purified via N-NTA affinity chromatography (see 3.2.2.3). The His-MBP tag was cleaved of during overnight dialysis against 2 L of Ni-NTA buffer A with one aliquot of TEV protease. Subsequently, remaining impurities, the cleaved MBP tag and the TEV protease were removed by reverse affinity chromatography (see 3.2.2.5). Pure protein fractions were pooled and concentrated via centrifugation with 4 mL Amicon Ultra

centrifugation filters. Kinetics of the SrtA-mediated ligation, as well as the efficiency of following purification steps were analyzed via SDS-PAGE.

### 3.2.4 Biophysical Methods

#### 3.2.4.1 Circular Dichroism Spectroscopy

Enantiomers of chiral substances differ in their absorption of left and right circularly polarized light. Protein chirality is based on the peptide backbone and drastically influenced by secondary structure elements and aromatic side chains. During CD spectroscopy, the resulting ellipticity as a function of the wavelength is used to describe and calculate structural features of a given protein (Kelly et al., 2005). In far-UV (190 – 250 nm) spectroscopy, the resulting spectrum depends on the percentage of  $\alpha$ -helices,  $\beta$ -sheets and random coil elements. For  $\alpha$ -helices, characteristic minima at 208 and 222 nm are obtained whereas  $\beta$ -sheets typically contribute minima at 218 nm. Additionally, the obtained structural information can be used to observe thermal unfolding of the protein when measured at different temperatures. Prior to the measurement, proteins were dialyzed overnight against phosphate buffer (50 mM  $\text{Na}_2\text{HPO}_4$  pH 7.5, 100 mM NaCl, 0.5 mM TCEP) and diluted to a concentration of 0.2 mg/mL. Spectra were recorded in a Chirascan CD Spectrometer (Applied Photophysics) together with a 1 mm cuvette. For far-UV spectra, measurements were conducted between 260 nm and 195 nm at a fixed temperature of 20 °C. For thermal transitions of Hsp90, the temperature was increased from 20 °C to 90 °C in 0.5 °C/min steps and the shifts of three independent, fixed wavelengths were monitored. For data comparison, obtained ellipticity values were converted into the respective mean residue weighted ellipticity  $[\Theta]_{MRW}$  of the protein. Equation 2 was used, where  $[\Theta]$  represents the measured ellipticity in degrees, M the molecular mass of the protein in g/mol, N the number of amino acids, d the pathlength in cm and c the concentration in g/ml.

$$\text{equation 2:} \quad [\Theta]_{MRW} = \frac{M * [\Theta]}{10 * c * d * (N - 1)}$$

#### 3.2.4.2 Thermo Shift Assay

A thermo shift assay can be used to monitor the unfolding of a target protein by thermal denaturation. Unfolded proteins expose otherwise buried hydrophobic patches, which allows non-specific binding of the dye Sypro® Orange (Huynh & Partch, 2015). In an aqueous environment, the fluorescent dye is quenched and upon binding to a protein fluorescence increases, which enables to track changes in signal intensity. For the assay, 5  $\mu\text{g}$  of Hsp90 at a total reaction volume of 20  $\mu\text{L}$  was used. Measurements were performed in 20 mM Hepes/KOH pH 7.5, 5 mM  $\text{MgCl}_2$ , 6 mM  $\beta$ -mercaptoethanol, 150 mM KCl or 500 mM  $(\text{NH}_4)_2\text{SO}_4$  with a 1:1000 dilution of Sypro® Orange. Additionally, the influence of ATP $\gamma$ S

was tested. For this purpose, Hsp90 was pre-incubated with 2 mM of the nucleotide at 37 °C for 4 h prior to the measurement. A real time PCR-cycler (Agilent Technologies Stratgene Mx3000P) was used to detect the fluorescence signal (excitation 490 nm/emission 575 nm). Thermal unfolding was measured between 25 °C and 95 °C with a stepwise increment of 1 °C per minute. Melting temperatures were calculated from triplicates using the 2<sup>nd</sup> derivative.

### **3.2.4.3 Absorbance Spectroscopy**

To measure the concentration of a protein in a given sample, UV/Vis spectrophotometry was utilized. Measurements are based on the fact, that aromatic amino acids, such as tryptophan and phenylalanine, display a maximum of absorption at 280 nm. All measurements were performed on a Nanodrop ND-100 UV/Vis spectrophotometer with 2.5 µL of sample volume. In a first step, the A280 method was used with the corresponding buffer of the protein, which automatically subtracts the spectrum from subsequent measurements. Afterwards, the protein was applied on the pedestal and the absorbance at 280 nm measured. Via the calculated molar extinction coefficient (ProtParam tool, Expasy) and the obtained absorbance value, the protein concentration can be determined by the Beer-Lambert law (eqn. 3). Nucleic acid contaminations were assed via the 260/280 nm ratio.

**equation 3:** 
$$A = \varepsilon * c * d$$

### **3.2.4.4 Analytical Ultracentrifugation**

Analytical ultracentrifugation (AUC) can be used to determine the molecular weight, shape and interaction of a macromolecule within a centrifugal field. The sedimentation velocity (SV) approach provides a fast way to study protein-protein interactions, conformational states and the oligomeric distribution of a known protein. Essential information of a protein can be gathered at low concentrations without the need of chemical crosslinking or the presence of a matrix. The centrifugal force of the ultracentrifuge results in the migration of sample sedimentation boundaries, which can be assigned to different distinct species. However, this requires an appropriate detection system to monitor the movement of the sedimentation boundaries over time (Schuck, 2013). Typically, this is achieved via Rayleigh interference or absorbance optics for native proteins or via a fluorescence detection system. The use of fluorescent-labeled proteins allows the detection of a target protein in a multi-component sample, since only complexes containing the target protein are observed. Additionally, fluorescent detectors offer a high sensitivity, providing the means to measure at nanomolar concentrations. Data analysis requires the Lamm equation (eqn. 4), which illustrates the time-dependent change of the solute concentration considering the radius, the solute diffusion constant, the sedimentation coefficient and rotor angular velocity.

**equation 4:** 
$$\frac{\partial c}{\partial t} = D \left[ \left( \frac{\partial^2 c}{\partial r^2} \right) + \frac{1}{r} \left( \frac{\partial c}{\partial r} \right) \right] - s\omega^2 \left[ r \left( \frac{\partial c}{\partial r} \right) + 2c \right]$$

For SV experiments, proteins were labeled with ATTO-488 (Atto-Tec) and diluted with closing buffer to a concentration of 1  $\mu\text{M}$  at a total volume of 300  $\mu\text{L}$  per cell. Closing of Hsp90 was initiated by the addition of 2 mM ATP $\gamma$ S and incubation at 37  $^{\circ}\text{C}$  for 1 h (30  $^{\circ}\text{C}$  for Hsp82). Re-opening with ADP (2 mM) and Radicicol (500  $\mu\text{M}$ ) was carried out for an additional hour at 37  $^{\circ}\text{C}$  (30  $^{\circ}\text{C}$  for Hsp82). Analytical ultracentrifugation was performed in an Optima XLA (Beckman Coulter) centrifuge, equipped with a Biomedical Fluorescence Detection System (Aviv). A Ti-50 rotor (Beckman) operating at 42,000 rpm and 20  $^{\circ}\text{C}$  was used for all experiments. To determine the buffer viscosity and calculate the partial specific volume of the protein Sednterp was utilized (Philo, 2023). Raw data evaluation was conducted in SedView, to obtain  $dc/dt$  profiles used to determine protein S-values (Schuck, 2000).

### 3.2.4.5 Transmission Electron Microscopy

Oligomers and large protein complexes can be easily visualized by electron microscopy. To detect formed oligomers or aggregates, Hsp90 was incubated for 4 h at 37  $^{\circ}\text{C}$  at a concentration of 0.5 mg/mL. Incubation was carried out in either 250 mM or 500 mM  $(\text{NH}_4)_2\text{SO}_4$  closing buffer in the presence of 2 mM ATP $\gamma$ S. 10  $\mu\text{L}$  of sample were pipetted on a 200-mesh activated copper grid and incubated for 1 min at room temperature. The grid was washed twice with 10  $\mu\text{L}$  ddH $_2\text{O}$  and negatively stained with 5  $\mu\text{L}$  of a 2 % (w/v) uranyl acetate solution. After 1 min excess solution was removed with a filter paper. All TEM micrographs were recorded on a JOEL JEM-1400 Plus transmission microscope at 120 kV (Jeol). Observed protein structures were documented at 50,000x magnification. All measurements were carried out by Ramona Absmeier (TUM).

### 3.2.4.6 Hydrogen Deuterium Exchange Mass Spectrometry

Hydrogen deuterium exchange (HDX) makes use of the phenomenon that solvent-exposed hydrogen atoms of the amide backbone interchange with deuterium atoms from the surrounding buffer. The rate of exchange is dependent on multiple factors, which include the given structure of a protein, interactions or the chemical environment (Wales & Engen, 2006). Therefore, the combination of HDX with mass spectrometry allows the acquisition of detailed and localized information of protein dynamics and specific protein-protein interaction sites (Percy et al., 2012). Hsp90 and Hsp82 were used for the hydrogen/deuterium exchange in the open and closed state to discern residues involved in the conformational rearrangements (Masson et al., 2019). 30  $\mu\text{M}$  of protein sample were incubated in 300  $\mu\text{L}$  buffer ( 500 mM  $(\text{NH}_4)_2\text{SO}_4$  / 500 mM KCl, 20 mM Hepes, 5 mM MgCl $_2$ , 6 mM  $\beta$ -mercaptoethanol) with or without 2 mM ATP $\gamma$ S for 1 h at 37  $^{\circ}\text{C}$  (30  $^{\circ}\text{C}$  for Hsp82) to form a

completely closed state. For the measurement, samples were diluted 1:20 in deuterated PBS buffer (pH 7.4) and incubated at 20 °C for 10 s, 1 min, 10 min, 30 min and 2 h. Subsequently, to stop the hydrogen exchange, protein samples were mixed 1:1 with quenching buffer at 1 °C. A Waters Enzymate BEH Pepsin Column (2.1 x 30 mm) at 20 °C was used for the proteolytic digestion of the proteins. Subsequently, obtained peptide fragments were loaded and separated via a Waters ACQUITY UPLC BEH C18 Column (1.0 x 100 mm). Elution was initiated by an acetonitrile/H<sub>2</sub>O gradient, with the liquid phase containing additional 0.1 % (v/v) formic acid. Electrospray ionization and time-of-flight analysis by a Synapt G2-S ESI-TOF were utilized for data acquisition. LC/MS was carried out on a Waters ACQUITY M-Class UPLC and the obtained data were analyzed in DynamX by Florian Rührnöbl (TUM).

### **3.2.4.7 Evolutionary Residue Conservation**

To evaluate the residue specific conservation of proteins, the ConSurf web tool (ConSurf Web Server) was utilized (Armon et al., 2001). Conservation grades were based on the respective crystal structure and sequence from the protein database (Hsp82: 2CG9; Hsc82: 6XLC; Hsp90 $\alpha$ : 7L7J; Hsp90 $\beta$ : 5FWK). The HMMR search algorithm (one iteration, E-value cutoff = 0.0001) assembles homologs from the UniRef-90 database, from which 150 random sequences with 70 – 95 % identity were selected for further calculations. For the creation of the multiple sequence alignment, the MAFFT-L-INS-I method was utilized. Evolutionary conservation calculations were carried out with the Bayesian method to fit the respective evolutionary substitution model.

### **3.2.4.8 Molecular Dynamic Simulations**

To simulate the effect of point mutations *in silico*, the group of Prof. Ville Kaile (Stockholm University) performed molecular dynamic (MD) simulations. All simulations, including mutants, are based on the full-length Hsp82 crystal structure in the dimeric closed state, which includes the ATP and Mg<sup>2+</sup> in the binding pocket (PDB: 2CG9) (Ali et al., 2006). The missing loops from the structure, especially from the flexible linker, were added via the MODELLER tool (Sali & Blundell, 1993). Each structure model was solvated in a TIP3 water box (176 x 176 x 115 Å), supplemented with 100 mM NaCl. The complete system comprised 303,000 independent atoms and was simulated as an NPT ensemble between 200 and 1000 ns (T = 310 K, p = 101.3 kPa). Calculations were carried out with the NAMD software, at 2 fs integration time steps using the CHARMM force field (MacKerell et al., 2000; Phillips et al., 2020). The Particle Mesh Ewald approach was utilized for long-range electrostatics (1 Å grid size, 12 Å switch-distance). For data visualization, Visual Molecular Dynamics (VMD) was used (Humphrey et al., 1996).

### 3.2.4.9 Size Exclusion Chromatography with Multi Angle Light Scattering

#### *Analytical Size Exclusion Chromatography HPCL:*

During its ATPase cycle, Hsp90 switches from an open v-shaped conformation to a more compact state with dimerized NTDs. This change in hydrodynamic volume results in a different elution time for the apo and nucleotide-bound state when loaded onto an analytical size exclusion column. Measurements were carried out on a Shimadzu HPLC system, equipped with a SPD-20A UV detector and a Superdex 200 10/300 GL column. Prior to any measurement, the system and column were equilibrated with the respective buffer for at least one hour at a flow rate of 0.5 mL/min. Protein samples were prepared at a concentration between 0.25 – 0.35 mg/mL in 110 µL of closing buffer. To determine conformational kinetics of Hsp90, the buffer reservoir of the system was cooled additionally. Closing of Hsp90 was initiated by the addition of 2 mM nucleotide and incubation at 37 °C (30 °C for Hsp82). Re-opening was triggered after 70 min of incubation with ATPγS via the addition of 2 mM ADP or 50 µM Radicicol. To assess the influence of co-chaperones on kinetics, the respective interactor was added at a molar ratio of 1:2 (Hsp90 : co-chaperone) during incubation. To access the conformational kinetics of Hsp90, the elution profiles after different defined time points were analyzed in OriginPro. UV absorbance profiles were fitted with a bi-Gaussian function to calculate the population of protein in the open and closed state (eq. 5).

**equation 5:** 
$$y = y_0 + \frac{A_1}{w_1\sqrt{\pi/2}} e^{-2\frac{(x-x_{c1})^2}{w_1^2}} + \frac{A_2}{w_2\sqrt{\pi/2}} e^{-2\frac{(x-x_{c2})^2}{w_2^2}}$$

#### *HPLC Multi Angle Light Scattering:*

After protein separation by the HPLC system, an additional multi-angle light scattering (MALS) detector provides the possibility to determine the molecular weight of the eluted species. The scattered light of the protein at multiple angles is used to calculate the absolute molar mass in addition to the average size of the sample. The Shimadzu system is equipped in line with a Dawn Helios II multi-angle light scattering detector, which was equilibrated with the respective buffer for at least one hour at a flow rate of 0.5 mL/min. To calibrate the method for a specific buffer, the delay volume between detectors, band broadening correction and signal normalization was carried out with BSA as protein standard. Since all measurements were made in addition to the UV detection system, samples could be analyzed with both methods. Obtained peaks were analyzed with the ASTRA software to determine the molar mass of eluted proteins.

### **3.2.4.10 Ensemble Förster Resonance Energy Transfer Spectroscopy**

Förster resonance energy transfer (FRET) describes the transfer of energy between a donor and an acceptor chromophore via dipole-dipole coupling. The efficiency of the transfer is largely dependent on the spectral overlap as well as on the intermolecular distance of the fluorophores. The contribution of the distance is inversely proportional to its sixth power ( $1/r^6$ ), making the transfer sensitive to small changes in donor-acceptor-distance. Therefore, FRET provides a powerful tool to study inter- and intramolecular interactions in addition to conformational rearrangements. To study the human Hsp90 ATPase cycle, a FRET system, based on the existing yeast Hsp82 system (Hessling et al., 2009), was created and used for ensemble measurements. To achieve selective labeling of Hsp90, the protein was expressed in two separate fragments. The N-terminal Hsp90 fragment, containing an introduced cysteine at position 63C and a C-terminal Sortase recognition motif, was labeled via cysteine-selective maleimide dyes (donor: ATTO-532 maleimide, acceptor: ATTO-643 maleimide). Afterwards, Sortase-mediated ligation with the C-terminal glycine fragment resulted in labeled full-length protein (described in 2.2.3.11). To form heterodimers containing both donor and acceptor labeled Hsp90, 1  $\mu$ M of the respective proteins were mixed at the used measurement buffer and incubated for 1 h at 37 °C. Measurements were carried out in closing buffer with varying salt concentrations (50 – 500 mM  $(\text{NH}_4)_2\text{SO}_4$  / KCl, 20 mM Hepes, 5 mM  $\text{MgCl}_2$ , 6 mM  $\beta$ -mercaptoethanol) at a total volume of 150  $\mu$ L. Experiments were conducted on a Jasco Fp-8500 Spectrofluorometer, operating at 37 °C. The excitation wavelength was set to 535 nm and emission spectras were recorded at 555 nm and 662 nm. 2 mM of nucleotide (ADP, ATP,  $\text{ATP}\gamma\text{S}$ , AMP-PNP) initiated the reaction.

### **3.2.4.11 Single Molecule Förster Resonance Energy Transfer Spectroscopy**

With single molecule FRET (smFRET) the diffusion of single molecules or complexes through the laser of a confocal microscope can be detected. Compared to bulk measurements, effects caused by a heterogeneous FRET pairs and quenching can be excluded. Additionally, the lifetime of single fluorophores can be calculated, which reveals conformational changes or intermolecular dynamics (Algar et al., 2019). To obtain single molecule pairs of labeled Hsp90, the sample was diluted to a concentration between 30 and 100 pM. For the single-pair measurements, a custom-build confocal microscope operated by Ganesh Agam (LMU) was used as previously described (Dahiya et al., 2019). In short, Hsp90 samples were incubated at different concentrations of closing buffer at 37 °C with or without the addition of 2 mM of nucleotide (ADP, ATP, AMP-PNP or  $\text{ATP}\gamma\text{S}$ ) for at least 30 min. Measurements were conducted at room temperature and for up to 90 min. By combining multi-parameter fluorescence detection with a pulsed interleaved excitation, fluorophore lifetime, anisotropy, FRET efficiency and stoichiometry can be assessed simultaneously. A 532 nm (PicoTA 530, Topica) and 640 nm laser (LDH-D-C-640, PicoQuant) at a synchronized repetition rate of 26.8 MHz with 18 ns delay

were used for excitation of the respective fluorescent dye. Events differing from a 0.5 dye stoichiometry, blinking and photo-bleaching effects were excluded. Data analysis was performed with PAM, a custom software for MATLAB (Schrimpf et al., 2018).

### 3.2.5 *In vitro* and *in vivo* Activity Assays

#### 2.2.5.1 Regenerative ATPase Assay

To determine the *in vitro* ATP turnover of Hsp90 under different conditions and to study the impact of mutations, a regenerative steady state ATPase assay was used (Ali et al., 1993). During the assay, a constant ATP concentration is provided by a coupled enzyme system, which bypasses the influence of formed ADP. Pyruvate kinase (PK), together with the co-factor phosphoenolpyruvate (PEP), converts ADP back into ATP. The additionally created pyruvate is reduced in a second reaction. Lactate dehydrogenase (LDH) and NADH catalyze the reduction of pyruvate into lactate and the oxidized NAD<sup>+</sup>. The decrease of NADH can be tracked photometrically via a decline of absorption at 340 nm. Since the consumption of NADH indirectly correlates with the ATP turnover, the ATPase activity of the target protein can be determined. For the measurements, 10 μM of Hsp90 (3 μM Hsp82) was diluted with the respective assay buffer and mixed with the prepared twofold enzyme premix. The final volume for a single measurement was 150 μL when quartz cuvettes were used and 120 μL in the case of the 96 well plate. The reaction was started by the addition of 2 mM ATP and carried out at 37 °C (30 °C for Hsp82) in a Cary 50/100 UV/Vis spectrometer or a Tecan Plate Reader. After a linear depletion of NADH was observed (30 – 60 min), 500 μM Radicol was added to the sample to stop Hsp90-specific ATP depletion. To determine the ATPase activity of Hsp90 and exclude background reactions, the Hsp90-specific inhibitor Radicol was added and the remaining slope was subtracted from the ‘ATP slope’. All measurements were performed in triplicates and the respective activity ( $k_{cat}$ ) was calculated with equation 6, where  $m$  is the fitted slope,  $d$  the thickness of the cuvette and  $\epsilon$  the molar extinction coefficient of NADH at 340 nm:

**equation 6:** 
$$k_{cat} = \frac{-m}{d \cdot c_{Hsp90} \cdot \epsilon_{NADH}}$$

**Table 16:** Buffers used for the regenerative ATPase assay.

Buffer	Volume/Concentration
<b>2x Assay Premix</b>	4156 μL Assay Buffer
	240 μL PEP (100 mM)
	48 μL NADH (50 mM)
	12 μL PK

	44 $\mu$ L LDH
<b>Assay Buffer</b>	20 mM Hepes/KOH pH 7.5 5 mM MgCl <sub>2</sub> 200 – 500 mM KCl/CaCl <sub>2</sub> /(NH <sub>4</sub> ) <sub>2</sub> SO <sub>4</sub> 6 mM $\beta$ -mercaptoethanol

### 3.2.5.2 5'-FOA Plasmid Shuffling Assay

To test the *in vivo* functionality of different Hsp82 mutants, a plasmid shuffling assay, based on the previously described method by the Lindquist lab, was performed (Nathan & Lindquist, 1995). This assay includes a yeast strain, which is deficient in genomic HSP82 and HSC82. Additionally the strain contains a plasmid with a URA3 selection marker coding for Hsp82 to rescue the lethality from the missing wildtype chaperone. This selection marker on the pKAT plasmid enables a selection of cells, which lost the pKAT Hsp82 plasmid in media supplemented with 5'-FOA. Hsp82 and variants were cloned into the p432GPD vector allowing constitutive expression under the control of the glyceraldehyde-3-phosphate dehydrogenase (GPD) promoter. Afterwards, the vector with the Hsp82 variant of interest was transformed into the yeast shuttling strain. Cells, which contained the 2 micron high-copy number plasmid and survived the shuffling, were tested for the loss of the original URA3 plasmid using media lacking uracil.

### 3.2.5.3 Temperature Sensitivity

The influence of mutations on the *in vivo* function of Hsp82 was monitored via a drop dilution assay. *S. cerevisiae* strains, which survived the 5'-FOA shuffling, were plated on yeast selection media, lacking histidine and leucine. After 2 d of incubation at 30 °C, colonies from the plates were used to inoculate liquid media, with the same composition. The next day, the OD<sub>600</sub> of the liquid culture was adjusted to 0.5 by diluting with –His/–Leu media. Based on the first sample, a dilution series with five subsequent 1:5 dilutions was prepared. 5  $\mu$ L of each dilution was plated on –His/–Leu yeast selection media and incubated for 48 h. For every mutant, the growth of the dilution series was monitored at 24 °C, 30 °C and 37 °C.

### 3.2.5.4 Radicicol Sensitivity

The inhibitor Radicicol binds with high affinity into the APTase binding pocket of Hsp90 and Hsp82 (Roe et al., 1999). As a result, the activity and functionality *in vivo* and *in vitro* is drastically impaired. To test the influence of Radicicol on the growth of Hsp82 and respective mutants, cells were grown in the presence of the inhibitor (0 - 100  $\mu$ M). *Cerevisiae* strains, which survived the 5'-FOA shuffling,

were plated on yeast selection media, lacking histidine and leucine. After 2 d of incubation at 30 °C, colonies from the plates were used to inoculate liquid media, with the same composition. The next day, the OD<sub>600</sub> of the liquid culture was adjusted to 0.1 by diluting with –His/–Leu media and different concentrations of Radicol. Afterwards, the samples were incubated over night at 30 °C and a dilution series was prepared the next day. Based on the first sample, five subsequent 1:5 dilutions were prepared. 5 µL of each dilution was plated on –His/–Leu yeast selection media and incubated for 48 h at 30 °C.

## 4 Results

### 4.1 Establishing a Human Hsp90 FRET-System

Fluorescence resonance energy transfer (FRET) is a powerful technique for studying protein-protein interactions (Piston & Kremers, 2007). To utilize this technique, site-specific labeling of the proteins with fluorescent donor and acceptor dyes is required. Maleimide dyes that react specifically with cysteine residues are commonly used for this purpose (Kim et al., 2008). The yeast Hsp90 isoforms, Hsp82 and Hsc82, do not contain any native cysteines, which simplifies the introduction and site-specific labeling of an engineered cysteine residue (Hessling et al., 2009). In contrast, the human  $\alpha$  and  $\beta$  Hsp90 isoforms contain six and seven cysteines, respectively, which makes the labeling process challenging (Fig. 13, 14). The reactivity of the solvent exposed native cysteines prevents the introduction of a site-specific label (Nardai et al., 2000). Additionally, post-translational modifications targeting the native cysteine residues affect the regulation of the conformational cycle (Retzlaff et al., 2009).

To address this issue, one possible approach is to express the protein in two fragments, with one protein fragment being labeled and the other containing the native cysteines. The two fragments can then be ligated using a technique called expressed protein ligation (EPL) based on the native chemical ligation (NCL). EPL is a powerful technique that enables the site-specific ligation of synthetic or recombinant proteins, while preserving the native protein backbone (Muir et al., 1998). For Hsp90, a successful expressed protein ligation has already been reported (Karagoz, Sinnige, et al., 2011). The mechanism of EPL involves three key steps: (1) formation of a C-terminal thioester, (2) transthioesterification with a thiol, and (3) ligation with an N-terminal cysteine residue (Fig. 13). The first step can be accomplished by different methods, but a common approach involves using inteins to create the thioester bond, which was employed in this work. The intein undergoes a series of self-catalyzed reactions, including an S-N acyl shift, which ultimately results in the formation of a C-terminal thioester bond between the protein and intein (Muir, 2003). The second step of EPL is the transthioesterification reaction, in which the C-terminal thioester of the protein fragment reacts with a thiol compound, typically 2-mercaptoethanesulfonic acid (MESNA), generating an S-acyl-MESNA intermediate (Hackeng et al., 1999). MESNA is a popular choice for EPL reactions because of its high solubility in aqueous buffers, its ability to reduce thioesters, and its low toxicity. MESNA is also a relatively small molecule, which reduces the likelihood of steric hindrance or interference with the ligation reaction (Kalia & Raines, 2006). Additionally, it is a mild reducing agent that is less likely to interfere with protein stability or activity compared to other more potent reducing agents, such as dithiothreitol (DTT). The third and final step of EPL involves the ligation of the C-terminal fragment to the N-terminal cysteine residue of the other protein fragment. The S-acyl-MESNA thioester intermediate is then ligated to the N-terminal cysteine residue of the other protein fragment, resulting in the formation of a native peptide bond and releasing MESNA. In the ligation step, the thioester reacts with the N-terminal cysteine residue of the

other protein fragment via a transthioesterification reaction, forming a new thioester bond between the two fragments. Once the thioester bond has been formed, an irreversible S-N acyl shift occurs, in which the intermediate acyl-S-thioester bond undergoes a nucleophilic attack by the N-terminal amine of the C-terminal fragment. This results in the formation of a native peptide bond and the release of the thiol byproduct (Dawson et al., 1994).

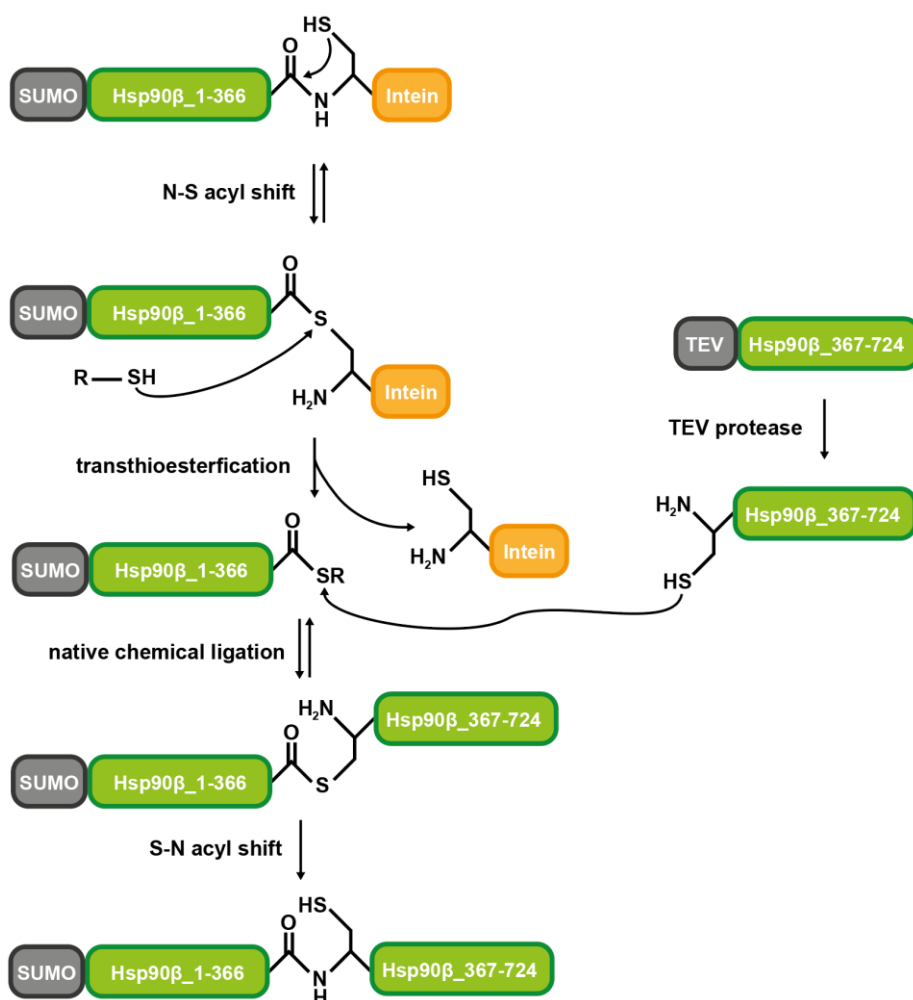


**Figure 13: Schematic overview of the expressed protein ligation.** After the N-S acyl shift, the intein of the N-terminal protein fragment is cleaved by the transthioesterification with MESNA. Subsequently, the cysteine of the C-terminal protein fragment reacts with the formed thioester ligating the two protein fragments. After an irreversible S-N acyl shift, the native backbone of the ligated protein is formed.

#### 4.1.1 Design of Hsp90 Fragments for the Expressed Protein Ligation (EPL)

In this work, three distinct positions were selected for the expressed protein ligation process (Fig. 14). The initial ligation site encompasses the natural cysteine residue at position 366, resulting in an unaltered protein sequence. The second position, as previously documented by Karagoz et al. (2011), includes an engineered cysteine at residue 235 positioned at the charged linker. The third site is located in the N-terminal domain (NTD) at an introduced cysteine residue at position 68. Notably, this residue exists within a loop region and does not appear to affect the protein's activity (Tippel, 2017). All three approaches include all the native cysteines (C366, C412, C521, C564, C589 and C590) in the C-terminal ligation fragment, which enables site-specific labeling of an engineered cysteine, analogous to the yeast Hsp82 FRET system.

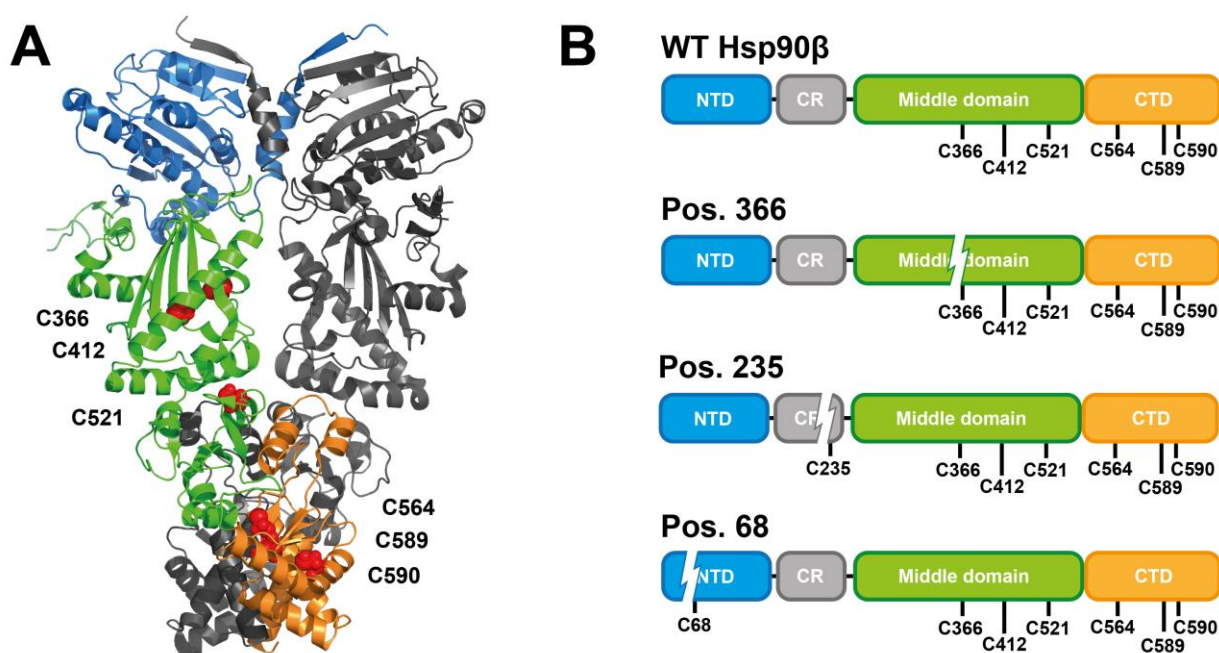


**Figure 14: Ligation sites for the expressed protein ligation of Hsp90 $\beta$ .** **A)** Native cysteines of Hsp90 $\beta$  highlighted as red spheres within the closed structure (PDB: 5fwk (Verba et al., 2016)). Three cysteines are located each in the middle domain (green) and the C-terminal domain (orange). **B)** Schematic illustration of the three possible ligation sites in wildtype Hsp90 $\beta$ . EPL at position 68 and 235 requires the introduction of an additional non-native cysteine at the N-terminus of the C-terminal fragment.

The protein thioester, required for the N-terminal fragment, involves the use of a mutated GyrA intein to create a protein with a C-terminal thioester (Southworth et al., 1999). The GyrA intein is a type of cis-splicing intein that is found in the gyrase A subunit of bacteria (Telenti et al., 1997). The mutated GyrA intein used in this work has a mutation that blocks the splicing of the intein, allowing it to remain attached to the N-terminal protein fragment and retain its C-terminal thioester (Evans et al., 1998). The thioester bond is formed between the intein and the N-terminal protein fragment by a thiolate ion, which is generated by the adjacent residue in the intein sequence. This thiolate ion attacks the carbonyl group of the C-terminal amino acid of the N-terminal protein fragment, forming a thioester intermediate.

Afterwards, the thioester intermediate can be converted into a stable thioester bond by the addition of a thiol reagent, such as MESNA. The thiol attacks the thioester intermediate, displacing the intein-derived thiol and forming a stable thioester bond between the N-terminal protein fragment and the MESNA molecule. Additionally, to improve the solubility and prevent protein misfolding, the fragment was expressed as a fusion protein carrying an N-terminal SUMO tag with an additional hexa-histidine (6xHis) tag and a chitin binding domain (CBD) attached to the intein (Peroutka Iii et al., 2011; Watanabe et al., 1994). This enabled the selective purification of the tagged protein via Ni-NTA affinity chromatography after bacterial expression and the removal of the intein after thioester formation.

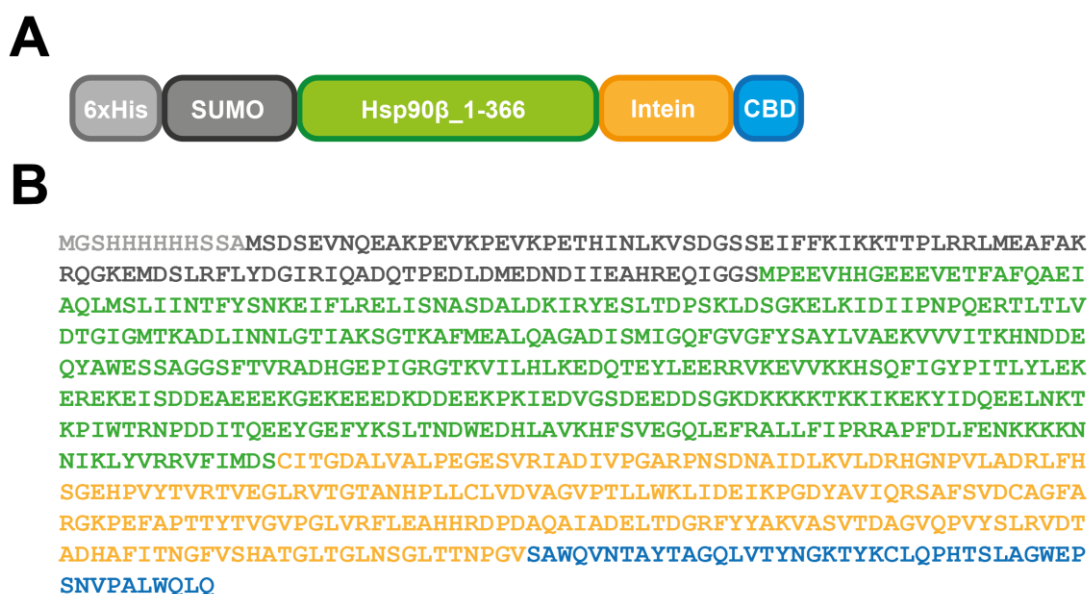


**Figure 15: Design of the N-terminal EPL fragment.** **A)** Schematic illustration of the Hsp90 $\beta$ -intein fragment for the ligation at position 366, which includes a hexa-His SUMO solubility tag and a chitin-binding domain. **B)** Exemplary full protein sequence for the N-terminal ligation fragment at the native cysteine residue 366. Functional elements are color coded according to (A).

To create the N-terminal cysteine residue in the recombinant protein fragment, various genetic engineering techniques can be used. One approach involves introducing a TEV (tobacco etch virus) cleavage site upstream of the desired cysteine residue (Fig. 16). After protein expression, the recombinant protein was purified and treated with TEV protease, which specifically cleaves the protein after the ENLYFQ motif (Chattopadhyaya et al., 2009). This generates an N-terminal cysteine residue, which was used for the ligation reaction. In the ligation step, the thioester group reacts with the N-terminal cysteine residue, resulting in a transthioesterification reaction. This intermediate then undergoes an S-N acyl shift, which generates a native peptide bond at the ligation site, forming a seamless protein backbone (Muir et al., 1998).



**Figure 16: Design of the C-terminal EPL fragment.** A) Schematic illustration of the Hsp90 $\beta$  fragment for the ligation at position 366, which includes a hexa-His tag and a TEV cleavage site. B) Exemplary full protein sequence for the C-terminal ligation fragment at the native cysteine residue 366. Functional elements are color coded according to (A).

#### 4.1.2 Expressed Protein Ligation of Hsp90

The N-terminal fragments for the EPL were cloned into a pET28b plasmid containing a 6xHis-SUMO solubility tag. Additionally, the intein from a pTXB1 plasmid, which includes a maltose binding protein (MBP), was cloned to the C-terminus of the respective Hsp90 fragment. Afterwards, proteins were expressed in *E. coli* and purified *via* affinity and size exclusion chromatography. The first steps of the expressed protein ligation involved the formation of the thioester and the transthioesterification of the intein with MESNA. An adapted protocol from the IMPACT™ Kit (New England Biolabs) was employed to initiate the intein cleavage. To test the efficiency of the thioester formation, 5 mg of the N-terminal Hsp90 $\beta$ \_1-366 fragment were incubated in cleavage buffer (20 mM HEPES pH 8/8.5/9, 500 mM NaCl, 1 mM EDTA, 50 mM MESNA) at 20 °C for 72 h. The kinetic of the resulting intein cleavage was monitored and analyzed by SDS-Page (Fig. 17A). An excess of MESNA in the buffer prevents the reverse reaction with the intein and results in the Hsp90 $\beta$ -MESNA thioester as the main reaction product. After 72 h, the formed band of the thioester (56 kDa), as well as the intein band can be observed (27 kDa). However, neither an increased temperature (Fig. 17B), nor variations of the pH value resulted in an acceptable amount (< 10 %) of thioester for the following ligation reactions.

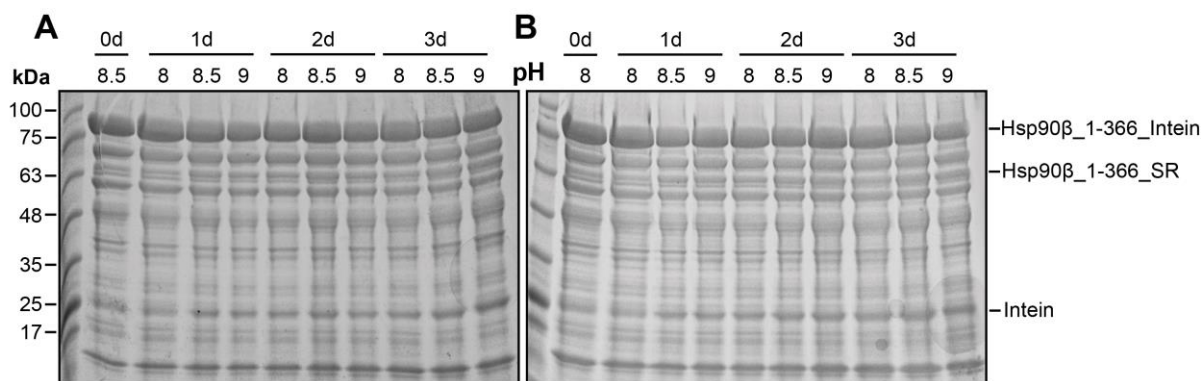


**Figure 17: Thioester formation of Hsp90 $\beta$ \_1-366.** The ability of the N-terminal Hsp90 fragment (1-366) to cleave the intein and form the reactive thioester was tested and analyzed via SDS-Page. The protein was incubated with cleavage buffer (20 mM HEPES, 500 mM NaCl, 1 mM EDTA, 50 mM MESNA) at 20 °C (**A**) and 30 °C (**B**) for up to 72 h. Furthermore, the influence of varying pH values (pH 8, 8.5, 9) on the kinetics was evaluated. The formed Hsp90 $\beta$  thioester band can be observed at 56 kDa, the cleaved intein at 27 kDa and the Hsp90 $\beta$  fragment with the intein attached at 83 kDa.

The efficiency of the intein cleavage and the accompanying thioester formation are strongly dependent on the N-terminal residue of the intein's cysteine. Serine N-terminal of the cysteine residue can lead to low thioester yields when used in combination with the GyrA intein (Goulatis et al., 2019; Xu, 2000). Therefore, the serine residues of the N-terminal fragments flanking the intein were mutated to asparagine for position 235 and 366 to improve the thioester formation (Chong et al., 1998). For both proteins, the mutation led to sufficient intein cleavage and the resulting thioester was used for the native chemical ligation.

The C-terminal fragments required for the ligation were cloned in a pET-M11 plasmid with a TEV cleavage motif upstream of the N-terminal cysteine. Proteins were expressed in *E. coli* and purified *via* affinity and size exclusion chromatography after incubation with TEV protease. However, for the ligation at residue 68, no sufficient expression for the C-terminal fragment was achieved. For the ligation at position 235 and 365, the N- and C-terminal fragments were mixed (1:2) and incubated for several days at room temperature. For the approach at residue 235, only a minimal formation of the ligated Hsp90 was observed, which could not be improved over several days of incubation (Figure 18A). The high structural flexibility of the charged linker limits the yields of the ligation at this position (Karagoz, Sinnige, et al., 2011). A deletion of the linker results in higher amounts of ligated product, but the protein drastically differs from the wildtype Hsp90. The ligation at position 365 displayed an increased formation of full-length Hsp90 with an efficiency between 5 – 10 % (Figure 18B). Low yields for this position are most likely caused by the location of the cysteine residue in the middle of the MD, limiting the accessibility of the C-terminal fragment.

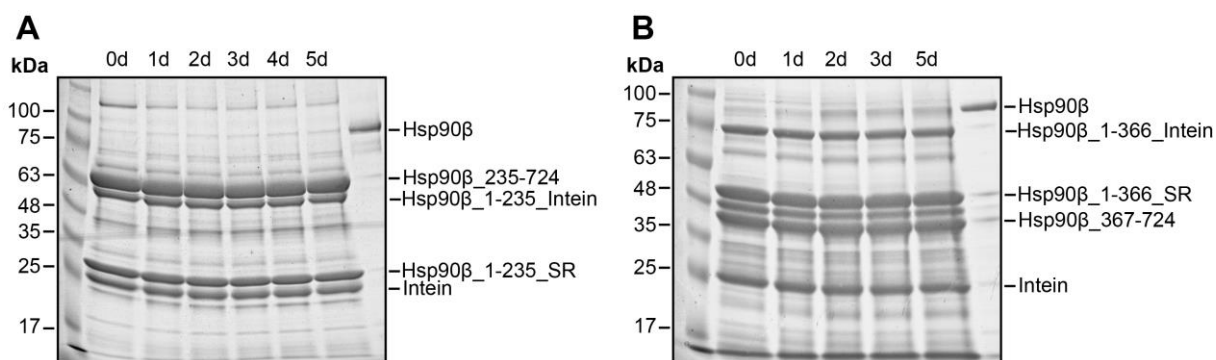


**Figure 18: Expressed protein ligation for full-length Hsp90 $\beta$ .** SDS-Page analysis of the one-pot reaction at position 235 (A) and 366 (B). The N-terminal intein fragment was incubated in cleavage buffer (pH 8) for 24 h at 20 °C to initiate the thioester formation. Samples were mixed with the C-terminal protein, containing the free cysteine residue, and incubated for five days at 20 °C (50  $\mu$ M final protein concentration). Varying time points of the diluted EPL reaction were loaded onto the gel to analyze the kinetics end efficiency of the full-length Hsp90 $\beta$  formation.

#### 4.1.3 Optimization of the Hsp90 Expressed Protein Ligation

The transthioesterification reaction after the MESNA-induced intein cleavage involves the reaction with free cysteines in the environment. To avoid the reverse reaction with the intein's cysteines and enhance the reaction with the C-terminal Hsp90 fragment to improve the yields, the intein was removed after MESNA cleavage by SEC. The EPL reaction is usually carried out at pH 7 – 8 to ensure chemoselectivity of the ligation (Muralidharan & Muir, 2006). However, depending on the protein, the efficiency of the reaction can be optimized by testing different pH values (Hauser & Ryan, 2007; Mills & Perler, 2005). Therefore, the ligation efficiency was tested and compared at pH 6.8, pH 8 and pH 9 (Fig. 19).

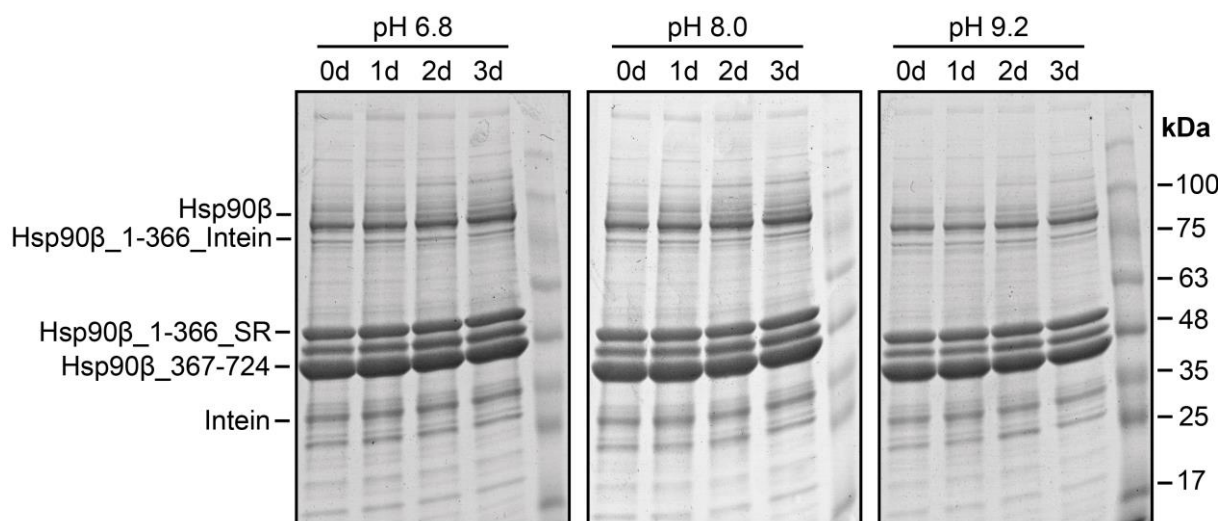


**Figure 19: EPL for the formation of full-length Hsp90 $\beta$  at varying pH values.** SDS-Page analysis of the ligation at position 366 at pH 6.8, 8 and 9.2. Cleaved intein was removed by SEC prior to the reaction. The N-terminal intein fragment was incubated in cleavage buffer (pH 8) for 24 h at 20 °C to initiate the thioester formation. Samples were mixed with the C-terminal protein, containing the free cysteine residue, and incubated for three days at 20 °C (50  $\mu$ M final protein concentration). Varying

## Results

time points of the diluted EPL reaction were loaded onto the gel to analyze the kinetics end efficiency of the full-length Hsp90 $\beta$  formation.

Neither basic nor more acidic conditions led to a significant improvement of the ligation. Similar to the reaction at pH 8, a maximal ligation efficiency of 3 – 8 % was achieved. Furthermore, longer incubation times did not increase the yield. Therefore, the limiting factor of the reaction is most likely the accessibility of the formed thioester for the C-terminal Hsp90 fragment. To exclude protein stability or aggregation as a cause for the low efficiency, the reaction was conducted in the presence of 250 mM L-arginine (Fig. 20A). Arginine is commonly used for protein refolding and can suppress protein aggregation (Buchner et al., 1992; Tsumoto et al., 2004). Additionally, to exclude deactivation of the formed MESNA thioester by hydrolysis, intein cleavage was performed using chitin beads as solid phase (Fig. 20B). The chitin-binding domain (CBD) fused to the intein enables the phase separation of the formed thioester and the ligation can be performed without the need to remove the intein. The thioester displays no affinity towards the chitin beads and is mainly present in the supernatant (Evans et al., 1998).

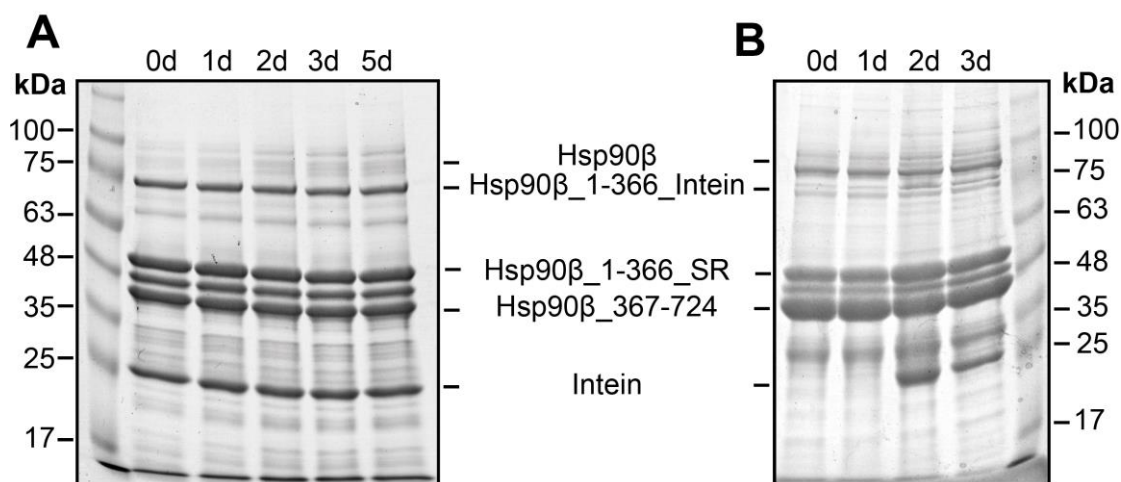


**Figure 20: EPL for the formation of full-length Hsp90 $\beta$  in the presence of L-arginine and chitin beads.** SDS-Page analysis of the ligation at position 366 in the presence of 250 mM arginine (A) and chitin beads (B). Samples were mixed with the C-terminal protein, containing the free cysteine residue, and incubated for up to five days at 20 °C (50  $\mu$ M final protein concentration). Varying time points of the diluted EPL reaction were loaded onto the gel to analyze the kinetics end efficiency of the full-length Hsp90 $\beta$  formation.

The addition of arginine to the ligation did not result in an increased formation of the ligated Hsp90. Therefore, a protein stability or aggregation related effect causing the low yields can be excluded. The ‘one-pot’ reaction with chitin beads displayed the same yields for the ligated product as without beads. Hence, intein deactivation by hydrolysis is unlikely. Heterodimer formation, low yields and several required subsequent purification steps of the ligated product complicate the goal of pure ligated Hsp90. Sterically demanding proteins often drastically influence yields of the expressed protein ligation (Muir et al., 1998). Different ligation sites, with increased accessibility, could improve the ligation efficiency. However, as alternative splicing sites would require the introduction of at least a cysteine residue in the

native sequence of Hsp90, this could result in non-native disulfide bonds, which would influence enzymatic activity and protein structure.

#### 4.1.4 Design of Hsp90 Fragments for SrtA Mediated Ligation

Ligation with Sortase A (SrtA) offers an alternative ligation method to the EPL reaction. Furthermore, Sortase A has already been successfully employed in the context of NMR experiments for Hsp90 (Freiburger et al., 2015). SrtA is a transpeptidase enzyme that is essential for the assembly of the cell wall in Gram-positive bacteria. It recognizes and cleaves the LPXTG (Leu-Pro-X-Thr-Gly) motif present in surface proteins, anchoring them to the cell wall. The enzyme recognizes the motif at the C-terminus of the protein and cleaves the amide bond between the threonine and glycine residues of the LPXTG motif. This generates a new N-terminal thioester on the C-terminal fragment of the protein or peptide substrate with the enzyme. In the final step, the N-terminal thioester reacts with an amino nucleophile present on the N-terminal fragment, typically an N-terminal glycine residue. This reaction results in the formation of a new peptide bond between the two fragments, mediated by the thioester formed during the cleavage step. Similar to the EPL (see 4.1.1), this approach enables the site-specific labeling of a cysteine in the N-terminal fragment. The C-terminal Hsp90 fragment, that includes the six native cysteine residues, can be ligated to the labeled protein afterwards (Fig. 21).

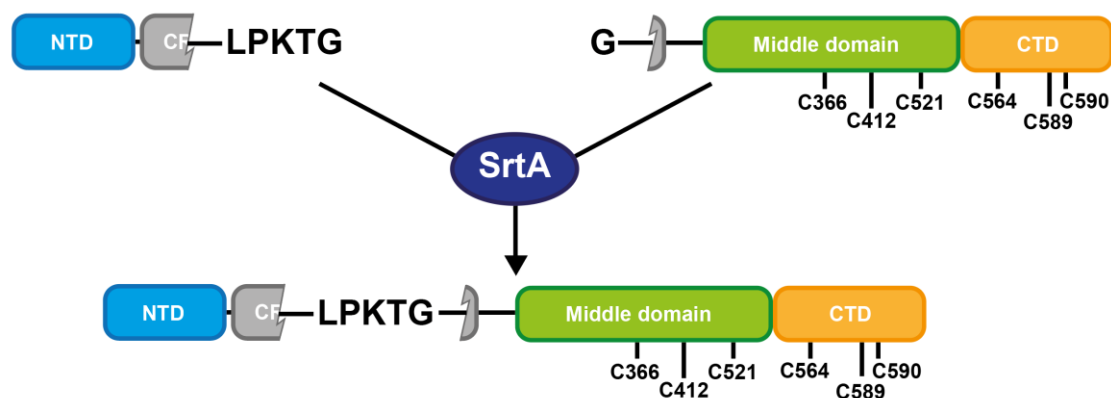


**Figure 21: Schematic illustration of the Sortase A ligation of Hsp90 $\beta$ .** The N-terminal fragment contains the LPKKTG Sortase recognition motif in the charged linker region. The C-terminal Hsp90 fragment includes the six native cysteines, the M and C domains and an N-terminal glycine required for the ligation. After the SrtA mediated ligation, full-length Hsp90 contains the LPKKTG motif in the charged linker.

The N-terminal fragment used for the Hsp90 ligations contains the LPXTG motif in order to be recognized and cleaved by the Sortase enzyme (Fig. 22). This motif consists of a conserved sequence of five amino acids: leucine (L), proline (P), any amino acid (X), threonine (T), and glycine (G). The LPXTG motif serves as a recognition signal for Sortase enzymes, allowing them to identify and specifically cleave the protein or peptide at the C-terminal side of the threonine residue within the motif.

Based on the preliminary work by Franziska Toppel, the Sortase A ligation motif was introduced in the flexible linker region of Hsp90. For the design of the N-terminal fragment, several aspects were considered. The protein is expressed with a maltose binding protein fusion tag, which enhances solubility and prevents aggregation during the recombinant expression. The 6xHis tag, N-terminal of the MBP, makes the removal of the TEV cleaved protein by affinity chromatography possible. Individual domains of Hsp90 are stable. Therefore, the ligation in the flexible linker does not interfere with the stability of the protein and facilitates accessibility for the enzyme. The X amino acid of the motif can either be D, E, A, N, Q or K to provide sufficient yields of the ligation. The Hsp90 charged linker region includes multiple lysine residues at the ligation site, rendering it a suitable amino acid for the incorporation into the Sortase ligation motif.

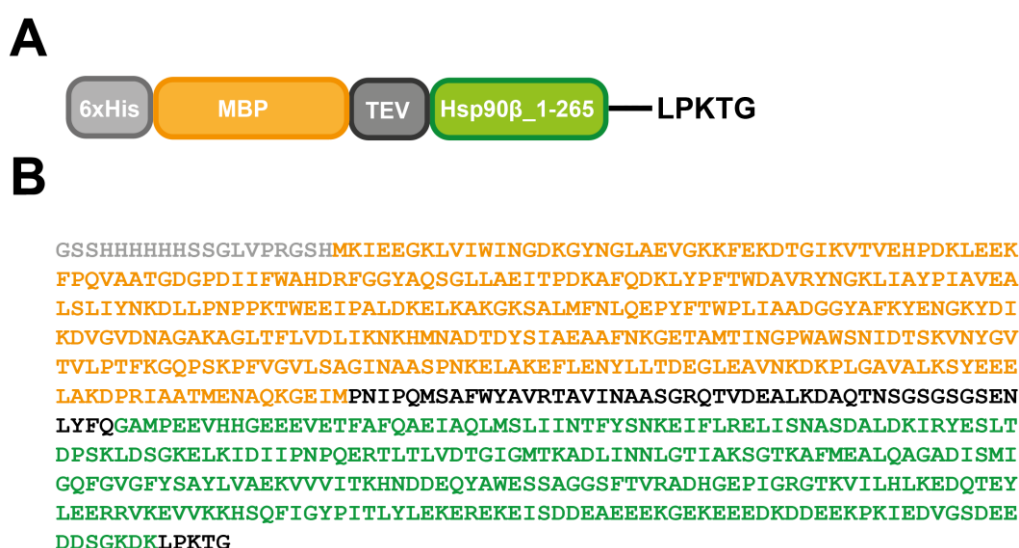


**Figure 22: Design of the N-terminal Sortase fragment.** **A)** Schematic illustration of the Hsp90 $\beta$ -LPKTG fragment for the ligation at the charged linker, which includes a hexa-His MBP solubility tag and the LPKTG motif. **B)** Full protein sequence for the N-terminal ligation fragment. Functional elements are color coded according to (A).

To create the N-terminal glycine residue in the recombinant protein fragment, a TEV cleavage site and a maltose binding protein upstream of the desired glycine residue was used (Fig. 23). After protein expression, the recombinant protein was purified and treated with TEV protease, which cleaves the protein after the ENLYFQ motif (Chattopadhyaya et al., 2009). This generates an N-terminal glycine residue, which was used for the ligation reaction. The MBP contains a 6xHis tag, which allowed the removal of the cleaved protein from the C-terminal fragment after TEV cleavage. Multiple N-terminal glycines enhance the recognition of the protein by SrtA (Chan et al., 2007). However, a successful ligation was already established for Hsp90 with only one glycine, which minimalizes the number of introduced mutations (Toppel, 2017). In the final ligation step, the N-terminal glycine residue reacts with the SrtA-Hsp90 thioester, resulting in the ligated protein.



**Figure 23: Design of the C-terminal Sortase ligation fragment.** A) Schematic illustration of the Hsp90 $\beta$  fragment for the ligation at the charged linker, which includes a hexa-His tag, MBP and a TEV cleavage site. B) Full protein sequence for the C-terminal ligation fragment. Functional elements are color coded according to (A).

#### 4.1.5 SrtA Mediated Ligation of Hsp90

In the first step of the ligation, Sortase A recognizes and binds to the LPKTG motif on the C-terminus of Hsp90 (Fig. 24). The enzyme recognizes the threonine (T) residue within this motif and forms a covalent bond between the carboxyl group of the threonine and its active site. The active site of Sortase A comprises a highly conserved cysteine residue that acts as a nucleophile during the cleavage step of the reaction. This cysteine residue attacks the carbonyl carbon of the scissile bond, forming a thioester intermediate with the recognized motif. This intermediate allows the Sortase A enzyme to cleave the peptide bond between the threonine and glycine residues within the LPKTG motif, resulting in the release of the C-terminal glycine and the formation of a thioester bond on the C-terminus of the Hsp90 fragment. During the ligation step, the reactive thioester bond is attacked by the amino group of the N-terminal glycine, resulting in the formation of a new peptide bond between the two Hsp90 fragments. After the SrtA mediated ligation, the full-length Hsp90 contains the LPKTG motif in the charged linker.

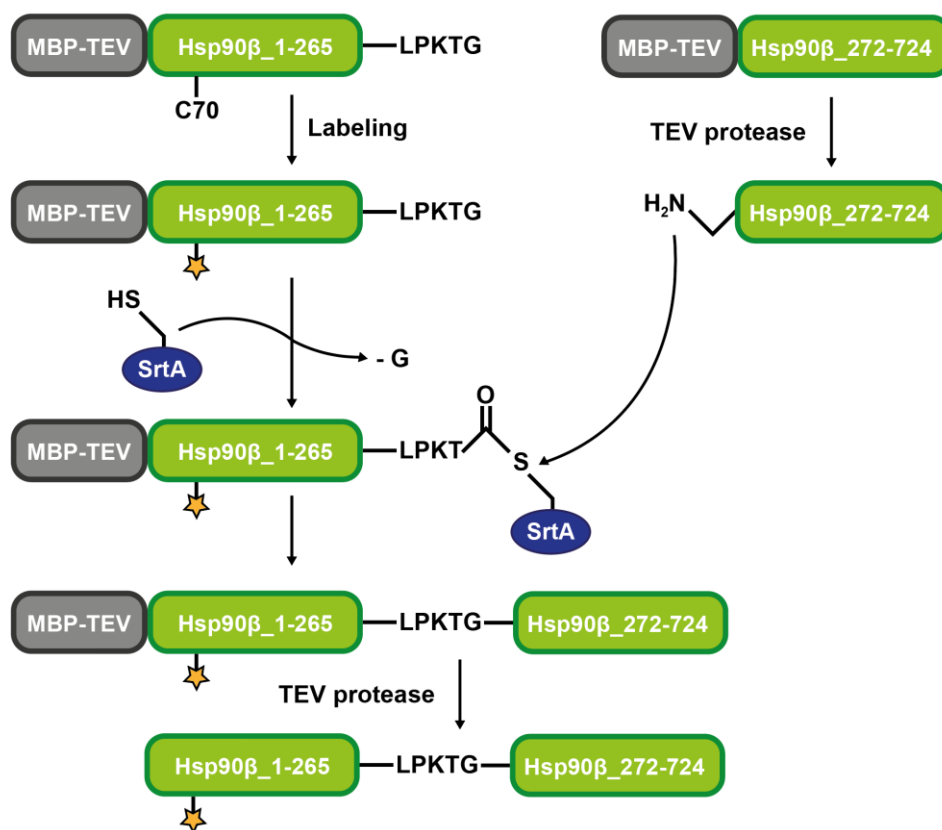


**Figure 24: Overview of the Sortase A mediated ligation.** After labeling of the N-terminal Hsp90 fragment, Sortase A recognizes the LPKTG motif, cleaves the peptide bond between threonine and glycine and forms a thioester intermediate. After the SrtA mediated ligation, full-length Hsp90 contains the LPKTG motif in the charged linker and a site-specific label at an introduced cysteine.

For the ligation of Hsp90, an optimized protocol for the Hsp90 constructs was used (Freiburger et al., 2015; Tippel, 2017). The published protocol recommends conducting the ligation in an amicon filter unit to remove the cleaved glycine during the reaction, in order to optimize the yields of the ligation. In this work, Sortase 5M was used, which has a 140-fold increased affinity to the LPXTG motif, resulting in a reduced reaction time and optimized yields (Chen et al., 2011). Therefore, the ligation reaction was performed in an Eppendorf tube at room temperature using 5 mg of each Hsp90 fragment and 5 mg of the Sortase 5M (Fig. 25). To assess the efficiency of the ligation, SDS-PAGE analysis was conducted. After just 30 minutes of reaction time, the ligated Hsp90, still containing the MBP solubility tag, was obtained. No further yield improvement was observed after prolonged incubation of the ligation mixture. However, multiple bands over 120 kDa were visible on the gel. During bacterial expression of the protein, the N-terminal methionine is excised by the methionyl-aminopeptidase (MAP) (Hirel et al., 1989). This results in the N-terminal Hsp90 ligation fragment having an exposed glycine, which can potentially lead to ligation with another N-terminal protein.

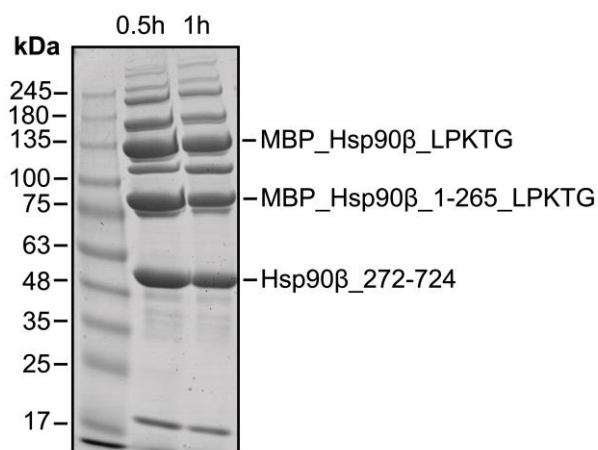


**Figure 25: SDS-Page of the Sortase 5M mediated ligation of Hsp90 $\beta$ .** A test reaction was performed at room temperature using 5 mg of each Hsp90 fragment and 5 mg of Sortase 5M in ligation buffer (50 mM Tris, pH 8.0, 150 mM NaCl, 20 mM CaCl<sub>2</sub>, 1 mM DTT). Samples were collected at 30 minutes and 1 hour, and analyzed by SDS-PAGE. The formation of MBP\_Hsp90 $\beta$ \_LPKTG (~127 kDa) from the two fragments (~53 kDa and ~74 kDa) indicates successful ligation.

#### 4.1.6 Optimization of the SrtA Mediated Protein Ligation

To improve the initial approach for Sortase-mediated ligation of Hsp90, the glycine residue following the start codon-encoded methionine was deleted through mutagenesis. This step excludes side product formation by self-ligation. Ligation with a labeled N-terminal fragment did not affect the reaction kinetics or efficiency (Fig. 26). Successful ligation was confirmed by the formation of a ~127 kDa band of MBP\_Hsp90 $\beta$ \_LPKTG\* by SDS-PAGE analysis. The decrease in band intensity of the N-terminal fragment (~74 kDa) further confirmed the ligation. Similar to the unlabeled protein, no additional product formation was observed after 30 minutes, indicating that the reaction was already complete at this point. Therefore, Sortase 5M as well as the glycine deletion significantly improved the efficiency and purity of the ligation reaction.

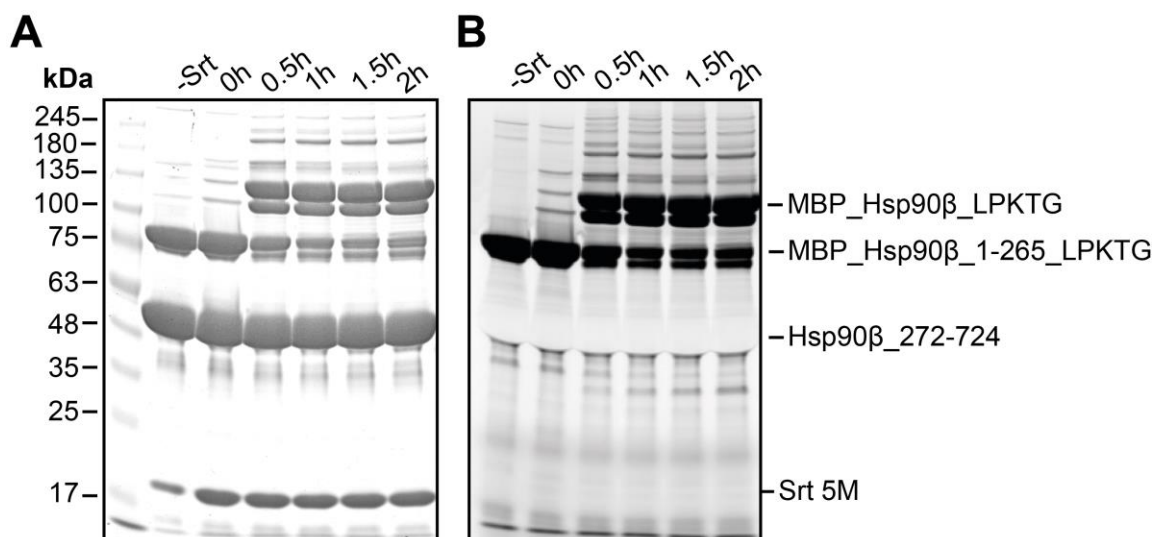


**Figure 26: SDS-Page of the Sortase 5M mediated ligation of Hsp90β.** **A)** The Sortase 5 M ligation was performed at room temperature using 2.5 mg of the labeled N-terminal Hsp90 fragment and 5 mg of the C-terminal protein in ligation buffer (50 mM Tris, pH 8.0, 150 mM NaCl, 20 mM CaCl<sub>2</sub>, 1 mM DTT). The reaction was initiated by the addition of 2.5 mg Sortase 5M. Samples were collected at varying time points, and analyzed by SDS-PAGE. The formation of MBP\_Hsp90β\_LPKTG (~127 kDa) from the two fragments (~53 kDa and ~74 kDa) indicates successful ligation. **B)** Gel shown in (A) analyzed by a fluorescent image scanner highlighting only labeled protein bands.

To prepare the protein for *in vitro* experiments, educts, side products, and Sortase 5M were removed via chromatography. The labeled N-terminal Hsp90 fragment was separated using ion exchange chromatography (IEX). However, Hsp90 dimers that included non-ligated MC protein could not be completely removed using this purification strategy (Fig. 27A). Separation of the MC protein would require impairing Hsp90's ability to dimerize, which was not feasible given the nanomolar affinity of the Hsp90 CTDs (REF). A subsequent TEV cleavage and reverse Ni-NTA affinity chromatography was employed to remove the MBP solubility tag and Sortase enzyme (Fig. 27B). Overall, the ligation produced sufficient amounts of ligated protein for multiple subsequent experiments and was of sufficient purity.

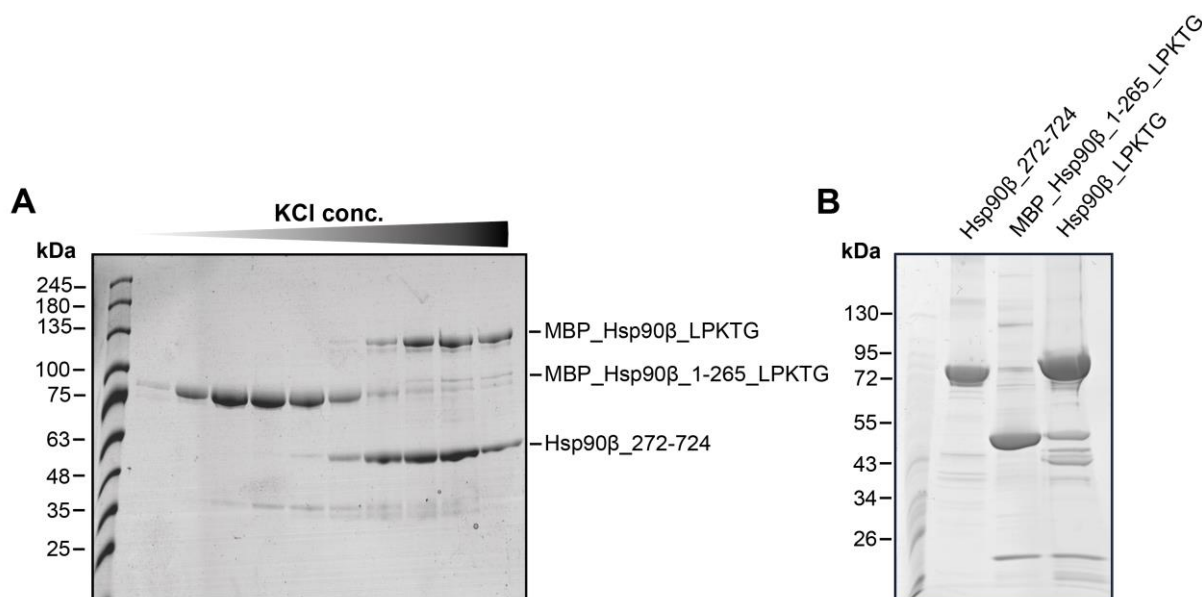


**Figure 27: SDS-Page analysis of the purification of ligated Hsp90 $\beta$ .** **A)** The separation of the N-terminal Hsp90 fragment by IEX was analyzed using a Coomassie stained SDS-Page gradient gel (4 – 12 %). During the first purification step, the ligated Hsp90 protein (~127 kDa) and heterodimers with non-ligated MC fragment (~53 kDa) were separated from the Sortase enzyme and side products. **B)** Cleavage of the MBP solubility tag using TEV protease and subsequent Ni-NTA affinity chromatography resulted in full-length Hsp90 protein, which was used for subsequent experiments (see right lane). Purity of the protein was analyzed *via* SDS-Page gradient gel (4 – 12 %) with Coomassie staining.

#### 4.1.7 *In Vitro* Characterization of SrtA Ligated Hsp90

To assess whether the introduced LPKTG motif in the charged linker region of Hsp90 affected its structure and function, *in vitro* characterization experiments were conducted. The mutated protein was compared to the wildtype protein. Far-UV CD spectra revealed that the mutated protein displays a nearly identical structure to wildtype Hsp90 (Fig. 28A). However, it is important to note that Far-UV CD spectroscopy can only detect secondary structural elements with chirality (Whitmore & Wallace, 2008). The charged linker region of Hsp90 is highly flexible and lacks structural elements, which most likely cannot be observed by CD spectroscopy. The structural integrity of the mutated Hsp90 was also confirmed by the thermal stability of the protein. Nearly identical thermal unfolding was observed in the presence of Sypro Orange compared to wildtype Hsp90 (Fig. 28B). The obtained melting point of 55 °C was very similar to that of wt Hsp90 (56 °C). Taken together with the CD spectroscopy measurements, this demonstrates that the introduced mutation does not appear to alter the protein's structure and stability. Hsp90 is an ATP-dependent chaperone (Obermann et al., 1998). Therefore, the enzymatic activity of the mutated protein was compared to that of wildtype Hsp90 (Fig. 28C). The obtained ATPase activity rate (0.79 min<sup>-1</sup>) did only slightly differ from the wildtype protein (0.90 min<sup>-1</sup>). Hence, the introduced LPKTG motif in the linker does most likely not influence the hydrolysis rate of the mutated protein.

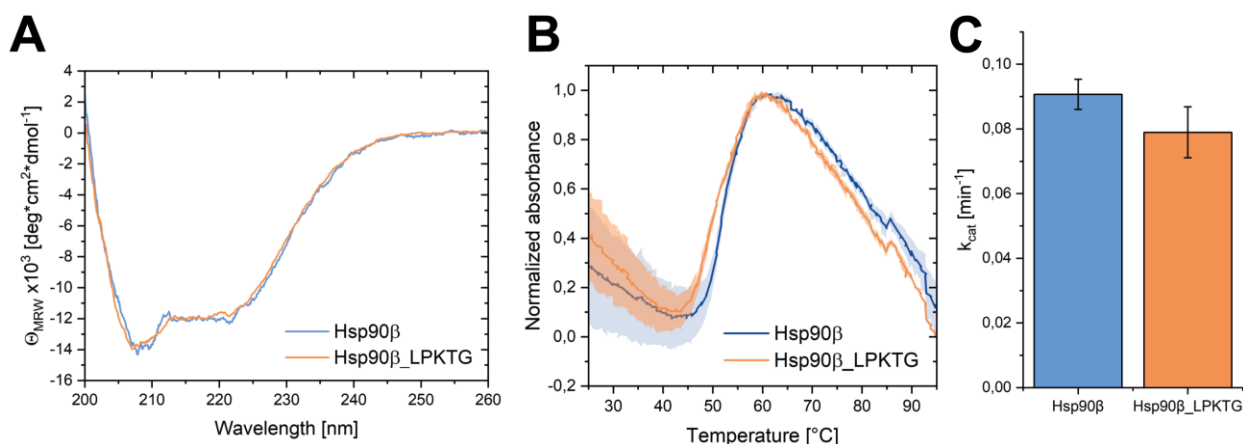


**Figure 28: *In vitro* characterization of Hsp90 $\beta$  containing the LPKTG motif. A)** The secondary structure of wt Hsp90 $\beta$  was compared to Hsp90 $\beta$ \_LPKTG by far UV spectroscopy. Spectra were recorded at a concentration of 0.2 mg/mL in 50 mM phosphate buffer (pH 7.4) at room temperature. **B)** Thermal stability of the proteins was compared by a thermal shift assay with Sypro orange. The assay was conducted in HKM buffer with 0.25 mg/mL of protein at a heating rate of 1 °C/min. **C)** Comparison of ATPase activity of wildtype and mutated Hsp90 $\beta$ . Hydrolysis rate was measured using a regenerative ATP system. The assay was performed in HKM buffer (40 mM HEPES, pH 7.4, 150 mM KCl, 5 mM MgCl $_2$ ) with 2 mM ATP and 10  $\mu$ M of Hsp90 at 37 °C. Measurements were performed as three independent technical replicates to calculate means and standard deviations. Obtained activity was corrected for background activity using Radicolol.

Hsp90's enzymatic activity requires the formation of a closed state, where the N-terminal domains (NTDs) dimerize, and ATP is hydrolyzed. To assess the ability of the mutated protein, containing the introduced LPKTG motif, to initiate this compact state, limited proteolysis was conducted. Limited proteolysis is a powerful technique that can be used to study protein structure and conformational changes by selectively cleaving a protein with a protease. By comparing the digestion patterns of the protein in different conditions, important insights can be gained into its structure and function. In this case, by incubating the protein with a slowly hydrolysable ATP analogue, such as ATP $\gamma$ S, Hsp90 can be trapped in the closed state. Protein pre-incubated with 2 mM ATP $\gamma$ S in high salt closing buffer (20 mM HEPES, pH 7.5, 500 mM KCl, 5 mM MgCl $_2$ , 6 mM  $\beta$ -mercaptoethanol), displayed an increased resistance against the protease  $\alpha$ -chymotrypsin compared to the apo protein (Fig. 29). The closed state of Hsp90 has a decreased accessibility to crucial cleavage sites, resulting in a prolonged presence of uncleaved peptides. This result suggests that the mutation does not affect the formation of the closed state of Hsp90. Overall, the *in vitro* experiments provide strong evidence that the introduced LPKTG motif does not perturb the structure conformational transitions and ATPase function of Hsp90.

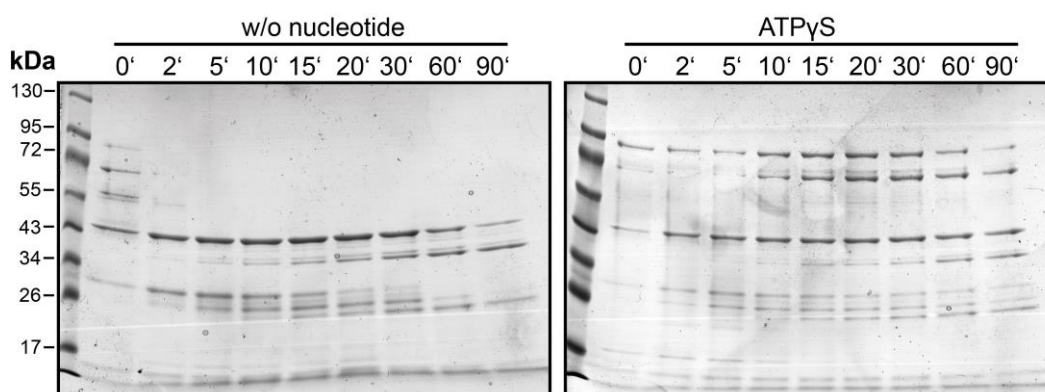


**Figure 29: Conformational rearrangements of Hsp90<sub>β</sub>\_LPKTG characterized by limited proteolysis.** Mutated Hsp90<sub>β</sub>, containing the LPKTG motif in the charged linker, was subjected to the protease  $\alpha$ -chymotrypsin (Hsp90: $\alpha$ -chymotrypsin 1:20). Proteolysis was conducted in HKM buffer at room temperature in the absence (left) or presence (right) of ATP $\gamma$ S. The reaction was stopped at the time points indicated with 2 mM PMSF and analyzed by SDS-Page analysis (4 – 12 % gradient).

#### 4.1.8 *In Vitro* Characterization of Labeled Hsp90

FRET is a method used to study the interaction between two molecules or regions of one protein by measuring energy transfer from an excited donor molecule to an acceptor molecule in close proximity (Jares-Erijman & Jovin, 2003). This technique has been used to investigate the conformational changes and interaction between Hsp90 and its co-chaperones as well as between the NTDs during the ATPase cycle (Hessling et al., 2009; Li et al., 2013). The ligated Hsp90<sub>β</sub>\_LPKTG was selectively labeled in the NTD with either Atto532 or Atto647N. Mixing the donor- and acceptor-labeled proteins results in a hetero-complex having both fluorescent dyes due to the subunit exchange of Hsp90 (Retzlaff et al., 2010). This FRET system was used to track changes in acceptor fluorescence following the addition of various nucleotides under different salt conditions (Fig. 30). The acceptor fluorescence signal depends solely on the energy transfer of the donor dye, allowing for exclusion of quenching and bleaching effects during measurement. Surprisingly, the highest increase in acceptor signal was observed under all tested conditions when no nucleotide was added. ATP, ATP $\gamma$ S, and AMP-PNP led to similar increases in signal. However, the data presented includes measurement times of up to 10 h, which exceeds the expected time frame required for Hsp90 to form the closed state (Zierer et al., 2016). Moreover, without any added nucleotide or with ATP added, Hsp90 predominantly populates an open conformation (Wolf et al., 2021). Therefore, the observed increase in the acceptor signal is unlikely to be caused by the formation of the closed state of Hsp90. One possible explanation for the observed signal increase could be aggregation or N-terminal oligomerization of the protein. The decreased signal compared to the sample without nucleotide added can be explained by the normal cycle progression of Hsp90 or the closed state competing with protein aggregation/oligomerization.

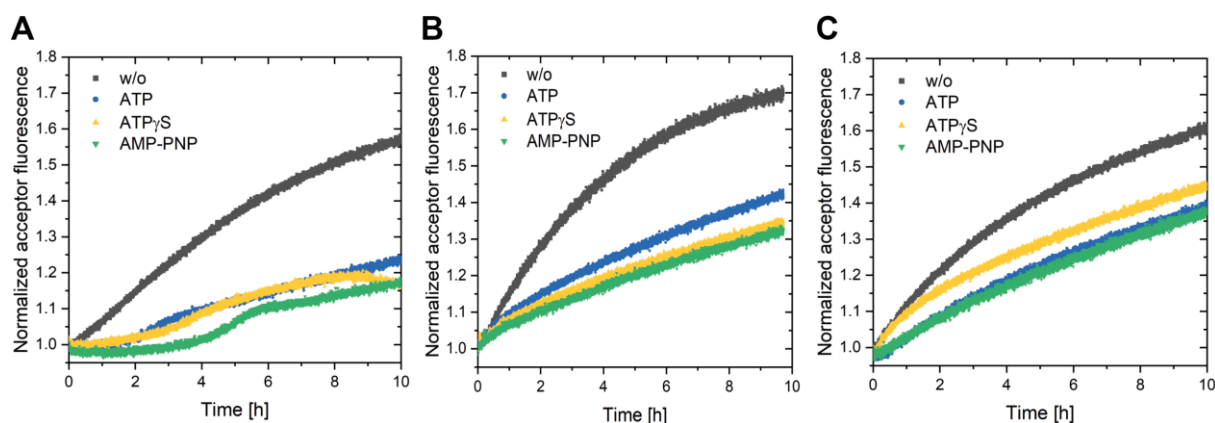


**Figure 30: Nucleotide induced conformational changes determined by FRET.** FRET kinetics of the acceptor fluorescent signal have been measured in closing buffer (20 mM HEPES, 5 mM MgCl $_2$ , 6 mM  $\beta$ -mercaptoethanol) with varying salt concentrations (**A**: 50 mM KCl, **B**: 500 mM KCl, **C**: 500 mM (NH $_4$ ) $_2$ SO $_4$ ). Donor- and acceptor-labeled protein were incubated at the measured buffer for 1 h at 37 °C to initiate labeled heterodimer formation via protein subunit exchange. Measurements were performed at 37 °C with a final protein concentration of 1  $\mu$ M. The addition of 2 mM nucleotide initiated the reaction.

To exclude aggregation as the cause for the increase in acceptor signal, light scattering at 360 nm was measured simultaneously with the fluorescent signal (Fig. 31A). The absence of a significant increase at 360 nm indicates that the protein is stable and does not precipitate under the buffer conditions used. Numerous publications on Hsp90 report temperature-dependent oligomerization (Chadli et al., 1999; Yonehara et al., 1996), which interestingly, correlates with the protein's melting point obtained from the thermal shift assay (see 4.1.7). To investigate the temperature dependence of the acceptor signal, the sample was cooled after 90 minutes of incubation at 37 °C (Fig. 31B). Following an initial increase in fluorescence, the signal starts to decrease as soon as the temperature is lowered to 20 °C, indicating a correlation with oligomerization and temperature. The co-chaperone p23 inhibits ATPase activity and is known to bind in the cleft of the NTDs in the closed state (Ali et al., 2006; McLaughlin et al., 2006). The addition of p23 during the ensemble FRET experiments significantly reduced the increase in acceptor signal (Fig. 31C). However, even with p23 added, no difference was observed between the absence of nucleotide and the presence of ATP $\gamma$ S. Nonetheless, the results strongly suggest that the observed increase is caused by N-terminal oligomerization of the protein. The addition of nucleotide or p23 initiates a closed state that prevents this reaction.

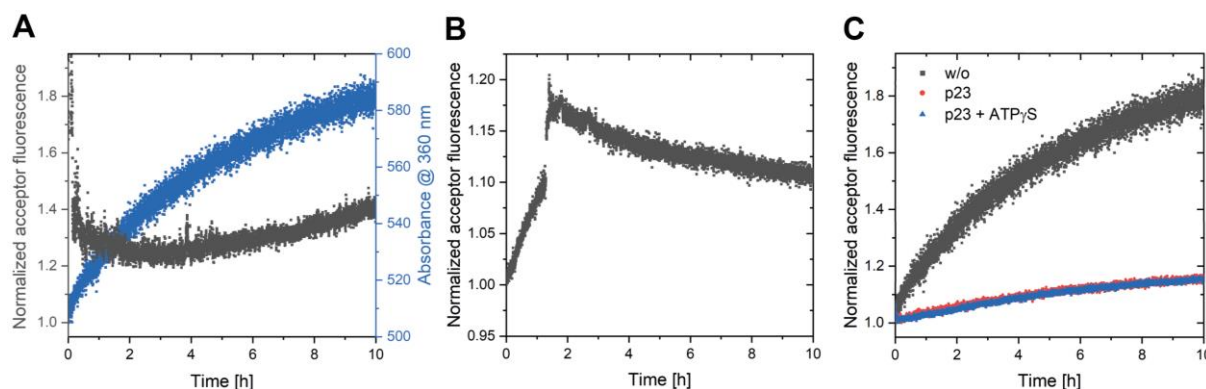


**Figure 31: Conformational changes of the quaternary structure determined by FRET.** FRET kinetics of the acceptor fluorescent signal have been measured in 500 mM  $(\text{NH}_4)_2\text{SO}_4$  closing buffer. Donor and acceptor labeled protein were incubated at the measured buffer for 1 h at 37 °C to initiate labeled heterodimer formation via protein subunit exchange. Measurements were performed at 37 °C with a final labeled protein concentration of 1  $\mu\text{M}$ . A) Light scattering at 360 nm was recorded to monitor aggregation of the sample. B) After 90 min of measurement, the temperature was reduced to 20 °C. Decrease of the acceptor fluorescent signal indicates reversibility of the reaction. C) The co-chaperone p23 was added during the preincubation (2  $\mu\text{M}$ ). Measurements were performed in the absence or presence of 2 mM  $\text{ATP}\gamma\text{S}$ .

Size exclusion chromatography was utilized to analyze the oligomerization reaction in detail. The comparison was made between wildtype Hsp90 randomly labeled on its native cysteine residues and the site-specific labeled ligated protein. Moreover, to test the effect of the nucleotide  $\text{ATP}\gamma\text{S}$ , the protein was incubated at 37°C for 1 h before analysis. The attached multiple angle light scattering (MALS) detector facilitated the estimation of the molecular weight of the eluted protein. The labeled wildtype protein was mainly present as a high molecular species (>1 MDa) eluting at 8.5 mL, with the protein in its dimeric state comprising only a fraction of the sample and eluting at 11 mL (Fig. 32A). The influence of  $\text{ATP}\gamma\text{S}$  shifted the peak slightly towards the dimer elution volume. Similar effects were also noted for the ligated protein (Fig. 32B). The oligomeric species constituted the largest fraction of the labeled protein that was eluted. Notably, a peak caused by non-ligated MC fragment of Hsp90 was observed at 12 mL. Therefore, in conjunction with the previous *in vitro* characterization of the ligated Hsp90, the oligomerization was found not to be induced by the introduced Sortase LPKTG motif. However, the labeling of the protein was found to significantly affect the quaternary structure of Hsp90, leading to oligomerization.

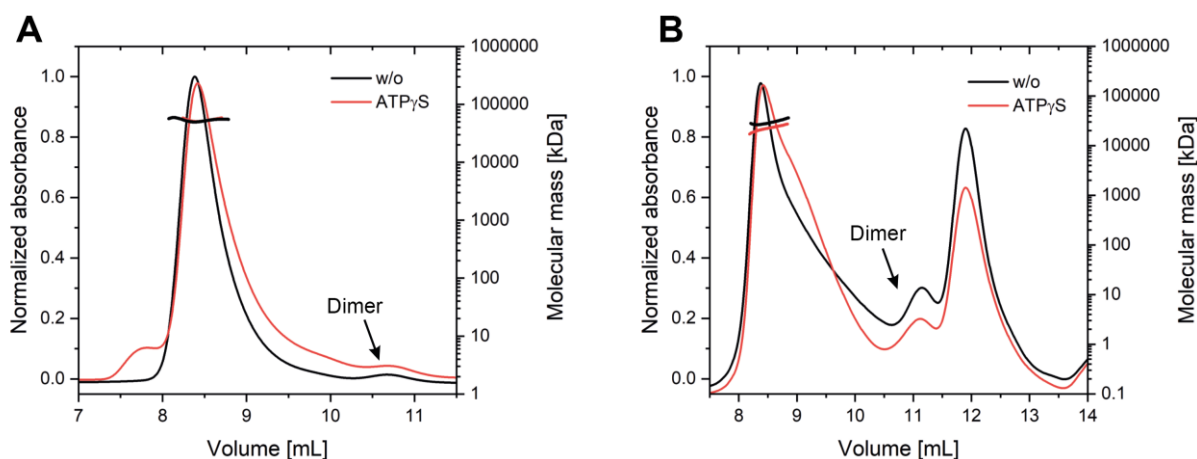


**Figure 32: Quaternary structure analysis of labeled Hsp90 $\beta$ .** SEC-elution profiles of wt Hsp90 $\beta$  (A) and ligated protein (B) labeled with Atto532. Proteins were incubated (0.25 mg/mL) without nucleotide or with ATP $\gamma$ S (2 mM) for 1 h in 200 mM KCl closing buffer at 37 °C. The early elution of the protein indicates the formation of high-molecular complexes. Additionally, heterodimers and non-ligated MC fragments are present in the sample (B).

#### 4.1.9 Single Molecule Characterization of Labeled Hsp90

Data generated from ensemble FRET experiments represents the average information obtained from the measured population. Due to the high amount of Hsp90 $\beta$  in non-native complexes, single molecule FRET (smFRET) was performed with the site-specific labeled and ligated Hsp90 $\beta$  (see 4.1.6). The method can distinguish between signal generated from dimer closing and oligomer formation and detect conformational dynamics and closing events of single particles. All measurements were carried out by Ganesh Agam and Ecenaz Bilgen (LMU Munich). In a first step, donor- and acceptor-labeled Hsp90 $\beta$  (Atto532 and Atto647) were mixed (1:1), incubated at 37 °C (1 h) to allow subunit exchange and subsequently diluted to a picomolar concentration with 200 mM KCl closing buffer. Prior to the measurement, the presence of donor and acceptor labeled species was confirmed using fluorescence cross-correlation spectroscopy (FCCS) in the presence of varying nucleotides (Fig. 33A). The obtained correlation of  $G(\tau)$  and the diffusion time  $\tau$ , was fitted to calculate the diffusion coefficient  $D(\tau)$ . In all cases, a diffusion coefficient in the expected range of the Hsp90 $\beta$  dimer was calculated (apo: 15.2  $\mu\text{m}^2/\text{s}$ , ATP: 11.6  $\mu\text{m}^2/\text{s}$ , ATP $\gamma$ S: 17.3  $\mu\text{m}^2/\text{s}$ , ADP: 20.5  $\mu\text{m}^2/\text{s}$ , AMP-PNP: 15.2  $\mu\text{m}^2/\text{s}$ ). Additionally, the scatter-corrected anisotropy for the donor and acceptor labeled protein ( $r_D/r_A$ ) was correlated with the respective fluorescence life time ( $\tau_{D(A)}/\tau_{(A)}$ ). The calculated low rotational correlation times ( $\rho$ ) indicate the prevention of oligomerization and unwanted surface-protein interactions (Fig. 33B).

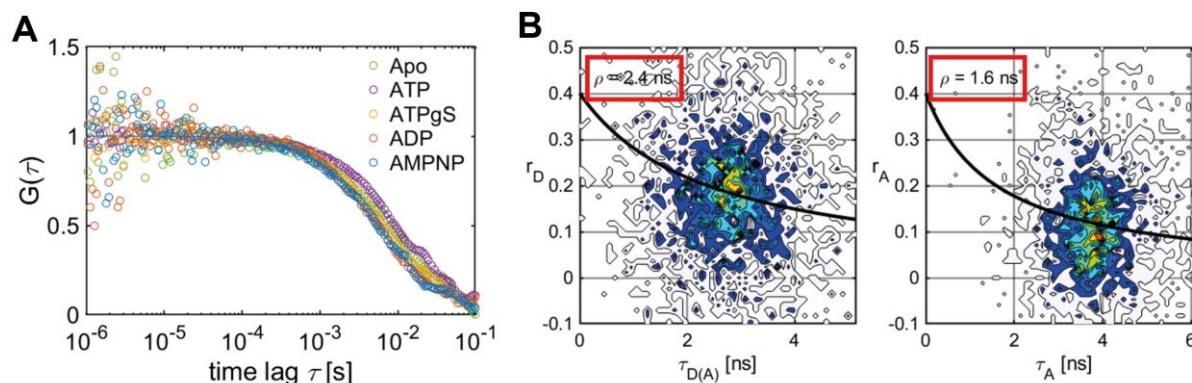


**Figure 33: Confirmation of the dimeric state of labeled Hsp90 $\beta$  by FCCS and anisotropy.** **A)** FCCS of Atto532 and Atto647 labeled Hsp90 $\beta$  was carried out in the presence of varying nucleotides (2 mM). The ligated protein was incubated in 200 mM KCl closing buffer at 37 °C for 1 h to allow subunit exchange. Prior to the measurement, the protein was diluted to a picomolar concentration while keeping the nucleotide concentration at 2 mM. Obtained data was fitted to calculate the diffusion coefficient  $D(\tau)$  of the respective sample. **B)** 2D heatmaps of anisotropy correlating with acceptor  $\tau_A$  and donor  $\tau_{D(A)}$  diffusion time of labeled protein in the apo state. Sample preparation was performed analogous to **(A)**. Measurements were carried out by Ganesh Agam and Ecenaz Bilgen (LMU Munich).

The smFRET measurements for Hsp90 $\beta$  in the absence of nucleotide showed low FRET peak (0 – 0.2) along with a broad distribution of higher FRET populations (0.4 – 1) (Fig. 34A). When ATP $\gamma$ S or AMP-PNP was added during the incubation to initiate the closed state formation, a shift of the population towards higher FRET efficiencies can be observed. Analysis of the fluorescence lifetime in correlation with the FRET efficiency additionally highlighted the dynamics of the closed state formation for AMP-PNP and ATP $\gamma$ S (Fig. 34E, F). For ADP no change on the FRET efficiency can be observed when compared to apo Hsp90 $\beta$ . However, the protein still displays dynamics towards higher FRET efficiencies without added nucleotide and when ADP was present (Fig. 34B, D). This result suggests, that Hsp90 $\beta$  in the apo state exhibits flexibility of the N-terminal domains, resulting in fluctuations of the FRET efficiency. Strikingly, when ATP was used, the FRET efficiency population shifted between the closed state and open state of Hsp90 $\beta$  (0.3 – 0.6). Furthermore, obtained dynamics highlight the cycling between high and low FRET states, due to the cycling of Hsp90 through the open and closed conformation. Summarized, smFRET results confirm previous observations of ensFRET experiments with labeled Hsp82. The protein predominantly is present in an open conformation in the absence of nucleotide or in the presence of ADP. When ATP $\gamma$ S or AMP-PNP is used, cycle progression is inhibited and accumulation of the closed state is observable. Furthermore, the dynamics of the conformational rearrangements during ATP hydrolysis can be detected and resolved using smFRET spectroscopy.

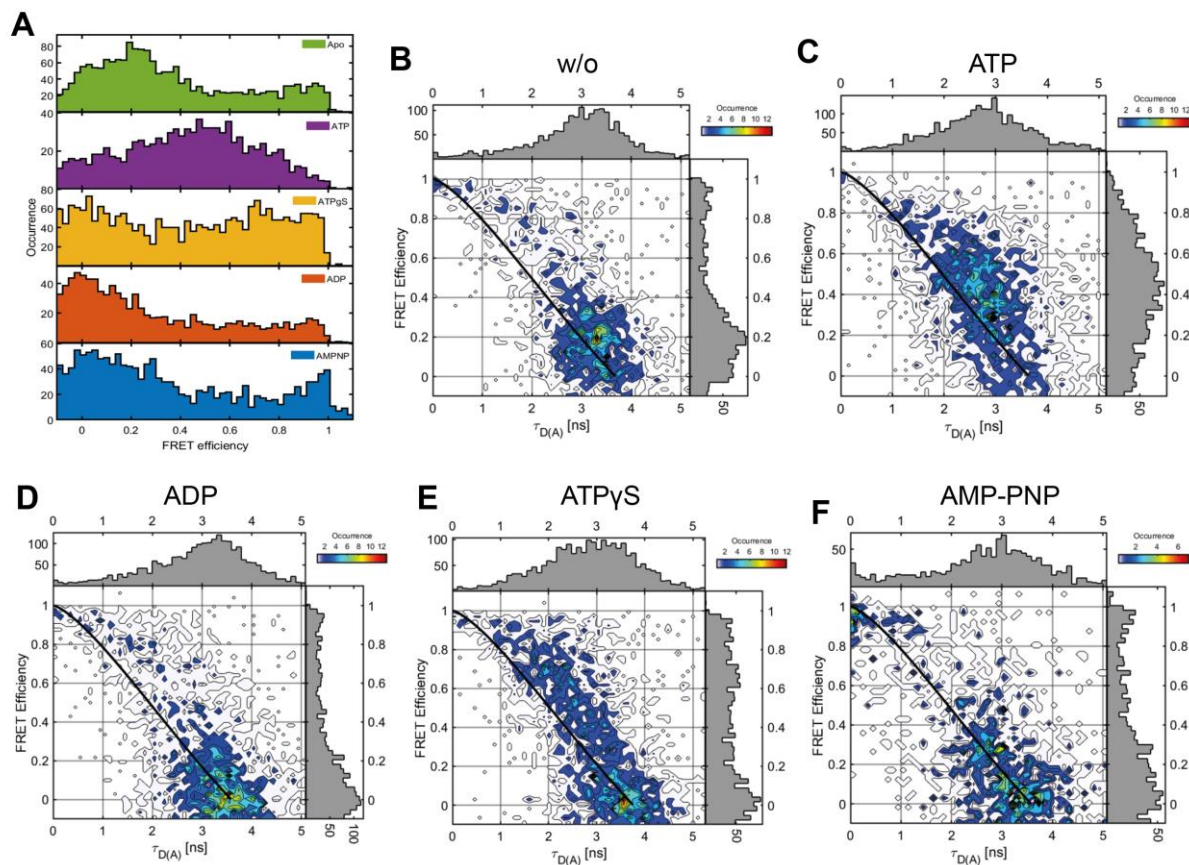


**Figure 34: Nucleotide dependent conformations and dynamics measured by smFRET.** **A)** smFRET efficiency histograms of Atto532 and Atto647 labeled Hsp90 $\beta$  in the presence of varying nucleotides: apo (green), ATP (purple), ATP $\gamma$ S (yellow), ADP (red) and AMP-PNP (blue). The ligated protein was incubated in 200 mM KCl closing buffer at 37 °C for 1 h to allow subunit exchange. Prior to the measurement, the protein was diluted to a picomolar concentration while keeping the nucleotide concentration at 2 mM. **B-F)** 2D histograms of FRET efficiency vs. donor fluorescence lifetime in the presence of an acceptor ( $\tau_{D(A)}$ ) in the presence of different nucleotides (2 mM). Black lines indicate the static FRET line. Sample preparation was performed analogous to **(A)**. All measurements were carried out by Ganesh Agam and Ecenaz Bilgen (LMU Munich).

## 4.2 Defining the Closed State Formation of Hsp90

The closed state formation of Hsp90 is limited by a complex structural process that involves several regions of the protein undergoing interdependent and coupled rearrangements. These rearrangements are essential for both active sites in the dimer to become catalytically functional and pose a rate-limiting step (Siligardi et al., 2004). For the yeast Hsp82, the association of the N-terminal domains 2 has been investigated using a broad spectrum of biophysical approaches (Hessling et al., 2009; Maruya et al., 1999; Prodromou et al., 2000). However, the extent to which human Hsp90 can attain a closed state under physiological conditions has not been sufficiently investigated, and the exact mechanisms underlying this closing process remain largely elusive. (Jussupow et al., 2022; Ratzke et al., 2012). Furthermore, previous analyses have relied on the use of specialized techniques, including crosslinking or high salt concentrations, to observe a closed conformation for human Hsp90 (Lee et al., 2021; Southworth & Agard, 2008). Therefore, the investigation of conformational rearrangements under physiological conditions would allow a more detailed investigation on the conformational cycle of human Hsp90.

### 4.2.1 Oligomer Formation during Hsp90 Closing

Closing of Hsp90 includes the formation of a compact state, which has a reduced hydrodynamic volume compared to the structure of the apo state. Using size exclusion chromatography, small differences in protein shape and volume can be separated, due to the increased retardation of smaller particles (Some et al., 2019). For Hsp90, this method has been already utilized to differentiate between the open and closed state as well as to investigate the interaction with co-chaperones (Lee et al., 2021). To observe the conformational cycle of unmodified, full-length Hsp90, the constitutive expressed human isoform Hsp90 $\beta$  was expressed and purified from *E. coli*. Closed state formation was initiated *via* incubation in 500 mM (NH<sub>4</sub>)<sub>2</sub>SO<sub>4</sub> closing buffer in the presence of 2 mM ATP $\gamma$ S at 37 °C. The protein sample was subjected to SEC after different time points to investigate the kinetics of the closed state formation (Fig. 35A). The obtained results suggest a complete closing of Hsp90 $\beta$  after 1 h of incubation, indicated by a shift to a larger elution volume. Prolonged exposure to ATP $\gamma$ S and 37 °C did not alter the elution profile of the dimeric protein. However, the formation of an additional high molecular (> 1000 kDa) species can be observed after 1 h. The peak area from this species only shows a slight increase with longer incubation of the sample beyond 1 h. These results suggest that the protein exhibits a more stable conformation in the closed state, which prevents the formation of the undefined oligomers. Data obtained from ensemble FRET experiments (see 4.1.8 Fig. 30) are in line with the observed formation of a non-dimeric species since complex formation with labeled protein resulted in an oligomeric species with an identical elution volume (8 – 9 mL). Ensemble FRET measurements suggested an inhibitory effect of p23 on the formation of the oligomeric complexes (see 4.1.8 Fig. 31). Therefore, the ability of

p23 to inhibit oligomer development was tested by SEC. Contrary to ensFRET experiments, the presence of p23 during the incubation with ATP $\gamma$ S did not show an influence on the oligomer formation (Fig. 35B). Even after 1 h, when the closed state of Hsp90 $\beta$  was achieved, an additional increase of the oligomeric population can be observed. Therefore, p23 only affects the N-terminal oligomerization of labeled protein, whereas the oligomer formation of unlabeled protein is caused by interactions of the MC domain as previously described (Moullintraffort et al., 2010).

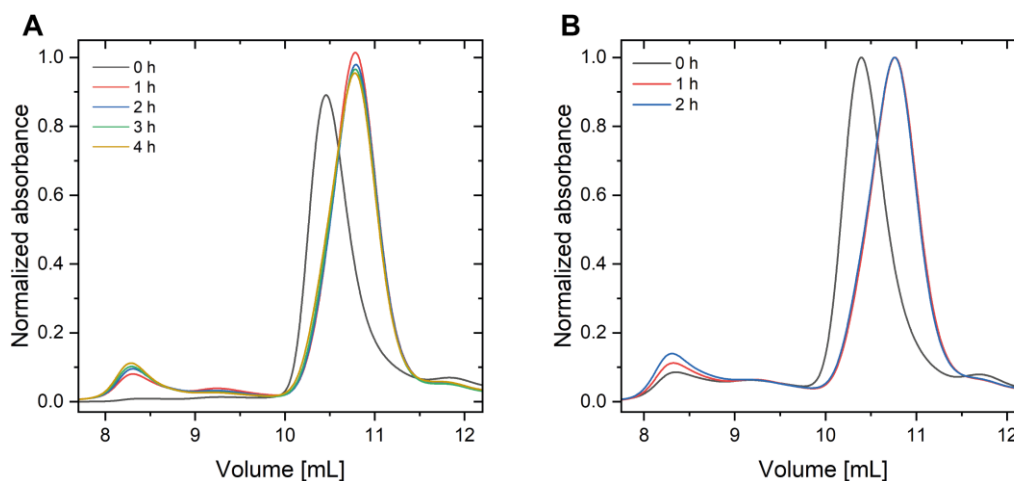


**Figure 35: Hsp90 $\beta$  closing inhibits oligomer formation.** **A)** Normalized SEC elution profiles of Hsp90 $\beta$  after varying time points of incubation at 37 °C. Proteins (0.25 mg/mL) were treated with 2 mM ATP $\gamma$ S in 500 mM (NH $_4$ ) $_2$ SO $_4$  closing buffer to initiate the closed state formation. **B)** Hsp90 $\beta$  was additionally incubated with p23 (1:2) for 30 min at room temperature to enable complex formation prior to the addition of ATP $\gamma$ S.

Native-PAGE is an electrophoretic technique, which can be used to separate proteins in their native, folded state (Wittig & Schagger, 2005). Similar to SEC, proteins are separated based on their hydrodynamic volume and isoelectric point. To characterize the formed oligomers and to monitor the closed state of Hsp90 $\beta$ , the purified full-length protein was incubated in different concentrations of closing buffer in the presence and absence of ATP $\gamma$ S. After varying time points of incubation at 37 °C, the protein samples were analyzed via Native-PAGE (Fig. 36A – E). Hsp90 $\beta$  can be identified as a broad band between 120 kDa and 220 kDa highlighting the flexibility of the protein. However, no difference between the open and closed state is observable. Yet, the increase of the ionic components in the buffer led to a more defined Hsp90 $\beta$  band at 120 kDa. The presence of two additional bands (~ 230 kDa and ~300 kDa) indicates the formation of the oligomeric population in the sample. After 18 h of incubation without ATP $\gamma$ S, only protein incubated in 500 mM (NH $_4$ ) $_2$ SO $_4$  was present in its dimeric state. Therefore, the kosmotropic properties of ammonium sulfate stabilize the dimeric Hsp90 $\beta$  state and inhibit the oligomerization. When ATP $\gamma$ S was present in the buffer, no significant decrease of the dimer band was observed except for 10 mM KCl. Hence, the closed state of Hsp90 $\beta$  is less prone to oligomerization. However, at a low salt concentration either Hsp90 $\beta$  does not form a closed state or the formation of oligomers is promoted.

## Results

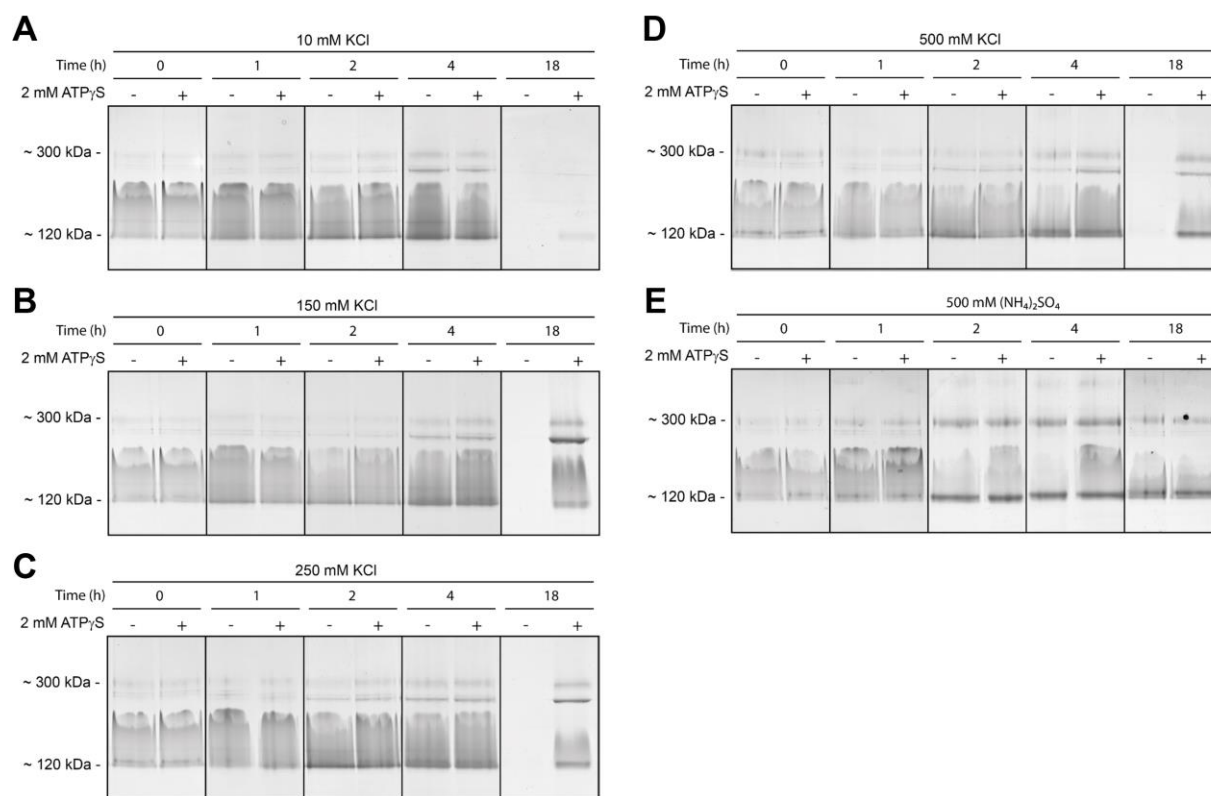


**Figure 36: Hsp90β oligomers characterized via Native-PAGE.** The formation of oligomers was monitored via Native-PAGE analysis. Hsp90β (0.3 mg/mL) was incubated with 2 mM ATP $\gamma$ S at 37 °C to initiate the closed state formation. The composition of the closing buffer was modified to observe the impact on oligomer formation (**A**: 10 mM KCl, **B**: 150 mM KCl, **C**: 250 mM KCl, **D**: 500 mM KCl, **E**: 500 mM (NH<sub>4</sub>)<sub>2</sub>SO<sub>4</sub>). After varying time points, samples were mixed with 2x sample buffer and subjected to electrophoresis.

Transmission electron microscopy (TEM) is often used to visualize the structure, shape, and size of proteins at high resolutions (Sato et al., 2014). By using TEM, detailed information about protein aggregates, fibrils, or complexes, which can aid in the understanding of protein folding, misfolding, and aggregation-related diseases, can be obtained (Goldsbury et al., 2011). To investigate and characterize the oligomerization of Hsp90β, the purified full-length protein was incubated in 250 mM and 500 mM ammonium sulfate closing buffer for 4 h. However, the TEM micrographs obtained from the prepared samples did not indicate the formation of higher-ordered protein structures (Fig. 37A, B). Together, the results from SEC experiments, Native-PAGE and TEM suggest the presence of Hsp90β oligomers in a broad mass distribution, agglomerating to larger complexes over time.

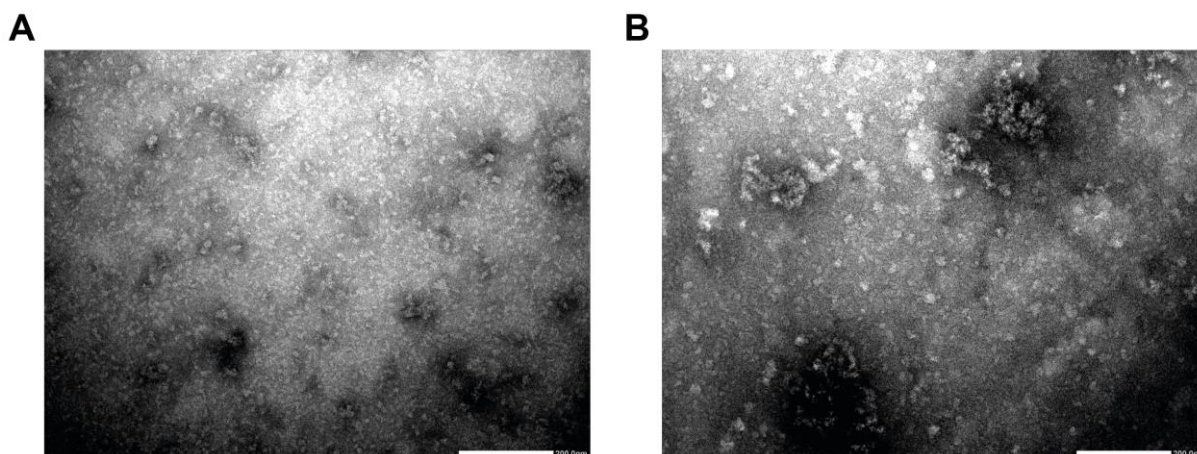


**Figure 37: Hsp90 $\beta$  oligomers characterized by TEM.** TEM micrographs of closed Hsp90 $\beta$  (0.5 mg/mL) after 4 h of incubation in 250 mM (A) or 500 mM (B) (NH<sub>4</sub>)<sub>2</sub>SO<sub>4</sub> closing buffer at 37 °C. TEM micrographs were obtained at a 50k x magnification. The white bar represents 200 nm.

#### 4.2.2 Ionic Components Modulate Hsp90 Stability and Closing

A thermos-shift assay monitors the unfolding of a target protein by thermal denaturation. The unfolded proteins expose otherwise buried hydrophobic patches, which allows non-specific binding of the dye Sypro Orange (Huynh & Partch, 2015). In an aqueous environment, the fluorescent dye is quenched and upon binding to a protein fluorescence increases, which enables to track changes in signal intensity. As a result, the stability of a protein under varying conditions can be tested. To compare the stability of Hsp90 $\beta$  in 200 mM KCl and 500 mM ammonium sulfate closing buffer, a thermos-shift assay with wt Hsp90 $\beta$  was conducted (Fig. 38A). A similar melting curve was observed for both buffer conditions, where the protein showed an onset of unfolding at approximately 46 °C and complete unfolding at 60 °C. The calculated melting temperature revealed a slight difference in stability between the two conditions: 52.8 °C with 200 mM KCl and 54.6 °C with 500 mM (NH<sub>4</sub>)<sub>2</sub>SO<sub>4</sub>. It is worth noting that these calculated temperatures align with the observed heat-induced oligomerization of Hsp90 (Chadli et al., 1999). Therefore, the slightly increased stability in the high salt ammonium sulfate buffer already prevents the formation of Hsp90 $\beta$  oligomers. To investigate the stability of Hsp90 $\beta$  under lower ammonium sulfate concentrations, the protein was incubated in 250 mM (NH<sub>4</sub>)<sub>2</sub>SO<sub>4</sub> with 2 mM ATP $\gamma$ S. Samples were taken at different time points and analyzed *via* SEC to observe protein closing and oligomer formation (Fig. 38B). Interestingly, the results showed increased oligomer formation compared to 500 mM (NH<sub>4</sub>)<sub>2</sub>SO<sub>4</sub> (see 4.2.1). However, the protein was unable to form a complete closed state within the measured incubation period. In contrast to the higher salt concentration, an incubation for 1 h did not result in a complete formation of the closed state, and prolonged incubation did not increase the closed population. Therefore, to obtain the closed state of Hsp90 and to avoid oligomerization requires the adjustment of the ionic compounds in the buffer.

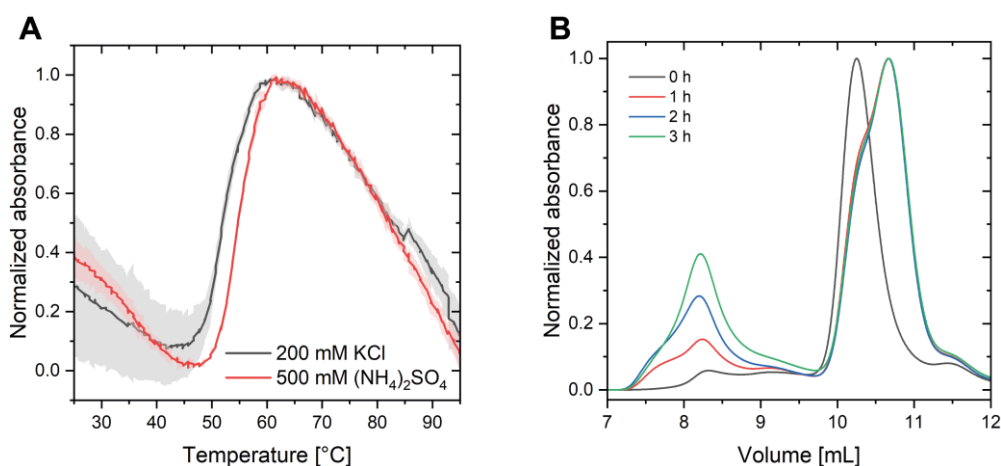


**Figure 38: Buffer components influence protein stability and oligomerization.** **A)** Thermal stability of the protein in 200 mM KCl (black) and 500 mM  $(\text{NH}_4)_2\text{SO}_4$  (red) was compared by a thermal shift assay with Sypro orange. The assay was conducted in a thermo cycler with 0.25 mg/mL of protein at a heating rate of  $1^\circ\text{C}/\text{min}$ . **B)** Normalized SEC elution profiles of Hsp90 $\beta$  after varying time points of incubation at  $37^\circ\text{C}$ . Proteins (0.25 mg/mL) were treated with 2 mM ATP $\gamma$ S in 250 mM  $(\text{NH}_4)_2\text{SO}_4$  closing buffer to initiate the closed state formation.

Additionally, the closing of Hsp90 $\beta$  with different potassium chloride concentrations, which are more representative of the physiological conditions (Melkikh & Sutormina, 2008), were tested using analytical ultracentrifugation (aUC). Similar to SEC-MALS, aUC separates molecules based on their size, shape, and density, and can be used to determine their molecular weight and shape. However, in aUC the separation is achieved in solution and in the absence of a matrix by applying a high centrifugal force on the sample. When labeled with a fluorophore, these proteins can be specifically tracked during their sedimentation, which can be used to study protein-protein interactions and conformational rearrangements under different solution conditions. Prior to the experiment, wt Hsp90 $\beta$  was labeled unspecifically with the fluorophore Atto550 via maleimide chemistry. Afterwards, the protein was incubated in three different concentrations of KCl (10 mM, 250 mM and 500 mM) in the presence or absence of 2 mM ATP $\gamma$ S. Additionally, the closing was compared to 500 mM  $(\text{NH}_4)_2\text{SO}_4$  (Fig. 39A - D). A shift toward higher Svedberg values indicates the formation of the closed state, due to the reduced hydrodynamic volume of Hsp90 $\beta$ . All used conditions, except 10 mM KCl, displayed a slight shift of the peak towards an increased Svedberg value. Therefore, Hsp90 $\beta$  requires an ionic concentration similar to physiological conditions to form a closed state with potassium chloride. Furthermore, these results are in line with Native-Page experiments (see 4.2.1), where 10 mM KCl displayed increased oligomerization even after incubation with ATP $\gamma$ S.

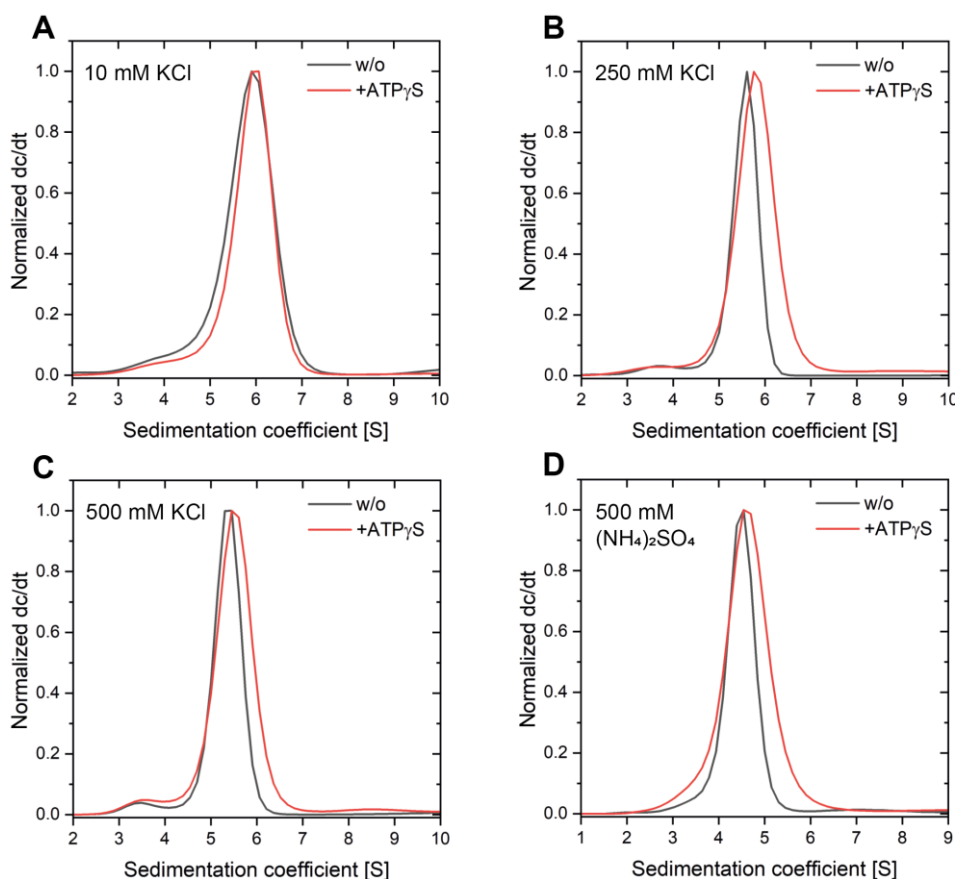


**Figure 39:** Closed state formation of labeled Hsp90 $\beta$  determined by AUC. Normalized dc/dt AUC sedimentation profiles of Atto550-labeled Hsp90 $\beta$ . Proteins were incubated (1  $\mu$ M) without nucleotide (black) or with 2mM ATP $\gamma$ S (red) for 1 h in closing buffer (A: 10 mM KCl, B: 250 mM KCl, C: 500 mM KCl, D: 500 mM (NH $_4$ ) $_2$ SO $_4$ ) at 37  $^{\circ}$ C.

### 4.2.3 Time-Resolved Closing of Hsp90

The formation of the closed state of Hsp90 $\beta$  can be observed *via* SEC due to the reduced hydrodynamic volume resulting from conformational rearrangements of the protein. The previously performed experiments suggest that complete closing occurs after 1 h of incubation in 500 mM (NH $_4$ ) $_2$ SO $_4$  in the presence of 2 mM ATP $\gamma$ S. To gain more insight into the kinetics of these conditions, samples were subjected to SEC after varying time points of incubation (Fig. 40). Closing, indicated by a shift in elution volume, can be observed after 10 and 20 min of incubation. A complete closed state was achieved after 30 min. Incubation for 40 and 50 min did not alter the elution profile of the protein. Furthermore, no increase in the oligomeric population was observed during the measured timeframe.

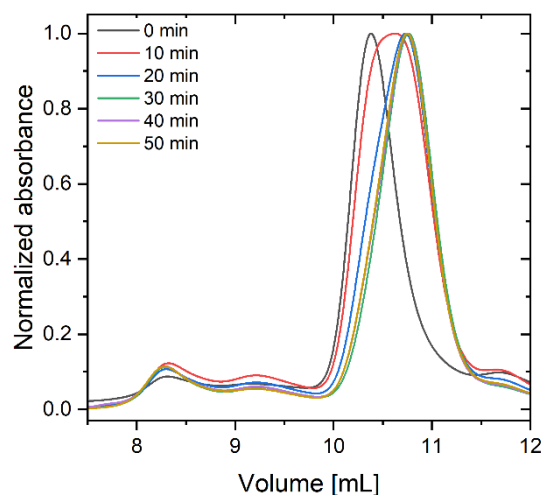


**Figure 40: Time-resolved closed state formation of Hsp90 $\beta$  characterized by SEC.** Normalized SEC elution profiles of Hsp90 $\beta$  after varying time points of incubation at 37 °C. Proteins (0.25 mg/mL) were treated with 2 mM ATP $\gamma$ S in 500 mM (NH<sub>4</sub>)<sub>2</sub>SO<sub>4</sub> closing buffer to initiate the closed state formation.

To get a more detailed view on the kinetics of Hsp90 $\beta$  closing, chemical crosslinking with disuccinimidyl glutarate (DSG) was performed. The compound covalently links side chain amino groups, which are in close proximity. Crosslinking is commonly used to study protein-protein interactions and conformational changes or to identify interaction partners (Sinz, 2006). Additionally, crosslinking stabilizes the closed state of Hsp90 and was employed to obtain cryo-EM structures (Southworth & Agard, 2011). To investigate the closing of Hsp90, incubation in the presence or absence of ATP $\gamma$ S (2 mM, 500 mM KCl, 37 °C) was carried out and DSG was added after varying time points. Subsequent to the crosslinking, samples were analyzed *via* SDS-Page (Fig. 41A). Without nucleotide added, Hsp90 $\beta$  is present in similar amounts of dimer (~ 250 kDa apparent mass) and monomer (~ 80 kDa apparent mass), which does not change with prolonged incubation. However, when ATP $\gamma$ S was present in the sample, the intensity of the dimeric band increases over time, while the monomeric band decreases. Therefore, the possibility of crosslinking is increased in the closed state, due to the protomers being in closer proximity. In line with SEC experiments, only a slight difference between 30 and 50 min of incubation is detectable, indicating a nearly complete formation of the closed state after 30 min of incubation. To investigate the kinetics of the closing in this time frame, dimer and monomer fractions were analyzed with ImageJ and fitted in OriginPro (Fig. 41B). A closing rate of 0.219 min<sup>-1</sup> was calculated for the Hsp90 $\beta$ , which is significantly slower as determined for Hsp82 (2.04 min<sup>-1</sup> (Tippel, 2017)). Therefore, the formation of the closed state largely contributes to the difference in ATPase activity of the two proteins.

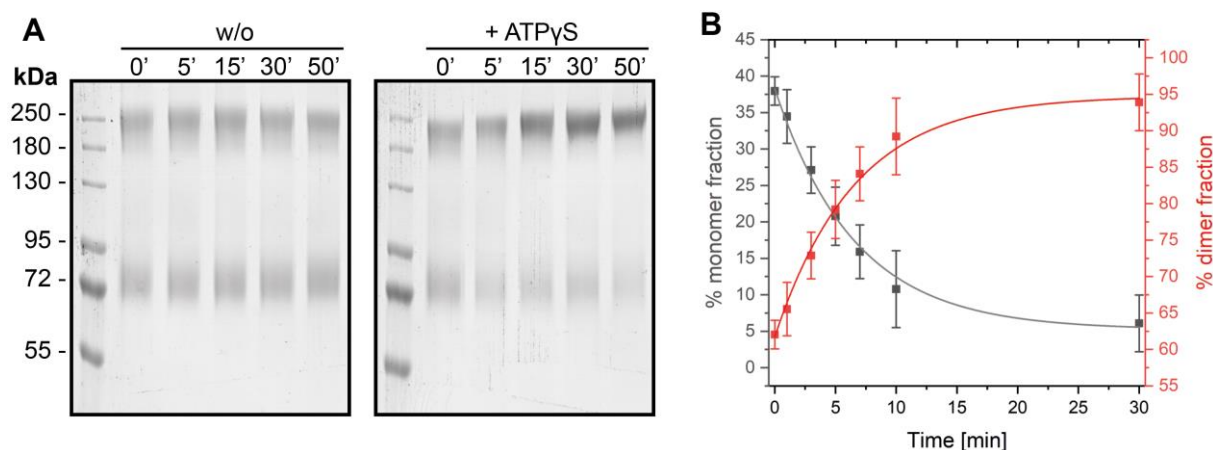


**Figure 41: Closed state formation kinetics of Hsp90 $\beta$  characterized by chemical crosslinking.** **A)** Exemplary SDS-PAGE analysis of crosslinked Hsp90 $\beta$  after varying time points. Protein samples were either incubated in the absence (left) or presence (right) of 2 mM ATP $\gamma$ S in 500 mM KCl closing buffer at 37 °C. Chemical crosslinking was achieved by the addition of 2 mM DSG for 45 min at room temperature. Subsequently, the reaction was quenched by the addition of 10 mM Tris. Samples were mixed with Laemmli buffer and analyzed by SDS-PAGE. **B)** Obtained closing kinetics Hsp90 $\beta$  in 500 mM KCl closing buffer with 2 mM ATP $\gamma$ S. Measurements at varying time points were carried out in triplicates and fitted (Hsp90 $\beta$   $k_{cat}$  = 0.219 min<sup>-1</sup>).

Crosslinking can be employed to distinguish between the open and closed state of Hsp90 $\beta$ . Therefore, the interaction with Hsp90 co-chaperones in the open and closed state was tested. Hsp90 $\beta$  was mixed with the respective co-chaperone (1:2) and incubated in either the absence or presence of 2 mM ATP $\gamma$ S for 1 h to initiate the formation of the closed state. After crosslinking with DSG, the formed protein complexes were analyzed by SDS-Page (Fig. 42). When Aha1 added to Hsp90 $\beta$ , an increase of the molecular mass of the dimer band can be observed (~ 290 kDa) for the open and closed state. A second band with an increased molecular weight is present for the closed state. In line with previous published data (Retzlaff et al., 2010), the results suggest that Aha1 binds in the open and closed state of Hsp90. Consequently, the two different formed bands in the presence of ATP $\gamma$ S can be contributed to the open and closed conformation of Hsp90 $\beta$  being in a complex with Aha1. The addition of Hop during the incubation resulted in an identical increase of the molecular mass (~ 270 kDa) in the presence and absence of ATP $\gamma$ S. Hop binds Hsp90 $\beta$  in the open state and inhibits ATPase activity by preventing the formation of the closed state (Richter et al., 2003; Southworth & Agard, 2011). Therefore, the closed state of Hsp90 $\beta$  is not observable on the gel, but only the complex of the open state crosslinked with Hop. Strikingly, when p23 was added during the incubation, no increase of the molecular mass is observed for Hsp90 $\beta$  in the open state. Only when the closed state was initiated with the addition of ATP $\gamma$ S, a shift towards an increased molecular mass is present (~ 270 kDa). This result is in line with existing cryo-EM structures of the Hsp90:p23/Sba1 complex, which demonstrates p23/Sba1 binding in the cleft of the dimerized NTDs (Ali et al., 2006; Lee et al., 2021). Therefore, as expected p23 predominantly forms a stable complex with Hsp90 $\beta$  in the closed state.

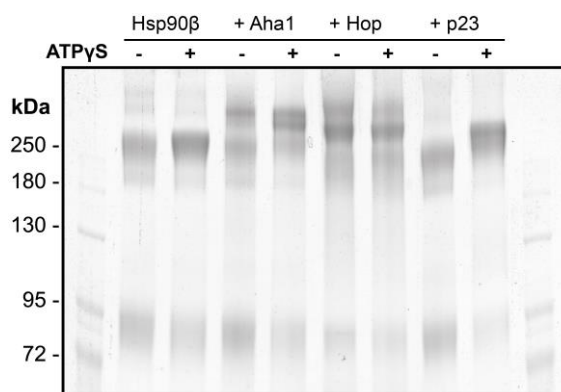


**Figure 42: Co-chaperone interaction with Hsp90 $\beta$  characterized by chemical crosslinking.** SDS-PAGE analysis of crosslinked Hsp90 $\beta$  (0.25 mg/mL) after incubation with different co-chaperones (Hsp90 $\beta$ :Co-chaperone = 1:2) and 2 mM ATP $\gamma$ S. Protein samples were either incubated in the absence (-) or presence (+) of ATP $\gamma$ S in 200 mM KCl closing buffer at 37 °C for 1 h. Chemical crosslinking was achieved by the addition of 2 mM DSG for 45 min. Subsequently, the reaction was quenched by the addition of 10 mM Tris. Samples were mixed with Laemmli buffer and analyzed by SDS-PAGE.

#### 4.2.4 Temperature Influence on the Hsp90 Closing Kinetics

The Hsp90 ATPase activity is strongly dependent on temperature (Prodromou et al., 2000). To investigate the temperature influence on the closing of the human Hsp90 $\beta$ , the protein was incubated in 500 mM (NH<sub>4</sub>)<sub>2</sub>SO<sub>4</sub> closing buffer at 30 °C. Closing was initiated by the addition of 2 mM ATP $\gamma$ S and samples subjected to SEC after varying time points. Previous experiments with this buffer suggest that complete closing occurs after 1 h of incubation at 37 °C (see 4.2.1). To gain more insights into the kinetics at a lower temperature (30 °C), samples were subjected to SEC in 1 h intervals (Fig. 43). Surprisingly, a complete formation of the closed state was not observed, even after 4 h of incubation. The closed population showed an increase in samples incubated for 1 hour and 2 hours, while a prolonged incubation of 3 and 4 hours did not alter the elution profile of the protein. Therefore, Hsp90 $\beta$  displays a decrease of the closing kinetic when the temperature is reduced, which is in line with a reduction of the ATPase activity. Furthermore, the incomplete closing of the protein indicates, that the human protein requires an increased temperature due to its adaption to the temperature of the human body. Therefore, it is highly probable that the elevated temperature also supplies the energy needed to surpass a conformational energy barrier crucial for the formation of the closed state.

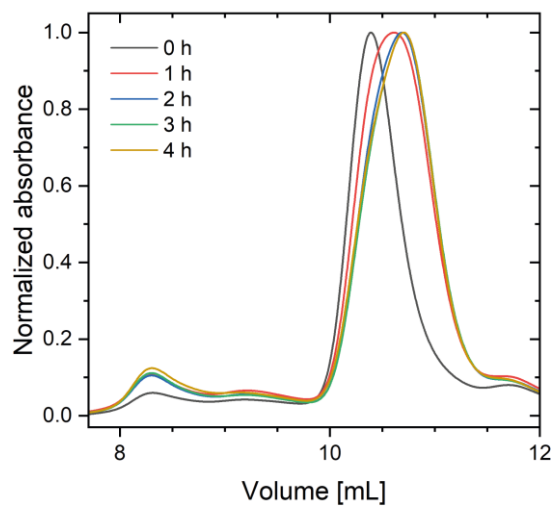


**Figure 43: Temperature influence on the closed state formation of Hsp90β.** Normalized SEC elution profiles of Hsp90β after varying time points of incubation at 30 °C. Proteins (0.25 mg/mL) were treated with 2 mM ATPγS in 500 mM (NH<sub>4</sub>)<sub>2</sub>SO<sub>4</sub> closing buffer to initiate the closed state formation.



### 4.3.1 Nucleotide-induced Closed State Formation

The conducted aUC and native-PAGE experiments with Hsp90 $\beta$  indicated that the closed state can be achieved with 150 mM and 250 mM KCl, respectively. To compare Hsp82 and Hsp90 $\beta$  *in vitro*, an initial investigation was carried out to assess the ability of both proteins to attain the closed state under physiological conditions (200 mM KCl). For this purpose, the proteins were incubated in the presence or absence of the slowly hydrolysable ATP analog ATP $\gamma$ S at 30 °C (Hsp82) or 37 °C (Hsp90 $\beta$ ) and analyzed *via* SEC (see 4.2.1). When incubated with ATP $\gamma$ S, both yeast Hsp82 and human Hsp90 $\beta$  exhibited a significant decrease in hydrodynamic volume, resulting in a shift of elution volume, while their molecular mass remained unchanged (Fig. 45A). However, Hsp90 $\beta$  displayed a larger shift in elution volume between the two populations ( $\Delta$ Hsp82 = 0.26 mL;  $\Delta$ Hsp90 $\beta$  = 0.36 mL), which indicates an increased difference between the hydrodynamic volume of the two states. Therefore, the human protein may experience larger conformational rearrangements upon nucleotide binding. In order to confirm observations from SEC experiments, closed state formation was additionally tested using aUC. Prior to the measurement, the proteins were labeled with the fluorescent dye Atto550. For Hsp82, the label was attached to an introduced cysteine (residue 61), while Hsp90 $\beta$  was labeled unspecifically (see 4.2.2). The obtained results are in line with SEC experiments, as both fluorescent-labeled proteins displayed a shift toward higher Svedberg values after incubation with ATP $\gamma$ S (Fig. 45B). Since the sedimentation coefficient is largely affected by the displaced mass of a given particle, this further confirms the formation of a more compact state of both Hsp90s. However, in this case the observed shift for Hsp90 $\beta$  was smaller than for Hsp82 ( $\Delta$ Hsp82 = 0.58 S;  $\Delta$ Hsp90 $\beta$  = 0.16 S). Similar to ensFRET measurements, the decreased closed state formation is most likely caused by the attached hydrophilic dye, which negatively affects the formation of the closed state. Nevertheless, the dimeric protein and the two different conformational states can be separated and distinguished during both aUC and SEC.

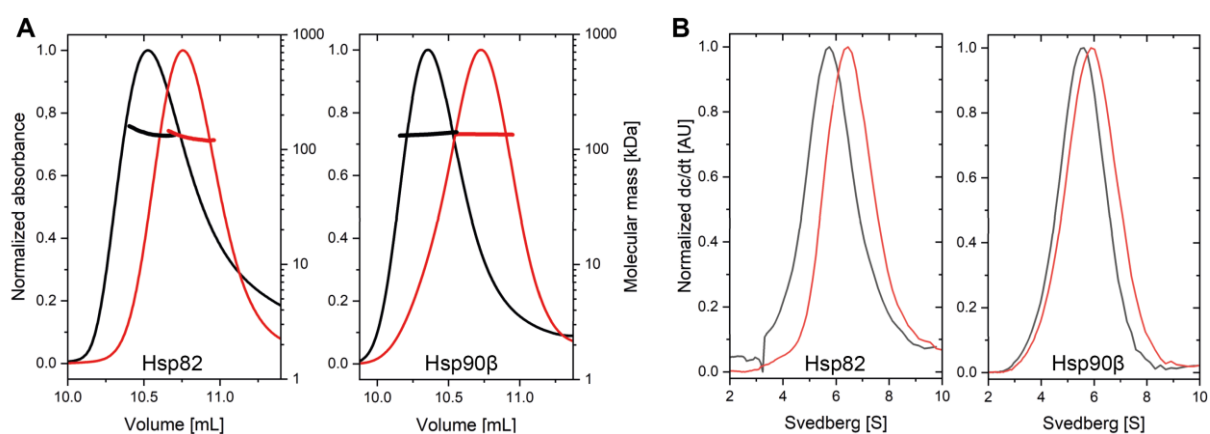


**Figure 45: Closed state formation of wt/labeled Hsp82 and Hsp90 $\beta$  determined by SEC and AUC.** **A)** Normalized SEC elution profiles of wt Hsp82 and wt Hsp90 $\beta$ . Proteins were incubated (0.25 mg/mL) without nucleotide (black) or with 2mM ATP $\gamma$ S (red) for 1 h in 200 mM KCl closing buffer (Hsp82 30 °C; Hsp90 $\beta$  37 °C). **B)** Normalized dc/dt AUC sedimentation profiles of Atto550-labeled Hsp82 and Hsp90 $\beta$ . Proteins were incubated (1  $\mu$ M) without nucleotide (black) or with 2mM ATP $\gamma$ S (red) for 1 h in 200 mM KCl closing buffer (Hsp82 30 °C; Hsp90 $\beta$  37 °C).

Additionally, limited proteolysis with  $\alpha$ -chymotrypsin was performed to detect a conformational difference between the open and closed conformation (Fig. 46A, B). The protease cleaves sequence independent after large hydrophilic sidechains (Tyr, Trp, Phe, Met, Leu) and has a similar number of cleavage sites for Hsp82 (138) and Hsp90 $\beta$  (140). The analysis of the digested full-length proteins by SDS-Page revealed a similar digestion pattern in the absence of ATP $\gamma$ S, which resulted in the formation of a main product at 45 kDa. However, Hsp90 $\beta$  preincubated with nucleotide exhibited a substantial increase in protection against the protease compared to the yeast protein. Digestion of Hsp90 is limited by the accessibility of the protease to cleavage sites. Therefore, in line with the results from SEC experiments, Hsp90 $\beta$  closing comprises structural rearrangements, which leads to the increased protection against  $\alpha$ -chymotrypsin. Furthermore, the digestion patterns of the closed state slightly differ between Hsp82 and Hsp90 $\beta$ . Since the digestion patterns of the open state are nearly identical, this further confirms a difference in the closing and the closed state of the proteins.

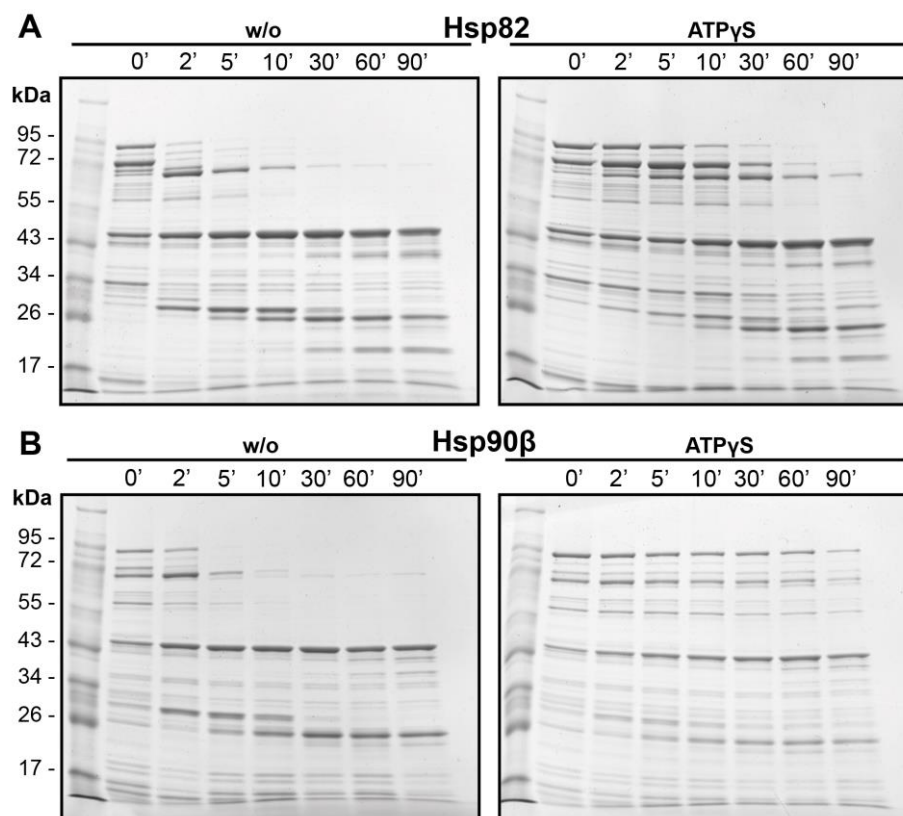


**Figure 46: Conformational rearrangements of Hsp82 and Hsp90 $\beta$  characterized by limited proteolysis.** Hsp82 (A) and Hsp90 $\beta$  (B) were subjected to the protease  $\alpha$ -chymotrypsin (Hsp90: $\alpha$ -chymotrypsin 1:20). Proteins (0.3 mg/mL) were pre-incubated in 200 mM KCl closing buffer for 1 h in the absence (left) or presence (right) of ATP $\gamma$ S (2 mM) to form the closed state (Hsp82: 30 °C; Hsp90 $\beta$  37 °C). Proteolysis was carried out at room temperature and stopped at several time points with 2 mM PMSF. Samples were mixed with 5x Laemmli buffer and analyzed by SDS-Page (4 – 12 % gradient).

To validate the ability of ATP $\gamma$ S to induce the closed conformation of Hsp82 and Hsp90 $\beta$ , SEC elution profiles after incubation with varying nucleotides were compared. Without any added nucleotide and in the presence of ADP, predominantly the open state was present for both proteins (Fig. 47A, B)). No shift towards a more compact formation was observed for either protein when incubated with ATP. This is in line with the prevailing notion that Hsp90 mainly populates an open conformation, even during the conformational cycle including ATP hydrolysis (Street et al., 2010; Zierer et al., 2016). Thus, the actual closing and opening motions as well as the closed state take up only a fraction of the cycle as the rate limiting step is the formation of the closed state (Hessling et al., 2009). Only the ATP analogues, ATP $\gamma$ S as well as AMP-PNP, led to a significant shift in elution caused by the decreased hydrodynamic volume of Hsp90 upon closing. Therefore, both ATP $\gamma$ S and AMP-PNP trap Hsp90 in the closed state and prevent cycle progression, resulting in the accumulation of the closed conformation. However, a significant difference was discovered for AMP-PNP. Whereas Hsp82 displayed a complete closing after 30 min, for Hsp90 $\beta$  this reaction required overnight incubation (Fig. 47C). Therefore, Hsp90 $\beta$  has a higher nucleotide specificity, which seems to involve the phosphoric acid anhydride bond of the  $\gamma$ -phosphate. To test this notion, the experiment was performed in the presence of the nucleotide ADP-AlF<sub>4</sub>. This compound has served as a proxy for the trigonal bipyramidal hydrolysis transition state of ATP (Fisher et al., 1995). In existing crystal structures ADP-AlF<sub>4</sub> is present in an octahedral geometry with four equatorial fluorines and the  $\beta$ -phosphate's oxygen with an axial water molecule (Xu et al., 1997). However, for Hsp90 ADP-AlF<sub>4</sub> did not lead to any change of the elution profile. Therefore, it can be concluded that the opening of the dimer occurs during the transition of the  $\gamma$ -phosphate from the tetrahedral conformation into the trigonal bipyramidal pre-hydrolysis state.

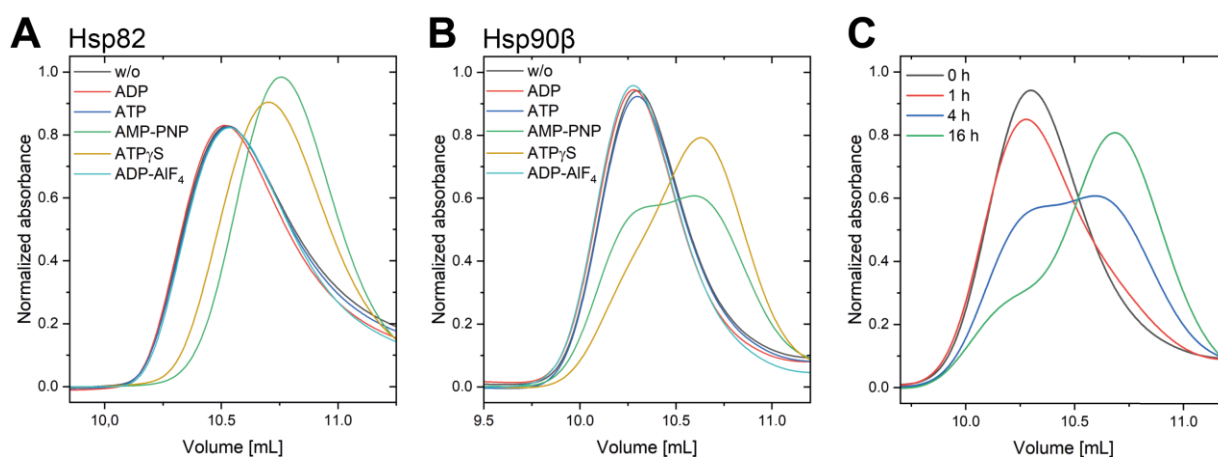


**Figure 47: Closed state formation of Hsp82 and Hsp90 $\beta$  with varying nucleotides characterized by SEC.** Normalized Hsp82 (A) and Hsp90 (B) elution profiles from size exclusion chromatography after incubation in 200 mM KCl closing buffer (Hsp82: 30 °C, 30 min, Hsp90: 37 °C, 4 h) with varying nucleotides (black: w/o, red: ADP, blue: ATP, green: AMP-PNP, yellow: ATP $\gamma$ S, teal: ADP-AlF<sub>4</sub>). C) Normalized SEC elution profiles of Hsp90 after different time points of incubation with AMP-PNP at 37 °C in 200 mM KCl closing buffer (black: 0 min, blue: 1 h, red: 4 h, green: 16 h).

### 4.3.2 Correlation of Hsp90 Closing Kinetics and ATPase Activity

The ATPase activity of Hsp90 drives conformational changes, which are essential for the proper folding, stability, and activation of a diverse set of proteins, including many involved in signal transduction and cell cycle control. Although the overall structure and function of Hsp90 is conserved between yeast and humans, there are some differences in their ATPase activities. Yeast Hsp82 has a higher turnover than the human Hsp90 $\beta$ , which may reflect differences in the regulatory mechanisms of the two proteins. Under steady state conditions, in this study, Hsp82 displayed an activity of 1.19 min<sup>-1</sup>, whereas Hsp90 $\beta$  was tenfold slower at a rate of 0.13 min<sup>-1</sup> (Fig. 48A). Previous studies excluded the difference in affinity and ATP binding as the rate-limiting step (Richter et al., 2008). Therefore, the observed difference in activity between yeast and human could be attributed to differences in changes during the conformational cycle or to the ATP hydrolysis reaction. To analyze the kinetics of the closed state formation, SEC was performed. Fitting the elution profiles of the peak with a bi-Gaussian function allows the calculation of the open and closed populations at a given time point (Fig. 48B - E). At 200 mM KCl, a closing rate of  $k_{\text{cat}} = 1.025 \text{ min}^{-1}$  was calculated for Hsp82, while Hsp90 $\beta$  displayed a tenfold slower rate of  $k_{\text{cat}} = 0.103 \text{ min}^{-1}$ , which is consistent with its lower ATPase activity. Therefore, we conclude that obtained results prove that the rate-limiting step for Hsp90 is the conformational transition to the closed state.

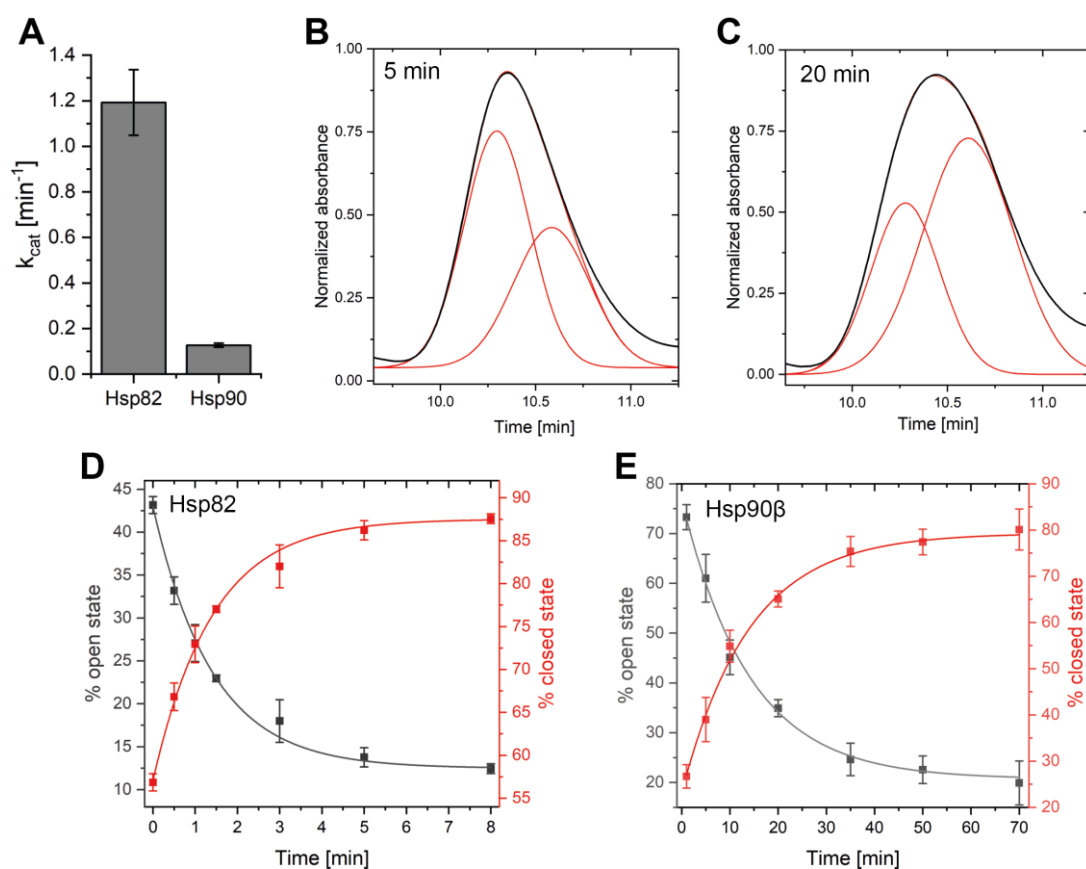


**Figure 48: Comparison of Hsp82 and Hsp90 $\beta$  ATPase activity and closing kinetics.** A) ATPase activity of Hsp82 and Hsp90 measured *via* the regenerative ATPase assay. Activity was measured in 200 mM KCl closing buffer (Hsp82: 30 °C,

3  $\mu\text{M}$ ; Hsp90 $\beta$ : 37  $^{\circ}\text{C}$ , 10  $\mu\text{M}$ ). Measurements were performed in triplicates and means as well as standard deviations were calculated. The obtained activity was corrected for background using Radicol. **B**) Normalized Hsp90 $\beta$  elution profiles from SEC after incubation in 200 mM KCl closing buffer at 37  $^{\circ}\text{C}$  for 5 min and 20 min **(C)**. Peaks were fitted with a bi-Gaussian function (red) to calculate populations of the open and closed state. **D, E**) Closing kinetics of Hsp82 and Hsp90 $\beta$ , respectively, in 200 mM KCl closing buffer with 2 mM ATP $\gamma\text{S}$ . Measurements at varying time points were carried out in triplicates and fitted (Hsp82 KCl  $k_{\text{cat}} = 1.025 \text{ min}^{-1}$ , Hsp90 $\beta$   $k_{\text{cat}} = 0.1030 \text{ min}^{-1}$ ).

Hsp82 and Hsp90 $\beta$  not only differ in their observed kinetics but also in the population of their closed apo states. Human Hsp90 $\beta$  has a closed state population of  $\sim 25\%$  without any added nucleotide, while for Hsp82, the closed population in the apo state was  $\sim 50\%$  (200 mM KCl; Hsp82: 30  $^{\circ}\text{C}$ , Hsp90 $\beta$ : 37  $^{\circ}\text{C}$ ). These results align with previous smFRET studies of Hsp82 (Wolf et al., 2021). To test these observations by an orthogonal method, the conformational changes of both proteins were tracked using chemical crosslinking with DSG and analysis by SDS-Page. Kinetics were obtained by calculating the dimer and monomer fraction on the gel after varying time points with ImageJ (Fig. 49A, B). Crosslinking in the presence of ATP $\gamma\text{S}$  showed similar kinetics of closed state formation as SEC experiments (Hsp90 $\beta$   $k_{\text{cat}} = 0.148 \text{ min}^{-1}$ ; Hsp82  $k_{\text{cat}} = 1.626 \text{ min}^{-1}$ ). Again, it can be observed that Hsp82 has a higher fraction of crosslinked dimer at  $t = 0 \text{ min}$ , indicating that the protomers of Hsp82 are in closer proximity and have a higher probability of being crosslinked. This may suggest a more compact formation of yeast Hsp82 NTDs or an increased propensity of the protein to form the closed state in its apo state. Both techniques used clearly demonstrate the difference between Hsp82 and Hsp90 $\beta$  in terms of the kinetics of closed state formation. However, it is possible that there may be additional kinetic differences during the hydrolysis step that have not been accounted for.

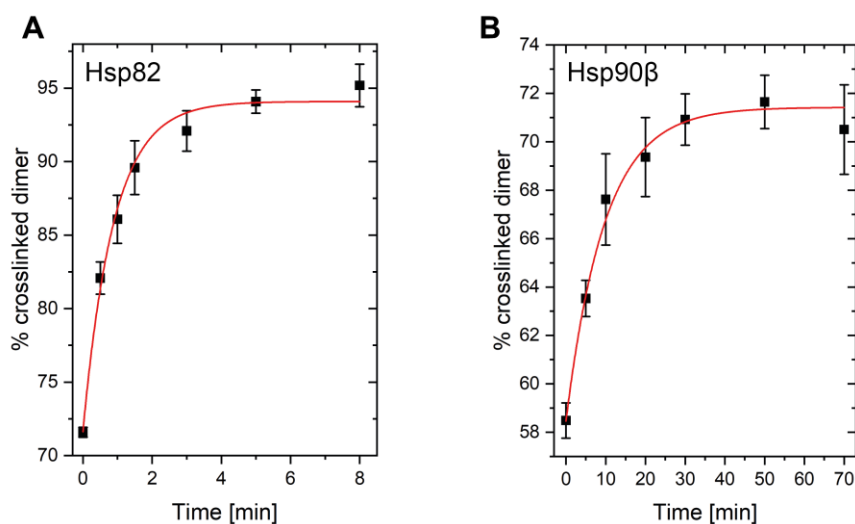


**Figure 49: Closed state formation kinetics of Hsp82 and Hsp90 $\beta$  characterized by chemical crosslinking.** . **A**) Obtained closing kinetics of Hsp82 and **(B)** Hsp90 $\beta$  in 200 mM KCl closing buffer with 2 mM ATP $\gamma\text{S}$  (Hsp82: 30  $^{\circ}\text{C}$ ; Hsp90 $\beta$ : 37  $^{\circ}\text{C}$ ). Measurements at varying time points were carried out in triplicates and fitted (Hsp82 KCl  $k_{\text{cat}} = 1.626 \text{ min}^{-1}$ , Hsp90 $\beta$   $k_{\text{cat}} = 0.148 \text{ min}^{-1}$ ). Chemical crosslinking was achieved by the addition of 2 mM DSG for 45 min. The reaction was quenched by the addition of 10 mM Tris. Samples were mixed with Laemmli buffer and analyzed by SDS-PAGE. Dimer and monomer fraction were determined using ImageJ.

To investigate the influence of co-chaperones on the closing kinetics of Hsp90, SEC was performed. Hsp90 was preincubated with the respective co-chaperone to initiate complex formation, followed by the addition of ATP $\gamma$ S and incubation for 10 minutes (1 minute for Hsp82), representing the half-time of the closing reaction. The resulting populations of the closed states were then analyzed and compared to Hsp90 without co-chaperone added (Fig. 50A, B)). Sba1 (p23 for Hsp90 $\beta$ ), which is known to bind into the cleft of the dimerized NTDs of the closed Hsp90 dimer (Ali et al., 2006), had only a slight negative effect on the closing kinetics. Therefore, it can be assumed that the inhibitory effect of Sba1 can be mostly contributed to hindering the re-opening and product release of Hsp90, which is in line with published data (Graf et al., 2014). In contrast, Sti1 (Hop for Hsp90 $\beta$ ), which interacts with Hsp90 in the open state and significantly inhibits ATPase activity (Richter et al., 2003; Wang et al., 2022), decelerated the closing kinetics effectively. The results for Aha1 are consistent with ATPase measurements (Panaretou et al., 2002; Prodromou et al., 1999), as a significant increase in the closed population was observed, indicating an acceleration of the closed state formation.

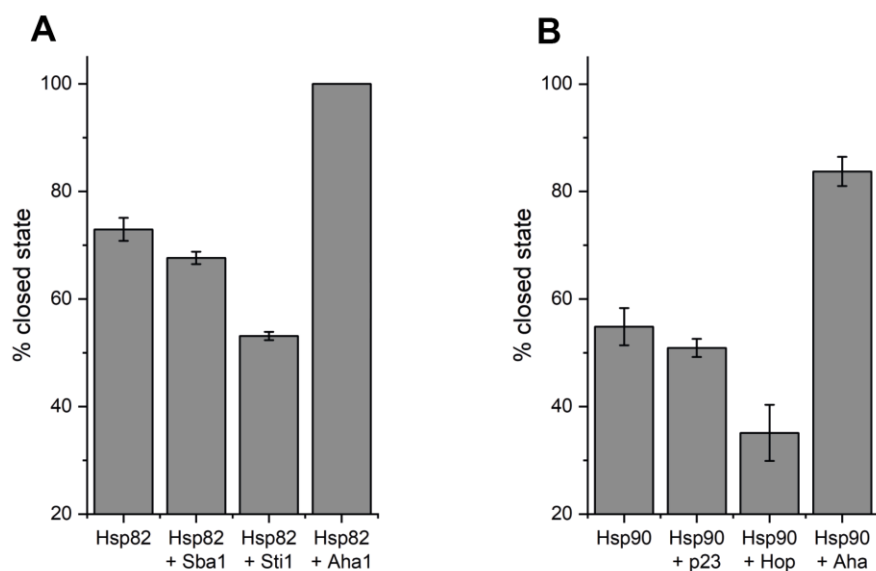


**Figure 50: Influence of co-chaperones on the closing kinetics of Hsp90. A&B)** Hsp90 closed state fraction after incubation with 2 mM ATP $\gamma$ S compared to protein additionally incubated with the respective co-chaperone (Hsp90:Co-Chaperone = 1:2). Samples were measured as independent triplicates. The data shown was obtained by fitting the SEC elution profiles with a bi-Gaussian fit. Incubation was carried out for Hsp82 for 1 min at 30 °C and 10 min at 37 °C for Hsp90 $\beta$ .

#### 4.3.3 Modulation of the Hsp90 Activity by Hydrophobic Interactions

To modify the underlying interactions and affect the ATPase activity, the ionic composition of the buffer was altered. Three salts were selected that represent different regions of the Hofmeister series (Hofmeister, 1888): ammonium sulfate on the kosmotropic side, calcium chloride on the chaotropic side, and potassium chloride in the middle. Furthermore, different concentrations of the respective salts were tested to differentiate the impact of the ionic compounds. The results obtained showed that

increasing the concentration of potassium chloride from 200 to 500 mM resulted only in a minor increase in ATPase activity for Hsp82, whereas Hsp90 $\beta$  showed a more significant gain of activity (Fig. 51A, B). Strikingly, the use of ammonium sulfate did not improve the ATPase activity of Hsp82 compared to potassium chloride. However, a slight direct correlation between an increase in ammonium sulfate concentration and ATPase activity was observable. For Hsp90 $\beta$ , on the other hand, ammonium sulfate led to a more evident concentration dependent increase in ATPase activity compared to potassium chloride. Between 200 and 500 mM (NH<sub>4</sub>)<sub>2</sub>SO<sub>4</sub>, an increase in activity from 10 % up to 50 % was determined. When calcium chloride was present in the buffer, both Hsp82 and Hsp90 $\beta$  showed a substantial decrease in activity. The chaotropic agent interferes with the hydration shell of the protein (Zhang & Cremer, 2006), highlighting the importance of the hydrophobic effect on closing. Furthermore, high calcium chloride concentrations led to a visible precipitation of the protein in the sample, therefore exhibiting the highest negative impact on the ATPase activity.

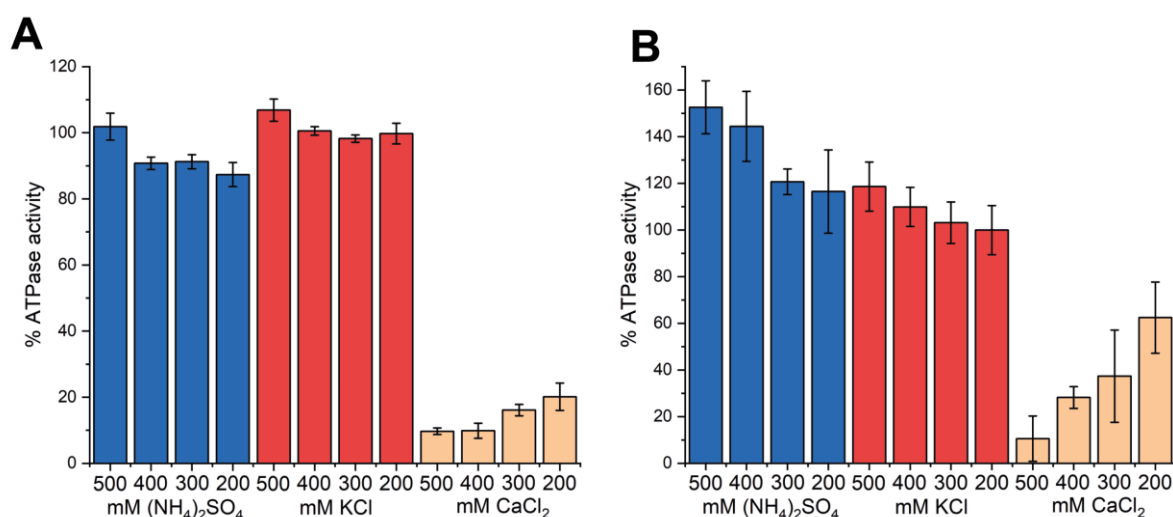


**Figure 51: Comparison of Hsp82 and Hsp90 $\beta$  ATPase activity under varying buffer composition.** ATPase activity of Hsp82 (A) and Hsp90 $\beta$  (B) measured via a regenerative ATPase assay. Activity was measured in closing buffer with varying salts and concentrations (Hsp82: 30 °C, 3  $\mu$ M; Hsp90 $\beta$ : 37 °C, 10  $\mu$ M). All measurements were performed as three independent technical replicates to calculate means and standard deviations. The obtained activity was corrected for background using Radicol. Data was normalized to the obtained ATPase activity of the respective chaperone at 200 mM KCl.

To compare the effect of the different salts on the closing kinetics, analytical SEC was performed (Fig. 52C, D). For both Hsp82 and Hsp90 $\beta$  an increase in the potassium chloride concentration led to a significant increase in the closed state population (Hsp82  $k_{\text{cat}} = 1.941 \text{ min}^{-1}$ ; Hsp90 $\beta$   $k_{\text{cat}} = 0.177 \text{ min}^{-1}$ ). With potassium being slightly on the kosmotropic side of the Hofmeister series, this demonstrates the importance of hydrophobic interactions during the closed state formation of the dimer. In line with the results of the ATPase activity measurements, ammonium sulfate did not significantly affect the closing rate for Hsp82 ( $k_{\text{cat}} = 1.258 \text{ min}^{-1}$ ). However, a larger fraction of the open population was present at any time point. During the measured timeframe, complete closing was not achieved. Hsp90 $\beta$ , on the other hand, displayed a considerable increase in closing kinetics when ammonium sulfate was used

( $k_{\text{cat}} = 0.4319 \text{ min}^{-1}$ ). This might hint towards an evolutionary difference between Hsp82 and Hsp90 $\beta$ , affecting the formation of the closed state.

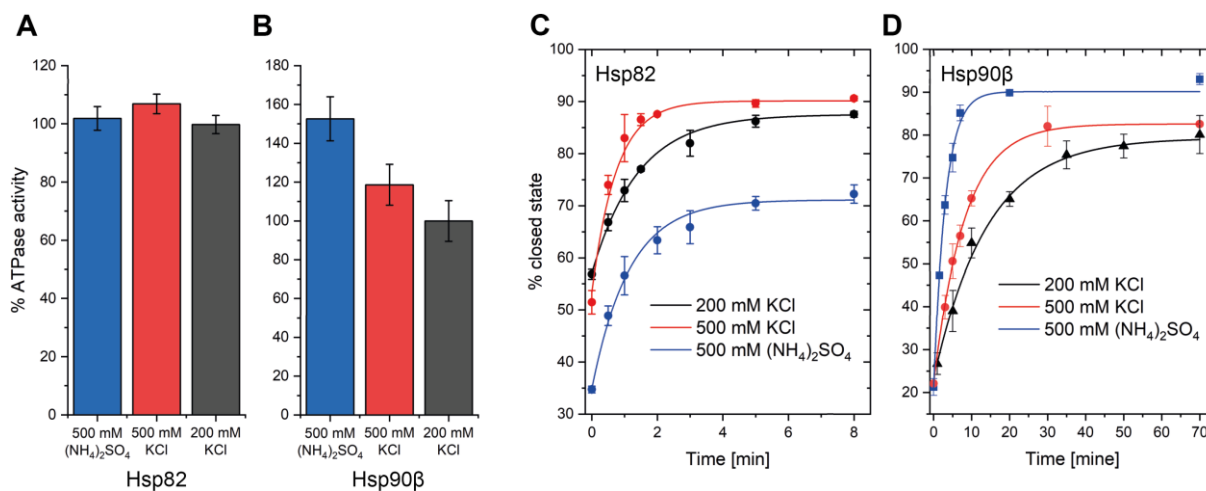


**Figure 52: Comparison of the Hsp82 and Hsp90 $\beta$  ATPase activities and closing kinetics at different buffer compositions.** ATPase activity of Hsp82 (A) and Hsp90 $\beta$  (B) measured via regenerative ATPase assay. Obtained closing kinetics of Hsp82 (C) and Hsp90 $\beta$  (D) in closing buffer with different salt concentrations. Measurements at varying time points were carried out in triplicates and fitted (Hsp82 200 mM KCl  $k_{\text{cat}} = 1.025 \text{ min}^{-1}$ , 500 mM KCl  $k_{\text{cat}} = 1.941 \text{ min}^{-1}$ , 500 mM (NH<sub>4</sub>)<sub>2</sub>SO<sub>4</sub>  $k_{\text{cat}} = 1.258 \text{ min}^{-1}$ ; Hsp90 $\beta$  200 mM KCl  $k_{\text{cat}} = 0.1030 \text{ min}^{-1}$ , 500 mM KCl  $k_{\text{cat}} = 0.1767 \text{ min}^{-1}$ , 500 mM (NH<sub>4</sub>)<sub>2</sub>SO<sub>4</sub>  $k_{\text{cat}} = 0.4391 \text{ min}^{-1}$ ).

When calcium chloride was used to initiate the closed state of Hsp90 $\beta$ , precipitation and aggregation of the protein could be observed in the sample. In the presence of 500 mM calcium chloride closing buffer, a significant population of the protein is present in an aggregated/oligomeric state (Fig. 53). After incubation in this buffer for 1 hour, the dimeric peak disappeared completely, leaving only the oligomeric species. Similar to the effect of hydrophilic dyes, the buffer promotes hydrophilic interaction, which result in protein misfolding and N-terminal aggregation. This results in a reduced ATPase activity or formation of an additional species during SEC. Therefore, Hsp90 requires a delicate balance between stabilizing and destabilizing interactions to form the closed conformation. Overall, these findings demonstrate that both Hsp82 and Hsp90 $\beta$  depend on the formation of hydrophobic interactions for ATPase cycle progression. However, when hydrophobic interactions were enhanced through buffer composition or mutation, the closing kinetics of Hsp90 $\beta$  were more strongly affected and a significant increase in ATPase activity was observed, highlighting an evolutionary difference between the two proteins.

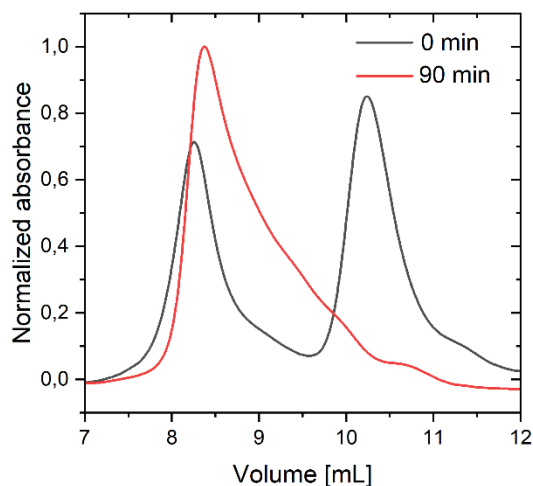


**Figure 53: SEC analysis of Hsp90 $\beta$  in the presence of CaCl<sub>2</sub>.** Normalized Hsp90 $\beta$  SEC elution profiles after incubation in 500 mM CaCl<sub>2</sub> closing buffer. Incubation was carried out in the presence of 2 mM ATP $\gamma$ S for 0 min (black) and 90 min (red) at 37 °C.

#### 4.3.4 Influence of Mutations on Hsp90

The underlying mechanistic difference explaining inherent divergence of the yeast and human Hsp90 are still elusive. However, several mutations have been identified in Hsp90 to either positively or negatively affect the overall ATPase activity. Remarkably, most of these mutations are located in the NTD either around the lid or near the  $\alpha$ 1-helix (Fig. 54A). In Hsp82, T101I and A107N (T110I and A116N in Hsp90 $\beta$ ) are both directly affecting lid movement. Whereas T101I inhibits ATPase activity by stabilizing the open state of the lid *via* hydrophobic interactions (Siligardi et al., 2004), A107N enhances ATPase activity by introducing a hydrogen bond between Asn-107 and Tyr-47, stabilizing the lid in the closed state (Fig. 54A, left) (Ali et al., 2006). T22I (T31I in Hsp90 $\beta$ ) increases the hydrophobicity of the  $\alpha$ 1-helix, augmenting its ability to interact with the helix of the opposing protomer, thus enhancing the ATPase activity. Similar effects of these mutations in yeast and human Hsp90 confirm the common underlying mechanism of the ATPase cycle (Vaughan et al., 2009), including lid rearrangement and dimerization through hydrophobic interactions *via* the  $\alpha$ 1-helix (Fig. 54A, right). To test the influence of the  $\alpha$ 1-helix and lid mutations on the closing of the dimer, we compared the fractions of protein in the closed state after incubation with ATP $\gamma$ S (Hsp82: 1 min, 30 °C; Hsp90 $\beta$ : 10 min, 37 °C). In line with the ATPase activity measurements, the Hsp82 lid mutations T101I and A107N displayed drastic changes of the closed population compared to the wild-type protein (Fig. 54B – E). T101I displayed nearly an unchanged population of the closed population, highlighting the importance of the lid rearrangement for Hsp90. Contrary, for the A107N mutation, nearly a complete transition to the closed state was observed. The human Hsp90 lid mutants T110I and A116N showed a similar behavior as the yeast mutants confirming the common mechanism of lid rearrangement upon nucleotide binding. Since both mutations do not alter nucleotide binding, the results indicate that lid rearrangement is not

only necessary for the formation of the closed state, but also is a decisive factor of the closing kinetics. The increased hydrophobicity of the  $\alpha$ 1-helix mutant T22I resulted in a distinct increase of the closed population for Hsp82 and Hsp90 $\beta$ . However, a direct comparison of the effect of the  $\alpha$ 1-helix mutant on the ATPase activity and closing rate demonstrates a more severe impact on Hsp90 $\beta$ . Similar to the influence of ammonium sulfate on the closing kinetics; this reveals the drastic dependency of Hsp90 $\beta$  on hydrophobic interactions during the formation of the closed state. Furthermore, the results also show that the closing kinetics do not necessarily match the ATPase activity. Although T31I exhibited the fastest closing kinetics for Hsp90 $\beta$ , the ATPase of the A116N lid mutant remained significantly higher.

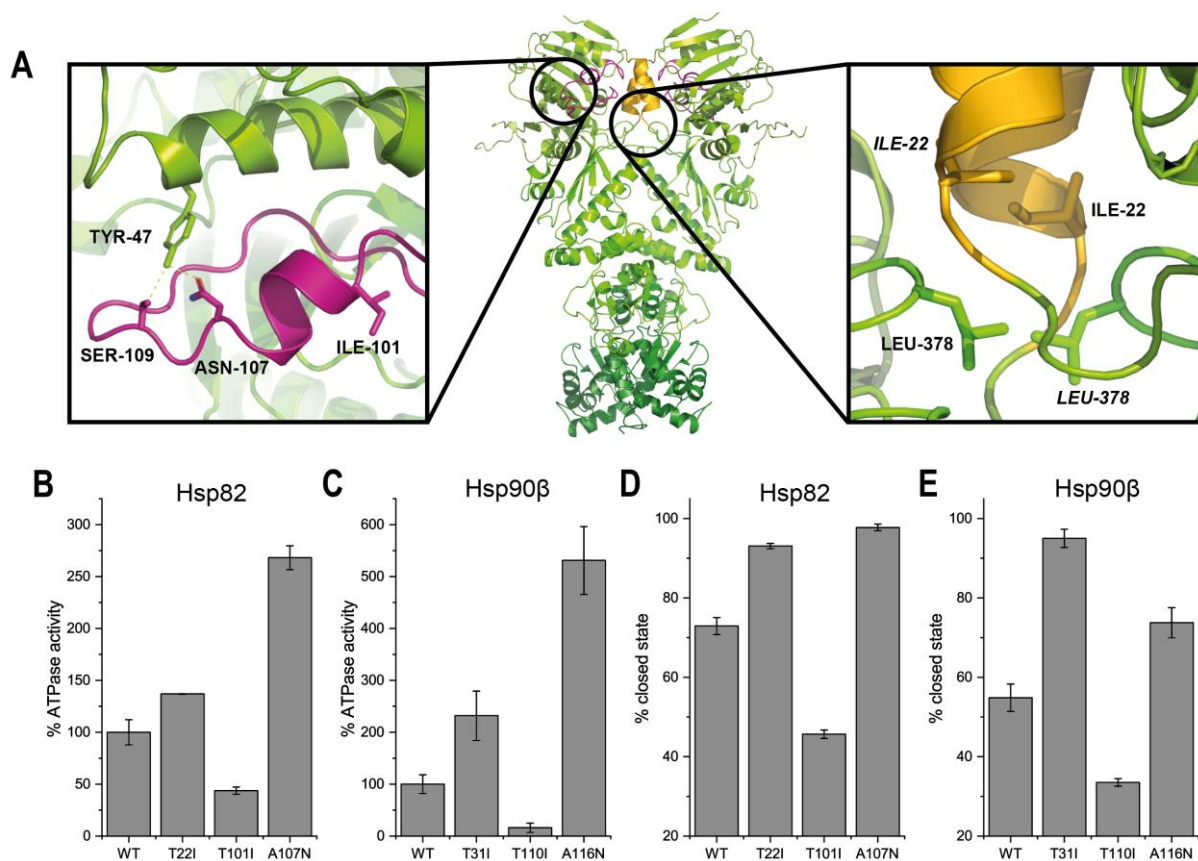


**Figure 54: Impact of mutations on the activity and closing kinetics of Hsp90.** **A**) Crystal structure of Hsp82 (PDB ID: 2cg9) highlighting mutations affecting ATPase activity. The ATP-lid (magenta) and  $\alpha$ 1-helix (yellow) are highlighted in the structure. **B, C**) Comparison of Hsp90 ATPase and activity mutants. The obtained activity was normalized to wt Hsp82 and Hsp90 $\beta$ , respectively. Activity was measured in 200 mM KCl closing buffer (Hsp82: 30 °C, 3  $\mu$ M; Hsp90 $\beta$ : 37 °C, 10  $\mu$ M). Measurements were performed as three independent technical replicates to calculate means and standard deviations. The obtained activity was corrected for background using Radicolol. **D, E**) Wt Hsp90 closed state fraction after incubation with 2 mM ATP $\gamma$ S compared to mutants. Data was obtained by fitting SEC elution profiles with a bi-Gaussian fit. Incubation was carried out for 1 min and at 30 °C for Hsp82 and for 10 min at 37 °C for Hsp90 $\beta$ .

#### 4.3.5 Dimer Re-Opening via Nucleotide Exchange

The general mechanistic understanding of Hsp90 involves the assumption that ATP hydrolysis is the trigger of dimer re-opening and cycle progression (McLaughlin et al., 2002; Prodromou et al., 2000). However, increasing evidence suggests that nucleotide exchange in the closed state is an alternative possibility for re-opening (Reidy & Masison, 2020; Zierer et al., 2016). To investigate the underlying mechanism of nucleotide exchange and dimer re-opening, the ability of various nucleotides to exchange the bound ATP $\gamma$ S was probed. In this experiment, prior to incubation with ATP, ADP or the Hsp90 inhibitor Radicicol, Hsp82 and Hsp90 $\beta$  were closed using ATP $\gamma$ S. After one hour of incubation in 200 mM KCl closing buffer, elution profiles obtained by SEC were compared. Radicicol led to the most significant shift towards lower elution volumes and therefore to an open conformation for both Hsp82 and Hsp90 $\beta$  (Fig. 55A, B). This indicates that nucleotides can trigger re-opening once the dimer is in a closed state. For ADP and ATP, shifts towards the open conformation were visible but to a lower extent than observed for Radicicol. Closed Hsp90 proteins incubated with ADP showed a more pronounced population of the open state compared to ATP. Strikingly, when AMP-PNP was used for closing, neither ADP, ATP nor Radicicol increased the open population after incubation (Fig. 55C, D). Together with the results from the closing experiments with AMP-PNP, this suggests either that the binding of AMP-PNP differs from ATP $\gamma$ S or that the  $\gamma$ -phosphate plays a crucial role during closing and opening. Since ADP, as well as Radicicol, have a lower dissociation constant than AMP-PNP, affinity based effects can be excluded (Roe et al., 1999; Zhang et al., 2015).

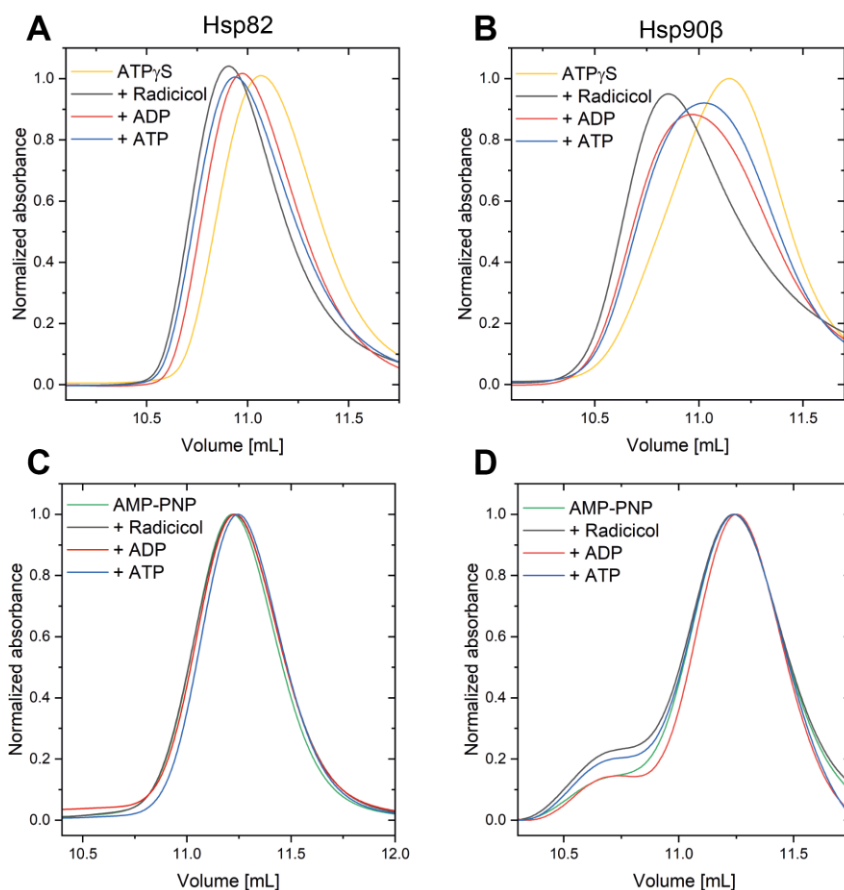


**Figure 55: Re-opening of the closed state of Hsp82 and Hsp90 $\beta$  in the presence of varying nucleotides characterized by SEC.** **A, B)** Normalized Hsp82 and Hsp90 elution profiles from SEC after incubation for 1 h in 200 mM KCl closing buffer (Hsp82: 30 °C, Hsp90: 37 °C) with 2 mM ATP $\gamma$ S (yellow) to initiate the closed state. Afterwards, ATP (blue), ADP (red) or Radicicol (black) were added and incubated for 1 h to probe dimer re-opening. **C, D)** Normalized Hsp82 and Hsp90 elution profiles from SEC after incubation in 200 mM KCl closing buffer (Hsp82: 30 °C, 1 h; Hsp90: 37 °C, 16 h) with 2 mM AMP-PNP (green) to initiate the closed state. Afterwards, ATP (blue), ADP (red) or Radicicol (black) were added and incubated for 1 h to probe dimer re-opening.

To confirm the results regarding re-opening, analytical ultracentrifugation was performed. Atto488-labeled Hsp82 (labeled at an introduced cysteine residue at position 61) and Hsp90 $\beta$  unspecifically labeled at its native cysteines were preincubated with ATP $\gamma$ S to initiate closing as previously described. Afterwards, ADP or Radicicol was added, and the samples were further incubated. Similar to the results obtained from SEC elution profiles, the Radicicol-treated proteins displayed the most significant shift towards lower Svedberg values (Fig. 56A, B). This indicates a less compact conformation of the protein and thus re-opening. The treatment of closed dimers with ADP did not lead to a complete decrease of the closed population, as observed in the SEC analyses. Therefore, it can be assumed that a fraction remains in the closed state due to the competitive binding with ATP $\gamma$ S.

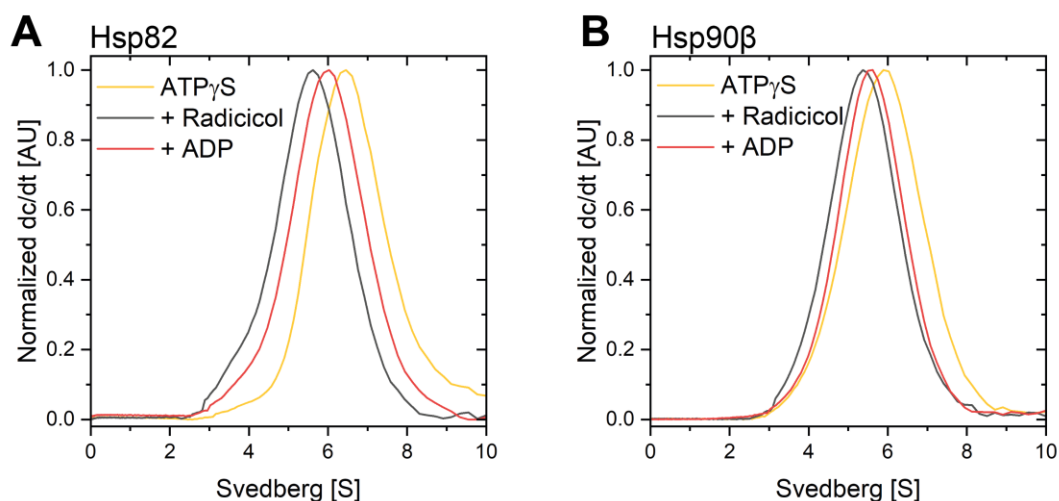


**Figure 56: Re-opening of the closed state of Hsp82 and Hsp90 $\beta$  with ADP and Radicicol characterized by AUC.** **A)** Normalized dc/dt AUC sedimentation profiles of Atto550 labeled Hsp82 (C61) and **B)** unspecifically labeled Hsp90 $\beta$ . Analytical ultracentrifugation was performed after incubation for 1 h in 200 mM KCl closing buffer (Hsp82: 30 °C, Hsp90: 37 °C) with 2 mM ATP $\gamma$ S (yellow) to initiate the closed state. Additionally, ADP (red) or Radicicol (black) were added and incubated for 1 h to probe dimer re-opening.

To get a more detailed view of this phenomenon, re-opening kinetics with ADP and Radicicol were acquired by SEC using the same fitting method as described earlier. Interestingly, Hsp82 and Hsp90 $\beta$  displayed similar kinetics (Hsp82  $k_{\text{cat}} = 0.3121 \text{ min}^{-1}$ ; Hsp90 $\beta$   $k_{\text{cat}} = 0.1763 \text{ min}^{-1}$ ) when incubated with Radicicol (Fig. 57A, B). Since it can be excluded that ATP $\gamma$ S hydrolyzation leads to re-opening during the measured timeframe (see 4.2.1), the conformational changes are induced by the exchange of ATP $\gamma$ S with Radicicol. For both proteins, the nucleotide exchange by ADP reaches an equilibrium, which leaves a fraction of dimer still in the closed state. Again, similar kinetics were observed (Hsp82  $k_{\text{cat}} = 0.1673 \text{ min}^{-1}$ ; Hsp90 $\beta$   $k_{\text{cat}} = 0.0742 \text{ min}^{-1}$ ). Since the same concentration of ATP $\gamma$ S and ADP is present in the buffer, the formation of an affinity- and diffusion-based equilibrium is the most plausible explanation. Therefore, for Radicicol a higher population of the open state is observed, due to its nanomolar affinity to Hsp90 (Roe et al., 1999). Furthermore, the results suggest that the opening of the dimer from the closed state is not the rate-limiting step for ATP hydrolysis.

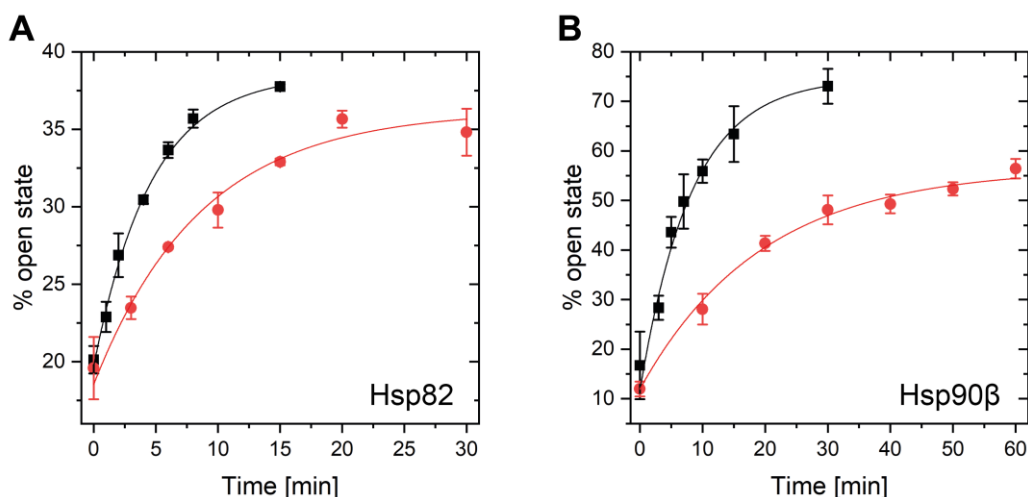


**Figure 57: Comparison of the Hsp82 and Hsp90 $\beta$  ATPase re-opening kinetics with ADP and Radiccol.** Re-opening kinetics of Hsp82 (A) and Hsp90 $\beta$  (B) in closing buffer with 50  $\mu$ M Radiccol or 2 mM ADP (red). Proteins were incubated with 2 mM ATP $\gamma$ S for 1 h prior to the measurement to initiate the closed state formation. Afterwards, SEC elution profiles at varying time points were obtained in triplicates and fitted (Radiccol: Hsp82  $k_{cat} = 0.3121 \text{ min}^{-1}$ ; Hsp90 $\beta$   $k_{cat} = 0.1763 \text{ min}^{-1}$ ; ADP: Hsp82  $k_{cat} = 0.1673 \text{ min}^{-1}$ ; Hsp90 $\beta$   $k_{cat} = 0.0742 \text{ min}^{-1}$ ).

Previous SEC experiments (see 4.3.2) demonstrated that the Hsp90 inhibitor and co-chaperone p23/Sba1 does only slightly affect the closed state formation. However, previous single ATP turnover and HD/X-MS experiments indicate that the co-chaperone inhibits ATPase activity by slowing down product release (Graf et al., 2014). To further investigate the interaction of p23/Sba1 with Hsp90, the co-chaperone was added to Hsp90 after the closed state had formed in the presence of 2 mM ATP $\gamma$ S. Afterwards, ADP was added, and the sample was incubated at 37  $^{\circ}$ C for 10 minutes (30  $^{\circ}$ C 5 min for Hsp82), representing half-time for Hsp90 re-opening. The resulting protein sample was analyzed using SEC, and the open population was calculated (Fig. 58). Consistent with previous findings, the presence of p23/Sba1 inhibited the opening of the dimer. Therefore, results obtained from crosslinking (see 4.2.3) and SEC suggest that the co-chaperone predominantly modulates the Hsp90 cycle during the closed state. Following ATP-induced N-terminal dimerization, p23/Sba1 binds stably to the formed cleft of the NTDs, contacting both protomers (Lee et al., 2021). The resulting complex impedes ADP release thereby inhibiting re-opening and ATPase activity (Graf et al., 2014).

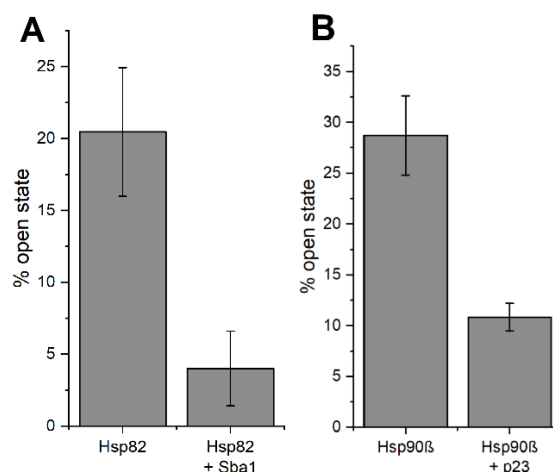


**Figure 58: Influence of the co-chaperone Sba1/p23 on dimer re-opening of Hsp90.** **A)** Hsp82 open state fraction after 5 min of incubation with Sba1 (Hsp82:Sba1 = 1:2). The protein was incubated in 200 mM KCl closing buffer (1h at 30 °C) with 2 mM ATP $\gamma$ S to initiate the closed state. **B)** Hsp90 $\beta$  re-opening compared to protein incubated with p23 after 10 min of incubation at 37 °C. The protein was incubated in 200 mM KCl closing buffer (1h at 37 °C) with 2 mM ATP $\gamma$ S to initiate the closed state. Samples were measured as independent triplicates and the data shown was obtained by fitting the SEC elution profiles with a bi-Gaussian fit.

#### 4.3.6 Domain Rearrangements during the Closed State Formation

H/DX (hydrogen-deuterium exchange) measures the exchange of hydrogen atoms with deuterium atoms in a protein's backbone amide groups (Konermann et al., 2011). This exchange occurs in response to changes in protein conformation, stability, and solvent accessibility. By comparing the H/DX patterns of Hsp90 in the open and closed state, insights into differing structural dynamics and interactions during the conformational rearrangements can be gained (Fig. 59A - E). The proteins were incubated in high salt closing buffer (Hsp82: 500 mM KCl, 30 min, 30°C; Hsp90 $\beta$ : 500 mM (NH<sub>4</sub>)<sub>2</sub>SO<sub>4</sub>, 60 min, 37 °C) in either the absence or presence of ATP $\gamma$ S to obtain a complete closed state. Afterwards, the proteins were subjected to H/DX-MS and the exchange rates of the different conformational states compared. In the N-terminal domain of Hsp82 and Hsp90 $\beta$ , two main structural elements that display significant differences in H/D could be identified: the  $\alpha$ 1-helix (Hsp82: residues 10-21; Hsp90 $\beta$ : residues 19-30) and the ATP-lid (Hsp82: residues 94-124; Hsp90 $\beta$ : residues 103-132) (Fig. 59C, D). Interestingly, based on the results, the  $\alpha$ 1-helix can be further divided into two areas with different exchange profiles. Residues oriented towards the  $\beta$ 1-sheet showed an increase in exchange, while residues near the catalytic loop showed a decreased exchange after closing. Upon nucleotide binding, the lid repositions over the binding pocket and exposes the N-terminal residues of the  $\alpha$ 1-helix, leading to an increase in exchange. Since the hydrophobic patch formed by the catalytic loop and the  $\alpha$ 1-helix is required for the dimerization of the NTDs, hydrogen exchange in the closed state is impeded. Strikingly, the lid displayed the largest decrease in exchange at the residues located near the hinges, highlighting the importance of these highly conserved residues. Both proteins showed a pronounced decrease in H/D

exchange upon closing in the middle domain at residues around the catalytic loop (Hsp82: residues 373-383; Hsp90 $\beta$ : residues 385-395). The arginine piston, which contacts the  $\gamma$ -phosphate of the nucleotide, is a key element for ATP hydrolysis (Cunningham et al., 2012). Therefore, essential rearrangements through hydrophobic interactions repositioning the catalytic loop lead to a reduction in exchange. For human Hsp90, the  $\beta$ -sheet connecting the subdomains of the MD, often referred to as M1 and M2, exhibited a notable decrease in exchange. Since Hsp82 did not show a similar behavior, an evolutionary divergence requiring Hsp90 $\beta$  to rearrange its MD during the ATPase cycle is a possible explanation for the different inherent enzymatic properties. On the other hand, for Hsp82, a more pronounced decrease was observed for the MD residues contacting the C-terminal domain (residues 494-498). Therefore, both proteins differ significantly in the way the MD rearranges during closing. In the C-terminal domain of Hsp90 $\beta$ , a slight decrease of H/D exchange in the helix (residues 604-610) forming an interface between the protomers, was discovered. Thus, all three domains of the protein are rearranged in the conformational cycle. In summary, the obtained H/DX results confirm a common hydrolysis mechanism involving the  $\alpha$ 1-helix, the lid, and the catalytic loop. However, variations in H/D exchange highlight differences regarding structural rearrangements.

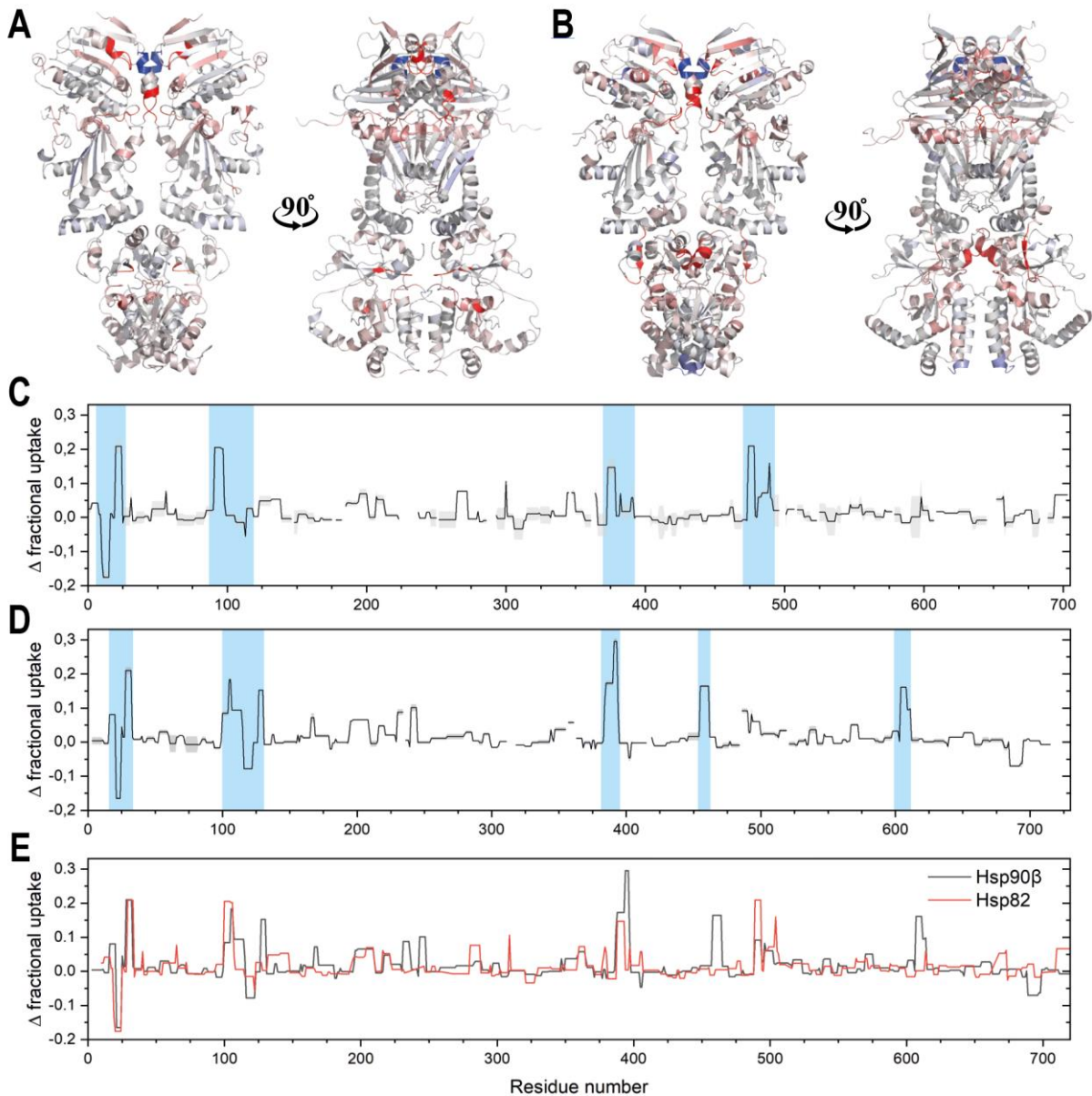


**Figure 59: H/DX comparison of the open and closed state of Hsp90.** **A)**  $\Delta$  fractional uptake between the open and closed state of Hsp82 plotted on its crystal structure in the closed state (PDB ID: 2cg9). Red indicates decreased exchange after closing; blue areas with increased exchange. Hsp82 was incubated for 1 h in 500 mM KCl closing buffer with 2 mM ATP $\gamma$ S to initiate the closed state. **B)**  $\Delta$  fractional uptake of Hsp90 $\beta$  plotted on its crystal structure (PDB ID: 5fwk). Hsp90 $\beta$  was incubated for 1 h in 500 mM ammonium sulfate closing buffer with 2 mM ATP $\gamma$ S to initiate the closed state. **C)**  $\Delta$  fractional uptake of Hsp82 and Hsp90 **(D)** plotted by residue. Blue highlights crucial elements exceeding the significance threshold. **D)** Residual alignment of Hsp82 and Hsp90 $\beta$  comparing  $\Delta$  fractional uptake.

#### 4.3.7 Evolutionary Divergence of Yeast and Human Hsp90

Previous experiments highlighted the effect of the ATP lid and the  $\alpha$ 1-helix for the formation of the closed state and the overall ATPase activity of Hsp90. The importance of the two elements can be visualized by a high conservation score of the respective residues (Fig. 60A). Furthermore, the catalytic loop and the residues forming the ATP binding pocket display a similar conservation score. However, a

direct comparison of the amino acid composition of the  $\alpha 1$ -helix and the lid reveals three amino acids in which Hsp82/Hsc82 and Hsp90 $\alpha$ /Hsp90 $\beta$  differ. In the  $\alpha 1$ -helix, both human isoforms contain an alanine residue (Hsp90 $\alpha$  residue 27, Hsp90 $\beta$  residue 22), whereas the yeast isoforms contain a serine at the respective positions (Hsp82 residue 13, Hsc82 residue 13). Strikingly, this residue displayed the highest change in deuterium uptake when the open and closed state were compared during H/DX measurements. This indicates that during the closed state formation this residue experiences a drastic increase in exposure towards the surrounding buffer. Therefore, the hydrophilic serine might provide a more stable closed state for the yeast Hsp90s. In the lid region, two residues differ between the yeast and human Hsp90. First, Hsp90 $\alpha$  and Hsp90 $\beta$  both contain a glutamine (Hsp90 $\alpha$  residue 122, Hsp90 $\beta$  residue 118) in the middle of the lid. In contrast, Hsp82 and Hsc82 both differ to the human isoforms, as a serine residue is present at this position (Hsp82 residue 109, Hsc82 residue 109). Similar to the A107N mutation, this residue might affect lid movement and stabilize the closed state by additional hydrogen bonds. The second differing lid residue includes an isoleucine residue for the human protein (Hsp90 $\alpha$  residue 128, Hsp90 $\beta$  residue 123), which is changed to a valine in yeast (Hsp82 residue 114, Hsc82 residue 114). However, this residue displayed generally a low conservation score and due to the similar properties of the amino acids, it is unlikely to influence the ATPase activity of the protein.

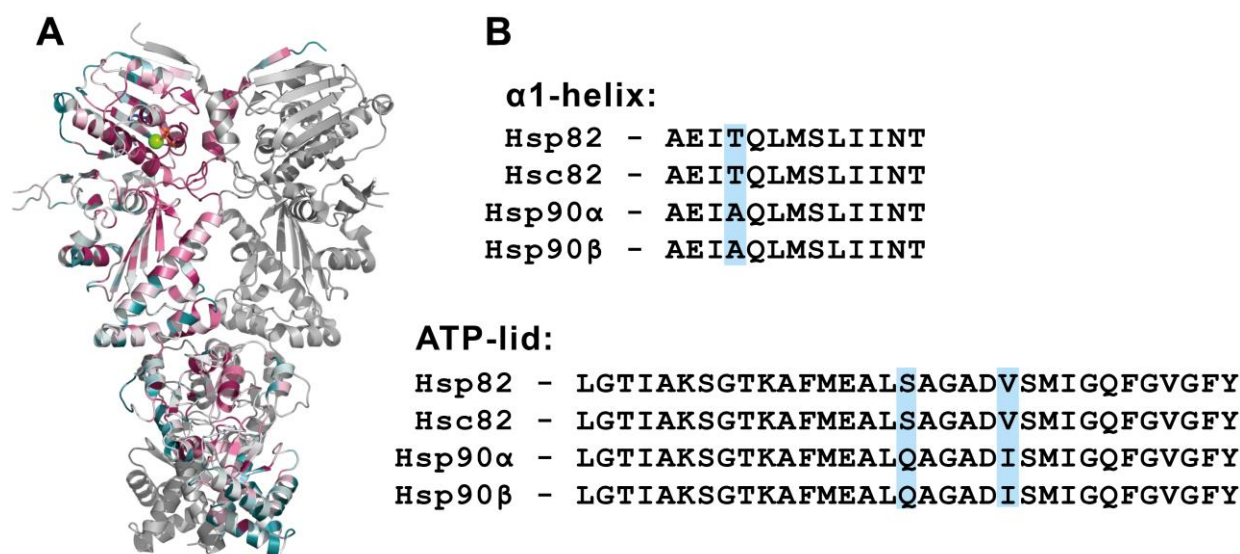


**Figure 60: Evolutionary conservation of Hsp82 and Hsp90 $\beta$ .** **A)** Conservation scores obtained via Consurf plotted on the structure of Hsp90 $\beta$  (PDB ID: 5FWK). Sequence homologs with a conserved identity between 35 – 95 % were selected to calculate scores. Magenta highlights residues with a high conservation value; teal coloring indicates a low conservation. **B)** Alignment of the residues comprising the  $\alpha 1$ -helix and ATP-lid residues from Hsp82, Hsc82, Hsp90 $\alpha$  and Hsp90 $\beta$ . Differing amino acids are highlighted in blue.

To address the impact of the T13A and S109Q mutation on the functionality of the Hsp82 dimer, molecular dynamic simulations were performed by the group of Prof. Ville Kaila (Stockholm University). Based on the crystal structure of closed Hsp82 (PDB ID: 2CG9), the two mutations were introduced in the primary structure and compared to the wildtype protein. Simulations were carried out for 300 ns and inter-/intramolecular distances of selected residues were monitored. For the T13A

mutation, the MD simulations suggest that T13 positions E11 (Fig. 61A, B), which leads to flickering of the E11-K98 ion-pair (Fig. 61E). In contrast, with A13, E11 moves towards the ATP lid, which in turn makes the E11-K98 ion-pair tighter (Fig. 61A, E). The E11-K98 ion-pair (E22-K107 for Hsp90 $\beta$ ) can be found in the crystal structure of the human Hsp90 $\beta$  (PDB ID: 5FWK), but is absent for wildtype Hsp82. K98 is located near the hinges of the ATP-lid, which displayed drastic changes during HD/X experiments (see 4.3.6). Therefore, the formed ion-pair hinders the lid rearrangement upon nucleotide binding. In the closed state of Hsp82, the lid is stabilized via hydrogen bonds, which includes the interaction of Y47 and S109. Therefore, the lid helices turn towards each other when ATP is bound. With the introduced glutamine at position 109, the loop around the residue is flipped outwards, abolishing the stabilizing hydrogen bond analogue to Hsp90 $\beta$  (Fig. 61C). This effect further propagates along the ATP-lid helix, moving K44-F104 further away from each other in the ATP-bound mutant (Fig. 61F). Additionally, the two helices contacting the adenine and ribose of ATP display an increased flexibility. Furthermore, the shifted interactions between the ATP lid and the first  $\alpha$ -helix of the NTD affect the  $\alpha$ 1- $\alpha$ 1 contacts within the Hsp90 dimer. The introduced mutations affect the motion of the  $\alpha$ 1-helices in the closed dimer state, which can influence the opening and closing of the dimer (Fig. 61D, G). Summarized, the obtained data suggests for Hsp82 a similar structural behavior as Hsp90 $\beta$ , resulting in a less stable closed state and a hindered lid movement.

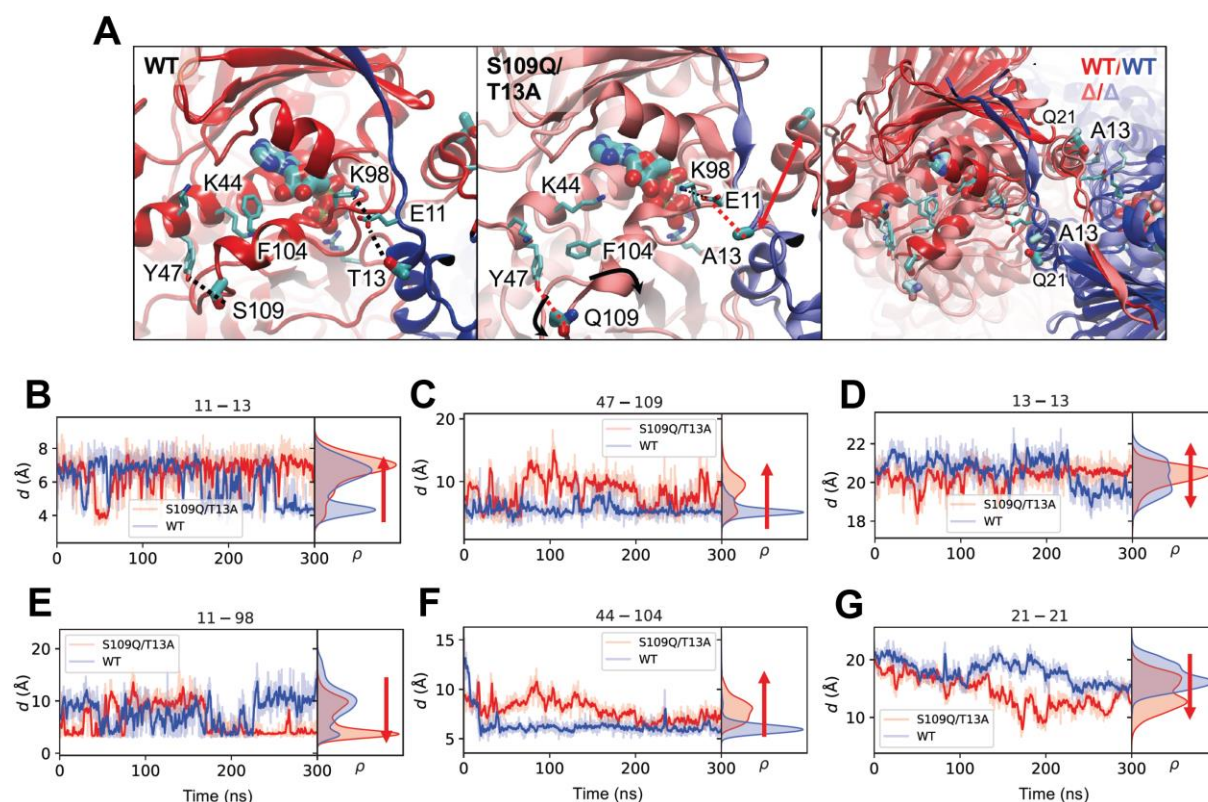


**Figure 61: MD simulations of wt Hsp82 and Hsp82 T13A S109Q. A)** Close view of the impact of the T13A mutation on the E11-K98 ion pair. **B)** Intramolecular distance of E11 and T/A13. The red arrow points towards the orientation required for the formation of the E11-K98 ion pair. **C)** Intramolecular distance of Y47 and S/Q109. The arrow indicates lid opening. **D)** Intermolecular distance of T/A13. The arrow indicates  $\alpha$ 1-helix movement. **E)** Intermolecular distance of E11 and K98. The

arrow indicates the formation of the E11-K98 ion pair. **F**) Intramolecular distance of K44 and F104. The arrow indicates lid opening. **G**) Intermolecular distance of N21. The arrow indicates  $\alpha$ 1-helix movement. All MD simulations were performed by the group of Prof. Ville Kaila (Stockholm University).

#### 4.3.8 *In Vitro* Characterization of Chimeric Human/Yeast-Mutants

Hsp82 and Hsp90 $\beta$  differ slightly in their amino acid composition in the  $\alpha$ 1-helix and ATP-lid. Obtained data from MD simulation suggests that two specific mutations have an impact on the formation of the closed state and lid stability. To confirm the effect of the T13A and S109Q mutations *in vitro*, the respective residues were changed to their human/yeast counterparts via site-directed mutagenesis. Subsequently, the influence on the ATPase activity and closing kinetics was investigated (Fig. 62 A, B). Hsp82 T13A displayed a drastic decrease in ATPase activity compared to the wildtype protein, whereas the human A22T mutation significantly increased its activity. Similar observations were made when comparing the formation of the closed state. For yeast, the introduced mutation led to a decreased closed population after 1 minute of incubation, whereas the human counterpart, Hsp90 $\beta$  A22T, displayed an increase in closing kinetics, resulting in a closed state population of over 83% after 10 minutes (Fig. 62C, D). The ATPase rate of Hsp82 S109Q was observed to be decreased by 32% compared to wildtype Hsp82. Additionally, a decrease in the closed population was present. For human Hsp90 $\beta$ , the Q118S mutation was found to stimulate ATPase activity by 57% and led to an increased closed state formation. However, when comparing the individual mutations, T13A/A22T had a more significant impact on the activity and N-terminal closing of the protein. Double mutants, containing both mutations, further enhanced the difference from the wildtype protein. Therefore, the mutations individually influence activity and closing kinetics. Consistent with MD simulations, the *in vitro* characterization demonstrated an evolutionary divergence of Hsp82 and Hsp90 $\beta$ . The facilitated lid movement of Hsp90 $\beta$  substantially affected its ATPase rate and potentiated the closed state formation. Contrary, when the respective mutations are present in yeast Hsp82, opposite effects are observed.

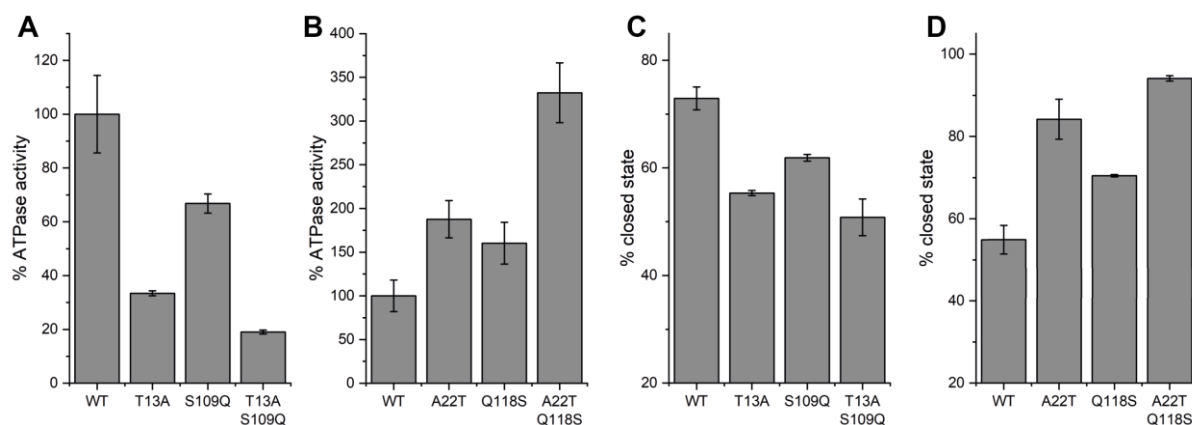


**Figure 62: Impact of mutations on the activity and closing kinetics of Hsp90.** **A)** Comparison of wt Hsp82 with chimeric mutants. The obtained activity was normalized to wt Hsp82. **B)** Comparison of analogous Hsp90 mutants. Activity was

measured in 200 mM KCl closing buffer (Hsp82: 30 °C, 3  $\mu$ M; Hsp90 $\beta$ : 37 °C, 10  $\mu$ M). Measurements were performed as three independent technical replicates to calculate means and standard deviations. The obtained activity was corrected for background activity using Radicol. **C)** Wt Hsp82 closed state fraction after 1 min of incubation at 30 °C with 2 mM ATP $\gamma$ S compared to chimeric mutants. Data was obtained by fitting SEC elution profiles with a bi-Gaussian fit. **D)** Wt Hsp90 compared to analogous mutants after 10 min of incubation at 37 °C.

#### 4.3.9 *In Vivo* Characterization of Chimeric Human/Yeast-Mutants

To determine the impact of the chimeric mutations on the viability of *S. cerevisiae*, p423GPD plasmids encoding the protein with the respective mutation were transformed into a yeast shuffling strain. Additionally, the strain contains the wt Hsp82 on a plasmid with a URA selection marker, which allowed to replace wt Hsp82 by the respective mutants. To ensure the loss of the original wt Hsp82 plasmid, cells were subjected to media supplemented with 5'-FOA. Therefore, only cells survive the complementation assay when the mutated Hsp82 provides sufficient functionality. The comparison of wt Hsp82 with the mutants indicates, that under optimal growing conditions the mutations have no impact on the viability of Hsp82 (Fig. 63A). Despite a significant reduction in ATPase activity, no inhibition of cell growth can be observed for the chimeric mutants. However, a comparison of the ATPase mutants to the wt Hsp82 protein reveals a reduced viability for T22I, T101I and A107N (Fig. 63B). Despite an increased ATPase activity of T22I, the cells displayed a drastic reduction in viability. Therefore, the ATPase activity does not necessarily correlate with viability (Zierer et al., 2016).

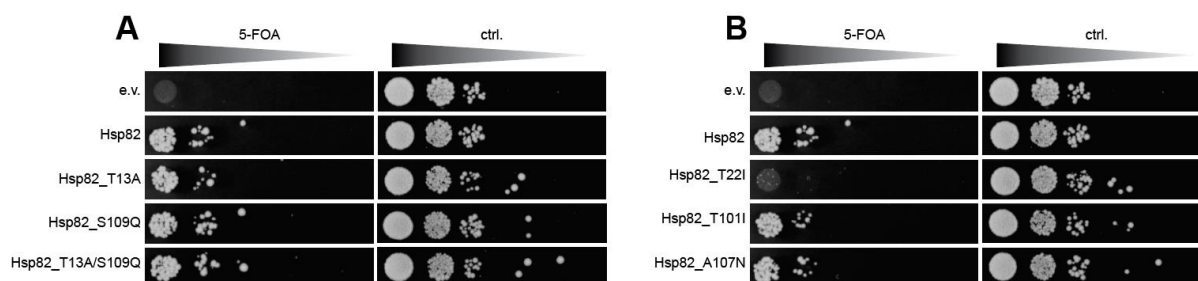


**Figure 63: *In vivo* viability of chimeric and ATPase mutants.** **A)** Viability of the chimeric mutants was tested after 5'-FOA plasmid shuffling at 30 °C. Mutants were cloned in a p423GPD plasmid in transformed into the yeast shuffling strain, which carried a wt Hsp82 plasmid with an URA marker. Cells were subjected to 5'-FOA at different dilutions to ensure loss of the wt Hsp82 plasmid. **B)** Viability of the ATPase mutants was tested after 5'-FOA plasmid shuffling.

## 5 Discussion

### Comparative Analysis of the Conformational Dynamics of Yeast and Human Hsp90

The viability of various organisms strongly relies on the precise regulation of Hsp90 activity (Yue et al., 1999; Zierer et al., 2016). A direct comparison of the yeast Hsp82 and human isoforms Hsp90 $\beta$  reveals a near identical dimeric structure and a 70 % shared sequence at the amino acid level. Furthermore, the proteins from both organisms are regulated by co-chaperones with similar functionality (Schopf et al., 2017). However, a tenfold difference in ATPase activity distinguishes Hsp82 from Hsp90 $\beta$ , with the yeast protein displaying an increased hydrolysis rate (Richter et al., 2008). Previous studies already confirmed a common conformational mechanism of the two proteins (Vaughan et al., 2009). However, additional mechanistic differences beyond a deviating ATPase rate and populations of the conformational states remain largely elusive (Graf et al., 2014; Southworth & Agard, 2008). Furthermore, the human Hsp90 comprises an extended set of co-chaperones (Johnson, 2012; Schopf et al., 2017). To obtain a detailed picture of the structural rearrangements of the hydrolysis driven conformational cycle, a comparative *in vitro* and *in silico* analysis was performed.

### Segmental Labeling and Domain Ligation of Hsp90 $\beta$ for FRET Analysis

In an attempt to label specific segments of Hsp90 $\beta$  without affecting the natural cysteines located exclusively in the M- and C-terminal domain, segmental labeling and ligation were carried out using EPL and Sortase 5M-mediated ligation. To achieve this, the respective modified N-terminal domain with an engineered cysteine was designed, expressed, purified, and labeled with a fluorescent dye before being ligated to the MC-domains of Hsp90. However, the chosen EPL ligation sites in the charged linker and middle domain did not yield sufficient full-length protein for further experiments. Decreased yields are most likely caused by steric factors and the flexibility of the linker (Karagoz, Sinnige, et al., 2011; Muir et al., 1998). The optimized strategy for the Srt5M-mediated ligation of full-length Hsp90 $\beta$  was successful, yielding approximately 50 % ligated full-length product (Fig. 26A), which is consistent with previous reports (Freiburger et al., 2015). However, fractions of non-ligated MC fragment could not be removed during the purification process after ligation, likely due to C-terminal dimerization. The construct that results after Srt5M ligation, containing the recognition motif LPKTG, was characterized *in vitro*. The experiments show that human Hsp90 $\beta$  carrying the LPKTG motif within the linker region behaves similarly compared to wt Hsp90 $\beta$  regarding the closed state formation and ATPase activity. However, labeling led to the formation of a fraction of undefined oligomers. As a result, ensemble FRET measurements were affected by the emergence of the additional species, and conformational changes during the closing reaction could not be detected unambiguously. To avoid oligomer formation, single-molecule FRET was performed at picomolar concentrations. These measurements confirmed the

presence of labeled Hsp90 $\beta$  in its dimeric state, as determined by anisotropy and FCCS analysis. The FRET measurements were performed in the presence of varying nucleotides to address their influence on conformational dynamics. Fluorescence lifetime analysis revealed that in the absence of nucleotide or in the presence of ADP, the protein mainly adopted an open conformation. However, the use of ATP $\gamma$ S or AMP-PNP inhibited cycle progression, resulting in the accumulation of the closed state. Interestingly, in the presence of ATP, the FRET efficiency shifted between the closed and open states of Hsp90 $\beta$ , indicating increased conformational dynamics. These experiments suggest that Hsp90 $\beta$  has extended flexibility in its N-terminal domains, leading to fluctuations in FRET efficiency even in the apo and ADP-bound states. The observed nucleotide-dependent closing and dynamics are consistent with single-molecule FRET experiments conducted for Hsp82 (Mickler et al., 2009; Wolf et al., 2021), highlighting a common mechanism, although Hsp90 $\beta$  displays greater structural flexibility. However, due to the observed oligomerization of labeled Hsp90 $\beta$ , it cannot be excluded that the fluorescent label affects protein dynamics and closing behavior.

### **Oligomerization of Hsp90**

The prevailing understanding of Hsp90 function includes the formation of an N-terminally associated state, which is necessary for ATP hydrolysis. However, in addition to the protein's dimeric state, several studies have reported Hsp90 self-association into larger oligomeric species. This oligomerization process has been observed *in vivo* (Nemoto & Sato, 1998) and *in vitro* (Garnier et al., 2002) and can be exacerbated under heat shock conditions (Chadli et al., 1999) or in the presence of divalent cations (Moullintraffort et al., 2010). Therefore, the presence of divalent cations, such as magnesium or calcium, in the closing buffer could explain the observed oligomer formation of Hsp90 during SEC experiments. In fact, when high concentrations of calcium chloride were used, both Hsp82 and Hsp90 $\beta$  showed increased oligomerization. Previous structural investigations of the oligomers revealed the presence of tetramers, hexamers, and dodecamers (Fig. 64) (Lee et al., 2011; Moullintraffort et al., 2010). In addition, the crystal structure of an MC-Hsp90 construct revealed a hexameric assembly, which has been termed "cozy nest" (Moullintraffort et al., 2010). Thus, the MC domain alone is sufficient for oligomerization, although the involvement of the NTDs cannot be excluded. The interaction between the NTDs from one dimer suggests that interactions between NTDs within oligomers may occur. Site-specific labeling of the N-terminal domain drastically increased the oligomeric population of Hsp90 $\beta$ . As interactions and close proximity of the NTDs likely occur in the formed oligomers, it is difficult to distinguish fluorescent signals from nucleotide-induced closing or the assembly into the undefined oligomeric species. Remarkably, the reported onset of the heat-induced oligomerization occurs around 50 °C (Chadli et al., 1999), which correlates with the observed thermal unfolding of Hsp90 $\beta$  during experiments with Sypro orange (Fig. 38A). Therefore, partial unfolding of the protein,

induced by temperature, hydrophilic interactions, divalent cations, or other external factors, is likely responsible for the formation of non-dimeric species.

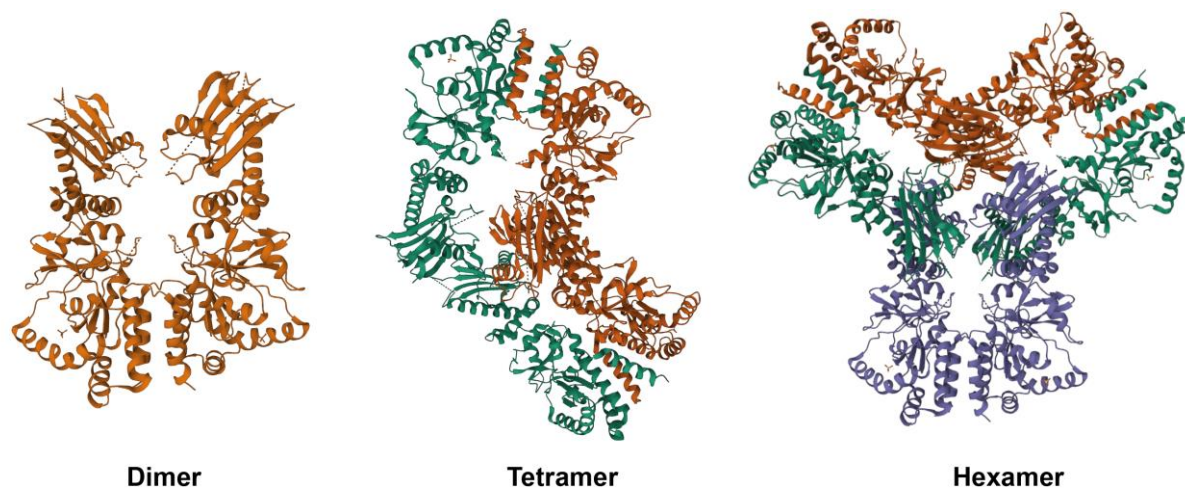


**Figure 64: Crystal structures of MC-Hsp90 $\alpha$  in different oligomeric states.** Dimer, tetramer and hexamer crystal structure obtained from oligomers from truncated Hsp90 $\beta$  (PDB: 3Q6M (Lee et al., 2011)). C-terminal associated dimers are colored in orange, green and blue, respectively.

### Hsp82 and Hsp90 $\beta$ Deviate in Hydrophobic Interactions

Both Hsp82 and Hsp90 $\beta$  display a salt-dependent closing kinetic and ATPase activity. An elevated ATP hydrolysis rate goes along with an accelerated closing kinetic of the dimer (Fig. 52). Additionally, Hsp82 displayed a tenfold faster closing kinetic compared to the human protein (Fig. 46). These results confirm that the formation of the closed state poses the rate-limiting step of the ATPase cycle for both Hsp82 and Hsp90 $\beta$ , in agreement with what previous ensFRET measurements indicated (Hessling et al., 2009). For Hsp90 $\beta$ , the ATPase activity strongly correlates with the ionic concentration and the ability of the respective salt to affect hydrophobic interactions (Fig. 51). The observed effects of these salts align with the well-established kosmotropic (strengthening) and chaotropic (weakening) classification of the Hofmeister series (Hofmeister, 1888). However, Hsp82 exhibits a slight deviation from this pattern as with ammonium sulfate a decrease in ATPase rate was observed. Additionally, SEC data indicate an incomplete formation of the closed population in the presence of ATP $\gamma$ S and (NH $_4$ ) $_2$ SO $_4$  (Fig. 52C). This leads to the assumption that the functionality of Hsp82 is partially impaired by the strengthened hydrophobic effects, caused by the kosmotropic properties of ammonium sulfate. It remains elusive whether this is the result of impaired conformational rearrangements or partial misfolding of the protein. On the other side of the spectrum, the chaotropic properties of calcium chloride resulted for both proteins in a reduced ATPase rate, visible aggregation and the formation of oligomers (Fig. 53). The chaotropic agent disrupts and weakens the hydrogen-bonding network highlighting the importance of hydrophobic interactions for Hsp90 (Zhang & Cremer, 2006). The attachment of hydrophilic, fluorescent dyes had a similar effect on Hsp90 $\beta$ , but not on Hsp82. Therefore, Hsp82 most likely has inherent stronger

hydrophobic interactions promoting the closed state formation upon nucleotide binding. These enhanced interactions could explain a reduced impact of hydrophilic dyes on the stability of the protein, as well as a faster closing kinetic of unlabeled Hsp82 compared to labeled protein (Hessling et al., 2009). Consequently, a further enhancement of Hsp82s hydrophobicity via ammonium sulfate negatively affects the closed state formation.

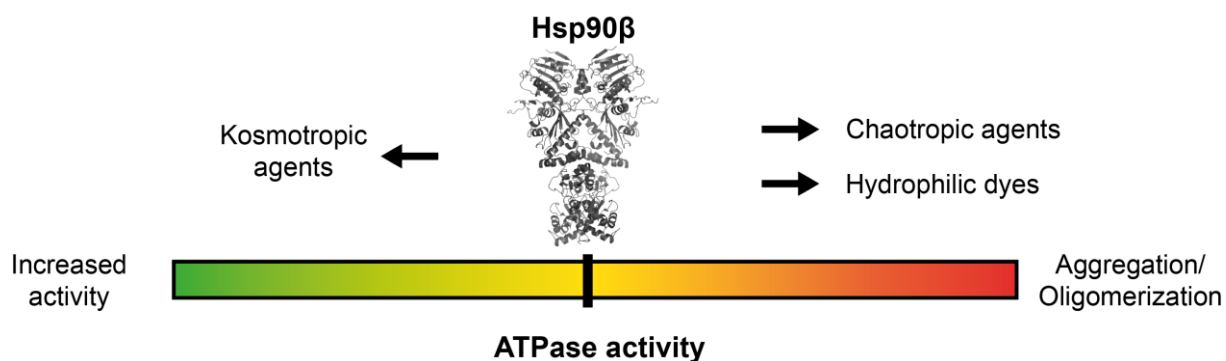


**Figure 65: Schematic illustration of the modulation of hydrophobic interactions.** Effects of buffer components and fluorescent labels on the closing kinetics and resulting ATPase activity for Hsp82 and Hsp90 $\beta$ . Green areas indicate an increased hydrolysis rate and formation of the close state; red areas indicate a decrease.

The difference of hydrophobic interactions is most likely caused by differences in single amino acid residues, as appropriate point mutations already drastically influence ATPase activity (Ali et al., 2006; Siligardi et al., 2004). T31I (T22I for Hsp82) increases the hydrophobicity of the  $\alpha$ 1-helix and contacts the hydrophobic residues of the catalytic loop. For both Hsp82 and Hsp90 $\beta$  the mutation results in an increased hydrolysis rate compared to the respective wildtype protein. Although the mutation displays a 37 % increase in activity for Hsp82, it caused a much larger increase of 141 % for the activity of Hsp90 $\beta$  (Fig. 54B, C). Additionally, T31I resulted in a larger percentage of the closed state population for the human protein compared to Hsp82 (Fig. 54D, E). This further confirms that the closing mechanism of human Hsp90 is more reliant on the formation of hydrophobic interactions compared to Hsp82.

### Nucleotide Exchange induced Dimer Re-Opening

The common understanding of the mechanism behind Hsp90 suggests that the initiation of dimer re-opening and cycle progression is triggered by ATP hydrolysis (McLaughlin et al., 2002; Prodromou et al., 2000). Nevertheless, a growing body of evidence suggests that the exchange of nucleotides while in the closed state could also lead to re-opening (Reidy & Masison, 2020; Zierer et al., 2016). Both ATP $\gamma$ S and AMP-PNP were able to accumulate the closed population of Hsp90 by preventing cycle progression *via* an inhibited hydrolysis (Fig. 47A, B). Surprisingly, a subsequent addition of ADP, ATP or Radicicol to the closed Hsp90 resulted in dimer re-opening, which was evident as a shift of the equilibrium towards

the open population. Effects caused by the hydrolysis of bound ATP $\gamma$ S can be excluded, since a prolonged incubation of Hsp90 $\beta$  (4 h) did not provide a sufficient time-frame for a hydrolysis associated re-opening (Fig. 35A). Therefore, the bound ATP $\gamma$ S most likely can be exchanged with ADP, ATP or Radicicol resulting a normal cycle progression and opening of the dimer (Fig. 55, 56, 57). For ATP, it could not be ruled out that the open Hsp90 population hydrolyzes the nucleotide and only the resulting ADP exchanges with the bound ATP $\gamma$ S. As Radicicol demonstrated a more prominent re-opening of Hsp90 compared to ADP, it is most likely that the exchange of ATP $\gamma$ S is influenced by the affinity of the respective compound (Radicicol  $K_D = 2.7$  nM; ADP  $K_D = 3.1$   $\mu$ M) (Roe et al., 1999; Zhang et al., 2015).

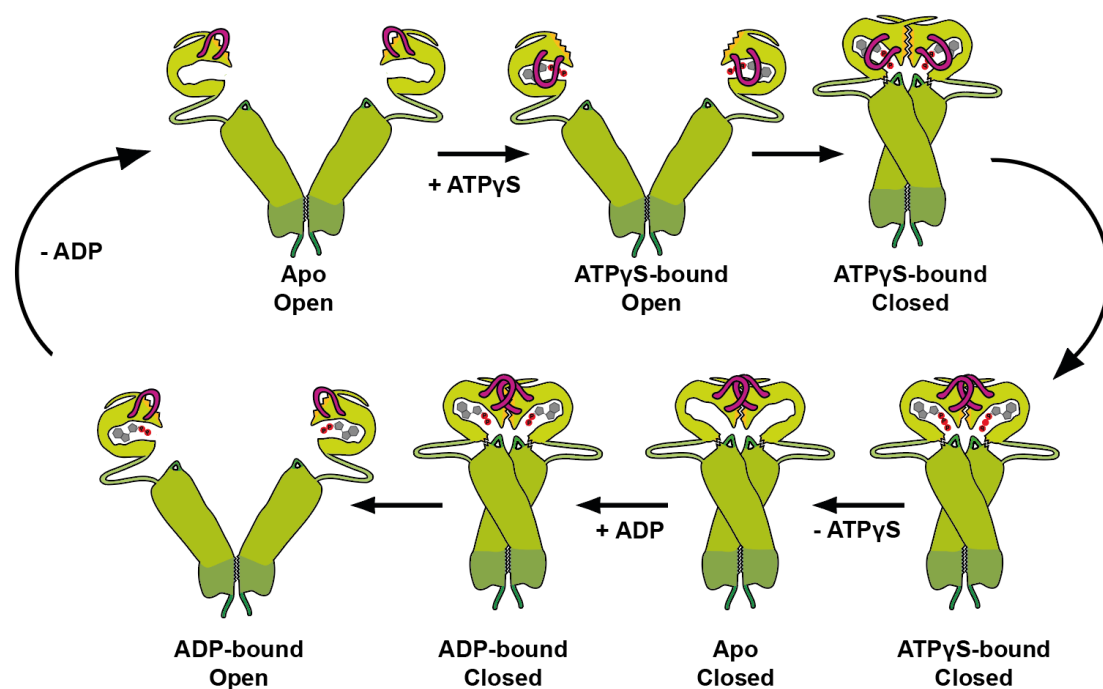


**Figure 66: Schematic illustration of nucleotide exchange-induced dimer re-opening.** ATP $\gamma$ S binding induces lid closure over the ATP binding pocket and subsequent dimerization of the N-terminal domains. Exchange of ATP $\gamma$ S with ADP in the closed state restores the ability of Hsp90 to progress through the cycle and triggers re-opening. The N-terminal lid (magenta), the  $\alpha$ 1-helix (yellow) and the catalytic loop (dark green) of Hsp90 are highlighted.

Previous experiments with shuffling strains have demonstrated the viability of the E33A mutant in yeast (Reidy & Masison, 2020; Zierer et al., 2016). This mutant replaces the glutamic acid that is located in the ATP binding pocket and is essential for ATP hydrolysis. Furthermore, the E33A mutant is still capable of initiating the closed conformation of Hsp82 upon nucleotide binding. Although a complete deletion of Hsp82 is lethal for cells (Fig. 63) (Nathan & Lindquist, 1995), the hydrolysis-deficient Hsp82 mutant provides enough functionality for the survival of yeast cells. Therefore, the exchange of bound ATP to ADP can serve as an alternative route for the conformational cycle progression of Hsp82. The exchange triggers re-opening similar to hydrolysis and eventually results in the necessary functionality of the E33A mutant. However, the distinct mechanism behind the exchange remains elusive. Most likely, the bound ATP $\gamma$ S can dissociate from the nucleotide-binding pocket in the closed state, as the lid and/or

the binding site provides sufficient flexibility to enable the exchange. Subsequent binding of ADP to the 'apo-closed' Hsp90 initiates the dissociation of the N-terminal domains and the re-opening of the dimer (Fig. 66). However, it cannot be ruled out that ADP/Radicicol trigger re-opening by an unknown mechanism independent of nucleotide binding.

### Impact of the $\gamma$ -Phosphate on Dimer Opening and Closing

Hsp82 and Hsp90 $\beta$  drastically differ in their closing behavior regarding AMP-PNP (Fig. 47C). Whereas for Hsp82 a similar closing kinetic to ATP $\gamma$ S was observed, Hsp90 $\beta$  required overnight incubation to achieve the closed state. Surprisingly, when AMP-PNP was used for closing, neither ADP, ATP nor Radicicol were able to trigger dimer re-opening for Hsp82 and Hsp90 $\beta$ . These findings, in combination with the outcomes of the closing experiments using AMP-PNP, suggest that the binding of AMP-PNP differs from ATP $\gamma$ S and that the  $\gamma$ -phosphate plays a critical role in the closing and opening process. Furthermore, it should be noted that affinity-based effects could be ruled out since ADP and Radicicol have lower dissociation constants than AMP-PNP (Radicicol  $K_D = 2.7$  nM; ADP  $K_D = 3.1$   $\mu$ M; AMP-PNP  $K_D = 7.9$   $\mu$ M) (Roe et al., 1999; Zhang et al., 2015). A direct comparison of the human Hsp90 in a closed conformation with ATP or AMP-PNP reveals slight conformational differences located in the lid region (Fig. 67). Strikingly, the difference is located near Gln118, which differs between human and yeast Hsp90 (Ser109). Structural differences of the closed states and conformational rearrangements of the ATP lid would provide a possible explanation for the inhibited closing of Hsp90 $\beta$  with AMP-PNP. Furthermore, MD simulations in yeast suggest, that small rearrangements in the lid area can influence stability and therefore activity (Fig. 61).

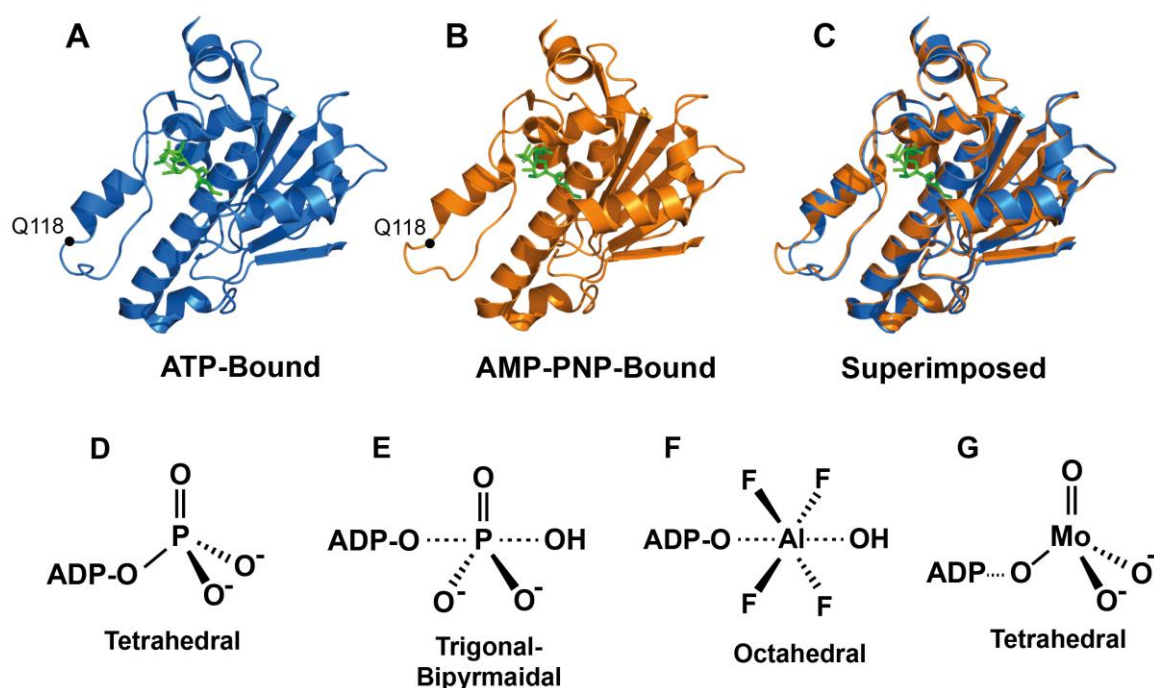


**Figure 67: Differences in nucleotide binding and  $\gamma$ -phosphate geometry.** Cryo-EM structure of the N-terminal domain from human Hsp90 $\beta$  in the closed state with ATP (**A**) (PDB: 5fwk (Verba et al., 2016)) and AMP-PNP (**B**) (PDB: 8EOB (Srivastava

et al., 2023)). The position of Ala22 is indicated on the ATP lid of the respective structure. C) Superimposition of the ATP and AMP-PNP bound structure. D-F) Different geometries of the  $\gamma$ -phosphate for ATP, the pre-hydrolysis state, ADP-AlF<sub>4</sub> and ADP-MoO<sub>4</sub> (Sullivan et al., 1997; Xu et al., 1997).

The importance of the  $\gamma$ -phosphate was confirmed when ADP-AlF<sub>4</sub> or ADP were tested for closing. ADP, which lacks the  $\gamma$ -phosphate, is unable to initiate the closed conformation, but was able to trigger re-opening *via* nucleotide exchange. Although ADP-AlF<sub>4</sub> mimics the trigonal bipyramidal pre-hydrolysis state of the  $\gamma$ -phosphate (Fig. 67E, F), it did not induce the closed state of Hsp90 (Fig. 47A, B) (Xu et al., 1997). Commonly, Molybdate (MoO<sub>4</sub>) is added to Hsp90 to stabilize the closed state (Verba et al., 2016). Molybdate is arranged a tetrahedral conformation, similar to phosphate, and can replace the  $\gamma$ -phosphate of hydrolyzed ATP (Fig. 67G) (Sullivan et al., 1997). These results suggest that the structure of the  $\gamma$ -phosphate determines the formation of the open or closed state. Furthermore, dimer re-opening is likely to occur during the transition from the tetrahedral conformation to the trigonal-bipyramidal state of the phosphate. After the transition, the repositioning of the ATP lid eliminates the hydrophobic interactions between the  $\alpha$ 1-helices and the catalytic loop, leading to conformational changes that promote the formation of the open state.

### **Hsp82 and Hsp90 $\beta$ Differ in Domain Rearrangements during the Closed State Formation**

H/DX data comparing Hsp82 and Hsp90 $\beta$  in their open and closed states revealed differences in the rearrangement of the MD and C-terminal domains of the two proteins (Fig. 59). For Hsp82, closing includes the structural changes of several residues located in the MD, which are in direct contact with the C-terminal domain. In contrast, the results suggest that structural changes in the MD are necessary for the closing process of human Hsp90. SEC data additionally confirms this assumption as it demonstrated a dissimilarity in the closing of Hsp82 and Hsp90 $\beta$  (Fig. 45). The elution volume of the closed population of human Hsp90 exhibited a more significant shift than for Hsp82, suggesting a greater disparity in the hydrodynamic volume between the two states. This implies that Hsp90 $\beta$  may undergo more extensive conformational changes upon nucleotide binding and closing. Additionally, differences in the open and closed populations of apo-Hsp90 can be observed, with apo Hsp82 showing a higher fraction of the closed population, as reported in previous studies (Southworth & Agard, 2008). Furthermore, limited proteolysis revealed that the divergence between Hsp82 and Hsp90 $\beta$  arises from differences in their closed states. Although the digestion patterns of their open states are nearly identical, slight variations in the digestion patterns of the closed state confirm a conformational difference (Fig. 46). Therefore, the evolutionary divergence between the two proteins is not limited to minor variations in the N-terminal domain, but rather extends to all three domains, impacting the complete dimer closing process. This notion is in agreement with previously published data comparing the conformational dynamics of eukaryotic Hsp90 proteins with HtpG of *E. coli* (Graf et al., 2014; Phillips et al., 2007). Hsp90 $\beta$  is likely to rely on a more flexible structure, allowing it to accommodate a broader range of

clients and providing an additional layer of regulation compared to Hsp82. Another explanation for the dynamic differences between Hsp90 $\beta$  and Hsp82 could be their interactions with a diverse set of co-chaperones (Johnson, 2012).

### Evolutionary Divergence of Yeast and Human Hsp90

The experiments conducted emphasize the significance of the ATP lid and  $\alpha$ 1-helix in both the formation of the closed state and overall ATPase activity of Hsp90. The essential role of these elements is highlighted by the nearly complete conservation of the corresponding residues between yeast and human isoforms (Fig. 60). The  $\alpha$ 1-helix and ATP-lid of Hsp82 and Hsp90 $\beta$  differ by only one amino acid each: Ala31 and Glu118 (Thr22 and Ser109 for yeast). Both hydrophilic and hydrophobic effects play a critical role in modulating the ATPase activity of Hsp82 and Hsp90 $\beta$  (Fig. 52). Therefore, mutating an alanine to threonine and *vice versa* altered the activity of both proteins, with the yeast protein experiencing a decreased ATPase while Hsp90 $\beta$  activity increased. The effects were further explained through MD simulations, which revealed that replacing Thr13 with Ala in Hsp82 caused Glu11 to move towards the ATP lid, resulting in a tighter ion-pair between Glu11 and Lys98. This ion-pair hindered the lid rearrangement upon nucleotide binding, thereby inhibiting ATPase activity. A similar effect to the Ala31/Thr22 mutation was observed for the Glu118/Ser109 mutation. This mutation directly affects the lid stability of the closed state by introducing an additional hydrogen bond to Tyr47 in Hsp90 $\beta$ . Previous studies have already shown a direct correlation between the ATPase rate and an enhanced lid closure (Ali et al., 2006). As a result, the human protein exhibited an increase in its hydrolysis rate and closing kinetics. Comparing the effect of both mutations on the hydrolysis and closing rates of Hsp90 revealed that the A22T/T13A mutant had a more significant impact on the protein. The importance of the lid flexibility is supported by H/DX experiments (Fig. 59), which indicate strong dynamics of the lid region upon nucleotide binding and closing. The residues surrounding Ala22/Thr13 demonstrated the most significant deuterium uptake during closing compared to the open state. This suggests that a hydrophilic amino acid, like threonine, could provide additional stability to the closed state. Altering both residues of the chimeric mutants to the respective yeast/human amino acid further amplified the observed changes in activity and closing. This leads to the assumption, that the mutation affecting lid movement and stability affect closing *via* independent mechanisms. In summary, the data obtained suggests that the two mutations in the NTD of Hsp82 lead to a similar structural behavior as Hsp90 $\beta$  (and *vice versa*), which exhibits a less stable closed state and hindered lid movement. Of note, the mutated Hsp82 still provides the functionality required to support viability of yeast cells (Fig. 63).

By comparing the  $\alpha$ 1-helix and ATP-lid sequence to a larger number of species, the evolution of Hsp90 can be observed (Fig. 68). All investigated animals, including nematodes like *C. elegans* and insects, have a nearly identical  $\alpha$ 1 and ATP lid sequence. However, differences were observed in the Hsp90s

from plants and fungi when compared to animal Hsp90s. For plants, the majority of differing residues is located in the  $\alpha 1$ -helix, but the differing amino acids also include the investigated residues Ala22 and Gln118. Interestingly, Hsp90 from fungi displayed fewer deviating residues when compared to human Hsp90 $\beta$ . This data suggests a common ancestor of both fungi and animals existed. Comparative genomics studies already confirmed the distinct evolution of the Hsp90 gene family in vertebrates and invertebrates compared to fungi and plantae (Chen et al., 2006). However, the reasons behind the sequence divergence and the subsequent alterations in ATPase rate and Hsp90 conformation remain unknown. It is highly probable that this evolutionary divergence is necessary to accommodate an expanded range of client proteins, provide additional regulation, and facilitate specific co-chaperone interactions.

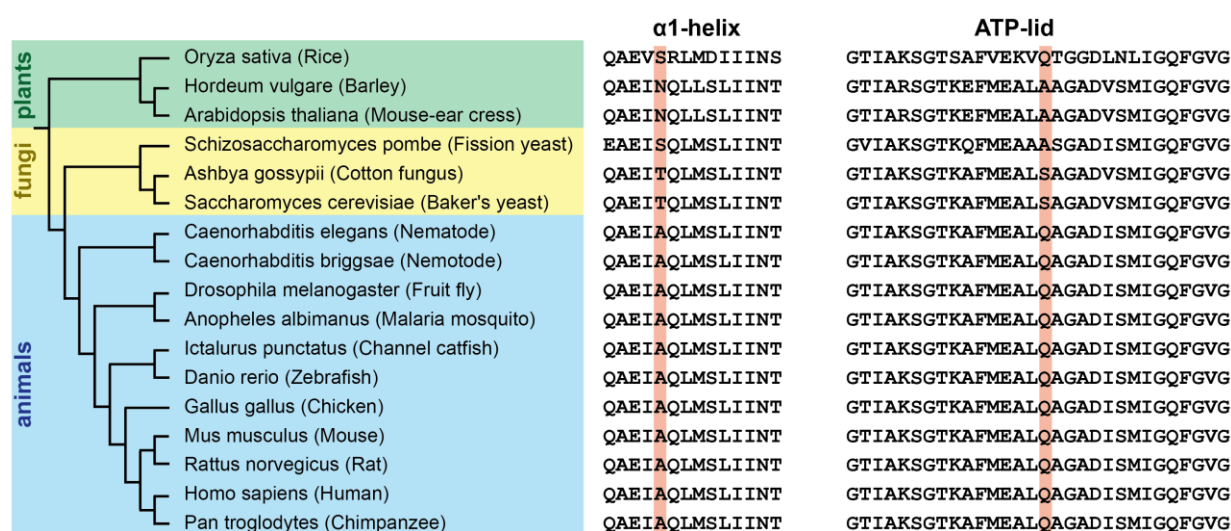


**Figure 68: Evolutionary conservation of the  $\alpha 1$ -helix and ATP-lid.** Phylogenetic tree with representative species of the plant, fungi and animal family. The sequence of the  $\alpha 1$ -helix and the ATP-lid of the respective organism is depicted on the right side. The two residues differing between Hsp82 and Hsp90 $\beta$  are highlighted in red.

## Conclusion and Outlook

In this study, the conformational cycle of Hsp90 $\beta$  and yeast Hsp82 were successfully investigated with various bioanalytical methods. However, the initial idea to investigate structural rearrangements via FRET measurements analogous to the established system for Hsp82 could only be realized to a certain degree. Fluorescent dyes negatively affected the dimeric structure of Hsp90 $\beta$ , which only allowed visualizing dynamics by single molecule FRET. Nevertheless, closing as well as re-opening under physiological conditions could be observed with various biophysical methods, which include SEC, aUC and limited proteolysis. The combined data identified the closing of Hsp90 $\beta$  as the rate-limiting step and explained the difference in ATPase activity to yeast. A direct comparison of the proteins revealed a common hydrolysis mechanism, which includes ATP-lid closure and N-terminal dimerization. However, differences regarding hydrophobic interactions, MC domain rearrangements, dynamics and

lid stability were revealed. Additionally, the created chimeric mutants demonstrated an evolutionary divergence between the two species and revealed the mechanisms of the ATPase activity and closing kinetics modulation. The collected data and established methods for the observation of closing and opening kinetics provide the tools to further investigate open questions in the field of Hsp90. Future investigations could aim at getting a more detailed view on how co-chaperone and client protein binding affects the overall dynamics of the protein. Furthermore, it is still unclear how the difference in MC domain rearrangements and the overall structural flexibility affect the activity and functionality of the protein. Moreover, Hsp90 is known to interact with a diverse range of client proteins, but it is unclear how the chaperone achieves specificity for individual clients. In summary, this work has made significant progress in understanding the conformational cycle of Hsp90 $\beta$  and its comparison to the yeast protein, providing a foundation for further investigations into the protein's dynamics and interactions with co-chaperones and client proteins.

## References

- Algar, W. R., Hildebrandt, N., Vogel, S. S., & Medintz, I. L. (2019). FRET as a biomolecular research tool - understanding its potential while avoiding pitfalls. *Nat Methods*, *16*, 815-829.
- Ali, J. A., Jackson, A. P., Howells, A. J., & Maxwell, A. (1993). The 43-kilodalton N-terminal fragment of the DNA gyrase B protein hydrolyzes ATP and binds coumarin drugs. *Biochemistry*, *32*, 2717-2724.
- Ali, M. M., Roe, S. M., Vaughan, C. K., Meyer, P., Panaretou, B., Piper, P. W., Prodromou, C., & Pearl, L. H. (2006). Crystal structure of an Hsp90-nucleotide-p23/Sba1 closed chaperone complex. *Nature*, *440*, 1013-1017.
- Alvira, S., Cuellar, J., Rohl, A., Yamamoto, S., Itoh, H., Alfonso, C., Rivas, G., Buchner, J., & Valpuesta, J. M. (2014). Structural characterization of the substrate transfer mechanism in Hsp70/Hsp90 folding machinery mediated by Hop. *Nat Commun*, *5*, 5484.
- Anfinsen, C. B. (1973). Principles that govern the folding of protein chains. *Science*, *181*, 223-230.
- Armon, A., Graur, D., & Ben-Tal, N. (2001). ConSurf: an algorithmic tool for the identification of functional regions in proteins by surface mapping of phylogenetic information. *J Mol Biol*, *307*, 447-463.
- Arrigo, A. P., & Tanguay, R. M. (1991). Expression of heat shock proteins during development in *Drosophila*. *Results Probl Cell Differ*, *17*, 106-119.
- Backe, S. J., Sager, R. A., Woodford, M. R., Makedon, A. M., & Mollapour, M. (2020). Post-translational modifications of Hsp90 and translating the chaperone code. *J Biol Chem*, *295*, 11099-11117.
- Bagneris, C., Bateman, O. A., Naylor, C. E., Cronin, N., Boelens, W. C., Keep, N. H., & Slingsby, C. (2009). Crystal structures of alpha-crystallin domain dimers of alphaB-crystallin and Hsp20. *J Mol Biol*, *392*, 1242-1252.
- Bai, Y., Sosnick, T. R., Mayne, L., & Englander, S. W. (1995). Protein folding intermediates: native-state hydrogen exchange. *Science*, *269*, 192-197.
- Balchin, D., Hayer-Hartl, M., & Hartl, F. U. (2016). In vivo aspects of protein folding and quality control. *Science*, *353*, aac4354.
- Basha, E., O'Neill, H., & Vierling, E. (2012). Small heat shock proteins and alpha-crystallins: dynamic proteins with flexible functions. *Trends Biochem Sci*, *37*, 106-117.
- Beraldo, F. H., Soares, I. N., Goncalves, D. F., Fan, J., Thomas, A. A., Santos, T. G., Mohammad, A. H., Roffe, M., Calder, M. D., Nikolova, S., Hajj, G. N., Guimaraes, A. L., Massensini, A. R., Welch, I., Betts, D. H., Gros, R., Drangova, M., Watson, A. J., Bartha, R., . . . Prado, M. A. (2013). Stress-inducible phosphoprotein 1 has unique

- cochaperone activity during development and regulates cellular response to ischemia via the prion protein. *FASEB J*, 27, 3594-3607.
- Biebl, M. M., Lopez, A., Rehn, A., Freiburger, L., Lawatscheck, J., Blank, B., Sattler, M., & Buchner, J. (2021). Structural elements in the flexible tail of the co-chaperone p23 coordinate client binding and progression of the Hsp90 chaperone cycle. *Nat Commun*, 12, 828.
- Blatch, G. L., & Lassle, M. (1999). The tetratricopeptide repeat: a structural motif mediating protein-protein interactions. *Bioessays*, 21, 932-939.
- Boorstein, W. R., Ziegelhoffer, T., & Craig, E. A. (1994). Molecular evolution of the HSP70 multigene family. *Journal of molecular evolution*, 38, 1-17.
- Borkovich, K. A., Farrelly, F. W., Finkelstein, D. B., Taulien, J., & Lindquist, S. (1989). hsp82 is an essential protein that is required in higher concentrations for growth of cells at higher temperatures. *Mol Cell Biol*, 9, 3919-3930.
- Bose, S., Weikl, T., Bugl, H., & Buchner, J. (1996). Chaperone function of Hsp90-associated proteins. *Science*, 274, 1715-1717.
- Brinker, A., Scheufler, C., Von Der Mulbe, F., Fleckenstein, B., Herrmann, C., Jung, G., Moarefi, I., & Hartl, F. U. (2002). Ligand discrimination by TPR domains. Relevance and selectivity of EEVD-recognition in Hsp70 x Hop x Hsp90 complexes. *J Biol Chem*, 277, 19265-19275.
- Bryngelson, J. D., Onuchic, J. N., Socci, N. D., & Wolynes, P. G. (1995). Funnels, pathways, and the energy landscape of protein folding: a synthesis. *Proteins*, 21, 167-195.
- Buchner, J. (1996). Supervising the fold: functional principles of molecular chaperones. *The FASEB journal*, 10, 10-19.
- Buchner, J., Pastan, I., & Brinkmann, U. (1992). A method for increasing the yield of properly folded recombinant fusion proteins: single-chain immunotoxins from renaturation of bacterial inclusion bodies. *Anal Biochem*, 205, 263-270.
- Butterfield, S. M., & Lashuel, H. A. (2010). Amyloidogenic protein-membrane interactions: mechanistic insight from model systems. *Angew Chem Int Ed Engl*, 49, 5628-5654.
- Cao, Y., Ohwatari, N., Matsumoto, T., Kosaka, M., Ohtsuru, A., & Yamashita, S. (1999). TGF-beta1 mediates 70-kDa heat shock protein induction due to ultraviolet irradiation in human skin fibroblasts. *Pflugers Arch*, 438, 239-244.
- Chadli, A., Ladjimi, M. M., Baulieu, E. E., & Catelli, M. G. (1999). Heat-induced oligomerization of the molecular chaperone Hsp90. Inhibition by ATP and geldanamycin and activation by transition metal oxyanions. *J Biol Chem*, 274, 4133-4139.
- Chan, L., Cross, H. F., She, J. K., Cavalli, G., Martins, H. F., & Neylon, C. (2007). Covalent attachment of proteins to solid supports and surfaces via Sortase-mediated ligation. *PLoS One*, 2, e1164.

- Chang, H. C., Nathan, D. F., & Lindquist, S. (1997). In vivo analysis of the Hsp90 cochaperone Sti1 (p60). *Mol Cell Biol*, *17*, 318-325.
- Chattopadhyaya, S., Abu Bakar, F. B., & Yao, S. Q. (2009). Expanding the chemical biologist's tool kit: chemical labelling strategies and its applications. *Curr Med Chem*, *16*, 4527-4543.
- Chen, B., Zhong, D., & Monteiro, A. (2006). Comparative genomics and evolution of the HSP90 family of genes across all kingdoms of organisms. *BMC Genomics*, *7*, 156.
- Chen, I., Dorr, B. M., & Liu, D. R. (2011). A general strategy for the evolution of bond-forming enzymes using yeast display. *Proc Natl Acad Sci U S A*, *108*, 11399-11404.
- Chong, S., Montello, G. E., Zhang, A., Cantor, E. J., Liao, W., Xu, M. Q., & Benner, J. (1998). Utilizing the C-terminal cleavage activity of a protein splicing element to purify recombinant proteins in a single chromatographic step. *Nucleic Acids Res*, *26*, 5109-5115.
- Csermely, P., Schnaider, T., Soti, C., Prohaszka, Z., & Nardai, G. (1998). The 90-kDa molecular chaperone family: structure, function, and clinical applications. A comprehensive review. *Pharmacol Ther*, *79*, 129-168.
- Cunningham, C. N., Krukenberg, K. A., & Agard, D. A. (2008). Intra- and intermonomer interactions are required to synergistically facilitate ATP hydrolysis in Hsp90. *J Biol Chem*, *283*, 21170-21178.
- Cunningham, C. N., Southworth, D. R., Krukenberg, K. A., & Agard, D. A. (2012). The conserved arginine 380 of Hsp90 is not a catalytic residue, but stabilizes the closed conformation required for ATP hydrolysis. *Protein Sci*, *21*, 1162-1171.
- Dahiya, V., Agam, G., Lawatscheck, J., Rutz, D. A., Lamb, D. C., & Buchner, J. (2019). Coordinated Conformational Processing of the Tumor Suppressor Protein p53 by the Hsp70 and Hsp90 Chaperone Machineries. *Mol Cell*, *74*, 816-830 e817.
- Daturpalli, S., Waudby, C. A., Meehan, S., & Jackson, S. E. (2013). Hsp90 inhibits alpha-synuclein aggregation by interacting with soluble oligomers. *J Mol Biol*, *425*, 4614-4628.
- Dawson, P. E., Muir, T. W., Clark-Lewis, I., & Kent, S. B. (1994). Synthesis of proteins by native chemical ligation. *Science*, *266*, 776-779.
- Dickey, C. A., Kamal, A., Lundgren, K., Klosak, N., Bailey, R. M., Dunmore, J., Ash, P., Shoraka, S., Zlatkovic, J., Eckman, C. B., Patterson, C., Dickson, D. W., Nahman, N. S., Jr., Hutton, M., Burrows, F., & Petrucelli, L. (2007). The high-affinity HSP90-CHIP complex recognizes and selectively degrades phosphorylated tau client proteins. *J Clin Invest*, *117*, 648-658.
- Dill, K. A., Bromberg, S., Yue, K., Fiebig, K. M., Yee, D. P., Thomas, P. D., & Chan, H. S. (1995). Principles of protein folding--a perspective from simple exact models. *Protein Sci*, *4*, 561-602.

- Dill, K. A., & Chan, H. S. (1997). From Levinthal to pathways to funnels. *Nature structural biology*, 4, 10-19.
- Doyle, S. M., & Wickner, S. (2009). Hsp104 and ClpB: protein disaggregating machines. *Trends Biochem Sci*, 34, 40-48.
- Dummler, A., Lawrence, A. M., & de Marco, A. (2005). Simplified screening for the detection of soluble fusion constructs expressed in *E. coli* using a modular set of vectors. *Microb Cell Fact*, 4, 34.
- Dunker, A. K., Brown, C. J., & Obradovic, Z. (2002). Identification and functions of usefully disordered proteins. *Adv Protein Chem*, 62, 25-49.
- Dutta, R., & Inouye, M. (2000). GHKL, an emergent ATPase/kinase superfamily. *Trends Biochem Sci*, 25, 24-28.
- Ellis, R. J., & Minton, A. P. (2006). Protein aggregation in crowded environments. *Biol Chem*, 387, 485-497.
- Esser, C., Scheffner, M., & Hohfeld, J. (2005). The chaperone-associated ubiquitin ligase CHIP is able to target p53 for proteasomal degradation. *J Biol Chem*, 280, 27443-27448.
- Evans, C. G., Wisen, S., & Gestwicki, J. E. (2006). Heat shock proteins 70 and 90 inhibit early stages of amyloid beta-(1-42) aggregation in vitro. *J Biol Chem*, 281, 33182-33191.
- Evans, T. C., Jr., Benner, J., & Xu, M. Q. (1998). Semisynthesis of cytotoxic proteins using a modified protein splicing element. *Protein Sci*, 7, 2256-2264.
- Fairbanks, G., Steck, T. L., & Wallach, D. F. (1971). Electrophoretic analysis of the major polypeptides of the human erythrocyte membrane. *Biochemistry*, 10, 2606-2617.
- Felts, S. J., Owen, B. A., Nguyen, P., Trepel, J., Donner, D. B., & Toft, D. O. (2000). The hsp90-related protein TRAP1 is a mitochondrial protein with distinct functional properties. *J Biol Chem*, 275, 3305-3312.
- Fenton, W. A., & Horwich, A. L. (2003). Chaperonin-mediated protein folding: fate of substrate polypeptide. *Q Rev Biophys*, 36, 229-256.
- Fernandez-Fernandez, M. R., & Valpuesta, J. M. (2018). Hsp70 chaperone: a master player in protein homeostasis. *F1000Res*, 7.
- Fink, A. L. (1998). Protein aggregation: folding aggregates, inclusion bodies and amyloid. *Fold Des*, 3, R9-23.
- Finkelstein, D. B., Strausberg, S., & McAlister, L. (1982). Alterations of transcription during heat shock of *Saccharomyces cerevisiae*. *J Biol Chem*, 257, 8405-8411.
- Fisher, A. J., Smith, C. A., Thoden, J. B., Smith, R., Sutoh, K., Holden, H. M., & Rayment, I. (1995). X-ray structures of the myosin motor domain of *Dictyostelium discoideum* complexed with MgADP.BeFx and MgADP.AIF<sub>4</sub>. *Biochemistry*, 34, 8960-8972.

- Freeman, B. C., Felts, S. J., Toft, D. O., & Yamamoto, K. R. (2000). The p23 molecular chaperones act at a late step in intracellular receptor action to differentially affect ligand efficacies. *Genes Dev*, *14*, 422-434.
- Freiburger, L., Sonntag, M., Hennig, J., Li, J., Zou, P., & Sattler, M. (2015). Efficient segmental isotope labeling of multi-domain proteins using Sortase A. *J Biomol NMR*, *63*, 1-8.
- Gaiser, A. M., Kaiser, C. J., Haslbeck, V., & Richter, K. (2011). Downregulation of the Hsp90 system causes defects in muscle cells of *Caenorhabditis elegans*. *PLoS One*, *6*, e25485.
- Garnier, C., Barbier, P., Devred, F., Rivas, G., & Peyrot, V. (2002). Hydrodynamic properties and quaternary structure of the 90 kDa heat-shock protein: effects of divalent cations. *Biochemistry*, *41*, 11770-11778.
- Girstmair, H., Toppel, F., Lopez, A., Tych, K., Stein, F., Haberkant, P., Schmid, P. W. N., Helm, D., Rief, M., Sattler, M., & Buchner, J. (2019). The Hsp90 isoforms from *S. cerevisiae* differ in structure, function and client range. *Nat Commun*, *10*, 3626.
- Goldsbury, C., Baxa, U., Simon, M. N., Steven, A. C., Engel, A., Wall, J. S., Aebi, U., & Muller, S. A. (2011). Amyloid structure and assembly: insights from scanning transmission electron microscopy. *J Struct Biol*, *173*, 1-13.
- Goulatis, L. I., Ramanathan, R., & Shusta, E. V. (2019). Impacts of the -1 Amino Acid on Yeast Production of Protein-Intein Fusions. *Biotechnol Prog*, *35*, e2736.
- Graf, C., Lee, C. T., Eva Meier-Andrejszki, L., Nguyen, M. T., & Mayer, M. P. (2014). Differences in conformational dynamics within the Hsp90 chaperone family reveal mechanistic insights. *Front Mol Biosci*, *1*, 4.
- Grammatikakis, N., Vultur, A., Ramana, C. V., Siganou, A., Schweinfest, C. W., Watson, D. K., & Raptis, L. (2002). The role of Hsp90N, a new member of the Hsp90 family, in signal transduction and neoplastic transformation. *J Biol Chem*, *277*, 8312-8320.
- Gupta, R. S. (1995). Phylogenetic analysis of the 90 kD heat shock family of protein sequences and an examination of the relationship among animals, plants, and fungi species. *Mol Biol Evol*, *12*, 1063-1073.
- Hackeng, T. M., Griffin, J. H., & Dawson, P. E. (1999). Protein synthesis by native chemical ligation: expanded scope by using straightforward methodology. *Proc Natl Acad Sci U S A*, *96*, 10068-10073.
- Hainzl, O., Lapina, M. C., Buchner, J., & Richter, K. (2009). The charged linker region is an important regulator of Hsp90 function. *J Biol Chem*, *284*, 22559-22567.
- Harris, S. F., Shiau, A. K., & Agard, D. A. (2004). The crystal structure of the carboxy-terminal dimerization domain of htpG, the *Escherichia coli* Hsp90, reveals a potential substrate binding site. *Structure*, *12*, 1087-1097.
- Hartl, F. U. (1996). Molecular chaperones in cellular protein folding. *Nature*, *381*, 571-580.

- Hartl, F. U., Bracher, A., & Hayer-Hartl, M. (2011). Molecular chaperones in protein folding and proteostasis. *Nature*, *475*, 324-332.
- Haslbeck, M., & Buchner, J. (2015). Assays to characterize molecular chaperone function in vitro. *Methods Mol Biol*, *1292*, 39-51.
- Hauser, P. S., & Ryan, R. O. (2007). Expressed protein ligation using an N-terminal cysteine containing fragment generated in vivo from a pelB fusion protein. *Protein Expr Purif*, *54*, 227-233.
- Hellenkamp, B., Wortmann, P., Kandzia, F., Zacharias, M., & Hugel, T. (2017). Multidomain structure and correlated dynamics determined by self-consistent FRET networks. *Nat Methods*, *14*, 174-180.
- Hessling, M., Richter, K., & Buchner, J. (2009). Dissection of the ATP-induced conformational cycle of the molecular chaperone Hsp90. *Nat Struct Mol Biol*, *16*, 287-293.
- Hirel, P. H., Schmitter, M. J., Dessen, P., Fayat, G., & Blanquet, S. (1989). Extent of N-terminal methionine excision from Escherichia coli proteins is governed by the side-chain length of the penultimate amino acid. *Proc Natl Acad Sci U S A*, *86*, 8247-8251.
- Hofmeister, F. (1888). *Zur Lehre von der Wirkung der Salze : Zweite Mittheilung* (Vol. 24). Archiv für pathologische Anatomie und Pathologie.
- Hong, J., & Gierasch, L. M. (2010). Macromolecular crowding remodels the energy landscape of a protein by favoring a more compact unfolded state. *J Am Chem Soc*, *132*, 10445-10452.
- Honore, B., Leffers, H., Madsen, P., Rasmussen, H. H., Vandekerckhove, J., & Celis, J. E. (1992). Molecular cloning and expression of a transformation-sensitive human protein containing the TPR motif and sharing identity to the stress-inducible yeast protein STII. *J Biol Chem*, *267*, 8485-8491.
- Horvat, N. K., Armstrong, H., Lee, B. L., Mercier, R., Wolmarans, A., Knowles, J., Spyropoulos, L., & LaPointe, P. (2014). A mutation in the catalytic loop of Hsp90 specifically impairs ATPase stimulation by Aha1p, but not Hch1p. *J Mol Biol*, *426*, 2379-2392.
- Houry, W. A., Frishman, D., Eckerskorn, C., Lottspeich, F., & Hartl, F. U. (1999). Identification of in vivo substrates of the chaperonin GroEL. *Nature*, *402*, 147-154.
- Hu, H., Wang, Q., Du, J., Liu, Z., Ding, Y., Xue, H., Zhou, C., Feng, L., & Zhang, N. (2021). Aha1 Exhibits Distinctive Dynamics Behavior and Chaperone-Like Activity. *Molecules*, *26*.
- Humphrey, W., Dalke, A., & Schulten, K. (1996). VMD: visual molecular dynamics. *J Mol Graph*, *14*, 33-38, 27-38.
- Huynh, K., & Partch, C. L. (2015). Analysis of protein stability and ligand interactions by thermal shift assay. *Curr Protoc Protein Sci*, *79*, 28 29 21-28 29 14.

- Irvine, G. B., El-Agnaf, O. M., Shankar, G. M., & Walsh, D. M. (2008). Protein aggregation in the brain: the molecular basis for Alzheimer's and Parkinson's diseases. *Molecular medicine*, *14*, 451-464.
- Jackson, F. (1998). *From metaphysics to ethics: A defence of conceptual analysis*. Clarendon Press.
- Jahn, M., Rehn, A., Pelz, B., Hellenkamp, B., Richter, K., Rief, M., Buchner, J., & Hugel, T. (2014). The charged linker of the molecular chaperone Hsp90 modulates domain contacts and biological function. *Proc Natl Acad Sci U S A*, *111*, 17881-17886.
- Jakob, U., Gaestel, M., Engel, K., & Buchner, J. (1993). Small heat shock proteins are molecular chaperones. *J Biol Chem*, *268*, 1517-1520.
- Jares-Erijman, E. A., & Jovin, T. M. (2003). FRET imaging. *Nat Biotechnol*, *21*, 1387-1395.
- Johnson, B. D., Schumacher, R. J., Ross, E. D., & Toft, D. O. (1998). Hop modulates Hsp70/Hsp90 interactions in protein folding. *J Biol Chem*, *273*, 3679-3686.
- Johnson, J. L. (2012). Evolution and function of diverse Hsp90 homologs and cochaperone proteins. *Biochim Biophys Acta*, *1823*, 607-613.
- Johnson, J. L., & Brown, C. (2009). Plasticity of the Hsp90 chaperone machine in divergent eukaryotic organisms. *Cell Stress Chaperones*, *14*, 83-94.
- Johnson, J. L., & Toft, D. O. (1994). A novel chaperone complex for steroid receptors involving heat shock proteins, immunophilins, and p23. *J Biol Chem*, *269*, 24989-24993.
- Johnson, J. L., & Toft, D. O. (1995). Binding of p23 and hsp90 during assembly with the progesterone receptor. *Mol Endocrinol*, *9*, 670-678.
- Jussupow, A., Lopez, A., Baumgart, M., Mader, S. L., Sattler, M., & Kaila, V. R. I. (2022). Extended conformational states dominate the Hsp90 chaperone dynamics. *J Biol Chem*, *298*, 102101.
- Kalia, J., & Raines, R. T. (2006). Reactivity of intein thioesters: appending a functional group to a protein. *ChemBiochem*, *7*, 1375-1383.
- Kampinga, H. H., Hageman, J., Vos, M. J., Kubota, H., Tanguay, R. M., Bruford, E. A., Cheetham, M. E., Chen, B., & Hightower, L. E. (2009). Guidelines for the nomenclature of the human heat shock proteins. *Cell Stress Chaperones*, *14*, 105-111.
- Karagoz, G. E., Duarte, A. M., Ippel, H., Uetrecht, C., Sinnige, T., van Rosmalen, M., Hausmann, J., Heck, A. J., Boelens, R., & Rudiger, S. G. (2011). N-terminal domain of human Hsp90 triggers binding to the cochaperone p23. *Proc Natl Acad Sci U S A*, *108*, 580-585.
- Karagoz, G. E., Sinnige, T., Hsieh, O., & Rudiger, S. G. (2011). Expressed protein ligation for a large dimeric protein. *Protein Eng Des Sel*, *24*, 495-501.

- Kawahara, M., & Kuroda, Y. (2000). Molecular mechanism of neurodegeneration induced by Alzheimer's beta-amyloid protein: channel formation and disruption of calcium homeostasis. *Brain Res Bull*, *53*, 389-397.
- Kelly, S. M., Jess, T. J., & Price, N. C. (2005). How to study proteins by circular dichroism. *Biochim Biophys Acta*, *1751*, 119-139.
- Kim, Y.-I., Levchenko, I., Fraczkowska, K., Woodruff, R. V., Sauer, R. T., & Baker, T. A. (2001). Molecular determinants of complex formation between Clp/Hsp100 ATPases and the ClpP peptidase. *Nature structural biology*, *8*, 230-233.
- Kim, Y., Ho, S. O., Gassman, N. R., Korlann, Y., Landorf, E. V., Collart, F. R., & Weiss, S. (2008). Efficient site-specific labeling of proteins via cysteines. *Bioconjug Chem*, *19*, 786-791.
- Kimmins, S., & MacRae, T. H. (2000). Maturation of steroid receptors: an example of functional cooperation among molecular chaperones and their associated proteins. *Cell Stress Chaperones*, *5*, 76-86.
- Kitagawa, K., Skowyra, D., Elledge, S. J., Harper, J. W., & Hieter, P. (1999). SGT1 encodes an essential component of the yeast kinetochore assembly pathway and a novel subunit of the SCF ubiquitin ligase complex. *Mol Cell*, *4*, 21-33.
- Kityk, R., Kopp, J., & Mayer, M. P. (2018). Molecular Mechanism of J-Domain-Triggered ATP Hydrolysis by Hsp70 Chaperones. *Mol Cell*, *69*, 227-237 e224.
- Kohler, V., & Andreasson, C. (2020). Hsp70-mediated quality control: should I stay or should I go? *Biol Chem*, *401*, 1233-1248.
- Konermann, L., Pan, J., & Liu, Y. H. (2011). Hydrogen exchange mass spectrometry for studying protein structure and dynamics. *Chem Soc Rev*, *40*, 1224-1234.
- Koulov, A. V., LaPointe, P., Lu, B., Razvi, A., Coppinger, J., Dong, M. Q., Matteson, J., Laister, R., Arrowsmith, C., Yates, J. R., 3rd, & Balch, W. E. (2010). Biological and structural basis for Aha1 regulation of Hsp90 ATPase activity in maintaining proteostasis in the human disease cystic fibrosis. *Mol Biol Cell*, *21*, 871-884.
- Kovacs, J. J., Murphy, P. J., Gaillard, S., Zhao, X., Wu, J. T., Nicchitta, C. V., Yoshida, M., Toft, D. O., Pratt, W. B., & Yao, T. P. (2005). HDAC6 regulates Hsp90 acetylation and chaperone-dependent activation of glucocorticoid receptor. *Mol Cell*, *18*, 601-607.
- Kriehuber, T., Rattei, T., Weinmaier, T., Bepperling, A., Haslbeck, M., & Buchner, J. (2010). Independent evolution of the core domain and its flanking sequences in small heat shock proteins. *FASEB J*, *24*, 3633-3642.
- Krukenberg, K. A., Street, T. O., Lavery, L. A., & Agard, D. A. (2011). Conformational dynamics of the molecular chaperone Hsp90. *Q Rev Biophys*, *44*, 229-255.
- Kundrat, L., & Regan, L. (2010). Identification of residues on Hsp70 and Hsp90 ubiquitinated by the cochaperone CHIP. *J Mol Biol*, *395*, 587-594.

- Laemmli, U. K. (1970). Cleavage of structural proteins during the assembly of the head of bacteriophage T4. *Nature*, *227*, 680-685.
- Laplante, A. F., Moulin, V., Auger, F. A., Landry, J., Li, H., Morrow, G., Tanguay, R. M., & Germain, L. (1998). Expression of heat shock proteins in mouse skin during wound healing. *J Histochem Cytochem*, *46*, 1291-1301.
- Lavery, L. A., Partridge, J. R., Ramelot, T. A., Elnatan, D., Kennedy, M. A., & Agard, D. A. (2014). Structural asymmetry in the closed state of mitochondrial Hsp90 (TRAP1) supports a two-step ATP hydrolysis mechanism. *Mol Cell*, *53*, 330-343.
- Lee, C. C., Lin, T. W., Ko, T. P., & Wang, A. H. (2011). The hexameric structures of human heat shock protein 90. *PLoS One*, *6*, e19961.
- Lee, K., Thwin, A. C., Nadel, C. M., Tse, E., Gates, S. N., Gestwicki, J. E., & Southworth, D. R. (2021). The structure of an Hsp90-immunophilin complex reveals cochaperone recognition of the client maturation state. *Mol Cell*, *81*, 3496-3508 e3495.
- Leitner, A., Joachimiak, L. A., Bracher, A., Monkemeyer, L., Walzthoeni, T., Chen, B., Pechmann, S., Holmes, S., Cong, Y., Ma, B., Ludtke, S., Chiu, W., Hartl, F. U., Aebersold, R., & Frydman, J. (2012). The molecular architecture of the eukaryotic chaperonin TRiC/CCT. *Structure*, *20*, 814-825.
- Levinthal, C. (1968). Are there pathways for protein folding? *Journal de chimie physique*, *65*, 44-45.
- Li, J., Richter, K., Reinstein, J., & Buchner, J. (2013). Integration of the accelerator Aha1 in the Hsp90 co-chaperone cycle. *Nat Struct Mol Biol*, *20*, 326-331.
- Li, M. Z., & Elledge, S. J. (2012). SLIC: a method for sequence- and ligation-independent cloning. *Methods Mol Biol*, *852*, 51-59.
- Lindquist, S. (1986). The heat-shock response. *Annu Rev Biochem*, *55*, 1151-1191.
- Lopez, A., Dahiya, V., Delhommel, F., Freiburger, L., Stehle, R., Asami, S., Rutz, D., Blair, L., Buchner, J., & Sattler, M. (2021). Client binding shifts the populations of dynamic Hsp90 conformations through an allosteric network. *Sci Adv*, *7*, eabl7295.
- Lopez, A., Elimelech, A. R., Klimm, K., & Sattler, M. (2021). The Charged Linker Modulates the Conformations and Molecular Interactions of Hsp90. *Chembiochem*, *22*, 1084-1092.
- Louvion, J. F., Warth, R., & Picard, D. (1996). Two eukaryote-specific regions of Hsp82 are dispensable for its viability and signal transduction functions in yeast. *Proc Natl Acad Sci U S A*, *93*, 13937-13942.
- MacKerell, A. D., Jr., Banavali, N., & Foloppe, N. (2000). Development and current status of the CHARMM force field for nucleic acids. *Biopolymers*, *56*, 257-265.
- Mao, H., Hart, S. A., Schink, A., & Pollok, B. A. (2004). Sortase-mediated protein ligation: a new method for protein engineering. *J Am Chem Soc*, *126*, 2670-2671.

- Martinez-Ruiz, A., Villanueva, L., Gonzalez de Orduna, C., Lopez-Ferrer, D., Higuera, M. A., Tarin, C., Rodriguez-Crespo, I., Vazquez, J., & Lamas, S. (2005). S-nitrosylation of Hsp90 promotes the inhibition of its ATPase and endothelial nitric oxide synthase regulatory activities. *Proc Natl Acad Sci U S A*, *102*, 8525-8530.
- Martinez-Yamout, M. A., Venkitakrishnan, R. P., Preece, N. E., Kroon, G., Wright, P. E., & Dyson, H. J. (2006). Localization of sites of interaction between p23 and Hsp90 in solution. *J Biol Chem*, *281*, 14457-14464.
- Maruya, M., Sameshima, M., Nemoto, T., & Yahara, I. (1999). Monomer arrangement in HSP90 dimer as determined by decoration with N and C-terminal region specific antibodies. *J Mol Biol*, *285*, 903-907.
- Marzec, M., Eletto, D., & Argon, Y. (2012). GRP94: An HSP90-like protein specialized for protein folding and quality control in the endoplasmic reticulum. *Biochim Biophys Acta*, *1823*, 774-787.
- Masson, G. R., Burke, J. E., Ahn, N. G., Anand, G. S., Borchers, C., Brier, S., Bou-Assaf, G. M., Engen, J. R., Englander, S. W., Faber, J., Garlish, R., Griffin, P. R., Gross, M. L., Guttman, M., Hamuro, Y., Heck, A. J. R., Houde, D., Jacob, R. E., Jorgensen, T. J. D., . . . Rand, K. D. (2019). Recommendations for performing, interpreting and reporting hydrogen deuterium exchange mass spectrometry (HDX-MS) experiments. *Nat Methods*, *16*, 595-602.
- Matz, J. M., LaVoi, K. P., Moen, R. J., & Blake, M. J. (1996). Cold-induced heat shock protein expression in rat aorta and brown adipose tissue. *Physiol Behav*, *60*, 1369-1374.
- Mayer, M. P., & Le Breton, L. (2015). Hsp90: breaking the symmetry. *Mol Cell*, *58*, 8-20.
- Mayer, M. P., Schroder, H., Rudiger, S., Paal, K., Laufen, T., & Bukau, B. (2000). Multistep mechanism of substrate binding determines chaperone activity of Hsp70. *Nat Struct Biol*, *7*, 586-593.
- Mayor, A., Martinon, F., De Smedt, T., Petrilli, V., & Tschopp, J. (2007). A crucial function of SGT1 and HSP90 in inflammasome activity links mammalian and plant innate immune responses. *Nat Immunol*, *8*, 497-503.
- Mayr, C., Richter, K., Lilie, H., & Buchner, J. (2000). Cpr6 and Cpr7, two closely related Hsp90-associated immunophilins from *Saccharomyces cerevisiae*, differ in their functional properties. *J Biol Chem*, *275*, 34140-34146.
- Mazmanian, S. K., Liu, G., Ton-That, H., & Schneewind, O. (1999). Staphylococcus aureus sortase, an enzyme that anchors surface proteins to the cell wall. *Science*, *285*, 760-763.
- McLaughlin, S. H., Smith, H. W., & Jackson, S. E. (2002). Stimulation of the weak ATPase activity of human hsp90 by a client protein. *J Mol Biol*, *315*, 787-798.
- McLaughlin, S. H., Sobott, F., Yao, Z. P., Zhang, W., Nielsen, P. R., Grossmann, J. G., Laue, E. D., Robinson, C. V., & Jackson, S. E. (2006). The co-chaperone p23 arrests the Hsp90 ATPase cycle to trap client proteins. *J Mol Biol*, *356*, 746-758.

- Melkikh, A. V., & Sutormina, M. I. (2008). Model of active transport of ions in cardiac cell. *J Theor Biol*, 252, 247-254.
- Meyer, P., Prodromou, C., Hu, B., Vaughan, C., Roe, S. M., Panaretou, B., Piper, P. W., & Pearl, L. H. (2003). Structural and functional analysis of the middle segment of hsp90: implications for ATP hydrolysis and client protein and cochaperone interactions. *Mol Cell*, 11, 647-658.
- Meyer, P., Prodromou, C., Liao, C., Hu, B., Mark Roe, S., Vaughan, C. K., Vlastic, I., Panaretou, B., Piper, P. W., & Pearl, L. H. (2004). Structural basis for recruitment of the ATPase activator Aha1 to the Hsp90 chaperone machinery. *EMBO J*, 23, 511-519.
- Mickler, M., Hessling, M., Ratzke, C., Buchner, J., & Hugel, T. (2009). The large conformational changes of Hsp90 are only weakly coupled to ATP hydrolysis. *Nat Struct Mol Biol*, 16, 281-286.
- Mills, K. V., & Perler, F. B. (2005). The mechanism of intein-mediated protein splicing: variations on a theme. *Protein Pept Lett*, 12, 751-755.
- Minami, Y., Kimura, Y., Kawasaki, H., Suzuki, K., & Yahara, I. (1994). The carboxy-terminal region of mammalian HSP90 is required for its dimerization and function in vivo. *Mol Cell Biol*, 14, 1459-1464.
- Mogk, A., Deuerling, E., Vorderwulbecke, S., Vierling, E., & Bukau, B. (2003). Small heat shock proteins, ClpB and the DnaK system form a functional triade in reversing protein aggregation. *Mol Microbiol*, 50, 585-595.
- Mogk, A., Kummer, E., & Bukau, B. (2015). Cooperation of Hsp70 and Hsp100 chaperone machines in protein disaggregation. *Front Mol Biosci*, 2, 22.
- Moran Luengo, T., Mayer, M. P., & Rudiger, S. G. D. (2019). The Hsp70-Hsp90 Chaperone Cascade in Protein Folding. *Trends Cell Biol*, 29, 164-177.
- Moullintraffort, L., Bruneaux, M., Nazabal, A., Allegro, D., Giudice, E., Zal, F., Peyrot, V., Barbier, P., Thomas, D., & Garnier, C. (2010). Biochemical and biophysical characterization of the Mg<sup>2+</sup>-induced 90-kDa heat shock protein oligomers. *J Biol Chem*, 285, 15100-15110.
- Muhlhofer, M., Peters, C., Kriehuber, T., Kreuzeder, M., Kazman, P., Rodina, N., Reif, B., Haslbeck, M., Weinkauff, S., & Buchner, J. (2021). Phosphorylation activates the yeast small heat shock protein Hsp26 by weakening domain contacts in the oligomer ensemble. *Nat Commun*, 12, 6697.
- Muir, T. W. (2003). Semisynthesis of proteins by expressed protein ligation. *Annu Rev Biochem*, 72, 249-289.
- Muir, T. W., Sondhi, D., & Cole, P. A. (1998). Expressed protein ligation: a general method for protein engineering. *Proc Natl Acad Sci U S A*, 95, 6705-6710.
- Muralidharan, V., & Muir, T. W. (2006). Protein ligation: an enabling technology for the biophysical analysis of proteins. *Nat Methods*, 3, 429-438.

- Murata, S., Chiba, T., & Tanaka, K. (2003). CHIP: a quality-control E3 ligase collaborating with molecular chaperones. *Int J Biochem Cell Biol*, *35*, 572-578.
- Nakamoto, H., & Vigh, L. (2007). The small heat shock proteins and their clients. *Cellular and Molecular Life Sciences*, *64*, 294-306.
- Nardai, G., Sass, B., Eber, J., Orosz, G., & Csermely, P. (2000). Reactive cysteines of the 90-kDa heat shock protein, Hsp90. *Arch Biochem Biophys*, *384*, 59-67.
- Nathan, D. F., & Lindquist, S. (1995). Mutational analysis of Hsp90 function: interactions with a steroid receptor and a protein kinase. *Mol Cell Biol*, *15*, 3917-3925.
- Nemoto, T., & Sato, N. (1998). Oligomeric forms of the 90-kDa heat shock protein. *Biochem J*, *330* ( Pt 2), 989-995.
- Nicolet, C. M., & Craig, E. A. (1989). Isolation and characterization of STI1, a stress-inducible gene from *Saccharomyces cerevisiae*. *Mol Cell Biol*, *9*, 3638-3646.
- Noddings, C. M., Johnson, J. L., & Agard, D. A. (2023). Cryo-EM reveals how Hsp90 and FKBP immunophilins co-regulate the Glucocorticoid Receptor. *bioRxiv*.
- Noddings, C. M., Wang, R. Y., Johnson, J. L., & Agard, D. A. (2022). Structure of Hsp90-p23-GR reveals the Hsp90 client-remodelling mechanism. *Nature*, *601*, 465-469.
- Obermann, W. M., Sondermann, H., Russo, A. A., Pavletich, N. P., & Hartl, F. U. (1998). In vivo function of Hsp90 is dependent on ATP binding and ATP hydrolysis. *J Cell Biol*, *143*, 901-910.
- Onuchic, J. N., Luthey-Schulten, Z., & Wolynes, P. G. (1997). Theory of protein folding: the energy landscape perspective. *Annu Rev Phys Chem*, *48*, 545-600.
- Oroz, J., Blair, L. J., & Zweckstetter, M. (2019). Dynamic Aha1 co-chaperone binding to human Hsp90. *Protein Sci*, *28*, 1545-1551.
- Panaretou, B., Prodromou, C., Roe, S. M., O'Brien, R., Ladbury, J. E., Piper, P. W., & Pearl, L. H. (1998). ATP binding and hydrolysis are essential to the function of the Hsp90 molecular chaperone in vivo. *EMBO J*, *17*, 4829-4836.
- Panaretou, B., Siligardi, G., Meyer, P., Maloney, A., Sullivan, J. K., Singh, S., Millson, S. H., Clarke, P. A., Naaby-Hansen, S., Stein, R., Cramer, R., Mollapour, M., Workman, P., Piper, P. W., Pearl, L. H., & Prodromou, C. (2002). Activation of the ATPase activity of hsp90 by the stress-regulated cochaperone aha1. *Mol Cell*, *10*, 1307-1318.
- Pearl, L. H. (2005). Hsp90 and Cdc37 -- a chaperone cancer conspiracy. *Curr Opin Genet Dev*, *15*, 55-61.
- Pearl, L. H. (2016). Review: The HSP90 molecular chaperone-an enigmatic ATPase. *Biopolymers*, *105*, 594-607.
- Pennisi, R., Ascenzi, P., & di Masi, A. (2015). Hsp90: A New Player in DNA Repair? *Biomolecules*, *5*, 2589-2618.

- Percy, A. J., Rey, M., Burns, K. M., & Schriemer, D. C. (2012). Probing protein interactions with hydrogen/deuterium exchange and mass spectrometry-a review. *Anal Chim Acta*, *721*, 7-21.
- Perez-Riba, A., & Itzhaki, L. S. (2019). The tetratricopeptide-repeat motif is a versatile platform that enables diverse modes of molecular recognition. *Curr Opin Struct Biol*, *54*, 43-49.
- Peroutka Iii, R. J., Orcutt, S. J., Strickler, J. E., & Butt, T. R. (2011). SUMO fusion technology for enhanced protein expression and purification in prokaryotes and eukaryotes. *Methods Mol Biol*, *705*, 15-30.
- Phillips, J. C., Hardy, D. J., Maia, J. D. C., Stone, J. E., Ribeiro, J. V., Bernardi, R. C., Buch, R., Fiorin, G., Henin, J., Jiang, W., McGreevy, R., Melo, M. C. R., Radak, B. K., Skeel, R. D., Singharoy, A., Wang, Y., Roux, B., Aksimentiev, A., Luthey-Schulten, Z., . . . Tajkhorshid, E. (2020). Scalable molecular dynamics on CPU and GPU architectures with NAMD. *J Chem Phys*, *153*, 044130.
- Phillips, J. J., Yao, Z. P., Zhang, W., McLaughlin, S., Laue, E. D., Robinson, C. V., & Jackson, S. E. (2007). Conformational dynamics of the molecular chaperone Hsp90 in complexes with a co-chaperone and anticancer drugs. *J Mol Biol*, *372*, 1189-1203.
- Philo, J. S. (2023). SEDNTERP: a calculation and database utility to aid interpretation of analytical ultracentrifugation and light scattering data. *Eur Biophys J*.
- Pirkl, F., & Buchner, J. (2001). Functional analysis of the Hsp90-associated human peptidyl prolyl cis/trans isomerases FKBP51, FKBP52 and Cyp40. *J Mol Biol*, *308*, 795-806.
- Piston, D. W., & Kremers, G. J. (2007). Fluorescent protein FRET: the good, the bad and the ugly. *Trends Biochem Sci*, *32*, 407-414.
- Polayes, D. A., Parks, T. D., Johnston, S. A., & Dougherty, W. G. (1998). Application of TEV Protease in Protein Production. *Methods Mol Med*, *13*, 169-183.
- Prodromou, C., Panaretou, B., Chohan, S., Siligardi, G., O'Brien, R., Ladbury, J. E., Roe, S. M., Piper, P. W., & Pearl, L. H. (2000). The ATPase cycle of Hsp90 drives a molecular 'clamp' via transient dimerization of the N-terminal domains. *EMBO J*, *19*, 4383-4392.
- Prodromou, C., Roe, S. M., O'Brien, R., Ladbury, J. E., Piper, P. W., & Pearl, L. H. (1997). Identification and structural characterization of the ATP/ADP-binding site in the Hsp90 molecular chaperone. *Cell*, *90*, 65-75.
- Prodromou, C., Siligardi, G., O'Brien, R., Woolfson, D. N., Regan, L., Panaretou, B., Ladbury, J. E., Piper, P. W., & Pearl, L. H. (1999). Regulation of Hsp90 ATPase activity by tetratricopeptide repeat (TPR)-domain co-chaperones. *EMBO J*, *18*, 754-762.
- Qi, R., Sarbeng, E. B., Liu, Q., Le, K. Q., Xu, X., Xu, H., Yang, J., Wong, J. L., Vorvis, C., Hendrickson, W. A., Zhou, L., & Liu, Q. (2013). Allosteric opening of the polypeptide-binding site when an Hsp70 binds ATP. *Nat Struct Mol Biol*, *20*, 900-907.
- Ratzke, C., Hellenkamp, B., & Hugel, T. (2014). Four-colour FRET reveals directionality in the Hsp90 multicomponent machinery. *Nat Commun*, *5*, 4192.

- Ratzke, C., Nguyen, M. N., Mayer, M. P., & Hugel, T. (2012). From a ratchet mechanism to random fluctuations evolution of Hsp90's mechanochemical cycle. *J Mol Biol*, *423*, 462-471.
- Rehn, A. B., & Buchner, J. (2015). p23 and Aha1. *Subcell Biochem*, *78*, 113-131.
- Reid, B. G., Fenton, W. A., Horwich, A. L., & Weber-Ban, E. U. (2001). ClpA mediates directional translocation of substrate proteins into the ClpP protease. *Proc Natl Acad Sci U S A*, *98*, 3768-3772.
- Reidy, M., & Masison, D. C. (2020). Mutations in the Hsp90 N Domain Identify a Site that Controls Dimer Opening and Expand Human Hsp90alpha Function in Yeast. *J Mol Biol*, *432*, 4673-4689.
- Reissmann, S., Joachimiak, L. A., Chen, B., Meyer, A. S., Nguyen, A., & Frydman, J. (2012). A gradient of ATP affinities generates an asymmetric power stroke driving the chaperonin TRIC/CCT folding cycle. *Cell Rep*, *2*, 866-877.
- Renart, J., Reiser, J., & Stark, G. R. (1979). Transfer of proteins from gels to diazobenzoyloxymethyl-paper and detection with antisera: a method for studying antibody specificity and antigen structure. *Proc Natl Acad Sci U S A*, *76*, 3116-3120.
- Retzlaff, M., Hagn, F., Mitschke, L., Hessling, M., Gugel, F., Kessler, H., Richter, K., & Buchner, J. (2010). Asymmetric activation of the hsp90 dimer by its cochaperone aha1. *Mol Cell*, *37*, 344-354.
- Retzlaff, M., Stahl, M., Eberl, H. C., Lagleder, S., Beck, J., Kessler, H., & Buchner, J. (2009). Hsp90 is regulated by a switch point in the C-terminal domain. *EMBO Rep*, *10*, 1147-1153.
- Richter, K., Haslbeck, M., & Buchner, J. (2010). The heat shock response: life on the verge of death. *Mol Cell*, *40*, 253-266.
- Richter, K., Muschler, P., Hainzl, O., & Buchner, J. (2001). Coordinated ATP hydrolysis by the Hsp90 dimer. *J Biol Chem*, *276*, 33689-33696.
- Richter, K., Muschler, P., Hainzl, O., Reinstein, J., & Buchner, J. (2003). Stil is a non-competitive inhibitor of the Hsp90 ATPase. Binding prevents the N-terminal dimerization reaction during the atpase cycle. *J Biol Chem*, *278*, 10328-10333.
- Richter, K., Soroka, J., Skalniak, L., Leskovar, A., Hessling, M., Reinstein, J., & Buchner, J. (2008). Conserved conformational changes in the ATPase cycle of human Hsp90. *J Biol Chem*, *283*, 17757-17765.
- Riffle, M., Jaschob, D., Zelter, A., & Davis, T. N. (2016). ProXL (Protein Cross-Linking Database): A Platform for Analysis, Visualization, and Sharing of Protein Cross-Linking Mass Spectrometry Data. *J Proteome Res*, *15*, 2863-2870.
- Roe, S. M., Prodromou, C., O'Brien, R., Ladbury, J. E., Piper, P. W., & Pearl, L. H. (1999). Structural basis for inhibition of the Hsp90 molecular chaperone by the antitumor antibiotics radicicol and geldanamycin. *J Med Chem*, *42*, 260-266.

- Rohl, A., Rohrberg, J., & Buchner, J. (2013). The chaperone Hsp90: changing partners for demanding clients. *Trends Biochem Sci*, *38*, 253-262.
- Rohl, A., Wengler, D., Madl, T., Lagleder, S., Tippel, F., Herrmann, M., Hendrix, J., Richter, K., Hack, G., Schmid, A. B., Kessler, H., Lamb, D. C., & Buchner, J. (2015). Hsp90 regulates the dynamics of its cochaperone Sti1 and the transfer of Hsp70 between modules. *Nat Commun*, *6*, 6655.
- Rosenzweig, R., Nillegoda, N. B., Mayer, M. P., & Bukau, B. (2019). The Hsp70 chaperone network. *Nature reviews Molecular cell biology*, *20*, 665-680.
- Rudiger, S., Buchberger, A., & Bukau, B. (1997). Interaction of Hsp70 chaperones with substrates. *Nat Struct Biol*, *4*, 342-349.
- Rutledge, B. S., Choy, W. Y., & Duennwald, M. L. (2022). Folding or holding?-Hsp70 and Hsp90 chaperoning of misfolded proteins in neurodegenerative disease. *J Biol Chem*, *298*, 101905.
- Rutz, D. A., Luo, Q., Freiburger, L., Madl, T., Kaila, V. R. I., Sattler, M., & Buchner, J. (2018). A switch point in the molecular chaperone Hsp90 responding to client interaction. *Nat Commun*, *9*, 1472.
- Saibil, H. (2013). Chaperone machines for protein folding, unfolding and disaggregation. *Nature reviews Molecular cell biology*, *14*, 630-642.
- Sali, A., & Blundell, T. L. (1993). Comparative protein modelling by satisfaction of spatial restraints. *J Mol Biol*, *234*, 779-815.
- Sambrook, J., Fritsch, E. F., & Maniatis, T. (1989). *Molecular cloning : laboratory manual* (2nd ed.). Cold Spring Harbor Laboratory Press.
- Sanchez, J., Carter, T. R., Cohen, M. S., & Blagg, B. S. J. (2020). Old and New Approaches to Target the Hsp90 Chaperone. *Curr Cancer Drug Targets*, *20*, 253-270.
- Sato, C., Mio, K., Kawata, M., & Ogura, T. (2014). 3D structure determination of protein using TEM single particle analysis. *Microscopy (Oxf)*, *63 Suppl 1*, i9-i10.
- Scheufler, C., Brinker, A., Bourenkov, G., Pegoraro, S., Moroder, L., Bartunik, H., Hartl, F. U., & Moarefi, I. (2000). Structure of TPR domain-peptide complexes: critical elements in the assembly of the Hsp70-Hsp90 multichaperone machine. *Cell*, *101*, 199-210.
- Schirmer, E. C., Glover, J. R., Singer, M. A., & Lindquist, S. (1996). HSP100/Clp proteins: a common mechanism explains diverse functions. *Trends in biochemical sciences*, *21*, 289-296.
- Schmid, A. B., Lagleder, S., Grawert, M. A., Rohl, A., Hagn, F., Wandinger, S. K., Cox, M. B., Demmer, O., Richter, K., Groll, M., Kessler, H., & Buchner, J. (2012). The architecture of functional modules in the Hsp90 co-chaperone Sti1/Hop. *EMBO J*, *31*, 1506-1517.
- Schopf, F. H., Biebl, M. M., & Buchner, J. (2017). The HSP90 chaperone machinery. *Nat Rev Mol Cell Biol*, *18*, 345-360.

- Schopf, F. H., Huber, E. M., Dodt, C., Lopez, A., Biebl, M. M., Rutz, D. A., Muhlhofer, M., Richter, G., Madl, T., Sattler, M., Groll, M., & Buchner, J. (2019). The Co-chaperone Cns1 and the Recruiter Protein Hgh1 Link Hsp90 to Translation Elongation via Chaperoning Elongation Factor 2. *Mol Cell*, *74*, 73-87 e78.
- Schrimpf, W., Barth, A., Hendrix, J., & Lamb, D. C. (2018). PAM: A Framework for Integrated Analysis of Imaging, Single-Molecule, and Ensemble Fluorescence Data. *Biophys J*, *114*, 1518-1528.
- Schuck, P. (2000). Size-distribution analysis of macromolecules by sedimentation velocity ultracentrifugation and lamm equation modeling. *Biophys J*, *78*, 1606-1619.
- Schuck, P. (2013). Analytical Ultracentrifugation as a Tool for Studying Protein Interactions. *Biophys Rev*, *5*, 159-171.
- Schulte, T. W., Akinaga, S., Soga, S., Sullivan, W., Stensgard, B., Toft, D., & Neckers, L. M. (1998). Antibiotic radicicol binds to the N-terminal domain of Hsp90 and shares important biologic activities with geldanamycin. *Cell Stress Chaperones*, *3*, 100-108.
- Schulze, A., Beliu, G., Helmerich, D. A., Schubert, J., Pearl, L. H., Prodromou, C., & Neuweiler, H. (2016). Cooperation of local motions in the Hsp90 molecular chaperone ATPase mechanism. *Nat Chem Biol*, *12*, 628-635.
- Scroggins, B. T., Robzyk, K., Wang, D., Marcu, M. G., Tsutsumi, S., Beebe, K., Cotter, R. J., Felts, S., Toft, D., Karnitz, L., Rosen, N., & Neckers, L. (2007). An acetylation site in the middle domain of Hsp90 regulates chaperone function. *Mol Cell*, *25*, 151-159.
- Seraphim, T. V., Gava, L. M., Mokry, D. Z., Cagliari, T. C., Barbosa, L. R., Ramos, C. H., & Borges, J. C. (2015). The C-terminal region of the human p23 chaperone modulates its structure and function. *Arch Biochem Biophys*, *565*, 57-67.
- Shiau, A. K., Harris, S. F., Southworth, D. R., & Agard, D. A. (2006). Structural Analysis of E. coli hsp90 reveals dramatic nucleotide-dependent conformational rearrangements. *Cell*, *127*, 329-340.
- Sigler, P. B., Xu, Z., Rye, H. S., Burston, S. G., Fenton, W. A., & Horwich, A. L. (1998). Structure and function in GroEL-mediated protein folding. *Annual review of biochemistry*, *67*, 581-608.
- Siligardi, G., Hu, B., Panaretou, B., Piper, P. W., Pearl, L. H., & Prodromou, C. (2004). Co-chaperone regulation of conformational switching in the Hsp90 ATPase cycle. *J Biol Chem*, *279*, 51989-51998.
- Sinz, A. (2006). Chemical cross-linking and mass spectrometry to map three-dimensional protein structures and protein-protein interactions. *Mass Spectrom Rev*, *25*, 663-682.
- Some, D., Amartely, H., Tsadok, A., & Lebendiker, M. (2019). Characterization of Proteins by Size-Exclusion Chromatography Coupled to Multi-Angle Light Scattering (SEC-MALS). *J Vis Exp*.

- Soroka, J., Wandinger, S. K., Mausbacher, N., Schreiber, T., Richter, K., Daub, H., & Buchner, J. (2012). Conformational switching of the molecular chaperone Hsp90 via regulated phosphorylation. *Mol Cell*, *45*, 517-528.
- Southworth, D. R., & Agard, D. A. (2008). Species-dependent ensembles of conserved conformational states define the Hsp90 chaperone ATPase cycle. *Mol Cell*, *32*, 631-640.
- Southworth, D. R., & Agard, D. A. (2011). Client-loading conformation of the Hsp90 molecular chaperone revealed in the cryo-EM structure of the human Hsp90:Hop complex. *Mol Cell*, *42*, 771-781.
- Southworth, M. W., Amaya, K., Evans, T. C., Xu, M. Q., & Perler, F. B. (1999). Purification of proteins fused to either the amino or carboxy terminus of the Mycobacterium xenopi gyrase A intein. *Biotechniques*, *27*, 110-114, 116, 118-120.
- Spiess, C., Meyer, A. S., Reissmann, S., & Frydman, J. (2004). Mechanism of the eukaryotic chaperonin: protein folding in the chamber of secrets. *Trends Cell Biol*, *14*, 598-604.
- Sreedhar, A. S., Kalmar, E., Csermely, P., & Shen, Y. F. (2004). Hsp90 isoforms: functions, expression and clinical importance. *FEBS Lett*, *562*, 11-15.
- Srivastava, D., Yadav, R. P., Singh, S., Boyd, K., & Artemyev, N. O. (2023). Unique interface and dynamics of the complex of HSP90 with a specialized cochaperone AIPL1. *Structure*, *31*, 309-317 e305.
- Storer, C. L., Dickey, C. A., Galigniana, M. D., Rein, T., & Cox, M. B. (2011). FKBP51 and FKBP52 in signaling and disease. *Trends Endocrinol Metab*, *22*, 481-490.
- Street, T. O., Krukenberg, K. A., Rosgen, J., Bolen, D. W., & Agard, D. A. (2010). Osmolyte-induced conformational changes in the Hsp90 molecular chaperone. *Protein Sci*, *19*, 57-65.
- Sullivan, W., Stensgard, B., Caucutt, G., Bartha, B., McMahon, N., Alnemri, E. S., Litwack, G., & Toft, D. (1997). Nucleotides and two functional states of hsp90. *J Biol Chem*, *272*, 8007-8012.
- Sun, H., Liu, X., Wang, L., Cui, B., Mu, W., Xia, Y., Liu, S., Liu, X., Jiao, Y., & Zhao, Y. (2022). Dexamethasone Sensitizes Acute Monocytic Leukemia Cells to Ara-C by Upregulating FKBP51. *Front Oncol*, *12*, 888695.
- Taherian, A., Krone, P. H., & Ovsenek, N. (2008). A comparison of Hsp90alpha and Hsp90beta interactions with cochaperones and substrates. *Biochem Cell Biol*, *86*, 37-45.
- Telenti, A., Southworth, M., Alcaide, F., Daugelat, S., Jacobs, W. R., Jr., & Perler, F. B. (1997). The Mycobacterium xenopi GyrA protein splicing element: characterization of a minimal intein. *J Bacteriol*, *179*, 6378-6382.
- Tippel, F. (2017). *Mechanistic Analysis of Conformational Dynamics of the Molecular Chaperone Hsp90* [Technische Universität München].

- Tomoyasu, T., Gamer, J., Bukau, B., Kanemori, M., Mori, H., Rutman, A. J., Oppenheim, A. B., Yura, T., Yamanaka, K., Niki, H., & et al. (1995). Escherichia coli FtsH is a membrane-bound, ATP-dependent protease which degrades the heat-shock transcription factor sigma 32. *EMBO J*, *14*, 2551-2560.
- Trepel, J., Mollapour, M., Giaccone, G., & Neckers, L. (2010). Targeting the dynamic HSP90 complex in cancer. *Nat Rev Cancer*, *10*, 537-549.
- Tsumoto, K., Umetsu, M., Kumagai, I., Ejima, D., Philo, J. S., & Arakawa, T. (2004). Role of arginine in protein refolding, solubilization, and purification. *Biotechnol Prog*, *20*, 1301-1308.
- Valpuesta, J. M., Martin-Benito, J., Gomez-Puertas, P., Carrascosa, J. L., & Willison, K. R. (2002). Structure and function of a protein folding machine: the eukaryotic cytosolic chaperonin CCT. *FEBS Lett*, *529*, 11-16.
- van Oosten-Hawle, P., Porter, R. S., & Morimoto, R. I. (2013). Regulation of organismal proteostasis by transcellular chaperone signaling. *Cell*, *153*, 1366-1378.
- Vaughan, C. K., Piper, P. W., Pearl, L. H., & Prodromou, C. (2009). A common conformationally coupled ATPase mechanism for yeast and human cytoplasmic HSP90s. *FEBS J*, *276*, 199-209.
- Verba, K. A., Wang, R. Y., Arakawa, A., Liu, Y., Shirouzu, M., Yokoyama, S., & Agard, D. A. (2016). Atomic structure of Hsp90-Cdc37-Cdk4 reveals that Hsp90 traps and stabilizes an unfolded kinase. *Science*, *352*, 1542-1547.
- Verghese, J., Abrams, J., Wang, Y., & Morano, K. A. (2012). Biology of the heat shock response and protein chaperones: budding yeast (*Saccharomyces cerevisiae*) as a model system. *Microbiol Mol Biol Rev*, *76*, 115-158.
- Verma, M., Vats, A., & Taneja, V. (2015). Toxic species in amyloid disorders: Oligomers or mature fibrils. *Ann Indian Acad Neurol*, *18*, 138-145.
- Verma, S., Goyal, S., Jamal, S., Singh, A., & Grover, A. (2016). Hsp90: Friends, clients and natural foes. *Biochimie*, *127*, 227-240.
- Wales, T. E., & Engen, J. R. (2006). Hydrogen exchange mass spectrometry for the analysis of protein dynamics. *Mass Spectrom Rev*, *25*, 158-170.
- Walter, S., & Buchner, J. (2002). Molecular chaperones--cellular machines for protein folding. *Angew Chem Int Ed Engl*, *41*, 1098-1113.
- Wandinger, S. K., Richter, K., & Buchner, J. (2008). The Hsp90 chaperone machinery. *J Biol Chem*, *283*, 18473-18477.
- Wang, J., Hartling, J. A., & Flanagan, J. M. (1997). The structure of ClpP at 2.3 Å resolution suggests a model for ATP-dependent proteolysis. *Cell*, *91*, 447-456.

- Wang, R. Y., Noddings, C. M., Kirschke, E., Myasnikov, A. G., Johnson, J. L., & Agard, D. A. (2022). Structure of Hsp90-Hsp70-Hop-GR reveals the Hsp90 client-loading mechanism. *Nature*, *601*, 460-464.
- Watanabe, T., Ito, Y., Yamada, T., Hashimoto, M., Sekine, S., & Tanaka, H. (1994). The roles of the C-terminal domain and type III domains of chitinase A1 from *Bacillus circulans* WL-12 in chitin degradation. *J Bacteriol*, *176*, 4465-4472.
- Wayne, N., & Bolon, D. N. (2007). Dimerization of Hsp90 is required for in vivo function. Design and analysis of monomers and dimers. *J Biol Chem*, *282*, 35386-35395.
- Weaver, A. J., Sullivan, W. P., Felts, S. J., Owen, B. A., & Toft, D. O. (2000). Crystal structure and activity of human p23, a heat shock protein 90 co-chaperone. *J Biol Chem*, *275*, 23045-23052.
- Weber-Ban, E. U., Reid, B. G., Miranker, A. D., & Horwich, A. L. (1999). Global unfolding of a substrate protein by the Hsp100 chaperone ClpA. *Nature*, *401*, 90-93.
- Wegrzyn, R. D., & Deuerling, E. (2005). Molecular guardians for newborn proteins: ribosome-associated chaperones and their role in protein folding. *Cell Mol Life Sci*, *62*, 2727-2738.
- Weickl, T., Abelmann, K., & Buchner, J. (1999). An unstructured C-terminal region of the Hsp90 co-chaperone p23 is important for its chaperone function. *J Mol Biol*, *293*, 685-691.
- Weickl, T., Muschler, P., Richter, K., Veit, T., Reinstein, J., & Buchner, J. (2000). C-terminal regions of Hsp90 are important for trapping the nucleotide during the ATPase cycle. *J Mol Biol*, *303*, 583-592.
- Whitesell, L., Mimnaugh, E. G., De Costa, B., Myers, C. E., & Neckers, L. M. (1994). Inhibition of heat shock protein HSP90-pp60v-src heteroprotein complex formation by benzoquinone ansamycins: essential role for stress proteins in oncogenic transformation. *Proc Natl Acad Sci U S A*, *91*, 8324-8328.
- Whitford, D. (2013). *Proteins: structure and function*. John Wiley & Sons.
- Whitmore, L., & Wallace, B. A. (2008). Protein secondary structure analyses from circular dichroism spectroscopy: methods and reference databases. *Biopolymers*, *89*, 392-400.
- Wittig, I., & Schagger, H. (2005). Advantages and limitations of clear-native PAGE. *Proteomics*, *5*, 4338-4346.
- Woerner, A. C., Frotin, F., Hornburg, D., Feng, L. R., Meissner, F., Patra, M., Tatzelt, J., Mann, M., Winklhofer, K. F., Hartl, F. U., & Hipp, M. S. (2016). Cytoplasmic protein aggregates interfere with nucleocytoplasmic transport of protein and RNA. *Science*, *351*, 173-176.
- Wolf, S., Sohmen, B., Hellenkamp, B., Thurn, J., Stock, G., & Hugel, T. (2021). Hierarchical dynamics in allostery following ATP hydrolysis monitored by single molecule FRET measurements and MD simulations. *Chem Sci*, *12*, 3350-3359.

- Xu, M.-Q. (2000). *Fusions to self-splicing inteins for protein purification* (Vol. 326). [https://doi.org/10.1016/S0076-6879\(00\)26066-7](https://doi.org/10.1016/S0076-6879(00)26066-7)
- Xu, Y. W., Morera, S., Janin, J., & Cherfils, J. (1997). AIF3 mimics the transition state of protein phosphorylation in the crystal structure of nucleoside diphosphate kinase and MgADP. *Proc Natl Acad Sci U S A*, *94*, 3579-3583.
- Yonehara, M., Minami, Y., Kawata, Y., Nagai, J., & Yahara, I. (1996). Heat-induced chaperone activity of HSP90. *J Biol Chem*, *271*, 2641-2645.
- Young, J. C., & Hartl, F. U. (2000). Polypeptide release by Hsp90 involves ATP hydrolysis and is enhanced by the co-chaperone p23. *EMBO J*, *19*, 5930-5940.
- Yue, L., Karr, T. L., Nathan, D. F., Swift, H., Srinivasan, S., & Lindquist, S. (1999). Genetic analysis of viable Hsp90 alleles reveals a critical role in Drosophila spermatogenesis. *Genetics*, *151*, 1065-1079.
- Zhang, H., Zhou, C., Chen, W., Xu, Y., Shi, Y., Wen, Y., & Zhang, N. (2015). A dynamic view of ATP-coupled functioning cycle of Hsp90 N-terminal domain. *Sci Rep*, *5*, 9542.
- Zhang, Y., & Cremer, P. S. (2006). Interactions between macromolecules and ions: The Hofmeister series. *Curr Opin Chem Biol*, *10*, 658-663.
- Zhao, G., Dong, X. Y., & Sun, Y. (2009). Ligands for mixed-mode protein chromatography: Principles, characteristics and design. *J Biotechnol*, *144*, 3-11.
- Zierer, B. K., Rubbelke, M., Toppel, F., Madl, T., Schopf, F. H., Rutz, D. A., Richter, K., Sattler, M., & Buchner, J. (2016). Importance of cycle timing for the function of the molecular chaperone Hsp90. *Nat Struct Mol Biol*, *23*, 1020-1028.
- Zimmerman, S. B., & Trach, S. O. (1991). Estimation of macromolecule concentrations and excluded volume effects for the cytoplasm of Escherichia coli. *J Mol Biol*, *222*, 599-620.
- Zuehlke, A., & Johnson, J. L. (2010). Hsp90 and co-chaperones twist the functions of diverse client proteins. *Biopolymers*, *93*, 211-217.
- Zuiderweg, E. R., Hightower, L. E., & Gestwicki, J. E. (2017). The remarkable multivalency of the Hsp70 chaperones. *Cell Stress Chaperones*, *22*, 173-189.
- Zwanzig, R., Szabo, A., & Bagchi, B. (1992). Levinthal's paradox. *Proc Natl Acad Sci U S A*, *89*, 20-22.

## Abbreviations

°C	Degree Celsius
µg	Microgram
µL	Microliter
µM	Micromol
5-FOA	5-Fluoroorotic acid
AAA+	ATPases associated with diverse cellular activities
ADP	Adenosine diphosphate
Aha1	Activator of Hsp90 ATPase
AMP-PNP	Adenylyl imidodiphosphate
ATP	Adenosine triphosphate
ATPgS	Adenosine-5'-O-(3-thiotriphosphate)
bp	Basepair
BSA	Bovine serum albumin
CD	Circular dichroism
DMSO	Dimethyl sulfoxide
DNA	Deoxyribonucleic acid
dNTP	Deoxyribonucleotide triphosphate
DOL	Degree of labeling
DSG	Disuccinimidyl glutarate
DTT	Dithiothreitol
EDTA	Ethylendiaminetetraacetic acid
EPL	Expressed protein ligation
FCCS	Fluorescence cross-correlation spectroscopy
Fig.	Figure
FRET	Förster resonance energy transfer
h	Hour
H/DX	Hydrogen/Deuterium exchange
HEPES	4-(2-hydroxyethyl)-1-piperazineethanesulfonic acid
Hop	Hsp70-Hsp90 organizing protein
Hsp	Heat shock protein
IPTG	Isopropyl β-D-1-thiogalactopyranoside
kDa	Kilodalton
KLD	Kinase, Ligase, Dpn1
MD	Molecular dynamics
MESNA	2-mercaptoethanesulfonic acid
mg	Milligram
min	Minute
mL	Milliliter
mM	Millimol
MRW	Mean residue weight
NBD	Nucleotide binding domain

## *Abbreviations*

---

ng	Nanogram
nm	Nanometer
OD	Optical density
PAGE	Poly acrylamide gel electrophoresis
PCR	Polymerase chain reaction
pmol	Picomol
PMSF	Phenylmethylsulfonyl fluoride
PPIase	Peptidyl-proline isomerase
PTM	Post translational modification
rpm	Rotations per minute
SDS	Sodium dodecyl sulfate
SEC	Size exclusion chromatography
SrtA	Sortase A
TEM	Transmission electron microscopy
TEMED	Tetramethylethylenediamine
TPR	Tetratricopeptide repeat
UV/Vis	Ultraviolet/Visible
WT	Wildtype

## **Acknowledgment**

First, I would like to express my gratitude to Professor Johannes Buchner, who not only provided me with the opportunity to conduct my thesis in his group but also ensured that I had access to exceptional scientific equipment and knowledge. Throughout my thesis journey, his guidance has been invaluable, and I am truly grateful for his unwavering support. I am also deeply appreciative of the opportunities he gave me to attend two captivating Hsp90 conferences and an EMBO conference in 2023.

I would like to extend special thanks to Ganesh Agam, Ecenaz Bilgen, Don Lamb, Christian Becker, and Ville Kaila for their incredibly productive and seamless collaboration on various Hsp90 projects during my thesis work. Their contributions have been instrumental in the success of my research.

I am grateful to my office and group members Maximilian Riedl, Benjamin Heim, Jannis Lawatschek, Maximilian Biebl, and Andreas Maier for their supportive assistance and stimulating discussions. I would also like to acknowledge the Buchner group as a whole for fostering a positive and inspiring work environment on a daily basis.

Furthermore, I extend my thanks to our exceptional lab technicians, especially Florian Rührnöbl, Martin Haslbeck, Margot Rubinstein, Anna Semm, and Laura Meier, who have ensured a smooth and efficient laboratory experience, handling both the scientific and bureaucratic aspects with proficiency.

Lastly, I would like to express my deepest gratitude to my family, friends, and my girlfriend. Their unwavering encouragement and support have been a constant source of strength throughout this journey, and I am truly fortunate to have them by my side.

## **Declaration**

I, Stefan Riedl, hereby declare that this thesis was prepared independently and using only references and resources stated herein. The work has not been presented to any examination board, yet. Parts of this work will be published in scientific journals.

Hiermit erkläre ich, Stefan Riedl, dass die vorliegende Arbeit selbstständig verfasst und keine anderen als die angegebenen Quellen und Hilfsmittel verwendet habe. Die Arbeit wurde bisher keiner Prüfungskommission vorgelegt. Teile dieser Arbeit werden in wissenschaftlichen Journalen veröffentlicht werden.

Stefan Riedl

Ort, Datum